NISTIR 8271

Face Recognition Vendor Test (FRVT)

Part 2: Identification

Patrick Grother
Mei Ngan
Kayee Hanaoka
Information Access Division
Information Technology Laboratory

This publication is available free of charge from:
https://doi.org/10.6028/NIST.IR.8271

2019/09/11

National Institute of Standards and Technology
U.S. Department of Commerce

NISTIR 8271

Face Recognition Vendor Test (FRVT)

Part 2: Identification

Patrick Grother
Mei Ngan
Kayee Hanaoka
Information Access Division
Information Technology Laboratory

This publication is available free of charge from:
https://doi.org/10.6028/NIST.IR.8271

November 2018

U.S. Department of Commerce
Wilbur Ross, Secretary

National Institute of Standards and Technology
Walter Copan, Director

ACKNOWLEDGMENTS

The authors are grateful to Wayne Salamon and Greg Fiumara at NIST for designing robust software infrastructure for image and template storage and parallel execution of algorithms across our computers. Thanks also to Brian Cochran at NIST for providing highly available computers and network-attached storage.

DISCLAIMER

Specific hardware and software products identified in this report were used in order to perform the evaluations described in this document. In no case does identification of any commercial product, trade name, or vendor, imply recommendation or endorsement by the National Institute of Standards and Technology, nor does it imply that the products and equipment identified are necessarily the best available for the purpose.

Executive Summary

This report updates and extends NIST Interagency Report 8238, documenting the evaluation of automated face recognition algorithms submitted to NIST in November 2018. The algorithms, which implement one-to-many identification of faces appearing in two-dimensional images, are prototypes from the research and development laboratories of mostly commercial suppliers, and are submitted to NIST as compiled black-box libraries implementing a NIST-specified C++ test interface. The report therefore does not describe how algorithms operate.

The evaluation used four datasets - frontal mugshots, profile views, webcam photos and wild images - and the report lists accuracy results alongside developer names. It will therefore be useful for comparison of face recognition algorithms and assessment of absolute capability. The primary dataset is comprised of 26.6 million reasonably well-controlled live portrait photos of 12.3 million individuals. The three smaller datasets contain more unconstrained photos: 3.2 million webcam images; 200 thousand side-view images; and 2.5 million photojournalism and amateur photographer photos. These datasets are sequestered at NIST, meaning that developers do not have access to them for training or testing. The last dataset, however, consists of images drawn from the internet for testing purposes so while it is not truly sequestered, its composition is unknown to the developers.

The evaluation was run in three phases, starting Feburary, June, and November 2018 respectively, with developers receiving technical feedback between phases. Results for 127 algorithms from 41 developers were published in November 2018 as NIST Interagency Report 8238. This update adds results for an additional 76 algorithms from 42 developers submitted in October 2018. At that time seven developers ceased participation, and nine developers started. The developer totals constitute a substantial majority of the face recognition industry.

The major result given in NIST IR 8238 was that massive gains in accuracy have been achieved in the last five years (2013-2018) and these far exceed improvements made in the prior period (2010-2013). While the industry gains were broad - at least 30 developers' algorithms outperformed the most accurate algorithm from late 2013 - there remains a wide range of capability. While this report shows accuracy gains only over the course of 2018, the most accurate algorithm reported here is substantially more accurate than anything reported in NIST IR 8238. This is evidence that face recognition development continues apace, and that FRVT reports are but a snapshot of contemporary capability.

From discussion with developers, the accuracy gains stem from the adoption of deep convolutional neural networks. As such, face recognition has undergone an industrial revolution, with algorithms increasingly tolerant of poorly illuminated and other low quality images, and poorly posed subjects. One related result is that a few algorithms correctly match side-view photographs to galleries of frontal photos, with search accuracy approaching that of the best c. 2010 algorithms executing frontal-frontal search. The capability to recognize under a 90-degree change in viewpoint - pose invariance - has been a long-sought milestone in face recognition research.

With good quality portrait photos, the most accurate algorithms will find matching entries, when present, in galleries containing 12 million individuals, with rank one miss rates of approaching 0.1%. The remaining errors are in large part attributable to long-run ageing, facial injury and poor image quality. In at least 5% of images identification often succeeds (i.e. the mate is returned at rank 1) but recognition similarity scores are weak such that true and false matches become indistinguishable, and human adjudication becomes necessary.

From Fall 2019 this report will be updated continuously as new algorithms are submitted to FRVT, and run on new datasets. Participation in the one-to-many identification track requires a devloper to first demonstrate high accuracy in the one-to-one verification track of FRVT.

Scope and Context

Audience: This report is intended for developers, integrators, end users, policy makers and others who have some familiarity with biometrics applications. The methods and metrics documented here will be of interest to organizations engaged in tests of face recognition algorithms. Some of these have been incorporated in the ISO/IEC 19795 Part 1 Biometric Testing and Reporting Framework standard, now under revision.

Prior benchmarks: Automated face recognition accuracy has improved massively in the two decades since initial commercialization of the various technologies. NIST has tracked that improvement through its conduct of regular independent, free, open, and public evaluations. These have fostered improvements in the state of the art. This report serves as an update to the NIST Interagency Report 8238 on performance of face identification algorithms, published in November 2018.

Scope: As with NIST IR 8238, this report documents recognition results for four databases containing in excess of 30.2 million still photographs of 14.4 million individuals. This constitutes the largest public and independent evaluation of face recognition ever conducted. It includes results for accuracy, speed, investigative vs. identification applications, scalability to large populations, use of multiple images per person, images of cooperative and non-cooperative subjects.

The report also includes results for ageing, recognition of twins, and recognition of profile-view images against frontal galleries. It otherwise does not address causes of recognition failure, neither image-specific problems nor subject-specific factors including demographics. Separate reports on demographic dependencies in face recognition will be published in the future. Additionally out of scope are: performance of live human-in-the-loop transactional systems like automated border control gates; human recognition accuracy as used in forensic applications; and recognition of persons in video sequences (which NIST evaluated separately [9]). Some of those applications share core matching technologies that *are* tested in this report.

Images: Three kinds of images are employed. The primary dataset is a set of law enforcement mugshot images (Fig. 3) which are enrolled and then searched with three kinds of images: 1) other mugshots (i.e. within-domain); 2) profile-view photographs (90 degree cross-view); 3) lower quality webcam images (Fig. 4) collected in similar detention operations (cross-domain); Additionally wild images (Fig. 6) are searched against other wild images.

Participation and industry coverage: The report includes performance figures for 203 prototype algorithms from the research laboratories of 51 commercial developers and one university. This represents a substantial majority of the face recognition industry, but only a tiny minority of the academic community. Participation was open worldwide. While there is no charge for participation, developers incur some software engineering expense in implementing their algorithms behind the NIST application programming interface (API). The test is a black-box test where the function of the algorithm, and the intellectual property associated with it, is hidden inside pre-compiled libraries.

Recent technology development: Most face recognition research with deep convolutional neural networks (CNNs) has been aimed at achieving invariance to pose, illumination and expression variations that characterize photojournalism and social media images. The initial research [18, 24] employed large numbers of images of relatively few ($\sim 10^4$) individuals to learn invariance. Inevitably much larger populations ($\sim 10^7$) were employed for training [11, 20] but the benchmark, Labeled Faces in the Wild with (essentially) an equal error rate metric [12], represents an easy task, one-to-one verification at very high false match rates. While a larger scale identification benchmark duly followed, Megaface [15], its primary metric, rank one hit rate, contrasts with the high threshold discrimination task required in most large-population applications of face recognition, namely credential de-duplication, and background checks. There, identification in galleries containing up to 10^8 individuals must be performed using a) very few images per individual and b) stringent thresholds to afford very low false positive identification rates. FRVT 2018 was launched to measure the capability of the new technologies, including in these two cases. FRVT has included open-set identification tests since 2002, reporting both false negative and positive identification rates [7].

Performance metrics for applications: This report documents the performance of one-to-many face recognition algorithms. The word "performance" here refers to recognition accuracy and computational resource usage, as measured by executing those algorithms on massive sequestered datasets.

This report includes extensive tabulation of recognition error rates germane to the main use-cases for face search technology. The Figure below, inspired by the Figure 1 in [25] differentiates different applications of the technolgy. The last row directs readers to the main tables relevant to those applications, respectively threshold-based and rank-based metrics that are special cases of the metrics given in section 3. The terms negative identification and positive identification are taken from the ISO/IEC 2382-37:2017 standardized biometrics vocabulary.

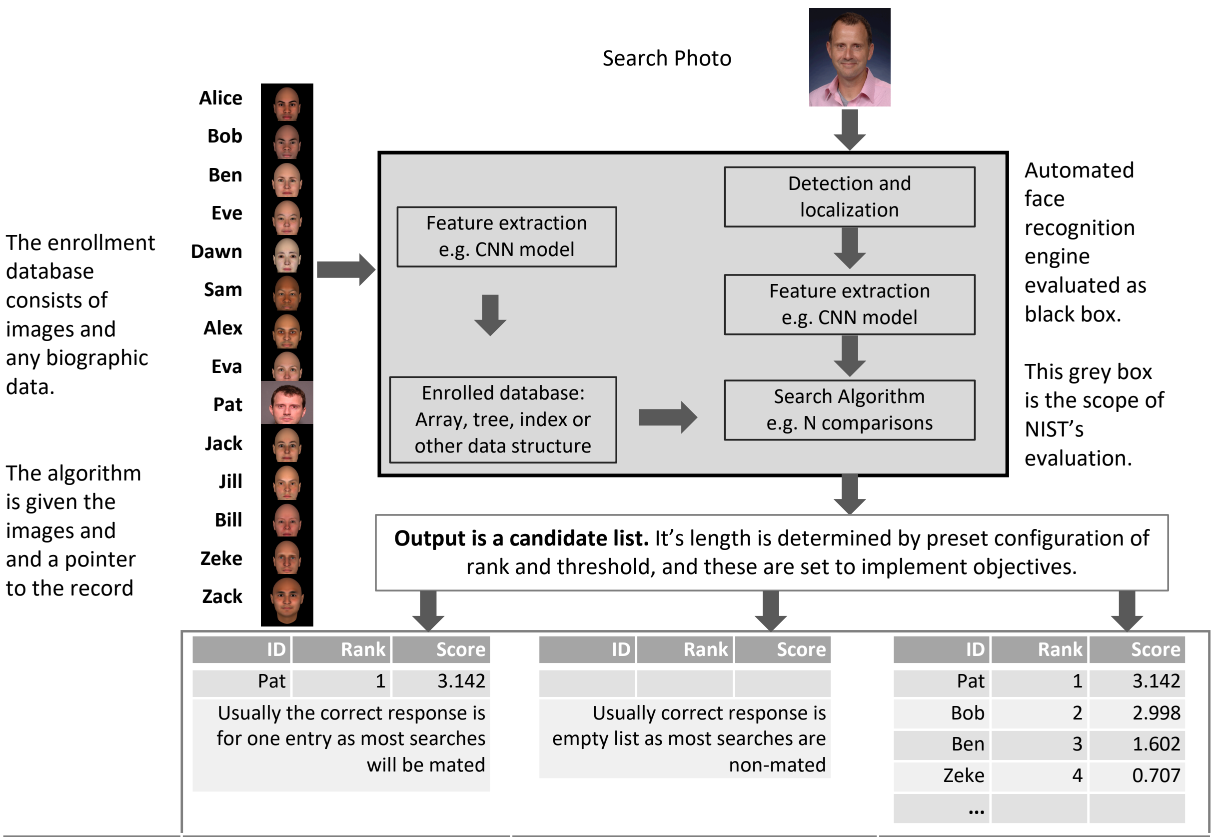

	Positive identification	Negative identification	Post-event investigation
Example	Access to a gym or cruise ship	Watchlist e.g. Detection of deportee or duplicate drivers license applications	Crime scene photos, or of detainee without ID documents.
Claim of identity	Implicit claim to be enrolled	Implicit claim to not be enrolled	No claim: Inquiry
Threshold	High, to implement security objective	High, to limit false positives	Zero
Num. candidates	1	0	L, set by request to algorithm
Human role	Review candidate to assist user in resolution of false negatives, or to detect impostor	Review candidate to determine false positive or correct hit	Review multiple candidates, refer possible hits to examiners see [26]
Intended human involvement frequency	Rare – approx. the false negative identification rate plus prior probability of impostor	Rare – approx. the false positive identification rate plus prior probability of an actual mate	Always
Performance metric of interest	**FNIR at low FPIR. See sec. 3.1, 3.2 and Tables 10, 19**	**FNIR at low FPIR. See sec. 3.1, 3.2 and Tables 10, 19**	**FNIR at ranks 1... 50, say. FPIR = 1. See sec. 3.2 and Table 12, 14, 16**

The algorithms are specifically configured for these applications by setting thresholds and candidate list lengths. Both rank-based metrics and threshold-based metrics include tradeoffs. In investigation, overall accuracy will be reduced if labor is only available to review a few candidates from the automated system. Note that when a fixed number of candidates are returned, the false positive identification rate of the automated face recognition engine will be 100%, because a probe image of anyone not enrolled will still return candidates. In identification applications where false positives must be limited to satisfy reviewer labor availability or a security objective, higher false negative rates are implied. This report includes extensive quantification of this threshold-based tradeoff. See Sec. 3

Template diversity: The FRVT is designed to evaluate black-box technologies with the consequence that the templates that hold features extracted from face images are entirely proprietary opaque binary data that embed considerable intellectual property of the developer. Despite migration to CNN-based technologies there is no consensus on the optimal feature vector dimension. This is evidenced by template sizes ranging from below 100 bytes to more than four kilobytes. This diversity of approaches, suggests there is no prospect of a standard template something that would require a common feature set to be extracted from faces. Interoperability in automated face recognition remains solidly based on images and documentary standards for those, in particular the ICAO portrait [29] specification deriving from the ISO/IEC 19794-5 Token frontal [26] standard, which are similar to certain ANSI/NIST Type 10 [28] formats.

Training: The algorithms submitted to NIST have been developed using image datasets that developers do not disclose. The development will often include application of machine learning techniques and will additionally involve iterative training and testing cycles. NIST itself does not perform any training and does not refine or alter the algorithm in any way. Thus the model, data files, and libraries that define an algorithm are fixed for the duration of the tests. This reflects typical operational reality where recognition software, once installed, is fixed and constant until upgraded. This situation persists because on-site training of algorithms on customer data is atypical essentially because training is not a turnkey process.

Automated search and human review: Virtually all applications using automated face search require human review of the outputs at some frequency: Always for investigational applications; rarely in positive identification applications, after rejection (false or otherwise); and rarely in negative identification applications, after an alarm (false or otherwise). The human role is usually to compare a reference image with the query image or the live-subject if present, to render either a definitive decision on “exclusion” (different subjects), or “identification” (same subject), or a declaration that one or both images have “no value” and that no decision can be made. Note that automated face recognition algorithms are not built to do exclusion - low scores from a face comparison arise from different faces *and* poor quality images of the same face.

Human reviewers make recognition errors [5, 19, 27] and are sensitive to image acquisition and quality. Accurate human review is supported by high resolution - as specified in the Type 50, 51 acquisition profiles of the ANSI/NIST Type 10 record [28], and by multiple non-frontal views as specified in the same standard. These often afford views of the ear. Organizations involved in image collection should consider supporting human adjudication by collecting high-resolution frontal and non-frontal views, preparing low resolution versions for automated face recognition [26], and retaining both for any subsequent resolution of candidate matches. Along these lines, the ISO/IEC Joint Technical Committee 1 subcommittee 37 on biometrics has just initiated projects on image quality assessment and face-aware capture.

Next steps: NIST expects to publish a first report on demographic dependencies in face recognition in 2019. This will include the effects of age, sex and race.

Technical Summary

▷ **Rank-based accuracy:** The inset table shows false negative "miss rates" realized when searching a 12 million person gallery populated with FRVT 2018 mugshots. The two most accurate algorithms fail to return the correct mate somewhere within the top 50 ranks in fewer than 0.1% of searches (Table 1, rows 1,2). This is achieved for galleries populated with multiple images per person. In the case where only the most recent image is present the miss rate is modestly higher (rows 3,4). The mates are almost always at rank 1, so in cases where only very short candidate lists must be used, the rank-1 miss rate is barely higher 0.12% (row 5) which again modestly rises when persons are enrolled with a single image (row 7). All the miss rates are measured over a fixed set of 154 549 searches, and the lowest false negative error rate recorded in this report (0.038%, row 10) corresponds to just 58 misses. Given such low error rates, what misses remain? By inspection they arise in five categories, those due to: a) ageing i.e. long-term time lapse between images; b) images of injured individuals e.g. bruised or bandaged faces; c) the presence of a second face e.g. printed on a T-shirt; d) images of some object that is not a face; e) profile-view images, and f) actual clerical ID label errors. As discussed in section 3.8.2, the first three categories are legitimately part of a test designed to measure accuracy on portrait images collected in law-enforcement settings. The latter three categories, however, should not be included in a test that is attempting to measure accuracy on only frontal images. Thus, by removing all known images in those categories, the rightmost column shows error rates that would be attainable in an application where exclusively frontal portrait images were collected without identity labeling errors.

	Investigation miss rate at	Num-subjects	Enrolled image	Num-images	Algorithm	FNIR Raw	FNIR Corrected
1	Rank-50	12M	Lifetime	26.1M	NEC-2	0.09%	0.09%
2	Rank-50	12M	Lifetime	26.1M	Microsoft-5	0.06%	**0.06%**
3	Rank-50	12M	Recent	12M	NEC-2	0.25%	**0.08%**
4	Rank-50	12M	Recent	12M	Microsoft-5	0.21%	0.09%
5	Rank-1	12M	Lifetime	26.1M	NEC-2	0.14%	**0.12%**
6	Rank-1	12M	Lifetime	26.1M	Microsoft-5	0.25%	0.24%
7	Rank-1	12M	Recent	12M	NEC-2	0.31%	**0.13%**
8	Rank-1	12M	Recent	12M	Microsoft-5	0.52%	0.37%
9	Rank-50	640K	Lifetime	1.25M	NEC-2	0.08%	0.08%
10	Rank-50	640K	Lifetime	1.25M	Microsoft-5	0.04%	**0.04%**

Table 1: Rank-based accuracy floor 2018.

Error rates today are two orders of magnitude below what they were in 2010, a massive reduction that stems from wholesale replacement of the old algorithms with those based on (deep) convolutional neural networks (CNNs). This constitutes a revolution rather than the evolution that defined the period 2010-2013. The rapid innovations around CNN architectures and loss functions including, both proprietary and published in the academic literature[1], may yet produce further gains. Even without that possibility, the results imply that prospective end-users should establish whether installed algorithms pre-date the development of the prototypes evaluated here and inquire with suppliers on availability of the latest versions. The gains mean that searches that had previously failed to yield candidates may now do so, such that unsolved cases could be revisited.

Given this impressive achievement - close to perfect recognition - an advocate might claim that frontal face recognition is a solved problem, a statement that should be refuted with the following context and caveats:

- ▷ **Algorithm accuracy spectrum:** Many algorithms do not achieve the low error rates tabulated above, and while many of those may still be useful and valuable to end-users, only the most accurate excel on poor quality images and those collected long after the initial enrollment sample.
- ▷ **Versioning:** While results for up to seven algorithms from each developer are reported here, the intra-provider accuracy variations are usually smaller than the inter-provider variations. That said different versions give order of magnitude fewer misses. Some developers demonstrate speed-accuracy tradeoffs[2]. See Figs. 17, 18.

[1] For example, Resnets [11], Inception [23], very deep networks [18, 21] and spatial transformers.
[2] NEC-0 prepares templates much faster than NEC-2 but gives twenty times more misses. Dermalog-5 executes a template search much more quickly than Dermalog-6 but is also much less accurate.

- ▷ **Quality:** The low error rates here are attained using mostly excellent cooperative live-capture mugshot images collected with an attendant present. Recognition in other circumstances, particularly those without a dedicated photographic environment and human or automated quality control checks, will lead to declines in accuracy. This is documented here for poorer quality webcam images and unconstrained "wild" images.

- ▷ **Low similarity scores:** In thousands of cases the correct gallery image is returned at rank 1 but its similarity score is nevertheless low, below some operationally required score threshold. This does not matter when face recognition is used for "lead generation" in investigational applications because human reviewers are specifically required to review potentially long candidate lists and the threshold is effectively 0. In applications where search volumes are higher and labor is not available to review the results from searches, a higher threshold can be applied. This reduces the length of candidate lists and false positive identification rates at the expense of increased false negative miss rates. The tradeoff between the two error rates is reported extensively later.

- ▷ **Population size:** As the number of enrolled subjects grows, some mates are displaced from rank one, decreasing accuracy. As tabulated later for N up to 12 million, false negative rates generally rise slowly with population size.

- ▷ **Database integrity:** An operational error rate should be added to all false negative rates in this report reflecting the proportion of images in a real database that are un-matchable. Such anomalies arise from images that: do not contain a face; include multiple persons; cannot be decoded; are rotated by 90° or 180°; depict a face on clothing; and others introduced by a long tail of various clerical errors. While the mugshot trials in this report have been constructed to minimize such effects, they are a real problem in actual operations.

▷ **Threshold-based accuracy:** Recognition accuracy is very strongly dependent on the algorithm and, more generally, on the developer of the algorithm. False negative error rates in a particular scenario range from a few tenths of one percent to beyond fifty percent. This is tabulated exhaustively later: For example Table 22 shows accuracy across datasets. The inset figure here compares algorithms on mugshot searches in a consolidated gallery of 12 million subjects and 26.1 million photos. In positive or negative identification applications, a score threshold is set to limit the rate at which non-mate searches produce false positives. This has the consequence that some mated searches will report the mate below threshold, i.e. a miss, even if it is at rank 1. The utility of this is that many non-mated searches will usually not return any candidate identities at all. As the

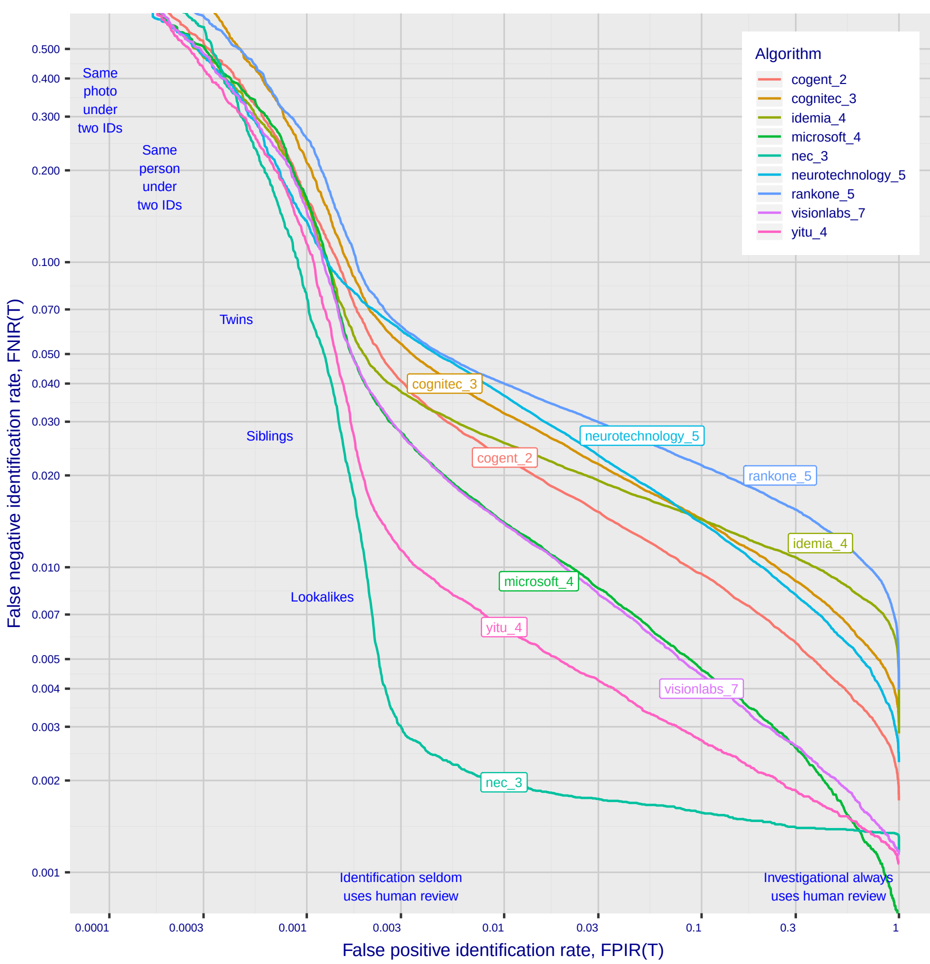

Figure 1: Miss rates across the false positive range

inset error-tradeoff characteristic
shows, investigational miss rates on the right side are very low but then rise steadily (in the center region) as threshold is increased to support "lights-out" applications, and ultimately rise quickly (left side) as discussed below. Thus, if we demand that just one in one thousand non-mate searches produce any false positives, the most accurate algorithm there (NEC-3) would fail on 7.9% of mated searches. Even though the graph shows results for the most accurate algorithms, all but two would fail to find the mate in more than 10% of mated searches. While the NEC algorithm produces a relatively flat error tradeoff until the threshold is raised to limit false positives to about 1 in 400 non-mated searches[3]

Thereafter, as the threshold is raised to further reduce false positives, miss rates rise rapidly. This means that low false positive identification rates are inaccesible with these algorithms, a result that does not apply for ten-finger identification algorithms. The rapid rise occurs because the lower mate scores are mixed with very high non-mate scores, the low scores from poor image quality and ageing, the high non-mates from the presence of lookalikes persons (doppelgangers), twins (discussed next) and, ultimately, the presence of a few unconsolidated subjects i.e. persons present under multiple IDs.

▷ **False positives from twins:** By enrolling 640 000 mugshots, adding photos of one twin, and then searching photos of those subjects and their twin the inset figure shows, for one typical algorithm, the similarity is generally greater when searching twins against themselves (A) than when searching twins against their sibling (B) but very often still above even stringent thresholds i.e. those corresponding to one in one thousand searches producing a false positive. Thus twins will very often produce a high-scoring non-match on a candidate list and a false alarm in an online identification system. The plot shows that some fraternal twins are correctly rejected at those thresholds - these are largely from different sex twins (at center). Figure 21 shows substantially similar behavior for all algorithms tested. In an investigative search, a twin would typically appear at rank 1, or rank 2 if their sibling happened to also be the gallery. Twins (and triplets etc.) constituted 3.3% of all live births [17] in recent years[4], and because that number is higher today than when the individuals in current adult databases were born, the false positives that arise from twins are now, and will increasingly be, an operational problem. Relative to the United States, twins are born with considerable regional variation. For example they are much less common in East Asia, and much more common in Sub-Saharan Africa [22]. The presence of twins in the mugshot database is inevitable given its size, around 12.3 million people. As this is not an insignificant sample of the domestic United States population, people with other familial ties will be present also. The data was collected over an extended period and because location information is not available, we are unable to estimate the proportion of the domestic population that is present in the dataset. However, if we assume twins are neither more or less disposed to arrest than the general population, we can estimate that hundreds of thousands of individuals in the dataset are twins. This will affect false positive rates because we randomly set aside 331 254 individuals for nonmate searches, and some proportion of those will be twins with siblings in the gallery.

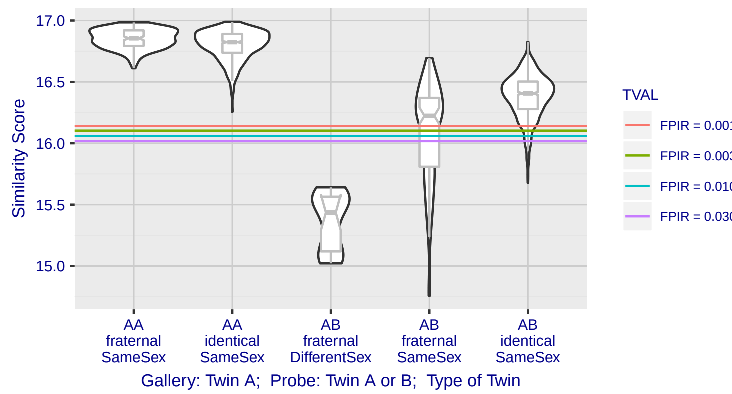

Figure 2: Intra- and inter-twin scores

[3] The gallery size here is 12 million people, 26.1 million images. Given 331 254 non-mated searches, an exhaustive implementation of one-too-many search would execute 8.6 trillion comparisons. At a false positive identification rate of 0.0025 the number of false positives is, to first order, 828 corresponding to single-comparison false match rate of 828 / 8.6 trillion = 9.6 10^{-11} i.e. about 1 in 10 billion. Strictly this FMRR computation meaningful only for algorithms that implement 1:N search using N 1:1 comparisons, which is not always the case.

[4] See the CDC's National Vital Statistics Report for 2017: https://www.cdc.gov/nchs/data/nvsr/nvsr67/nvsr67_08-508.pdf

▷ **False negatives from ageing:** A large source of error in long-run applications where subjects are not re-enrolled on a schedule is ageing. This is a function of the time elapsed between photographs. Change in facial appearance causes recognition similarity scores to decline such that over the longer term, accuracy will decline. All faces age and while this usually proceeds in a graceful and progressive manner, drug use can accelerate this [30]. Elective surgery may be effective in delaying it although this has not been formally quantified with face recognition. As ageing is essentially unavoidable, it can only be mitigated by scheduled re-capture, as in passport re-issuance. To quantify ageing effects, we used the more accurate algorithms to enroll the earliest image of 3.1 million adults and then search with 10.3 million newer photos taken up to 18 years after the the initial enrollment photo. In the inset table, accuracy is seen to degrade progressively with time, as mate scores decline and non-mates displace mates from rank 1 position. More accurate algorithms tend to be less sensitive to ageing. The more accurate algorithms give fewer errors after 18 years of ageing than middle tier algorithms give after four. Note also we do not quantify an ageing rate - more formal methods [2] borrowed from the longitudinal analysis literature have been published for doing so (given suitable repeated measures data). See Figures 62, 72 and 77.

Algorithm	Metric, FNIR@	(0,2]	(2,4]	(4,6]	(6,8]	(8,10]	(10,12]	(12,14]	(14,18]
nec-2	Rank = 1	0.3	0.4	0.4	0.4	0.4	0.5	0.6	0.4
microsoft-4	Rank = 1	0.3	0.5	0.6	0.7	0.9	1.0	1.3	1.6
yitu-4	Rank = 1	0.6	0.8	0.8	0.8	0.9	1.1	1.5	2.1
everai-3	Rank = 1	0.5	0.7	0.9	1.1	1.3	1.5	1.8	2.2
idemia-4	Rank = 1	1.1	1.5	1.9	2.3	2.8	3.1	3.7	5.1
cogent-3	Rank = 1	0.8	1.1	1.3	1.5	1.7	1.9	2.4	3.1
cognitec-2	Rank = 1	1.0	1.4	1.7	2.0	2.4	2.6	3.1	3.9
nec-2	FPIR = 0.001	0.7	0.9	1.1	1.3	1.5	1.7	2.1	2.7
microsoft-4	FPIR = 0.001	2.7	4.7	7.2	10.1	12.9	16.1	20.5	25.9
yitu-4	FPIR = 0.001	1.2	2.0	3.1	4.7	6.7	9.6	14.2	20.1
everai-3	FPIR = 0.001	3.5	6.2	9.3	12.9	16.2	19.6	24.1	29.2
idemia-4	FPIR = 0.001	3.7	5.9	8.3	11.0	13.4	15.8	19.1	24.8
cogent-3	FPIR = 0.001	5.8	9.7	14.2	19.2	23.8	28.4	34.4	42.1
cognitec-2	FPIR = 0.001	5.2	8.8	12.7	17.1	21.0	24.6	29.2	35.3

Table 2: Impact of ageing on accuracy.

▷ **Image quality matters:** Poor quality photographs undermine recognition, either because the imaging system is poor (lighting, camera, etc.) or because the subject mis-presents to the camera (head orientation, facial expression, occlusion, etc.). Imaging problems can be mitigated by design i.e. ensuring adherence to long-standing face image capture standards. Presentation problems, however, must be detected at capture time, either by the photographer, or by an automated system, and re-capture performed. The most accurate algorithms in FRVT are highly tolerant of image quality problems. This derives from the invariances afforded by CNN-based algorithms, and this is the fundamental reason why accuracy has improved since 2013. For example, the Microsoft algorithms are can match many profile-view images to frontal mugshots - see Figures 100 and 102. As the inset table shows, rank-1 false negative identification rates are much higher with wild images than webcams and, in turn, mugshots. Further, even with the most capable algorithms, comparison scores are lower with unconstrained images, so that when (high) thresholds are necessary to limit false positives, here to 1 in 100 searches, error rates are very high. Such figures should guide prospective users of face recognition to consider whether face recognition can meet a formal written accuracy requirement.

Algorithm	Metric, FNIR@	Wild	Mugshot	Webcam
cognitec-3	Rank = 1	5.1	0.9	2.5
everai-3	Rank = 1	3.8	0.5	1.9
idemia-5	Rank = 1	4.4	1.1	3.9
microsoft-5	Rank = 1	3.3	0.3	1.1
nec-3	Rank = 1	8.8	0.3	1.0
ntechlab-6	Rank = 1	3.8	0.6	1.7
visionlabs-5	Rank = 1	4.3	0.4	1.9
yitu-4	Rank = 1	4.4	0.4	0.8
cognitec-3	FPIR = 0.01	32.5	2.8	10.0
everai-3	FPIR = 0.01	35.7	1.8	6.0
idemia-5	FPIR = 0.01	34.0	2.8	10.2
microsoft-5	FPIR = 0.01	34.4	1.2	4.1
nec-3	FPIR = 0.01	38.0	0.4	1.3
ntechlab-6	FPIR = 0.01	38.1	2.1	5.9
visionlabs-5	FPIR = 0.01	34.4	2.2	8.7
yitu-4	FPIR = 0.01	30.6	0.7	1.7

Table 3: Impact of image quality on accuracy.

▷ **Accuracy in large populations:** This report documents identification accuracy in galleries containining up to 12 million people and 26.1 million images. False negative rates climb very slowly as population size increases. For the most accurate algorithm, NEC-2, when searching a database of size 640 000, about 0.26% of searches fail to produce the correct mate as its best hypothesized identity. In a database of 12 000 000 this rises to just 0.31%. This benign growth in miss rates is fundamentally the reason for the utility of face recognition in large scale one-to-many search applications. See Table 12 and Figure 22.

The reason for this is that as more identities are enrolled into an database, the possibility of a false positive increases due to lookalike faces that yield extreme values from the right tail of the non-mate score distribution. However, these scores are lower than most mate scores such that when an identification algorithm is configured with a threshold of zero (so human adjudication is always necessary), rank-one identification miss rates scale very favorably with population size, N, growing slowly, approximately as a power law, aN^b with $b \ll 1$. This dependency was first noted in 2010. Depending on the algorithm, the exponent b for mugshot searches is low, around 0.06 for the some of the more accurate algorithms with up to 12 million identities. See Table 12.

In any case, variations in accuracy with increasing population size are small relative to both ageing and algorithm choice. See Figure 20.

▷ **Utility of adjudicating long candidate lists:** In the regime where a system is configured with a threshold of zero, and where human adjudication is always necessary, the reviewer will find some mates quite far down candidate lists. This usually occurs because either the probe image or its corresponding enrolled mate image have poor quality, or large time-lapse. The accuracy benefits of traversing say 50 candidates versus just the first one is broadly a reduction in error by up to a factor of two. See Figure 30 and compare Tables 12 and 13.

However, accuracy from the leading algorithm is now so high - mates that in 2013 were placed at rank > 1, are now at rank 1 - such that reviewers can expect to review substantially fewer candidates. Note, however, for the proportion of searches where there is no mate, reviewers might still examine all candidates, fruitlessly. This report does not address the issue of human error in adjudicating candidates produced in one-to-many searches.

▷ **Utility of enrolling multiple images per subject:** We run three kinds of enrollment: First, by enrolling just the most recent image; second by creating a single template from a person's full lifetime history of images; and third by enrolling multiple images of a person separately, as though under different identities. The overall effect is that the enrollment of multiple images yields as much as a factor of two lower miss rates. This occurs due to higher information content and because the most recent image may sometimes be of poorer quality than historical images. See Table 12.

Gains depend on the number of available images: FNIR drops steadily. Some algorithms reduce FPIR or maintain it - the desirable behaviors - but others give higher false positive rates. See Figures leading up to Figure 87.

▷ **Reduced template sizes:** There has been a trend toward reduced template sizes, i.e. a smaller feature representation of an image. In 2014, the most accurate algorithm used a template of size 2.5KB; the figure in 2018 is around 1600 bytes. Close competitors produce templates of size 256, 364, 512, and about 2KB bytes. In 2014, the leading competitors had templates of size 4KB to 8KB. Some algorithms, when enrolling more than one image of a person, produce a template whose size is independent of the number of images given to the algorithm. This can be achieved by selecting a "best" image, or by integrating (fusing) information from the images. See Table 16.

▷ **Template generation times:** Template generation times, as measured on a single circa-2016 server processor core [5], vary from below 20 milliseconds up to nearly 1 second. This wide variation across developers may be relevant to end-users who have high-volume workflows. There has not been a wide downward trend since 2014. Note that speed may be expedited over the figure reported here by exploiting new vector instructions on recent chips. Note that GPUs were not used and, while indispensable for training CNNs, are not necessary for feeding an image forward through a network. See Table 16.

▷ **Search duration and scalability:** Template search times, as measured on circa-2016 Intel server processor cores,

[5] Intel Xeon CPU E5-2630 v4 running at 2.20GHz.

vary massively across the industry. For a database of size 1 million subjects, and the more accurate implementations, durations range from below 1 to 500 milliseconds, with other less accurate algorithms going much slower still. Several algorithms exhibit sublinear search time i.e. the duration does not double with a doubling of the enrolled population size, N. This was noted also in 2014. This has improved in 2018, however, such that close-to-logarithmic growth is evident for several developers' algorithms and extremely fast search. The consequence of this is that as N increases even the fastest linear algorithm (NEC-3) will quickly become much slower than the strongly sublinear algorithms. For the Dermalog-5 algorithm, search of a template against a database of N = 12 million images takes 850 microseconds on a single core of a contemporary CPU. That number is faster than any other algorithm even with the smallest gallery we tested (N = 640 000). See Table 6 and Figure 111.

▷ **Accuracy gains June - October 2018** NIST Interagency Report 8238 documented massive gains from 2013 to 2018. This report shows most developers achieved gains over the four month interval between June and October 2018. For a set of 12 million subjects enrolled with their most recent mugshot image, the inset table shows, for selected algorithms, the proportion of searches where mates are not returned against the given criteria (column 2). The result is that substantial reductions in false negatives - by a factor of two or more - were realized by algorithms submitted by Cogent, Cognitec, Dermalog, Hikvision, Innovatrics, NEC, Rank One, Shaman, Tiger-IT, and Vigilant Solutions. In particular, in this same time period one developer, NEC, which had produced broadly the most accurate algorithms in 2010 and 2013, submitted algorithms that are substantially more accurate than their June 2018 versions, and on many measures are now the most accurate. A number of other developers produced slightly less accurate implementations.

Application	Metric	Algorithm		FNIR
Mode: Mugshot	Miss rate	Date	Name	
Investigation	at Rank=1	2018-JUN	NEC-0	3.20%
Investigation	at Rank=1	2018-OCT	NEC-2	0.31%
Investigation	at Rank=1	2018-JUN	Microsoft-4	0.45%
Investigation	at Rank=1	2018-OCT	Microsoft-5	0.52%
Investigation	at Rank=1	2018-JUN	Yitu-2	0.55%
Investigation	at Rank=1	2018-OCT	Yitu-5	0.55%
Identification	at FPIR=0.001	2018-JUN	NEC-0	20.0%
Identification	at FPIR=0.001	2018-OCT	NEC-3	5.8%
Identification	at FPIR=0.001	2018-JUN	Microsoft-4	15.8%
Identification	at FPIR=0.001	2018-OCT	Microsoft-6	15.6%
Identification	at FPIR=0.001	2018-JUN	Yitu-2	12.4%
Identification	at FPIR=0.001	2018-OCT	Yitu-5	11.1%

Table 4: Accuracy gains since June - October 2018

See Tables 16 and 19, and Figure 19.

▷ **Non-technical considerations:** Recognition accuracy is likely the most important technical indicator for an algorithm. But even among the more accurate developers accuracy, template size, and resource consumption vary widely. This, incidentally, implies that technological diversity remains, that there is no consensus on approach and that algorithms are not commoditized. But beyond the performance statements in this report, face recognition outcomes in complete systems will be influenced by things like code and model size, software maturity, extensibility, reliability, ease of integration and maintenance, cost, availability of monitoring tools, and support for human review of true and false matches using, for example, capable graphical user interfaces.

▷ **Conclusions:** As with other biometrics, accuracy of facial recognition implementations varies greatly across the industry. Absent other performance or economic parameters, users should prefer the most accurate algorithm. Note that accuracy, and algorithm rankings, vary somewhat with the kinds of images used and the mode of operation: investigation with zero threshold; or identification with high threshold.

▷ **Supplementary Data:** This document is accompanied by a supplement that includes a three page report for each of the algorithms evaluated. Each report includes various performance plots pertinent to the particular algorithm under test. The supplement, which currently runs to more than 600 pages, is available from the same webpage as this report.

Release Notes

FRVT Activities: NIST restarted FRVT's one-to-many track in February 2018, inviting participants to send up to seven prototype algorithms. Since February 2017, NIST has been evaluating one-to-one verification algorithms on an ongoing basis. This allows developers to submit updated algorithms to NIST at any time but no more frequently than four calendar months. This more closely aligns development and evaluation schedules. Results are posted to the web within a few weeks of submission. Details and full report are linked from the Ongoing FRVT site.

FRVT Reports: The results of the FRVT appear in the series NIST Interagency Reports tabulated below. The reports were developed separately and released on different schedules. In prior years NIST has mostly reported FRVT results as a single report; this had the disadvantage that results from completed sub-studies were not published until all other studies were complete.

Date	Link	Title	No.
2014-03-20	PDF	FRVT Performance of Automated Age Estimation Algorithms	7995
2015-04-20	PDF	Face Recognition Vendor Test (FRVT) Performance of Automated Gender Classification Algorithms	8052
2014-05-21	PDF	FRVT Performance of face identification algorithms	8009
2017-03-07	PDF	Face In Video Evaluation (FIVE) Face Recognition of Non-Cooperative Subjects	8173
2017-11-23	PDF	The 2017 IARPA Face Recognition Prize Challenge (FRPC)	8197
2018-04-13	WWW	Ongoing Face Recognition Vendor Test (FRVT)	Draft

Details appear on pages linked from `https://www.nist.gov/programs-projects/face-projects`.

Appendices: This report is accompanied by appendices which present exhaustive results on a per-algorithm basis. These are machine-generated and are included because the authors believe that visualization of such data is broadly informative and vital to understanding the context of the report.

Typesetting: Virtually all of the tabulated content in this report was produced automatically. This involved the use of scripting tools to generate directly type-settable LaTeX content. This improves timeliness, flexibility, maintainability, and reduces transcription errors.

Graphics: Many of the Figures in this report were produced using the ggplot2 package running under R, the capabilities of which extend beyond those evident in this document.

Contents

Acknowledgments 1

Disclaimer 1

Executive Summary 2

Scope and Context 3

Technical Summary 6

Release Notes 12

1 Introduction 14

2 Evaluation datasets 14

3 Performance metrics 20

4 Results 36

Appendices 65

A Accuracy on large-population FRVT 2018 mugshots 65

B Effect of time-lapse: Accuracy after face ageing 110

C Effect of enrolling multiple images 138

D Accuracy with poor quality webcam images 145

E Accuracy for profile-view to frontal recognition 155

F Accuracy when identifying wild images 159

G Search duration 170

H Gallery Insertion Timing 177

1 Introduction

One-to-many identification represents the largest market for face recognition technology. Algorithms are used across the world in a diverse range of biometric applications: detection of duplicates in databases, detection of fraudulent applications for credentials such as passports and driving licenses, token-less access control, surveillance, social media tagging, lookalike discovery, criminal investigation, and forensic clustering.

This report contains a breadth of performance measurements relevant to many applications. Performance here refers to accuracy and resource consumption. In most applications, the core accuracy of a facial recognition algorithm is the most important performance variable. Resource consumption will be important also as it drives the amount of hardware, power, and cooling necessary to accommodate high volume workflows. Algorithms consume processing time, they require computer memory, and their static template data requires storage space. This report documents these variables.

1.1 Open-set searches

FRVT tested open-set identification algorithms. Real-world applications are almost always "open-set", meaning that some searches have an enrolled mate, but some do not. For example, some subjects have truly not been issued a visa or drivers license before; some law enforcement searches are from first-time arrestees[6]. In an "open-set" application, algorithms make no prior assumption about whether or not to return a high-scoring result, and for a mated search, the ideal behaviour is that the search produces the correct mate at high score and first rank. For a non-mate search, the ideal behavior is that the search produces zero high-scoring candidates.

Too many academic benchmarks execute only closed-set searches. The proportion of mates found in the rank one position is the default accuracy metric. This hit rate metric ignores the score with which a mate is found; weak hits count as much as strong hits. This ignores the real-world imperative that in many applications it is necessary to elevate a threshold to reduce the number of false positives.

2 Evaluation datasets

This report documents accuracy for four kinds of images - mugshots, webcam, profiles and wild - as described in the following sections.

2.1 Mugshot images

The main mugshot dataset used is referred to as the FRVT 2018 set. This set was collected over the period 2002 to 2017 in routine United States law enforcement operations. This set has been extracted from a larger operational parent set by excluding non-face images, and setting aside webcam and profile-view images, for use in separate tests.

NIST Interagency Report 8238 includes a comparison of this set of mugshots with the smaller and easier sets of mugshots used in tests run in 2010 and 2014.

[6] Operationally closed-set applications are rare because it is usually not the case that all searches have an enrolled mate. One counter-example, however, is a cruise ship in which all passengers are enrolled and all searches should produce exactly one identity. Another example is forensic identification of dental records from an aircraft crash.

▷ **Mugshots**: Mugshots comprise about 86% of the database. They have reasonable compliance with the ANSI/NIST ITL1-2011 Type 10 standard's subject acquisition profiles levels 10-20 for frontal images [28]. The most common departure from the standard's requirements is the presence of mild pose variations around frontal - the images of Figure 3 are typical. The images vary in size, with many being 480x600 pixels with JPEG compression applied to produce filesizes of between 18 and 36KB with many images outside this range, implying that about 0.5 bits are being encoded per pixel.

▷ **Profile images**: Profile-view images have been collected in law enforcement for more than 100 years, as human capability is improved with orthogonal information. The profile images used in this report were collected during the same session as the frontal mugshot photograph, in the same standardized photographic setup. These would not therefore be used with automated face recognition. A small subset, 200 000 images, were set aside for testing.

▷ **Webcam images**: The remaining 14% of the images were collected using an inexpensive webcam attached to a flexible operator-directed mount. These images are all of size 240x240 pixels, that are in considerable violation of most quality-related clauses of all face recognition standards. As evident in the figure, the most common defects are non-frontal pose (associated with the rotational degrees of freedom of the camera mount), low contrast (due to varying and intense background lights), and poor spatial resolution (due to inexpensive camera optics) - see examples in Fig 4. The images are overly JPEG compressed, to between 4 and 7KB, implying that only 0.5 to 1 bits are being encoded per color pixel.

Example images are shown in Figures 3, 4 and 5 These are drawn from NIST Special Database 32 which may be downloaded here.

These images were partitioned in galleries and probesets for the various experiment listed in Table 5.

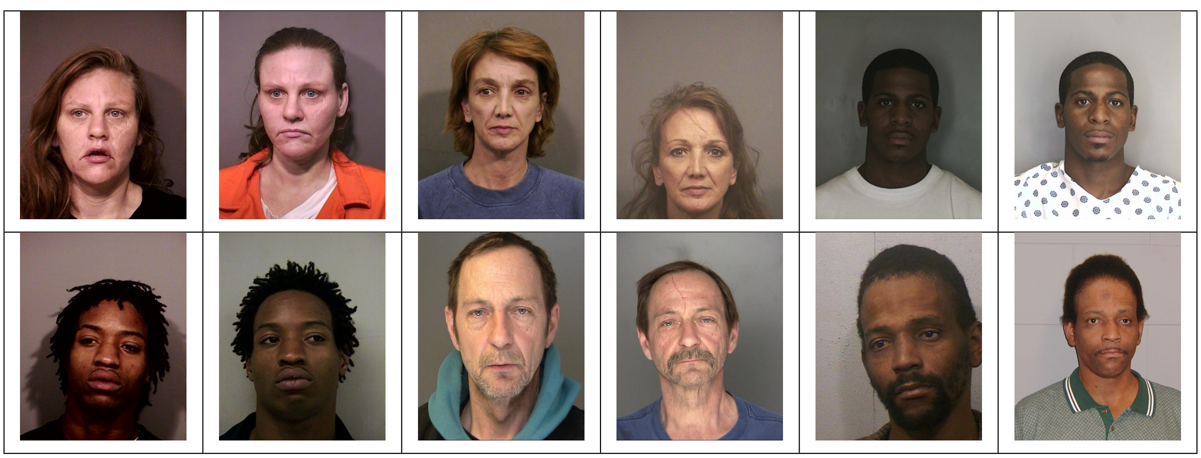

Figure 3: Six mated mugshot pairs representative of the FRVT-2014 (LEO) and FRVT-2018 datasets. The images are collected live, i.e. not scanned from paper. Image source: NIST Special Database 32

Figure 5: **[Profile views]** *The three images are a frontal enrollment, subsequent frontal probe, and same-session ninety degree profile view. While collection of both frontal and profile views has been typical in law enforcement for more than a century, the recognition of profile to frontal views has essentially been impossible. However, reasonbly high accuracy results is now possible - see section E.*

Figure 4: Twelve webcam images representative of probes against the FRVT-2018 mugshot gallery. The first eight images are four mated pairs. Such images present challenges to recognition including pose, non-uniform illumination, low contrast, compression, cropping, and low spatial sampling rate. Image source: NIST Special Database 32

2.2 Unconstrained "wild" images

In addition to portrait-styled mugshots, algorithms were also evaluated on a "wild" dataset composed of non-cooperative and unconstrained photojournalism and amateur photography imagery. The images are closely cropped from the parent images as shown in Figure 6. A portion of the images are collected by professional photographers and as such are captured, and selected, to not exhibit exposure and focus problems. Some of the photos were downloaded from websites with substantial amateur photographer imagery, which may contain images that do exhibit exposure and focus problems. Resolution varies widely as these images were downloaded from the internet with varying resampling and compression practices. The primary difficulties for face recognition is unconstrained yaw and pitch pose variation, with some images extending to profile view. Additionally faces can be occluded, including by hair and hands.

The images are cropped prior to passing them to the algorithm. The cropping is done per human-annotated rectangular bounding boxes. The algorithm must further localize the face and extract features. In many cases, there were multiple images of the subject provided to the algorithm, and the output was a single template representation of the subject.

$N_P = 332\,574$ subjects were searched against two galleries, where the number of enrolled subjects in each gallery were $N_{G1} = 1\,106\,777$ and $N_{G2} = 1\,107\,778$. Both gallery and search images were composed of unconstrained wild imagery.

Figure 6: Examples of "in the wild" stills. The top row gives the full original images; the second row gives the manually specified face region that is cropped and passed to the algorithms. The source images in this figure are attributed to, from left, Rita Molnr, Eva Rinaldi, and Gage Skidmore under the [cc-by-sa-2.5], [cc-by-sa-2.0], [cc-by-sa-3.0] creative commons licenses respectively.

2.3 Enrollment strategies

Many operational applications include collection and enrollment of biometric data from subjects on more than one occasion. This might be done on a regular basis, as might occur in credential (re-)issuance, or irregularly, as might happen in a criminal recidivist situation [4]. The number of images per person will depend on the application area. In civil identity credentialing (e.g. passports, driver's licenses), the images will be acquired approximately uniformly over time (e.g. ten years for a passport). While the distribution of dates for such images of a person might be assumed uniform, a number of factors might undermine this assumption[7]. In criminal applications, the number of images would depend on the number of arrests. The distribution of dates for arrest records for a person (i.e. the recidivism distribution) has been modeled using the exponential distribution but is recognized to be more complicated[8].

In any case, the 2010 NIST evaluation of face recognition showed that considerable accuracy benefits accrue with retention and use of *all* historical images [6].

To this end, the FRVT API document provides $K \geq 1$ images of an individual to the enrollment software. The software is tasked with producing a single proprietary undocumented "black-box" template[9] from the K images. This affords the algorithm an ability to generate a *model* of the individual, rather than to simply extract features from each image on a sequential basis.

As depicted in Figure 7, the i-th individual in the FRVT 2018 dataset has K_i images. These are labelled as x_k for $k = 1 \ldots K_i$ in chronological order of capture date. To measure the utility of having multiple enrollment images, this report evaluates three kinds of enrollment:

[7] For example, a person might skip applying for a passport for one cycle, letting it expire. In addition, a person might submit identical images (from the same photography session) to consecutive passport applications at five year intervals.
[8] A number of distributions have been considered to model recidivism, see for example [3].
[9] There are no formal face template standards. Template standards only exist for fingerprint minutiae - see ISO/IEC 19794-2:2011.

Image				
Encounter	1	...	$K_i - 1$	K_i
Capture Time	T_1	...	$T_{K_i - 1}$	T_{K_i}
Role RECENT	Not used	Not used	Enrolled	Search
Role LIFETIME	Enrolled	Enrolled	Enrolled	Search

Figure 7: Depiction of the "recent" and "lifetime" enrollment types. Image source: NIST Special Database 32

- **Recent**: Only the second most recent image, x_{K_i-1} is enrolled. This strategy of enrollment mimics the operational policy of retaining the imagery from the most recent encounter. This might be done operationally to ameliorate the effects of face ageing. Obviously retaining only the most recent image should only be done if the identity of the person is trusted to be correct. For example, in an access control situation retention of the most recent successful *authentication* image would be hazardous if it could be a false positive.

- **Lifetime-consolidated**: All but the most recent image are enrolled, $x_1 \dots x_{K_i-1}$. This subject-centric strategy might be adopted if quality variations exist where an older image might be more suitable for matching, despite the ageing effect.

- **Lifetime-unconsolidated**: Again all but the most recent image are enrolled $x_1 \dots x_{K_i-1}$ but now separately, with different identifiers, such that the algorithm is not aware that the images are from the same face. This kind of event- or encounter-centric enrollment is very common when operational constraints preclude reliable consolidation of the historical encounters into a single identity. This aspect also prevents the recognition algorithm from a) building a holistic model of identity (as is common in speaker recognition systems) and b) implementing fusion, for example template-level fusion of feature vectors, or post-search score-level fusion. The result is that searches will typically yield more than one image of a person in the top ranks. This has consequences for appropriate metrics, as detailed in section 3.2.1

  NIST first evaluated this kind of enrollment in mid 2018, and the results tables include some comparison of accuracy available from all three enrollment styles.

In all cases, the most recent image, x_{K_i}, is reserved as the search image. For the 1.6 million subject enrollment partition of the FRVT 2018 data, $1 \leq K_i \leq 33$ with $K_i = 1$ in 80.1% of the individuals, $K_i = 2$ in 13.4%, $K_i = 3$ in 3.7%, $K_i = 4$ in 1.4%, $K_i = 5$ in 0.6%, $K_i = 6$ in 0.3%, and $K_i > 6$ is 0.2% for everyone else. This distribution is substantially dependent on United States recidivism rates.

We did not evaluate the case of retaining only the highest quality image, since automated quality assessment is out of scope for this report. We do not anticipate that such strategies will prove beneficial when the quality assessment apparatus is imperfect and unvalidated.

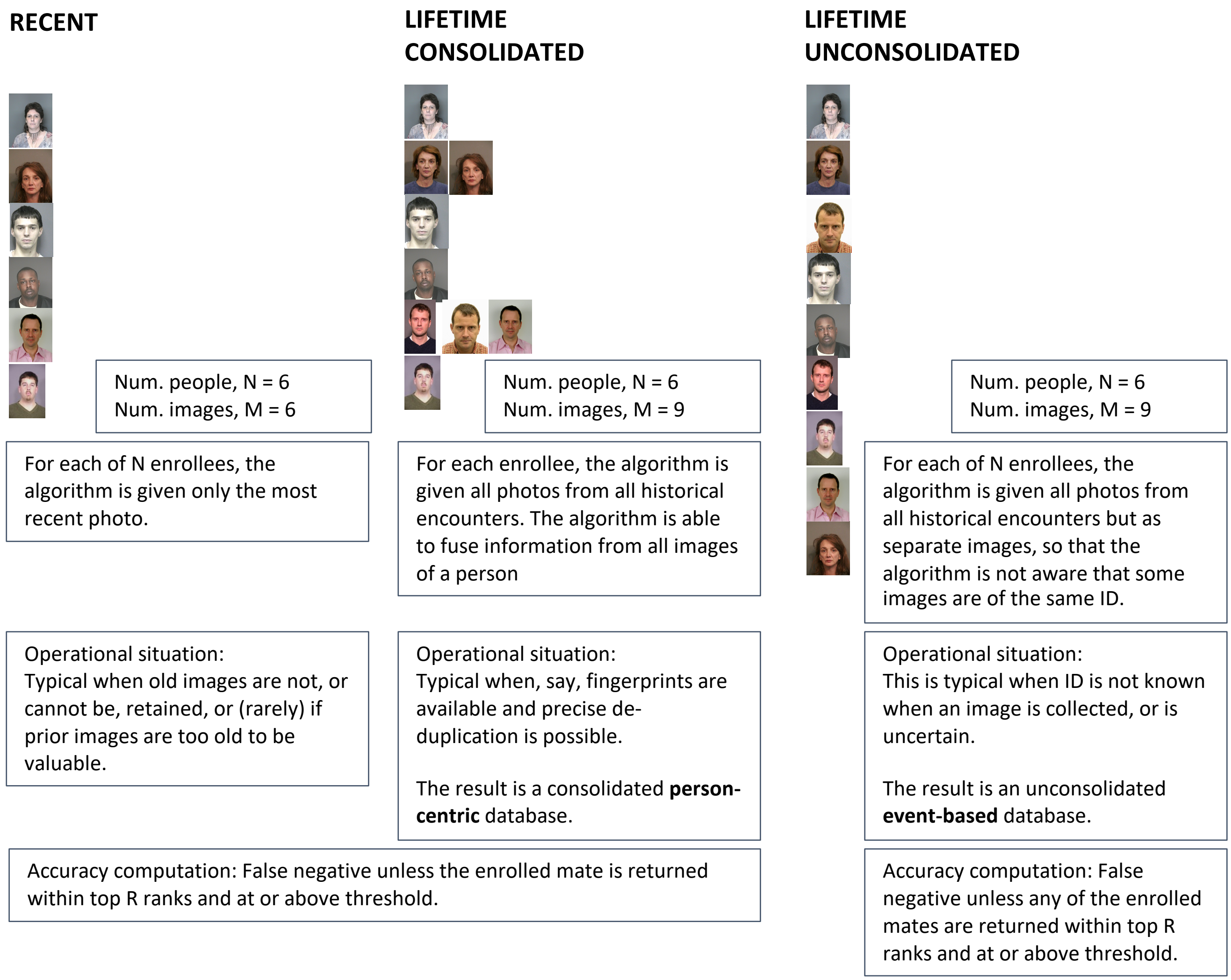

Figure 8: **Enrollment strategies**. *The figure shows the three kinds of enrollment databases examined in this report. Image source: NIST Special Database 32*

	ENROLLMENT				SEARCH			
	TYPE SEE	POPULATION			MATE		NON-MATE	
	SECTION 2.3	FILTER	N-SUBJECTS	N-IMAGES	N-SUBJECTS	N-IMAGES	N-SUBJECTS	N-IMAGES
Mugshot trials from enrollment of single images								
1	RECENT	NATURAL	640 000	640 000	154 549	154 549	331 254	331 254
2	RECENT	NATURAL	1 600 000	1 600 000				
3	RECENT	NATURAL	3 000 000	3 000 000				
4	RECENT	NATURAL	6 000 000	6 000 000				
5	RECENT	NATURAL	12 000 000	12 000 000				
Mugshot trials from enrollment of lifetime images								
6	CONSOL	NATURAL	640 000	1 247 331				
7	CONSOL	NATURAL	1 600 000	3 351 206				
8	CONSOL	NATURAL	3 000 000	6 417 057				
9	CONSOL	NATURAL	6 000 000	12 976 185				
10	CONSOL	NATURAL	12 000 000	26 107 917				
11	UN-CONSOL	NATURAL	640 000	1 247 331				
12	UN-CONSOL	NATURAL	1 600 000	3 351 206				
Cross-domain								
13	MUGSHOTS AS ON ROW 2				82 106 WEBCAM	82 106 WEBCAM	331 254 WEBCAM	331 254 WEBCAM
Cross-view								
14	MUGSHOTS AS ON ROW 2				100 000 PROFILE	100 000 PROFILE	100 000 PROFILE	100 000 PROFILE
Ageing								
17	OLDEST	NATURAL	3 068 801	3 068 801	2 853 221	10 951 064	0	0

Table 5: ***Enrollment and search sets****. Each row summarizes one identification trial. Unless stated otherwise, all entries refer to mugshot images. The term "natural" means that subjects were selected without heed to demographics, i.e. in the distribution native to this dataset. The probe images were collected in a different calendar year to the enrollment image. Missing values in rows 2-12 are the same as in row 1.*

3 Performance metrics

This section gives specific definitions for accuracy and timing metrics. Tests of open-set biometric algorithms must quantify frequency of two error conditions:

- ▷ **False positives**: Type I errors occur when search data from a person who has never been seen before is incorrectly associated with one or more enrollees' data.
- ▷ **Misses**: Type II errors arise when a search of an enrolled person's biometric does not return the correct identity.

Many practitioners prefer to talk about "hit rates" instead of "miss rates" - the first is simply one minus the other as detailed below. Sections 3.1 and 3.2 define metrics for the Type I and Type II performance variables.

Additionally, because recognition algorithms sometimes fail to produce a template from an image, or fail to execute a one-to-many search, the occurrence of such events must be recorded. Further because algorithms might elect to not produce a template from, for example, a poor quality image, these failure rates must be combined with the recognition error rates to support algorithm comparison. This is addressed in section 3.5.

Finally, section 3.7 discusses measurement of computation duration, and section 3.8 addresses the uncertainty associated with various measurements. Template size measurement is included with the results.

3.1 Quantifying false positives

It is typical for a search to be conducted into an enrolled population of N identities, and for the algorithm to be configured to return the closest L candidate identities. These candidates are ranked by their score, in descending order, with all scores required to be greater than or equal to zero. A human analyst might examine either all L candidates, or just the top $R \leq L$ identities, or only those with score greater than threshold, T. The workload associated with such examination is discussed later, in 3.6.

False alarm performance is quantified in two related ways. These express how many searches produces false positives, and then, how many false positives are produced in a search.

False positive identification rate: The first quantity, FPIR, is the proportion of non-mate searches that produce an adverse outcome:

$$\text{FPIR}(N,T) = \frac{\text{Num. non-mate searches where one or more enrolled candidates are returned with score at or above threshold}}{\text{Num. non-mate searches attempted.}} \tag{1}$$

Under this definition, FPIR can be computed from the highest non-mate candidate produced in a search - it is not necessary to consider candidates at rank 2 and above. FPIR is the primary measure of Type I errors in this report.

Selectivity: However, note that in any given search, several non-mate may be returned above threshold. In order to quantify such events, a second quantity, selectivity (SEL), is defined as the *number* of non-mates returned on a candidate list, averaged over all searches.

$$\text{SEL}(N,T) = \frac{\text{Num. non-mate enrolled candidates returned with score at or above threshold}}{\text{Num. non-mate searches attempted.}} \tag{2}$$

where $0 \leq$ SEL(N, T) $\leq$L. Both of these metrics are useful operationally. FPIR is useful for targeting how often an adverse false positive outcome can occur, while SEL as a number is related to workload associated with adjudicating candidate lists. The relationship between the two quantities is complicated - it depends on whether an algorithm concentrates the false alarms in the results of a few searches or whether it disburses them across many. This was detailed in FRVT 2014, NISTIR 8009. It has not yet been detailed in FRVT 2018.

3.2 Quantifying hits and misses

If L candidates are returned in a search, a shorter candidate list can be prepared by taking the top $R \leq L$ candidates for which the score is above some threshold, $T \geq 0$. This reduction of the candidate list is done because thresholds may be applied, and only short lists might be reviewed (according to policy or labor availability, for example). It is useful then to state accuracy in terms of R and T, so we define a "miss rate" with the general name **false negative identification rate** (FNIR), as follows:

$$\text{FNIR}(N,R,T) = \frac{\text{Num. mate searches with enrolled mate found outside top R ranks or score below threshold}}{\text{Num. mate searches attempted.}} \tag{3}$$

This formulation is simple for evaluation in that it does not distinguish between causes of misses. Thus a mate that is not reported on a candidate list is treated the same as a miss arising from face finding failure, algorithm intolerance of poor quality, or software crashes. Thus if the algorithm fails to produce a candidate list, either because the search failed, or because a search template was not made, the result is regarded as a miss, adding to FNIR.

Hit rates, and true positive identification rates: While FNIR states the "miss rate" as how often the correct candidate is either not above threshold or not at good rank, many communities prefer to talk of "hit rates". This is simply the **true positive identification rate**(TPIR) which is the complement of FNIR giving a positive statement of how often mated searches are successful:

$$\text{TPIR}(N, R, T) = 1 - \text{FNIR}(N, R, T) \quad (4)$$

This report does not report true positive "hit" rates, preferring false negative miss rates for two reasons. First, costs rise linearly with error rates. For example, if we double FNIR in an access control system, then we double user inconvenience and delay. If we express that as decrease of TPIR from, say 98.5% to 97%, then we mentally have to invert the scale to see a doubling in costs. More subtly, readers don't perceive differences in numbers near 100% well, becoming inured to the "high nineties" effect where numbers close to 100 are perceived indifferently.

Reliability is a corresponding term, typically being identical to TPIR, and often cited in automated (fingerprint) identification system (AFIS) evaluations.

An important special case is the **cumulative match characteristic**(CMC) which summarizes accuracy of mated-searches only. It ignores similarity scores by relaxing the threshold requirement, and just reports the fraction of mated searches returning the mate at rank R or better.

$$\text{CMC}(N, R) = 1 - \text{FNIR}(N, R, 0) \quad (5)$$

We primarily cite the complement of this quantity, FNIR$(N, R, 0)$, the fraction of mates *not* in the top R ranks.

The **rank one hit rate** is the fraction of mated searches yielding the correct candidate at best rank, i.e. CMC(N, 1). While this quantity is the most common summary indicator of an algorithm's efficacy, it is not dependent on similarity scores, so it does not distinguish between strong (high scoring) and weak hits. It also ignores that an adjudicating reviewer is often willing to look at many candidates.

3.2.1 False negative rates for unconsolidated galleries

As detailed in section 2.3 a common type of gallery, here referred to as the lifetime unconsolidate type, is populated with all images of an individual without any association between them. That is, the gallery construction algorithm is not provided with any ID labels that would support processing of a person's images jointly. This constrasts with the lifetime consolidate type where an algorithm may explicitly fuse features from multiple images of a person, or select a best image. In such cases, where the number of enrolled images is a random variable, we define two false negative rates as follows.

The first demands that the algorithm place any of the K_i mates in the top $R \geq 1$ ranks. The proportion of searches for which this does not occur forms a false negative identification rate:

$$\text{FNIR}_{\text{any}}(N, R, T) = 1 - \frac{\text{Num. mate searches where any enrolled mate is found in the top R ranks and at-or-above threshold}}{\text{Num. mate searches attempted.}} \quad (6)$$

The second demands that the algorithm place all K_i mates in the top $R \geq K_i$ ranks. The proportion of searches for which this does not occur forms a false negative identification rate:

$$\text{FNIR}_{\text{all}}(N, R, T) = 1 - \frac{\text{Num. mate searches where all enrolled mates are found in the top R ranks and at-or-above threshold}}{\text{Num. mate searches attempted.}} \quad (7)$$

Placing all mates in the top ranks is a more difficult task than correctly retrieving any image, so it holds that: $\text{FNIR}_{\text{all}} \geq \text{FNIR}_{\text{any}}$. This is evident in the results presented for November 2018 algorithms in Tables starting at 25.

The information retrieval community might prefer to compute and plot *precision* and *recall*; this is a valid approach, but we advance the two metrics above because they relate to our normal definition of consolidated FNIR, and they cover the two extreme use-cases of wanting any hit vs. all hits.

3.3 DET interpretation

In biometrics, a false negative occurs when an algorithm fails to match two samples of one person a Type II error. Correspondingly, a false positive occurs when samples from two persons are improperly associated a Type I error.

Matches are declared by a biometric system when the native comparison score from the recognition algorithm meets some threshold. Comparison scores can be either similarity scores, in which case higher values indicate that the samples are more likely to come from the same person, or dissimilarity scores, in which case higher values indicate different people. Similarity scores are traditionally computed by fingerprint and face recognition algorithms, while dissimilarities are used in iris recognition. In some cases, the dissimilarity score is a distance possessing metric properties. In any case, scores can be either mate scores, coming from a comparison of one persons samples, or nonmate scores, coming from comparison of different persons samples.

The words ”genuine” or ”authentic” are synonyms for mate, and the word ”impostor” is used as a synonym for nonmate. The words ”mate” and ”nonmate” are traditionally used in identification applications (such as law enforcement search, or background checks) while genuine and impostor are used in verification applications (such as access control).

An error tradeoff characteristic represents the tradeoff between Type II and Type I classification errors. For identification this plots false negative vs. false positive identification rates i.e. FNIR vs. FPIR parametrically with T. Such plots are often called detection error tradeoff (DET) characteristics or receiver operating characteristic (ROC). These serve the same function $-$ to show error tradeoff $-$ but differ, for example, in plotting the complement of an error rate (e.g. TPIR = 1 $-$ FNIR) and in transforming the axes, most commonly using logarithms, to show multiple decades of FPIR. More rarely, the function might be the inverse of the Gaussian cumulative distribution function.

The slides of Figures 9 through 15 discuss presentation and interpretation of DETs used in this document for reporting face identification accuracy. Further detail is provided in formal biometrics testing standards, see the various parts of ISO/IEC 19795 Biometrics Testing and Reporting. More terms, including and beyond those to do with accuracy, appear in ISO/IEC 2382-37 Information technology – Vocabulary – Part 37: Harmonized biometric vocabulary.

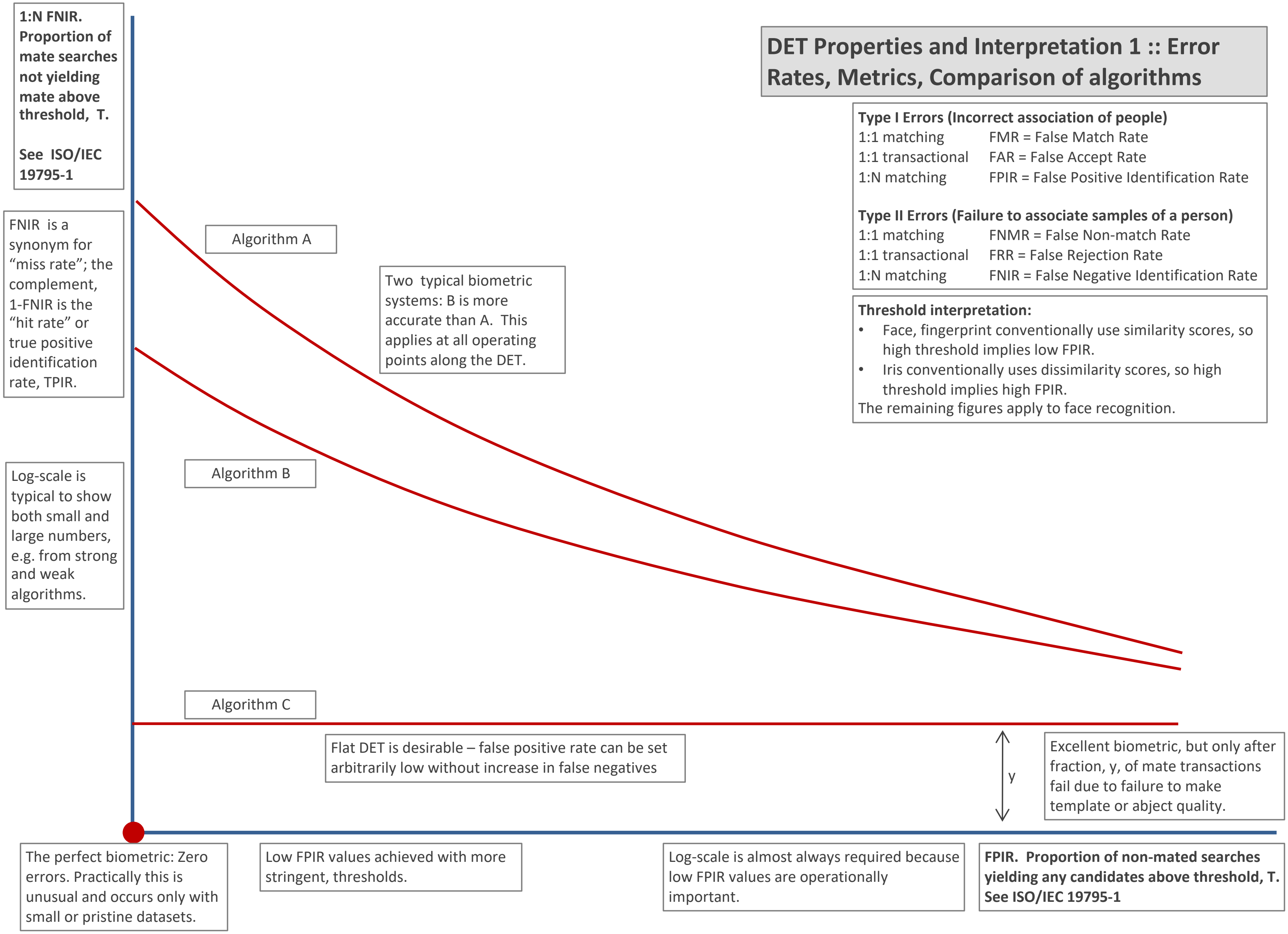

Figure 9: **DET as the primary performance reporting mechanism**.

2019/09/11 16:09:13

FNIR(N, R, T) = False neg. identification rate
FPIR(N, T) = False pos. identification rate
N = Num. enrolled subjects
R = Num. candidates examined
T = Threshold
T = 0 → Investigation
T > 0 → Identification

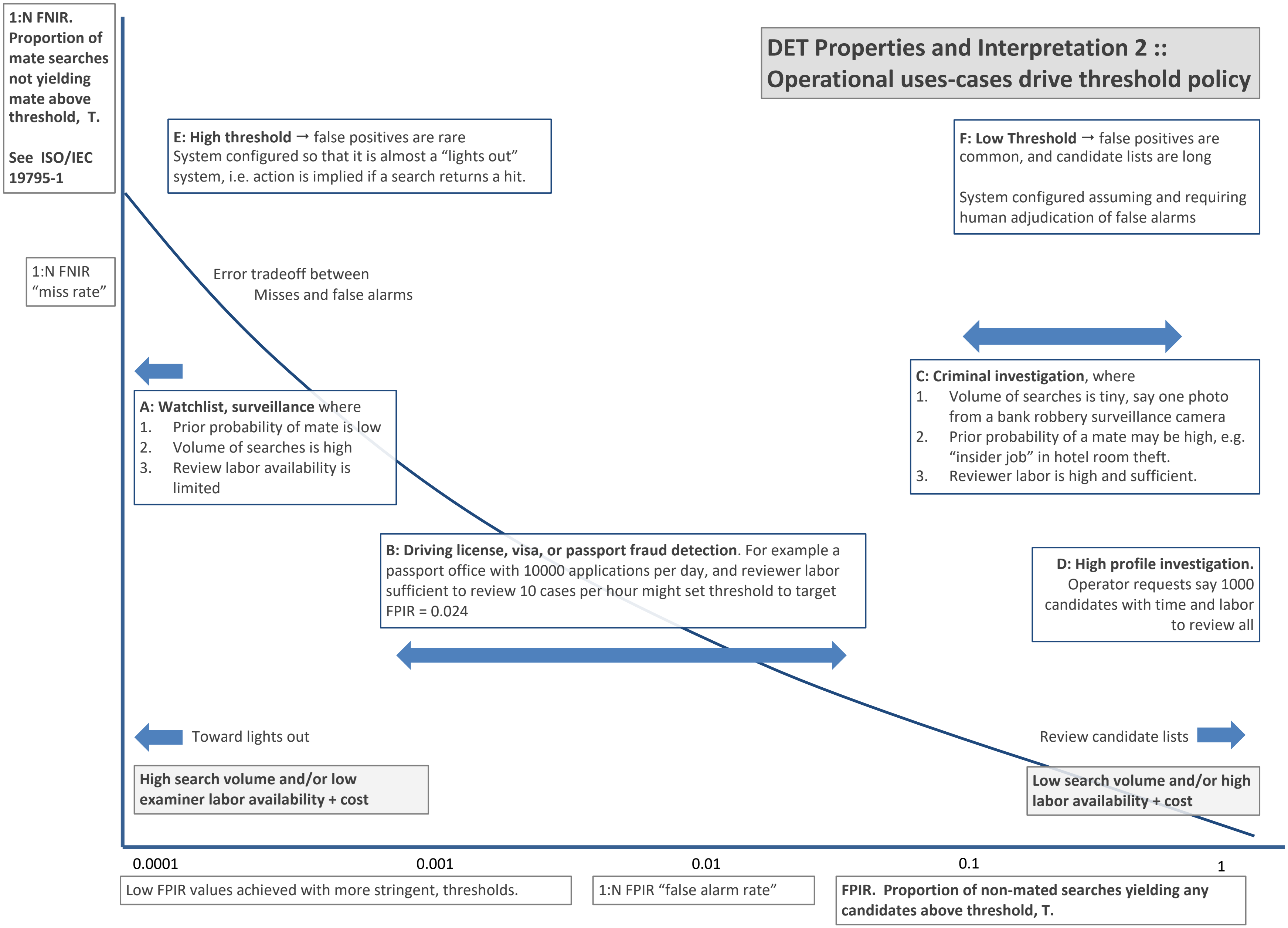

Figure 10: **DET as the primary performance reporting mechanism.**

2019/09/11 16:09:13

FNIR(N, R, T) = False neg. identification rate
FPIR(N, T) = False pos. identification rate
N = Num. enrolled subjects
R = Num. candidates examined
T = Threshold
T = 0 → Investigation
T > 0 → Identification

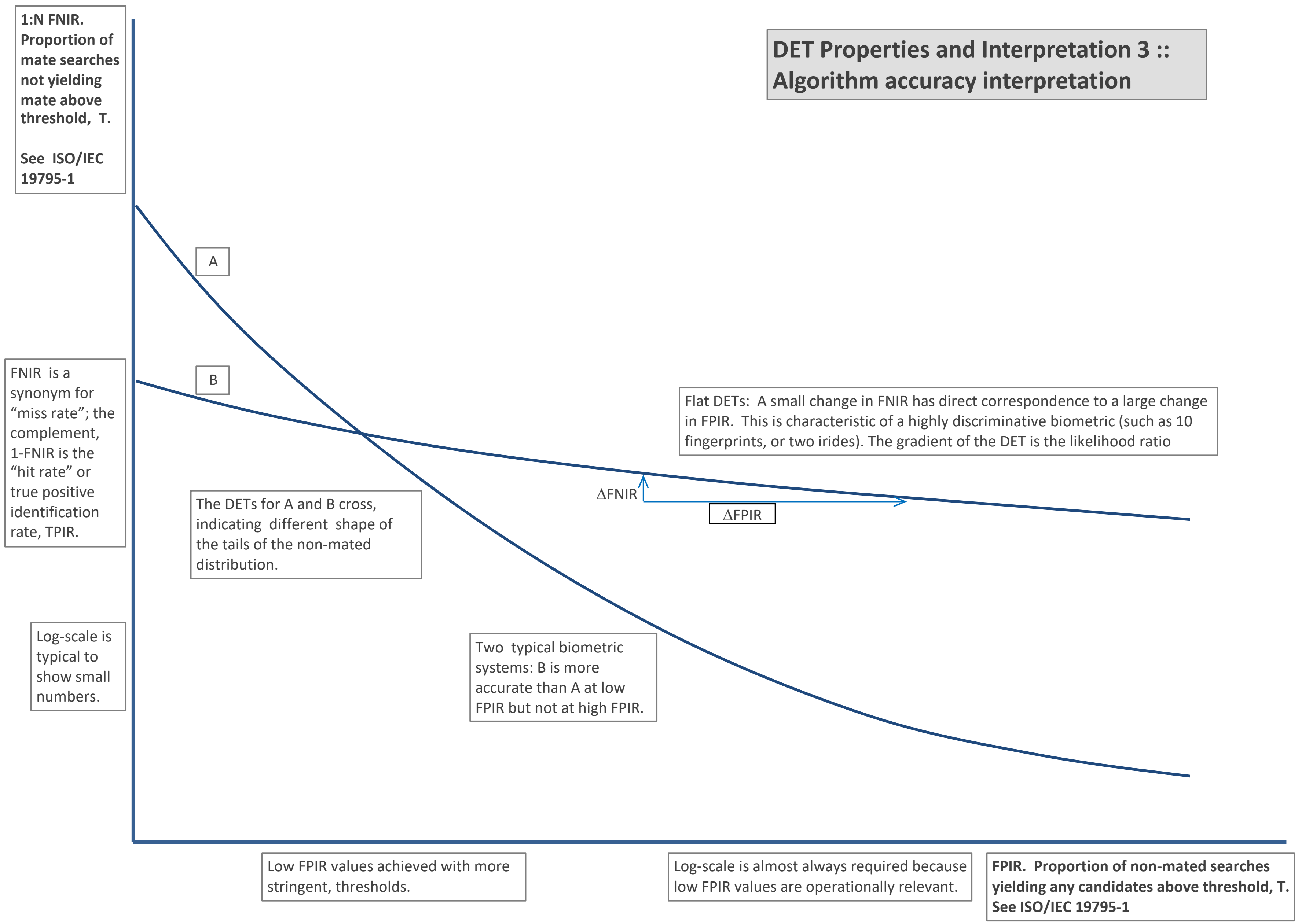

Figure 11: **DET as the primary performance reporting mechanism**.

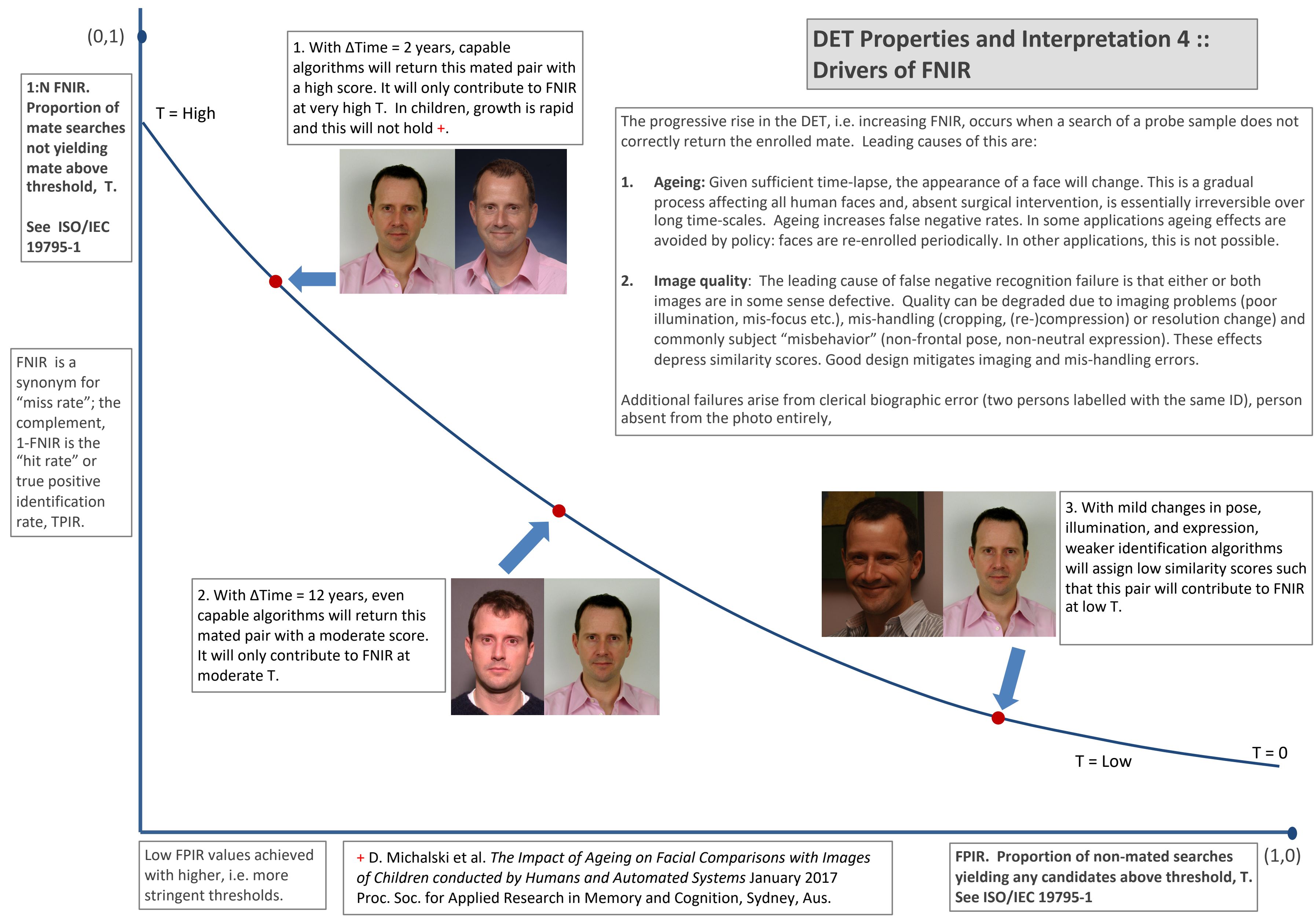

Figure 12: **DET as the primary performance reporting mechanism.**

FNIR(N, R, T) = False neg. identification rate
FPIR(N, T) = False pos. identification rate
N = Num. enrolled subjects
R = Num. candidates examined
T = Threshold
T = 0 → Investigation
T > 0 → Identification

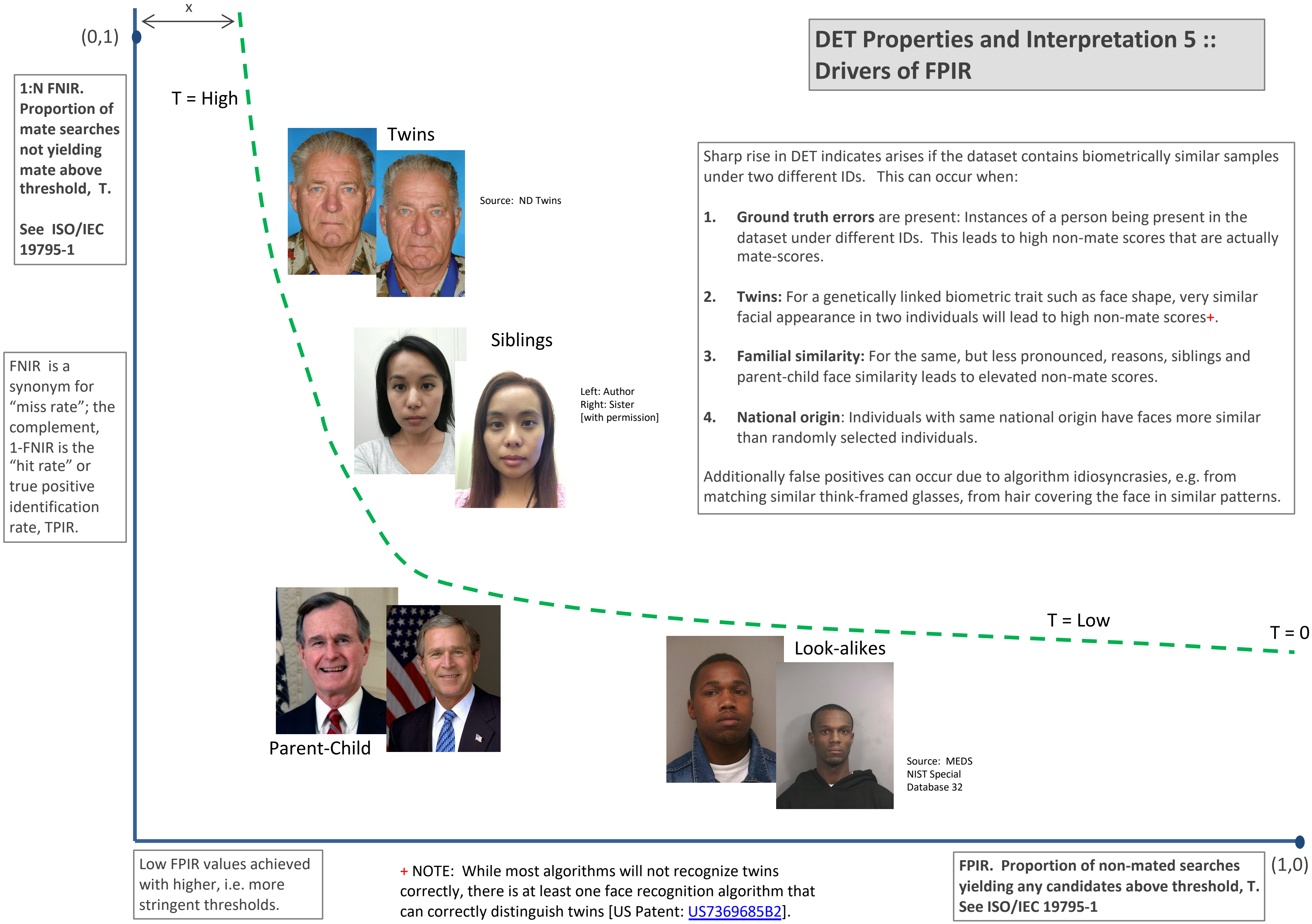

Figure 13: **DET as the primary performance reporting mechanism.**

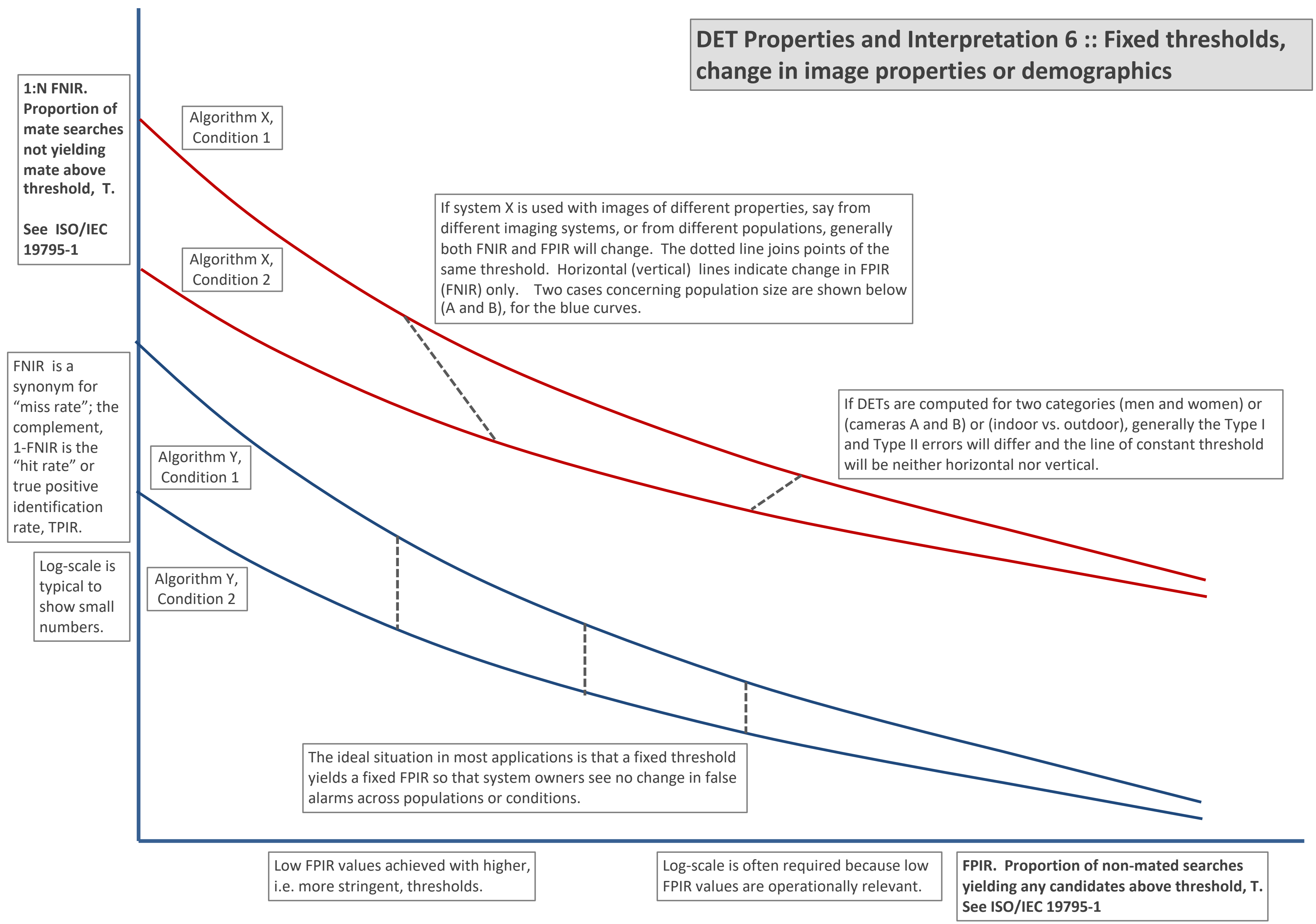

Figure 14: **DET as the primary performance reporting mechanism**.

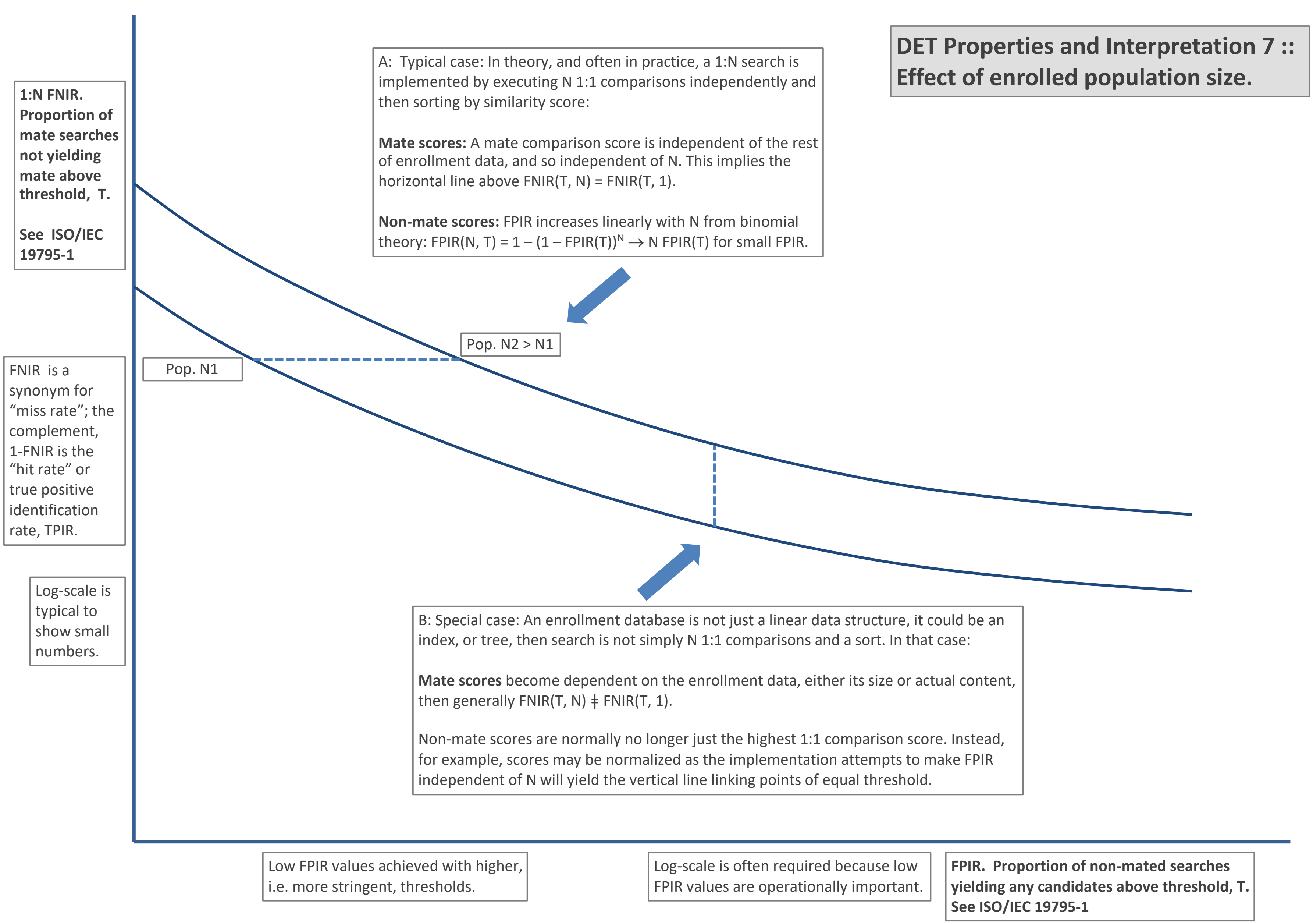

Figure 15: **DET as the primary performance reporting mechanism.**

FNIR(N, R, T) = False neg. identification rate
FPIR(N, T) = False pos. identification rate
N = Num. enrolled subjects
R = Num. candidates examined
T = Threshold
T = 0 → Investigation
T > 0 → Identification

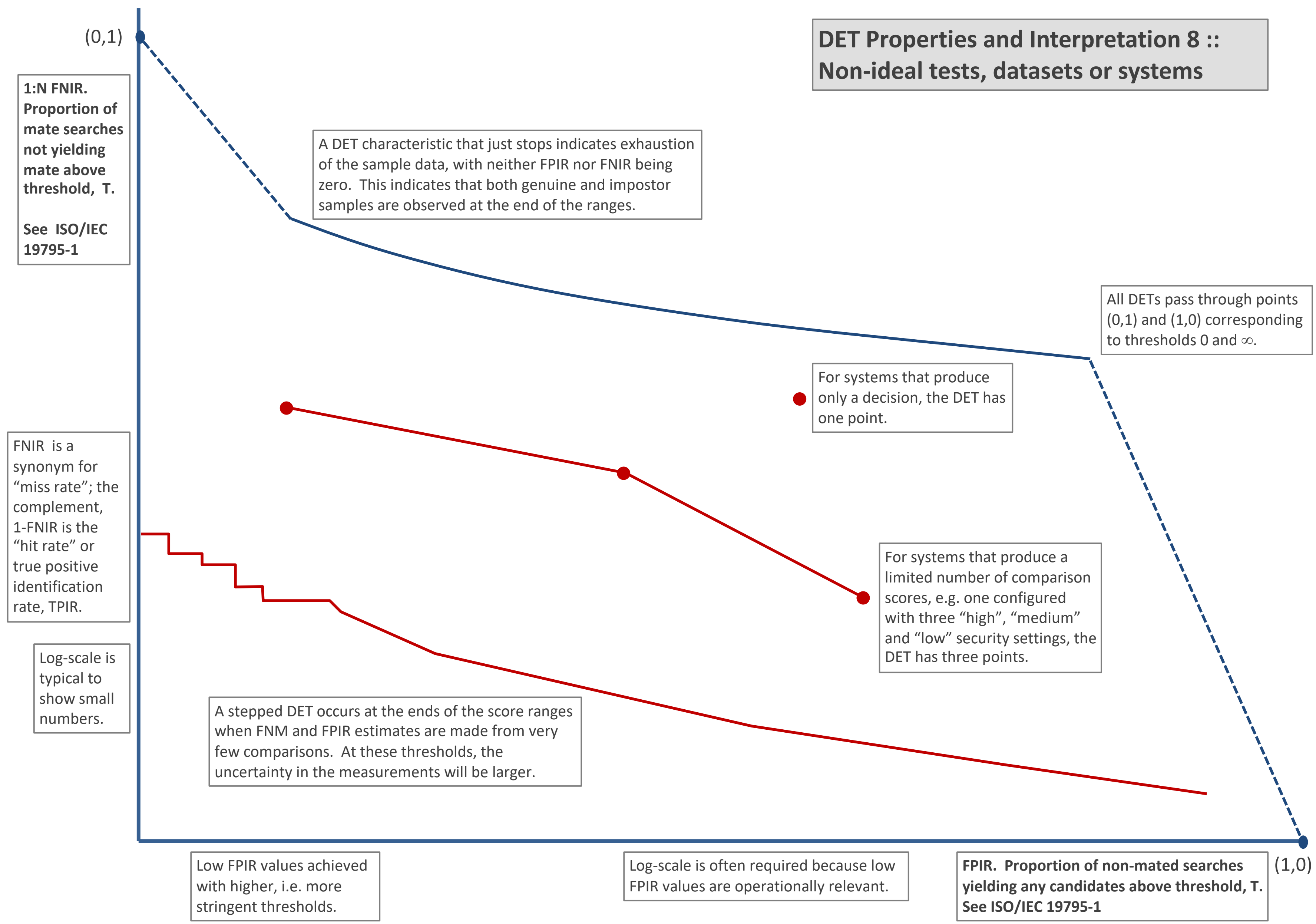

Figure 16: **DET as the primary performance reporting mechanism.**

3.4 Best practice testing requires execution of searches with and without mates

FRVT embeds 1:N searches of two kinds: Those for which there is an enrolled mate, and those for which there is not. The respective numbers for these types of searches appear in Table 5. However, it is common to conduct only mated searches[10]. The cumulative match characteristic is computed from candidate lists produced in mated searches. Even if the CMC is the only metric of interest, the actual trials executed in a test should nevertheless include searches for which no mate exists. As detailed in Table 5 the FRVT reserved disjoint populations of subjects for executing true non-mate searches.

3.5 Failure to extract features

During enrollment some algorithms fail to convert a face image to a template. The proportion of failures is the failure-to-enroll rate, denoted by FTE. Similarly, some search images are not converted to templates. The corresponding proportion is termed failure-to-extract, denoted by FTX.

We do not report FTX because we assume that the same underlying algorithm is used for template generation for enrollment and search.

Failure to extract rates are incorporated into FNIR and FPIR measurements as follows.

- ▷ **Enrollment templates**: Any failed enrollment is regarded as producing a zero length template. Algorithms are required by the API [10] to transparently process zero length templates. The effect of template generation failure on search accuracy depends on whether subsequent searches are mated, or non-mated: Mated searches will fail giving elevated FNIR; non-mated searches will not produce false positives so, to first order, FPIR will be reduced by a factor of $1-\mathrm{FTE}$.

- ▷ **Search templates and 1:N search**: In cases where the algorithm fails to produce a search template from input imagery, the result is taken to be a candidate list whose entries have no hypothesized identities and zero score. The effect of template generation failure on search accuracy depends on whether searches are mated, or non-mated: Mated searches will fail giving elevated FNIR; Non-mated searches will not produce false positives, so FPIR will be reduced. Thus given a measurement of false negative and positive rates made over only those where failures-to-extract did not occur, those rates - call them $\mathrm{FNIR}^{\dagger}$ and $\mathrm{FPIR}^{\dagger}$ - could be adjusted by an explicit measurement of FTX as follows

$$\mathrm{FNIR} = \mathrm{FTX} + (1 - \mathrm{FTX})\mathrm{FNIR}^{\dagger} \tag{8}$$

$$\mathrm{FPIR} = (1 - \mathrm{FTX})\mathrm{FPIR}^{\dagger} \tag{9}$$

This approach is the correct treatment for positive-identification applications such as access control where cooperative users are enrolled and make attempts at recognition. This approach is not appropriate to negative identification applications, such as visa fraud detection, in which hostile individuals may attempt to evade detection by submitting poor quality samples. In those cases, template generation failures should be investigated as though a false alarm had occurred.

[10]For example, the Megaface benchmark. This is bad practice for several reasons: First, if a developer knows, or can reasonably assume, that a mate always exists, then unrealistic gaming of the test is possible. A second reason is that it does not put FPIR on equal footing with FNIR and that matters because in most applications, not all searches have mates - not everyone has been previously enrolled in a driving license issuance or a criminal justice system - so addressing between-class separation becomes necessary.

3.6 Fixed length candidate lists, threshold independent workload

Suppose an automated face identification algorithm returns L candidates, and a human reviewer is retained to examine up to R candidates, where $R \leq L$ might be set by policy, preference or labor availability. For now, assume also that the reviewer is not provided with, or ignores, similarity scores, and thresholds are not applied. Given the algorithm typically places mates at low (good) ranks, the number of candidates a reviewer can be expected to review can be derived as follows. Note that the reviewer will:

- ▷ Always inspect the first ranked image — Frac. reviewed = 1
- ▷ Then inspect those candidates where mate not confirmed at rank 1 — Frac. reviewed = 1-CMC(1)
- ▷ Then inspect those candidates where mate not confirmed at rank 1 or 2 — Frac. reviewed = 1-CMC(2)

etc. Thus if the reviewer will stop after a maximum of R candidates, the expected number of candidate reviews is

$$M(R) = 1 + (1 - CMC(1)) + (1 - CMC(2)) + \ldots + (1 - CMC(R-1)) \tag{10}$$

$$= R - \sum_{r=1}^{R-1} CMC(r) \tag{11}$$

A recognition algorithm that front-loads the cumulative match characteristic will offer reduced workload for the reviewer. This workload is defined only over the searches for which a mate exists. In the cases where there truly is no mate, the reviewer would review all R candidates. Thus, if the proportion of searches for which a mate does exist is β, which in the law enforcement context would be the recidivism rate [3], the full expression for workload becomes:

$$M(R) = \beta \left(R - \sum_{r=1}^{R-1} CMC(r) \right) \quad + \quad (1-\beta)R \tag{12}$$

$$= R - \beta \sum_{r=1}^{R-1} CMC(r) \tag{13}$$

3.7 Timing measurement

Algorithms were submitted to NIST as implementations of the application programming interface(API) specified by NIST in the Evaluation Plan [10]. The API includes functions for initialization, template generation, finalization, search, gallery insert, and gallery delete. Two template generation functions are required, one for the preparation of an enrollment template, and one for a search template.

In NIST's test harness, all functions were wrapped by calls to the C++ std::chrono::high resolution clock which on the dedicated timing machine counts 1ns clock ticks. Precision is somewhat worse than that however.

3.8 Uncertainty estimation

3.8.1 Random error

This study leverages operational datasets for measurement of recognition error rates. This affords several advantages. First, large numbers of searches are conducted (see Table 5) giving precision to the measurements. Moreover, for the two mugshot datasets, these do not involve reuse of individuals so binomial statistics can be expected to apply to recognition error counts. In that case, an observed count of a particular recognition outcome (i.e. a false negative or false positive) in M trials will sustain 95% confidence that the actual error rate is no larger than some value.

As an example, the minimum number of mugshot searches conducted in this report is M =154 549, and for an observed FNIR around 0.002, the measurement supports a conclusion that the actual FNIR is no higher than 0.00228 at 99% confidence level. On the false positive side, we tabulate FNIR at FPIR values as low as 0.001. Given estimates based on 331 254 non-mate trials, the actual FPIR values will be below 0.00115 at 99% confidence. In conclusion, large scale evaluation, without reuse of subjects, supports tight uncertainty bounds on the measured error rates.

3.8.2 Systematic error

The FRVT 2018 dataset includes anomalies discovered as a result of inspecting images involved in recognition failures from the most accurate algorithms. Two kinds of failure occur: False negatives (which, for the purpose here, include failures to make templates) and false positives.

False negative errors: We reviewed 600 false negative pairs for which either or both of the leading two algorithms did not put the correct mate in the top 50 candidates. Given 154 549 searches, this number represents 0.39% of the total, resulting in FNIR ~ 0.0039. Of the 600 pairs:

- ▷ **A: Poor quality**: About 20% of the pairs included images of very low quality, often greyscale, low resolution, blurred, low contrast, partially cropped, interlaced, or noisy scans of paper images. Additionally, in a few cases, the face is injured or occluded by bandages or heavy cosmetics.
- ▷ **B: Ground truth identity label bugs**: About 15% of the pairs are not actually mated. We only assigned this outcome when a pair is clearly not mated.
- ▷ **C: Profile views**: About 35% included an image of a profile (side) view of the face, or, more rarely, an image that was rotated 90 degrees in-plane (roll).
- ▷ **D: Tattoos**: About 30% included an image of a tattoo that contained a face image. These arise from mis-labelling in the parent dataset metadata.
- ▷ **E: Ageing**: There is considerable time-lapse between the two captures.

All these estimates are approximate. Of these, the tattoo and mislabled images can never be matched. These constitute an accuracy floor in the sample implying that FNIR cannot be below 0.0018[11]. The profile-views, low-quality images, and images with considerable ageing can, in principle, be successfully matched - indeed some algorithms do so - so are not part of the accuracy floor.

[11] This value is the sum of two partial false negative rates: FNIR_B = 0.15 * 0.0039 plus FNIR_D = 0.3 * 0.0039

For the microsoft-4 algorithm the lowest miss rate from (recent entry in Table 16) is FNIR(640 000, 50, 0) = 0.0018. This is close to the value estimated from the inspection of misses. It is below the 0.0039 figure because the algorithm does match some profile and poor quality images, that the yitu-2 algorithm does not.

For many tables (e.g. Table 16), the FNIR values obtained for the FRVT-2018 mugshots could be corrected by reducing them by 0.0018. The best values would then be indistinct from zero. The results in this report *were not* adjusted to account for this systematic error.

False positive errors: As depicted in Figure 9 many of the DET characteristics in this report exhibit a pronounced turn upward at low false positive rates. The shape can be caused by identity labelling errors in the ground truth of a dataset, specifically persons present in the database under two IDs such that some proportion of non-mate pairs are actually mated. We merged the highest 1000 non-mate pairs produced by three different algorithms which resulted in 1839 unique pairs. This constitutes 0.56% of all non-mate searches. We assert that it is *very* difficult for human reviewers to assign the pairs into the following three categories: twins; doppelgangers; or ground-truth errors (instances of the same person under two IDs). Given this difficulty we made no attempt to correct any ground truth except by removing 57 pairs in the following categories:

- ▷ **A: Profile views**: Thirteen pairs included one or two profile-view images. As described in Figure 102, these can cause false positives.
- ▷ **B: Same-session photographs**: For twelve pairs, the images were identical or trivially altered (e.g. cropped) versions of the same photo. These were present under a different ID likely due to some clerical or procedural mistake.
- ▷ **C: Tattoos of faces**: There were fourteen instances of tattoo photographs that contained faces causing false matches.
- ▷ **D: T-shirt faces**: There were six instances of T-shirt photographs (of Bob Marley and Che Guevara) being detected instead of the face and causing false positives.
- ▷ **E: Background faces**: There were twelve instances of one subject appearing in the background of two otherwise correct portrait photos.

Note we did not remove any images where there was a chance that the pair was actually a different person.

In any case, the results in this report have not been adjusted for this systematic error.

4 Results

This section gives extensive results for algorithms submitted to FRVT 2018. Three page "report cards" for each algorithm are contained in the separate supplement. Performance metrics were described in section 3. The main results are summarized in tabular form with more exhaustive data included as DET, CMC and related graphs in appendices as follows:

▷ The three tables 6-8 list algorithms alongside full developer names, acceptance date, size of the provided configuration data, template size and generation time, and search duration data.

- The **template generation duration** is most important to applications that require fast response. For example, an eGate taking more than two seconds to produce a template might be unacceptable. Note that GPUs may be of utility in expediting this operation for some algorithms, though at additional expense. Two additional factors should be considered[12][13].
- The **search duration** is the time taken for a search of a search template into a gallery of N enrollment templates. This performance variable, together with the volume of searches, is influential on the amount of hardware needed to sustain an operational deployment. This is measured here with the algorithm running on a single core of a contemporary CPU. Search is most simply implemented as N computations of a distance metric followed by a sort operation to find the closest enrollments. However, considerable optimization of this process is possible, up to and including fast-search algorithms that, by various means, avoid computation of all N distances.
- The **template size** is the size of the extracted feature vector (or vectors) and any needed header information. Large template sizes may be influential on bus or network bandwidth, storage requirements, and on search duration. While the template itself is an opaque data blob, the feature dimensionality might be estimated by assuming a four-bytes-per-float encoding. There is a wide range of encodings. For the more accurate algorithm, sizes range from 256 bytes to about 2KB bytes, indicating essentially no consensus on face modeling and template design.
- The **template size multiplier** column shows how, given k input images, the size of the template grows. Most implementations internally extract features from each image and concatenate them, and implement some score-level fusion logic during search. Other implementations, including many of the most accurate algorithms, produce templates whose size does not grow with k. This could be achieved via selection of the best quality image - but this is not optimal in handling ageing where the oldest image could be the best quality. Another mechanism would be feature-level fusion where information is fused from all k inputs. In any case, as a black-box test, the fusion scheme is proprietary and unknown.
- The size of the **configuration data** is the total size of all files resident in a vendor-provided directory that contains arbitrary read-only files such as parameters, recognition models (e.g caffe). Generally a large value for this quantity may prohibit the use of the algorithm on a resource-constrained device.

[12] The FRVT 2018 API prohibited threading, so some gains from parallelism may be available on multiple-cores or multiple processors, if the feature extraction code could be distributed across them.

[13] Note also that factors of two or more may be realizable by exploiting modern vector processing instructions on CPUs. It is not clear in our measurements whether all developers exploited Intel's AVX2 instructions, for example. Our machine was so equipped, but we insisted that the same compiled library should also run on older machines lacking that instruction. The more sophisticated implementations may have detected AVX2 presence and branched accordingly. The less sophisticated may be defaulted to the reduced instruction set. Readers should see the FRVT 2018 API document for the specific chip details.

▷ Tables 16-17 report core rank-based accuracy for mugshot images. The population size is limited to N = 1.6 million identities because this is the largest gallery size on which all algorithms were executed. Notable observations from these tables are as follows:

- **Accuracy gains during 2018**: NIST Interagency Report 8238 documented massive gains over those reported in the FRVT 2014 report, NIST Interagency Report 8009.

  Further gains are documented in this report. Comparing the most accurate algorithm in June 2018, Microsoft-4, with the most accurate in November 2018, NEC-2, the value of FNIR(N, 1, 0) reduced from 0.0031 to 0.0028 with N = 1.6 million recent images. For lifetime enrollments, Microsoft-4 remained the most accurate algorithm as the newer variants from Microsoft did not reduce this error rate.

  We further note that the revolution is not over: Figure 19 shows that many developers have made great advances in the four months between Phases 1 and 2 of FRVT 2018, Feburary to June. Most developers saw a two-fold reduction in errors, with Neurotechnology seeing a five fold reduction.

- **Wide range in accuracy**: The rank-1 miss rates vary from FNIR(N, 1, 0) = 0.001 for nec-3 up to about 0.5 for the very fast but inaccurate microfocus-x algorithms. Among the developers who are superior to NEC in 2013, the range is from 0.002 to 0.035 for camvi-3. This large accuracy range is consistent with the buyer-beware maxim, and indicates that face recognition software is far from being commoditized.

▷ Tables 19-20 report threshold-based error rates, FNIR(N, L, T), for N = 1.6 million for mugshot-mugshot accuracy on FRVT 2014, FRVT 2018, and also (in pink) mugshot-webcam accuracy using FRVT 2018 enrollments. Notable observations from these tables are as follows:

- **Order of magnitude accuracy gains since 2014**: As with rank-based results, the gains in accuracy are substantial, though somewhat reduced. At FPIR = 0.01, the best improvement over NEC in 2014 is a nine-fold reduction in FNIR using the Microsoft_4 algorithm. At FPIR = 0.001, the largest gain is a six-fold reduction in FNIR via the Yitu_2 algorithm.

- **Broad gains across the industry**: About 19 companies realize accuracy better than the NEC benchmark from 2014. This is somewhat lower than the 28 developers who succeeded on the rank-1 metric. This may be due to the ubiquity of, and emphasis on, the rank-1 metric in many published algorithm development papers.

- **Webcam images**: Searches of webcam images give FNIR(N, T) values around 2 to 3 times higher than mugshot searches. Notably the leading developers with mugshots are approximately the same with poorer quality webcams. But some developers e.g. Camvi, Megvii, TongYi, and Neurotechnology do improve their relative rankings on webcams, perhaps indicating their algorithms were tailored to less constrained images.

▷ Tables 10, 12, 13 and show, respectively, high-threshold, rank 1, nd rank 50 FNIR values for all algorithms performing searches into five different gallery sizes, N = 640 000, N = 1 600 000, N = 3 000 000, N = 6 000 000 and 12 000 000. The FPIR = 0.001 table is included to inform high-volume duplicate detection applications. The Rank-1 table is included as a primary accuracy indicator. The Rank-50 table is included to inform agencies who routinely produce 50 candidates for human-review. The notable results are:

- **Slow growth in rank-based miss rates:** FNIR(N, R) generally grows as a power law, aN^b. From the straight lines of many graphs of Figure 22 this is clearly a reasonable model for most, but not all, algorithms. The coefficient a can be interpreted as FNIR in a gallery of size 1. The more important coefficient b indicates scalability, and often, $b \ll 1$, implies very benign growth in FNIR. The coefficients of the models appear in the Tables 12 and 13.

- **Slow growth in threshold-based miss rates:** FNIR(N, T) also generally grows as a power law, aN^b except at the high threshold values corresponding to low FPIR values. This is visible in the plots of Figure 38 which show straight lines except for FPIR = 0.001, which increase more rapidly with N above 3 000 000. Each trace in those figures shows FNIR(N, T) at fixed FPIR with both N and T varying. Thus at large N, it is usually necessary to elevate T to maintain fixed FPIR. This causes increased FNIR. Why that would no-longer obey a power-law is not known. However, if we expect large galleries to contain individuals with familial relations to the non-mate search images - in the most extreme case, twins - then suppression of false positives becomes more difficult. This is discussed in the Figures starting at Fig. 9

▷ Figure 21 shows false positives from twins against their enrolled siblings, broken out by type of twin: fraternal or identical. The Figure is based on the enrollment of 104 single images on one of a pair of twins, and then the search of 2354 second images. Note that the dataset is heavily skewed towards identical twins which is not representative of the true population. There is also a skew towards same sex fraternal twin pairs compared to different sex fraternal twin pairs again not representative of the true population.

The notable results are:

- For all algorithms tested, the 1087 mated searches (Twin A vs. Twin A) produce scores almost always above typical operational thresholds, with (not shown) matches at rank 1. The images are of good quality, so this is the result expected from the rest of this report.
- For the 1066 identical twin searches (AB), almost all produce the twin at rank 1, with a few producing the mate at further down the candidate lists rank and low score.
- For the 169 fraternal searches (AB) from same sex pairs, most algorithms give a large number of very high scores, implying false positives at all thresholds. However, there there are long tails containing lower scores that are correctly below threshold. In general, scores that are higher in this distribution are all rank 1 whereas the lower scores have much higher ranks.
- (Not shown) Of the 169, there are 24 fraternal searches (AB) involving different sex twins. Here most algorithms correctly report scores well below the lowest threshold, and usually not on the candidate list at all.

This publication is available free of charge from: https://doi.org/10.6028/NIST.IR.8271

FNIR(N, R, T) = False neg. identification rate
FPIR(N, T) = False pos. identification rate
N = Num. enrolled subjects
R = Num. candidates examined
T = Threshold
T = 0 → Investigation
T > 0 → Identification

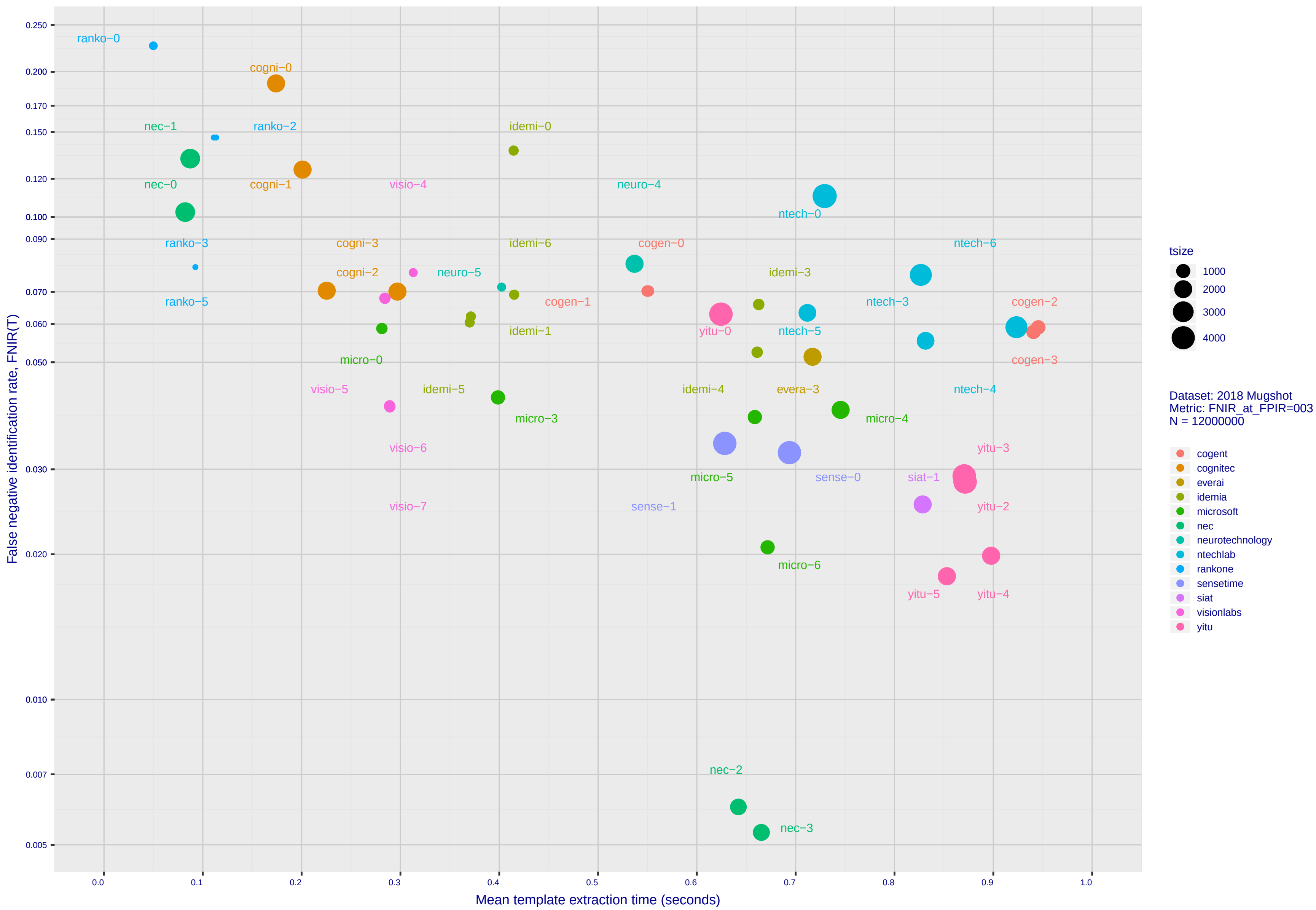

Figure 17: **[Mugshot Dataset] Speed-accuracy tradeoff**. *For developers of the more accurate algorithms the plot shows the tradeoff of high-threshold recognition miss-rates, FNIR(N, N, T) for FPIR(N, T) = 0.003, and template generation time. Developers are coded by color. Template size is encoded by the size of the circle. Some labels are quite distant from the respective point, to avoid superposing text. Without any other influences, the assumption would be that taking time to localize the face, and extract features, would lead to better accuracy. The most notable result, for NEC, is that their slower algorithms are much more accurate than the version that extract features in fewer than 90 milliseconds.*

This publication is available free of charge from: https://doi.org/10.6028/NIST.IR.8271

FNIR(N, R, T) = False neg. identification rate
FPIR(N, T) = False pos. identification rate
N = Num. enrolled subjects
R = Num. candidates examined
T = Threshold
T = 0 → Investigation
T > 0 → Identification

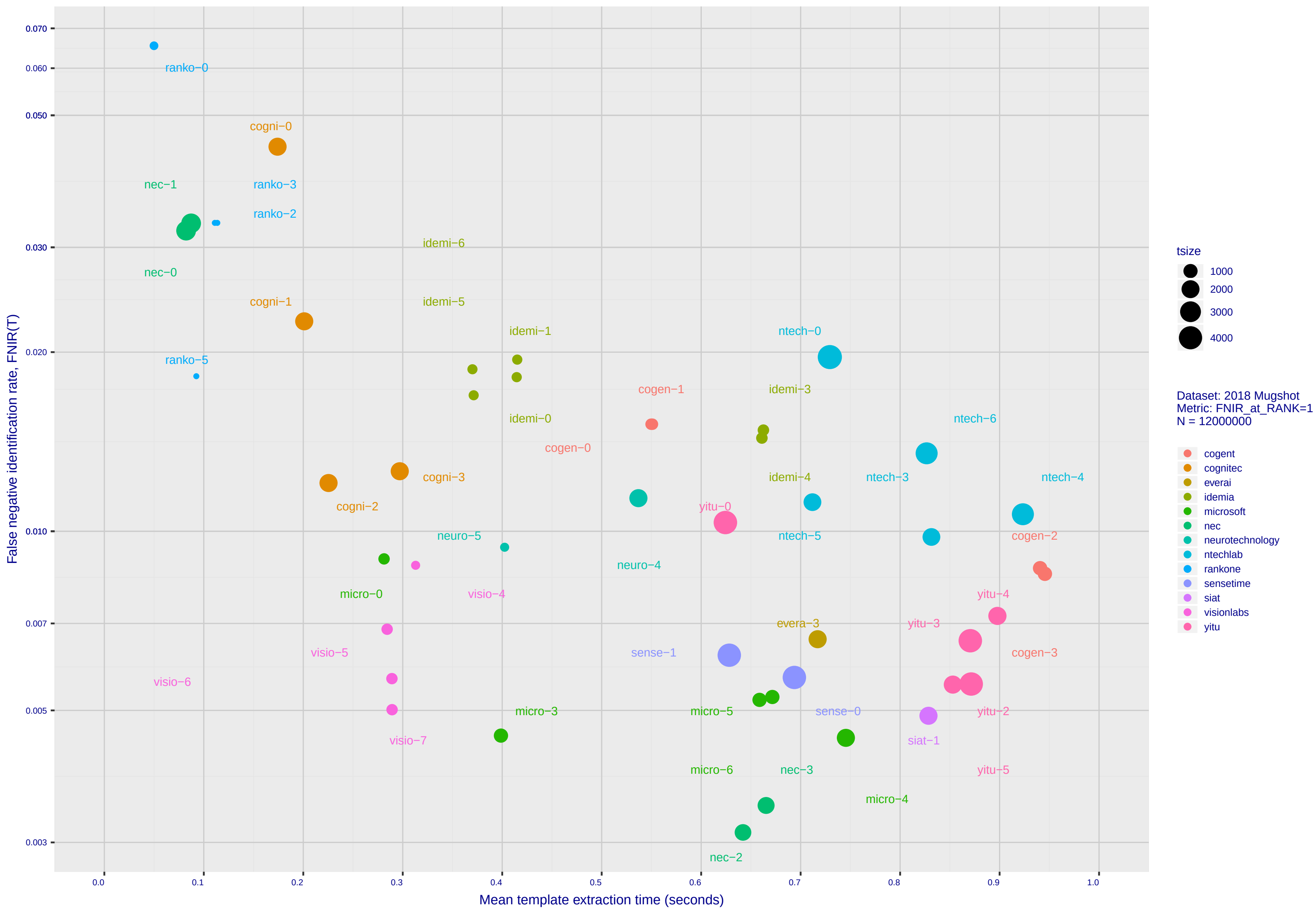

Figure 18: **[Mugshot Dataset] Speed-accuracy tradeoff**. *For developers of the more accurate algorithms the plot shows the tradeoff of rank-one recognition miss-rates, FNIR(N, 1, 0), and template generation time. Developers are coded by color. Template size is encoded by the size of the circle. Some labels are quite distant from the respective point, to avoid superposing text. Without any other influences, the assumption would be that taking time to localize the face, and extract features, would lead to better accuracy. This occurs for NEC with their slower algorithm being much accurate than the version that extract features in fewer than 90 milliseconds.*

FNIR(N, R, T) = False neg. identification rate
FPIR(N, T) = False pos. identification rate
N = Num. enrolled subjects
R = Num. candidates examined
T = Threshold
T = 0 → Investigation
T > 0 → Identification

	DEVELOPER FULL NAME	SHORT NAME	SEQ. NUM.	VALIDATION DATE	CONFIG[1] DATA (MB)	TEMPLATE GENERATION SIZE (B)	MULT[2]	TIME (MS)[3]	SEARCH DURATION[4] MILLISEC L=1 N=1.6M	L=50 N=1.6M	L=50 N=3M	L=50 N=6M	L=50 N=12M	POWER LAW (μs)
1	3Divi	3divi	0	2018-02-09	186	[183]4096	k	[90]426	-	[107]553	-	-	-	
2	3Divi	3divi	1	2018-02-15	187	[195]4224	k	[94]428	-	[19]37	-	-	-	
3	3Divi	3divi	2	2018-02-15	187	[47]528	k	[92]428	-	[17]33	-	-	-	
4	3Divi	3divi	3	2018-06-19	165	[41]512	k	[130]625	[15]76	[23]76	-	-	-	
5	3Divi	3divi	4	2018-06-19	186	[180]4096	k	[131]628	[73]604	[126]801	-	-	-	
6	3Divi	3divi	5	2018-10-26	186	[178]4096	k	[138]653	[67]537	[104]537	[51]1376	[48]2612	[41]5524	[71]0.07 $N^{1.1}$
7	3Divi	3divi	6	2018-10-26	187	[49]528	k	[141]653	[10]33	[15]33	-	-	-	
8	Alchera	alchera	0	2018-06-30	168	[146]2048	k	[42]263	[120]3296	[193]5420	-	-	-	
9	Alchera	alchera	1	2018-06-30	46	[124]2048	k	[8]66	[121]3516	[194]5489	-	-	-	
10	Alchera	alchera	2	2018-10-30	7	[143]2048	k	[16]115	[118]2920	[179]2926	-	-	-	
11	Alchera	alchera	3	2018-10-30	251	[113]2048	k	[117]548	[119]2952	[181]2953	[79]6540	[74]14998	[70]35227	[84]0.10 $N^{1.2}$
12	Anke Investments	anke	0	2018-10-30	779	[165]2072	k	[96]431	[74]675	[123]748	[53]1482	[50]2965	[43]6142	[58]0.21 $N^{1.1}$
13	Anke Investments	anke	1	2018-10-30	779	[164]2072	k	[97]433	[76]707	[124]769	-	-	-	
14	Aware	aware	0	2018-02-16	261	[99]1564	k	[139]653	-	[60]251	-	-	-	
15	Aware	aware	1	2018-02-16	232	[100]1564	k	[136]651	-	[61]251	-	-	-	
16	Aware	aware	2	2018-02-16	349	[167]2076	k	[197]912	-	[62]252	-	-	-	
17	Aware	aware	3	2018-06-22	350	[166]2076	k	[163]716	[114]2426	[174]2508	[74]4495	-	-	[41]1.09 $N^{1.0}$
18	Aware	aware	4	2018-06-22	349	[2]92	k	[160]712	[89]1232	[140]1187	-	-	-	
19	Aware	aware	5	2018-10-30	368	[173]3100	k	[182]827	[18]94	[26]97	[13]202	[11]370	[9]251	[11]4.13 $N^{0.7}$
20	Aware	aware	6	2018-10-30	368	[3]124	k	[175]818	[27]157	[39]162	-	-	-	
21	Ayonix	ayonix	0	2018-06-21	57	[77]1036	k	[1]10	[47]283	[74]298	-	-	-	
22	Ayonix	ayonix	1	2018-10-29	74	[81]1036	k	[3]12	[44]277	[70]277	-	-	-	
23	Ayonix	ayonix	2	2018-10-30	74	[79]1036	1	[2]11	[43]277	[69]274	[27]531	[25]1079	[22]2268	[50]0.11 $N^{1.0}$
24	Camvi Technologies	camvitech	1	2018-02-16	94	[69]1024	1	[24]177	-	[12]23	-	-	-	
25	Camvi Technologies	camvitech	2	2018-02-16	442	[74]1024	1	[172]774	-	[11]20	-	-	-	
26	Camvi Technologies	camvitech	3	2018-06-30	233	[72]1024	1	[158]707	[7]10	[9]11	-	-	-	
27	Camvi Technologies	camvitech	4	2018-10-30	233	[66]1024	1	[165]718	[11]33	[14]32	[8]38	[6]40	[4]48	[2]8492.66 $N^{0.1}$
28	Camvi Technologies	camvitech	5	2018-10-30	257	[61]1024	1	[170]769	[9]31	[13]30	-	-	-	
29	Thales	cogent	0	2018-06-20	533	[46]525	k	[118]551	[63]494	[110]558	[42]1047	[41]2060	[33]4141	[21]0.46 $N^{1.0}$
30	Thales	cogent	1	2018-06-20	533	[45]525	k	[119]552	[64]498	[108]556	[43]1048	[42]2082	[35]4263	[26]0.39 $N^{1.0}$
31	Thales	cogent	2	2018-10-30	681	[84]1043	k	[203]987	[108]2017	[166]2144	[73]4298	[69]8472	[65]16429	[37]1.08 $N^{1.0}$
32	Thales	cogent	3	2018-10-30	681	[83]1043	k	[202]960	[88]1230	[146]1311	[63]2687	[60]5398	[55]10184	[39]0.62 $N^{1.0}$
33	Cognitec Systems GmbH	cognitec	0	2018-06-21	364	[155]2052	k	[23]176	[100]1748	[154]1780	[68]3672	[64]7093	[63]15224	[55]0.57 $N^{1.0}$
34	Cognitec Systems GmbH	cognitec	1	2018-06-21	412	[149]2052	k	[28]202	[103]1835	[156]1805	[71]3971	[67]7484	[64]16249	[60]0.49 $N^{1.1}$
35	Cognitec Systems GmbH	cognitec	2	2018-10-30	463	[151]2052	k	[34]227	[99]1733	[153]1763	[67]3660	[66]7279	[59]13895	[40]0.83 $N^{1.0}$
36	Cognitec Systems GmbH	cognitec	3	2018-10-30	465	[157]2052	k	[52]297	[98]1719	[155]1791	[66]3638	[65]7277	[61]14904	[52]0.66 $N^{1.0}$
37	Dahua Technology Co. Ltd	dahua	0	2018-10-29	276	[131]2048	k	[72]378	-	[65]256	-	-	-	
38	Dahua Technology Co. Ltd	dahua	1	2018-10-29	276	[115]2048	k	[68]371	-	[64]256	[33]601	[31]1199	[30]3001	[78]0.02 $N^{1.2}$
39	Dermalog	dermalog	0	2018-02-16	0	[5]128	1	[65]344	-	[88]404	-	-	-	
40	Dermalog	dermalog	1	2018-02-16	0	[8]128	1	[22]171	-	[91]407	-	-	-	
41	Dermalog	dermalog	2	2018-02-16	0	[18]256	k	[64]344	-	[119]640	-	-	-	
42	Dermalog	dermalog	3	2018-06-21	0	[7]128	1	[31]211	[17]92	[24]92	-	-	-	
43	Dermalog	dermalog	4	2018-06-21	0	[4]128	1	[29]208	[16]91	[25]93	-	-	-	
44	Dermalog	dermalog	5	2018-10-26	0	[6]128	1	[109]532	[2]0	[1]0	[1]0	[1]0	[1]0	[4]66.21 $N^{0.2}$
45	Dermalog	dermalog	6	2018-10-26	0	[24]256	1	[105]514	[25]141	[35]143	[18]267	[16]527	[14]1285	[53]0.05 $N^{1.0}$
46	Ever AI	everai	0	2018-06-21	142	[140]2048	1	[99]438	[4]4	[5]3	[2]5	-	-	[9]42.41 $N^{0.3}$
47	Ever AI	everai	1	2018-06-21	200	[111]2048	1	[125]590	[51]336	[81]356	[35]651	-	-	[74]0.03 $N^{1.1}$
48	Ever AI	everai	2	2018-10-30	224	[132]2048	1	[71]377	[46]278	[72]283	-	-	-	
49	Ever AI	everai	3	2018-10-30	438	[112]2048	1	[167]735	[45]278	[71]281	[30]572	[29]1146	[23]2278	[48]0.12 $N^{1.0}$
50	Eyedea Recognition	eyedea	0	2018-02-16	644	[194]4152	k	[89]424	-	[120]640	-	-	-	
51	Eyedea Recognition	eyedea	1	2018-02-16	287	[82]1036	k	[56]311	-	[76]307	-	-	-	
52	Eyedea Recognition	eyedea	2	2018-02-16	287	[78]1036	k	[95]429	-	[75]305	-	-	-	

Notes	
1	Configuration size does not capture static data present in libraries. Libraries are not counted because most implementations include common ancillary libraries for image processing (e.g. openCV) or numerical computation (e.g. blas).
2	This multiplier expresses the increase in template size when k images are passed to the template generation function.
3	All durations are measured on Intel®Xeon®CPU E5-2630 v4 @ 2.20GHz processors. Estimates are made by wrapping the API function call in calls to std::chrono::high_resolution_clock which on the machine in (3) counts 1ns clock ticks. Precision is somewhat worse than that however.
4	Search durations are measured as in the prior note. The power-law model in the final column mostly fits the empirical results in Figure 111. However in certain cases the model is not correct and should not be used numerically.

Table 6: Summary of algorithms and properties included in this report. The blue superscripts give ranking for the quantity in that column. Missing search durations, denoted by "-", are absent because those runs were not executed, usually because we did not run on the larger galleries. Caution: The power-law model is sometimes an incorrect model. It is included here only to show broad sublinear behavior, which is flagged in green. The models should not be used for prediction.

2019/09/11 16:09:13

FNIR(N, R, T) = False neg. identification rate
FPIR(N, T) = False pos. identification rate
N = Num. enrolled subjects
R = Num. candidates examined
T = Threshold
T = 0 → Investigation
T > 0 → Identification

	DEVELOPER FULL NAME	SHORT NAME	SEQ. NUM.	VALIDATION DATE	CONFIG[1] DATA (MB)	TEMPLATE GENERATION SIZE (B)	MULT[2]	TIME (MS)[3]	SEARCH DURATION[4] MILLISEC L=1 N=1.6M	L=50 N=1.6M	L=50 N=3M	L=50 N=6M	L=50 N=12M	POWER LAW (μs)
53	Eyedea Recognition	eyedea	3	2018-06-18	284	[80]1036	k	[73]385	[48]309	[78]311	-	-	-	
54	Glory Ltd	glory	0	2018-06-30	0	[33]418	k	[18]160	[70]575	[112]575	-	-	-	
55	Glory Ltd	glory	1	2018-06-30	0	[103]1726	k	[81]405	[104]1864	[159]1978	-	-	-	
56	Gorilla Technology	gorilla	0	2018-02-01	95	[202]8300	k	[91]427	-	[200]10426	-	-	-	
57	Gorilla Technology	gorilla	1	2018-06-19	91	[170]2156	k	[21]169	[128]5254	[190]5156	-	-	-	
58	Gorilla Technology	gorilla	2	2018-10-29	91	[87]1132	k	[62]341	[26]145	[37]146	[19]293	[17]612	[17]1509	[66]$0.02\ N^{1.1}$
59	Gorilla Technology	gorilla	3	2018-10-26	94	[169]2156	k	[124]563	[105]1934	[161]2047	-	-	-	
60	loginface Corp	hbinno	0	2018-02-01	88	[44]520	-	[43]265	-	[95]419	-	-	-	
61	Hikvision Research Institute	hikvision	0	2018-02-12	378	[105]1808	1	[194]875	-	[171]2360	-	-	-	
62	Hikvision Research Institute	hikvision	1	2018-02-12	378	[107]1808	1	[178]820	-	[172]2403	-	-	-	
63	Hikvision Research Institute	hikvision	2	2018-02-12	378	[106]1808	1	[176]820	-	[173]2408	-	-	-	
64	Hikvision Research Institute	hikvision	3	2018-06-30	408	[91]1408	1	[133]633	[84]904	[138]1108	[60]2377	[53]3785	[45]7570	[20]$0.91\ N^{1.0}$
65	Hikvision Research Institute	hikvision	4	2018-06-30	334	[88]1152	1	[104]510	[79]784	[134]1024	[58]2094	[52]3254	[44]7117	[19]$0.86\ N^{1.0}$
66	Hikvision Research Institute	hikvision	5	2018-10-29	593	[90]1408	-	[129]619	[83]883	[132]895	[55]1908	[54]3792	[52]9387	[72]$0.10\ N^{1.1}$
67	Hikvision Research Institute	hikvision	6	2018-10-29	593	[89]1408	1	[126]610	[82]871	[131]877	-	-	-	
68	Idemia	idemia	0	2018-02-16	371	[32]364	1	[86]416	-	[28]133	[14]249	[12]502	-	[33]$0.08\ N^{1.0}$
69	Idemia	idemia	1	2018-02-16	371	[30]364	1	[87]417	-	[33]138	-	-	-	
70	Idemia	idemia	2	2018-02-16	371	[31]364	1	[88]417	-	[34]138	-	-	-	
71	Idemia	idemia	3	2018-06-21	472	[48]528	1	[149]689	[50]318	[82]361	[34]631	[28]1104	[24]2332	[12]$5.03\ N^{0.8}$
72	Idemia	idemia	4	2018-06-21	472	[50]528	1	[147]669	[29]168	[53]211	[25]475	[23]995	[21]2225	[73]$0.02\ N^{1.1}$
73	Idemia	idemia	5	2018-10-29	417	[28]352	1	[70]374	[20]137	[32]138	[23]437	[19]724	[19]1630	[82]$0.01\ N^{1.2}$
74	Idemia	idemia	6	2018-10-29	417	[29]352	1	[69]373	[21]137	[31]138	[24]442	[22]827	[20]1646	[83]$0.01\ N^{1.2}$
75	Imagus Technology Pty Ltd	imagus	0	2018-02-14	35	[37]512	k	[5]43	-	[48]202	-	-	-	
76	Imagus Technology Pty Ltd	imagus	2	2018-06-21	35	[34]512	k	[9]76	[37]200	[52]208	-	-	-	
77	Imagus Technology Pty Ltd	imagus	3	2018-06-21	46	[39]512	k	[7]57	[38]201	[50]206	-	-	-	
78	Incode Technologies	incode	0	2018-06-29	23	[75]1024	k	[27]190	[93]1293	[185]3510	-	-	-	
79	Incode Technologies	incode	1	2018-06-29	151	[144]2048	k	[151]690	[94]1542	[188]4497	-	-	-	
80	Incode Technologies	incode	2	2018-10-29	71	[120]2048	1	[49]291	[59]411	[89]404	-	-	-	
81	Incode Technologies	incode	3	2018-10-29	133	[139]2048	1	[156]704	[58]408	[94]412	[38]846	[35]1606	[36]4482	[69]$0.05\ N^{1.1}$
82	Innovatrics	innovatrics	0	2018-02-16	0	[53]530	k	[100]455	-	[118]625	-	-	-	
83	Innovatrics	innovatrics	1	2018-02-16	0	[51]530	k	[58]316	-	[117]625	-	-	-	
84	Innovatrics	innovatrics	2	2018-06-21	0	[52]530	k	[40]255	[3]1	[3]2	-	-	-	
85	Innovatrics	innovatrics	3	2018-06-21	0	[54]530	k	[41]255	[109]2020	[157]1882	-	-	-	
86	Innovatrics	innovatrics	4	2018-10-30	0	[85]1076	k	[83]406	[6]8	[8]8	[4]11	[3]9	[2]13	[7]$668.38\ N^{0.2}$
87	Alivia / Innovation Sys.	isystems	0	2018-02-14	262	[134]2048	1	[33]222	-	[85]393	-	-	-	
88	Alivia / Innovation Sys.	isystems	1	2018-02-14	263	[63]1024	1	[32]222	-	[55]240	-	-	-	
89	Alivia / Innovation Sys.	isystems	2	2018-06-25	268	[126]2048	1	[59]316	[55]385	[99]484	[50]1275	[39]1770	[31]3063	[16]$0.68\ N^{0.9}$
90	Alivia / Innovation Sys.	isystems	3	2018-10-30	350	[142]2048	1	[189]856	[54]384	[84]387	[41]976	[40]1817	[51]9319	[86]$0.00\ N^{1.3}$
91	Lookman Electroplast Industries	lookman	3	2018-10-28	203	[26]292	1	[63]342	[77]739	[122]745	[52]1394	[49]2817	[46]8286	[64]$0.13\ N^{1.1}$
92	Lookman Electroplast Industries	lookman	4	2018-10-28	184	[55]548	1	[60]325	[85]981	[133]998	-	-	-	
93	Megvii	megvii	0	2018-02-15	1327	[138]2048	1	[174]794	-	[73]284	[26]530	[24]1060	-	[30]$0.18\ N^{1.0}$
94	Megvii	megvii	1	2018-10-28	1703	[184]4096	1	[137]652	[68]551	[111]560	[49]1219	[45]2316	[42]5956	[68]$0.08\ N^{1.1}$
95	Megvii	megvii	2	2018-10-28	1735	[182]4096	1	[142]656	[69]552	[109]557	-	-	-	
96	Microfocus	microfocus	0	2018-02-12	101	[21]256	k	[106]525	-	[42]184	-	-	-	
97	MicroFocus	microfocus	1	2018-02-16	101	[13]256	k	[107]527	-	[20]39	-	-	-	
98	Microfocus	microfocus	2	2018-02-16	101	[22]256	k	[108]529	-	[4]2	-	-	-	
99	Microfocus	microfocus	3	2018-06-22	101	[14]256	k	[46]269	[33]185	[45]188	-	-	-	
100	Microfocus	microfocus	4	2018-06-22	102	[20]256	k	[47]270	[34]186	[46]189	-	-	-	
101	Microfocus	microfocus	5	2018-10-29	94	[25]256	k	[45]266	[31]182	[44]186	[20]353	[18]706	[15]1422	[34]$0.11\ N^{1.0}$
102	Microfocus	microfocus	6	2018-10-29	94	[19]256	k	[44]265	[32]182	[43]186	-	-	-	
103	Microsoft	microsoft	0	2018-01-30	126	[43]512	1	[48]283	-	[114]593	[47]1193	[46]2395	[38]4936	[51]$0.22\ N^{1.0}$
104	Microsoft	microsoft	1	2018-02-12	165	[68]1024	1	[66]349	-	[130]869	-	-	-	

Notes	
1	Configuration size does not capture static data present in libraries. Libraries are not counted because most implementations include common ancillary libraries for image processing (e.g. openCV) or numerical computation (e.g. blas).
2	This multiplier expresses the increase in template size when k images are passed to the template generation function.
3	All durations are measured on Intel®Xeon®CPU E5-2630 v4 @ 2.20GHz processors. Estimates are made by wrapping the API function call in calls to std::chrono::high_resolution_clock which on the machine in (3) counts 1ns clock ticks. Precision is somewhat worse than that however.
4	Search durations are measured as in the prior note. The power-law model in the final column mostly fits the empirical results in Figure 111. However in certain cases the model is not correct and should not be used numerically.

Table 7: Summary of algorithms and properties included in this report. The blue superscripts give ranking for the quantity in that column. Missing search durations, denoted by "-", are absent because those runs were not executed, usually because we did not run on the larger galleries. Caution: The power-law model is sometimes an incorrect model. It is included here only to show broad sublinear behavior, which is flagged in green. The models should not be used for prediction.

	DEVELOPER	SHORT	SEQ.	VALIDATION	CONFIG[1]	TEMPLATE GENERATION			SEARCH DURATION[4] MILLISEC					
	FULL NAME	NAME	NUM.	DATE	DATA (MB)	SIZE (B)	MULT[2]	TIME (MS)[3]	L=1	L=50	L=50	L=50	L=50	POWER LAW
									N=1.6M	N=1.6M	N=3M	N=6M	N=12M	(μs)
105	Microsoft	microsoft	2	2018-02-12	228	[73] 1024	1	[120] 555	-	[129] 869	-	-	-	
106	Microsoft	microsoft	3	2018-06-20	230	[65] 1024	1	[80] 404	[96] 1638	[148] 1603	[65] 3260	[63] 6730	[58] 13833	[56] $0.51\ N^{1.1}$
107	Microsoft	microsoft	4	2018-06-20	437	[127] 2048	1	[171] 773	[117] 2662	[177] 2691	[75] 5260	[71] 11070	[67] 22748	[57] $0.83\ N^{1.1}$
108	Microsoft	microsoft	5	2018-10-29	381	[70] 1024	1	[148] 673	[95] 1604	[150] 1671	[64] 3073	[61] 6296	[57] 13147	[38] $0.79\ N^{1.0}$
109	Microsoft	microsoft	6	2018-10-29	478	[62] 1024	1	[152] 695	[97] 1640	[149] 1617	[69] 3707	[62] 6394	[56] 12879	[47] $0.68\ N^{1.0}$
110	NEC	nec	0	2018-06-21	131	[172] 2592	k	[10] 82	[49] 317	[96] 426	[37] 738	[33] 1315	[27] 2737	[14] $0.73\ N^{0.9}$
111	NEC	nec	1	2018-06-29	131	[171] 2592	k	[11] 88	[36] 193	[51] 208	[22] 388	[20] 750	[18] 1577	[18] $0.21\ N^{1.0}$
112	NEC	nec	2	2018-10-30	705	[101] 1616	k	[140] 653	[57] 405	[93] 409	[44] 1072	[37] 1755	[34] 4255	[70] $0.06\ N^{1.1}$
113	NEC	nec	3	2018-10-30	774	[102] 1712	k	[150] 690	[5] 7	[7] 7	[5] 14	[5] 40	[6] 82	[80] $0.00\ N^{1.2}$
114	Neurotechnology	neurotech	0	2018-02-16	331	[197] 5214	k	[154] 702	-	[182] 3040	-	-	-	
115	Neurotechnology	neurotech	1	2018-02-16	331	[198] 5214	k	[145] 661	-	[184] 3054	-	-	-	
116	Neurotechnology	neurotech	2	2018-02-16	331	[199] 5214	k	[144] 658	-	[183] 3051	-	-	-	
117	Neurotechnology	neurotech	3	2018-06-27	265	[116] 2048	k	[116] 547	[87] 1084	[135] 1059	[59] 2111	[57] 4779	[49] 8793	[31] $0.73\ N^{1.0}$
118	Neurotechnology	neurotech	4	2018-06-27	265	[145] 2048	k	[115] 543	[86] 1060	[136] 1061	[57] 2091	[56] 4263	[47] 8736	[17] $1.22\ N^{1.0}$
119	Neurotechnology	neurotech	5	2018-10-30	266	[17] 256	k	[84] 412	[80] 835	[127] 839	[54] 1690	[51] 3219	[50] 8955	[62] $0.19\ N^{1.1}$
120	Neurotechnology	neurotech	6	2018-10-30	564	[16] 256	k	[169] 746	[81] 839	[128] 842	-	-	-	
121	Newland Computer Co. Ltd	newland	2	2018-10-30	96	[110] 2048	-	[191] 868	[134] 8653	[199] 8765	[86] 17713	[81] 38963	-	[67] $1.32\ N^{1.1}$
122	Noblis	noblis	1	2018-10-30	114	[128] 2048	1	[30] 211	[91] 1273	[143] 1272	-	-	-	
123	Noblis	noblis	2	2018-10-30	153	[200] 6144	1	[110] 535	[116] 2513	[175] 2522	[76] 5649	[72] 12432	[73] 44262	[85] $0.04\ N^{1.3}$
124	N-Tech Lab	ntech	0	2018-02-16	2124	[196] 4442	k	[166] 730	-	[83] 382	[36] 673	[34] 1344	-	[22] $0.27\ N^{1.0}$
125	N-Tech Lab	ntech	1	2018-02-16	851	[104] 1736	k	[82] 405	-	[38] 161	-	-	-	
126	N-Tech Lab	ntech	3	2018-06-21	3664	[174] 3484	k	[184] 831	[53] 384	[80] 326	[31] 596	[30] 1192	[25] 2411	[24] $0.24\ N^{1.0}$
127	N-Tech Lab	ntech	4	2018-06-21	3766	[175] 3484	k	[198] 929	[52] 378	[79] 312	[32] 597	[32] 1204	[26] 2416	[29] $0.21\ N^{1.0}$
128	N-Tech Lab	ntech	5	2018-10-30	1685	[108] 1940	k	[164] 717	[42] 243	[57] 246	[28] 538	[26] 1100	[28] 2867	[75] $0.02\ N^{1.1}$
129	N-Tech Lab	ntech	6	2018-10-30	1686	[109] 1940	k	[187] 841	[41] 243	[56] 246	[29] 546	[27] 1104	[29] 2873	[77] $0.02\ N^{1.1}$
130	Quantasoft	quantasoft	1	2018-10-30	276	[117] 2048	k	[76] 396	[135] 15422	[201] 14858	[85] 14717	-	[66] 18323	
131	Rank One Computing	rankone	0	2018-02-07	0	[12] 228	k	[6] 50	-	[22] 75	[11] 142	[10] 220	[10] 502	[15] $0.12\ N^{0.9}$
132	Rank One Computing	rankone	1	2018-02-15	0	[27] 324	k	[17] 136	-	[41] 169	-	-	-	
133	Rank One Computing	rankone	2	2018-06-19	0	[10] 133	k	[14] 113	[22] 138	[29] 137	[16] 258	[14] 517	[12] 1029	[25] $0.10\ N^{1.0}$
134	Rank One Computing	rankone	3	2018-06-19	0	[11] 133	k	[15] 114	[23] 138	[30] 137	[15] 258	[13] 515	[11] 1027	[28] $0.09\ N^{1.0}$
135	Rank One Computing	rankone	4	2018-10-09	0	[1] 85	k	[4] 36	[19] 101	[27] 101	[12] 190	-	-	[27] $0.07\ N^{1.0}$
136	Rank One Computing	rankone	5	2018-10-24	0	[9] 133	k	[12] 94	[24] 140	[36] 144	[17] 266	[15] 525	[13] 1049	[23] $0.11\ N^{1.0}$
137	RealNetworks	realnetworks	0	2018-06-21	96	[185] 4100	1	[38] 244	[123] 4257	[178] 2740	-	-	-	
138	RealNetworks	realnetworks	1	2018-06-21	105	[189] 4104	k	[37] 243	[122] 3568	[164] 2107	-	-	-	
139	RealNetworks	realnetworks	2	2018-10-30	105	[187] 4104	k	[39] 245	[107] 2006	[160] 2046	[72] 4190	[70] 8633	[62] 15020	[36] $1.08\ N^{1.0}$
140	KanKan Ai	remarkai	0	2018-10-30	187	[129] 2048	k	[127] 615	[131] 5685	[195] 5723	-	-	-	
141	KanKan Ai	remarkai	1	2018-10-30	187	[114] 2048	k	[98] 434	[130] 5680	[196] 5761	[84] 12475	[80] 28726	[76] 59618	[81] $0.37\ N^{1.2}$
142	Sensetime Group Ltd	sensetime	0	2018-10-30	525	[186] 4104	k	[162] 715	[65] 498	[100] 501	[48] 1212	[43] 2281	[40] 5032	[65] $0.09\ N^{1.1}$
143	Sensetime Group Ltd	sensetime	1	2018-10-30	525	[188] 4104	k	[143] 656	[66] 516	[101] 502	[45] 1146	[44] 2301	[37] 4765	[63] $0.09\ N^{1.1}$
144	Shaman Software	shaman	0	2018-02-12	0	[181] 4096	k	[113] 538	-	[102] 523	-	-	-	
145	Shaman Software	shaman	1	2018-02-12	0	[179] 4096	k	[121] 557	-	[103] 524	-	-	-	
146	Shaman Software	shaman	2	2018-02-12	0	[201] 8192	k	[122] 557	-	[121] 688	-	-	-	
147	Shaman Software	shaman	3	2018-06-30	0	[125] 2048	k	[155] 704	[75] 692	[77] 310	-	-	-	
148	Shaman Software	shaman	4	2018-06-30	0	[136] 2048	k	[135] 642	[61] 434	[66] 267	-	-	-	
149	Shaman Software	shaman	6	2018-10-26	0	[133] 2048	k	[157] 706	[72] 594	[115] 603	-	-	-	
150	Shaman Software	shaman	7	2018-10-26	0	[123] 2048	k	[159] 709	[71] 593	[116] 605	[46] 1169	[47] 2411	[39] 5007	[49] $0.25\ N^{1.0}$
151	Shenzhen Inst. Adv. Tech. CAS	SIAT	0	2018-02-14	306	[86] 1096	k	[67] 358	-	[147] 1343	-	-	-	
152	Shenzhen Inst. Adv. Tech. CAS	SIAT	1	2018-06-30	521	[147] 2052	1	[188] 842	[125] 4512	[186] 4402	[81] 9103	[76] 18391	[71] 38745	[44] $2.06\ N^{1.0}$
153	Shenzhen Inst. Adv. Tech. CAS	SIAT	2	2018-02-30	521	[153] 2052	1	[195] 906	[126] 5101	[189] 4884	[82] 9556	[77] 18834	[72] 39717	[45] $2.08\ N^{1.0}$
154	Smilart	smilart	0	2018-02-15	105	[64] 1024	k	[20] 168	-	[144] 1285	-	-	-	
155	Smilart	smilart	1	2018-02-15	120	[71] 1024	k	[146] 662	-	[139] 1135	-	-	-	
156	Smilart	smilart	2	2018-02-15	109	[67] 1024	k	[123] 560	-	[145] 1302	-	-	-	

Notes	
1	Configuration size does not capture static data present in libraries. Libraries are not counted because most implementations include common ancillary libraries for image processing (e.g. openCV) or numerical computation (e.g. blas).
2	This multiplier expresses the increase in template size when k images are passed to the template generation function.
3	All durations are measured on Intel®Xeon®CPU E5-2630 v4 @ 2.20GHz processors. Estimates are made by wrapping the API function call in calls to std::chrono::high_resolution_clock which on the machine in (3) counts 1ns clock ticks. Precision is somewhat worse than that however.
4	Search durations are measured as in the prior note. The power-law model in the final column mostly fits the empirical results in Figure 111. However in certain cases the model is not correct and should not be used numerically.

Table 8: Summary of algorithms and properties included in this report. The blue superscripts give ranking for the quantity in that column. Missing search durations, denoted by "-", are absent because those runs were not executed, usually because we did not run on the larger galleries. Caution: The power-law model is sometimes an incorrect model. It is included here only to show broad sublinear behavior, which is flagged in green. The models should not be used for prediction.

	DEVELOPER	SHORT	SEQ.	VALIDATION	CONFIG[1]	TEMPLATE GENERATION			SEARCH DURATION[4] MILLISEC					
	FULL NAME	NAME	NUM.	DATE	DATA (MB)	SIZE (B)	MULT[2]	TIME (MS)[3]	L=1 N=1.6M	L=50 N=1.6M	L=50 N=3M	L=50 N=6M	L=50 N=12M	POWER LAW (μs)
157	Smilart	smilart	4	2018-10-30	65	^{36}512	k	^{19}167	^{136}15879	^{202}15382	-	-	-	
158	Smilart	smilart	5	2018-10-30	562	^{130}2048	k	^{101}464	-	-	-	-	-	
159	Synesis	synesis	0	2018-02-15	332	^{38}512	k	^{36}237	-	^{40}162	-	-	-	
160	Synesis	synesis	3	2018-10-30	237	^{177}4096	k	^{13}103	^{78}784	^{125}796	^{56}1928	^{55}3861	^{48}8748	^{76}0.07 $N^{1.1}$
161	Tevian	tevian	0	2018-02-16	666	^{122}2048	1	^{75}394	-	^{90}405	-	-	-	
162	Tevian	tevian	1	2018-02-16	666	^{137}2048	1	^{79}398	-	^{87}403	-	-	-	
163	Tevian	tevian	2	2018-02-16	666	^{135}2048	1	^{77}397	-	^{86}402	-	-	-	
164	Tevian	tevian	3	2018-06-20	707	^{118}2048	1	^{54}300	^{62}473	^{106}539	-	-	-	
165	Tevian	tevian	4	2018-06-20	707	^{141}2048	1	^{53}299	^{60}434	^{105}537	-	-	-	
166	Tevian	tevian	5	2018-10-30	773	^{121}2048	1	^{85}416	^{56}405	^{92}407	^{39}852	^{36}1753	^{32}3373	^{54}0.14 $N^{1.0}$
167	TigerIT Americas LLC	tiger	0	2018-06-29	333	^{152}2052	k	^{93}428	^{102}1822	^{180}2942	-	-	-	
168	TigerIT Americas LLC	tiger	1	2018-06-27	333	^{148}2052	k	^{78}398	^{1}0	^{2}1	-	-	-	
169	TigerIT Americas LLC	tiger	2	2018-10-29	416	^{156}2052	k	^{103}464	^{101}1814	^{158}1919	^{70}3829	^{68}7519	^{60}14805	^{43}0.83 $N^{1.0}$
170	TigerIT Americas LLC	tiger	3	2018-10-30	416	^{154}2052	k	^{102}464	^{35}191	^{47}189	-	-	-	
171	TongYi Transportation Technology	tongyi	0	2018-06-29	1701	^{163}2070	k	^{26}190	^{113}2256	^{169}2272	-	-	-	
172	TongYi Transportation Technology	tongyi	1	2018-06-29	1701	^{161}2070	1	^{25}189	^{112}2238	^{168}2257	-	-	-	
173	Toshiba	toshiba	0	2018-10-30	961	^{98}1548	k	^{200}930	^{133}6147	^{197}6230	^{83}12209	^{79}25330	^{75}49398	^{79}0.36 $N^{1.2}$
174	Toshiba	toshiba	1	2018-10-30	961	^{159}2060	k	^{201}931	^{132}6001	^{198}6349	-	-	-	
175	Visidon	visidon	0	2018-06-20	208	^{76}1028	k	^{61}337	^{106}2006	^{176}2566	-	-	-	
176	Visidon	visidon	1	2018-10-30	166	^{150}2052	k	^{153}695	^{124}4357	^{187}4458	^{80}8429	^{75}17210	^{69}34185	^{35}2.40 $N^{1.0}$
177	Vigilant Solutions	vigilant	0	2018-02-08	335	^{95}1544	k	^{180}823	-	^{162}2058	-	-	-	
178	Vigilant Solutions	vigilant	1	2018-02-14	249	^{158}2056	k	^{168}739	-	^{163}2075	-	-	-	
179	Vigilant Solutions	vigilant	2	2018-02-14	335	^{97}1544	k	^{177}820	-	^{165}2121	-	-	-	
180	Vigilant Solutions	vigilant	3	2018-06-21	335	^{94}1544	k	^{185}832	^{115}2453	^{170}2307	-	-	-	
181	Vigilant Solutions	vigilant	4	2018-06-21	337	^{93}1544	k	^{183}830	^{110}2050	^{167}2251	-	-	-	
182	Vigilant Solutions	vigilant	5	2018-10-30	335	^{96}1544	k	^{173}778	-	^{152}1720	-	-	-	
183	Vigilant Solutions	vigilant	6	2018-10-30	337	^{92}1544	k	^{186}834	-	^{151}1713	-	-	-	
184	VisionLabs	visionlabs	3	2018-02-16	624	^{15}256	1	^{35}228	-	^{6}5	^{3}5	^{2}6	-	^{6}417.37 $N^{0.2}$
185	VisionLabs	visionlabs	4	2018-06-22	299	^{23}256	1	^{57}315	^{8}19	^{10}17	^{6}20	^{4}26	^{3}29	^{3}2663.29 $N^{0.1}$
186	VisionLabs	visionlabs	5	2018-06-22	305	^{35}512	1	^{55}300	^{13}54	^{16}33	^{7}37	^{8}56	^{7}88	^{10}166.84 $N^{0.4}$
187	VisionLabs	visionlabs	6	2018-10-30	360	^{40}512	1	^{50}292	^{12}36	^{18}36	^{9}39	^{7}44	^{5}53	^{5}3211.93 $N^{0.2}$
188	VisionLabs	visionlabs	7	2018-10-30	360	^{42}512	1	^{51}293	^{14}63	^{21}63	^{10}72	^{9}80	^{8}115	^{8}2076.32 $N^{0.2}$
189	Vocord	vocord	0	2018-02-16	872	^{56}608	k	^{111}536	-	^{67}268	-	-	-	
190	Vocord	vocord	1	2018-02-16	872	^{57}608	k	^{112}536	-	^{68}268	-	-	-	
191	Vocord	vocord	2	2018-02-16	924	^{119}2048	k	^{134}635	-	^{59}248	-	-	-	
192	Vocord	vocord	3	2018-06-30	627	^{59}896	k	^{161}714	^{39}215	^{58}247	-	-	-	
193	Vocord	vocord	4	2018-06-30	627	^{60}896	k	^{114}538	^{40}216	^{63}253	-	-	-	
194	Vocord	vocord	5	2018-10-30	1035	^{58}768	k	^{179}822	^{28}158	^{49}204	^{21}383	^{21}767	^{16}1466	^{32}0.12 $N^{1.0}$
195	Vocord	vocord	6	2018-10-30	1035	^{203}10240	k	^{181}825	^{30}170	^{54}216	-	-	-	
196	Zhuhai Yisheng Electronics Tech.	yisheng	0	2018-02-14	473	^{168}2108	k	^{128}615	-	^{113}587	-	-	-	
197	Zhuhai Yisheng Electronics Tech.	yisheng	1	2018-06-19	474	^{176}3704	k	^{74}387	^{111}2228	^{137}1108	-	-	-	
198	Shanghai Yitu Technology	yitu	0	2018-02-12	1774	^{191}4136	1	^{132}633	-	^{98}464	^{40}868	^{38}1769	-	^{59}0.12 $N^{1.1}$
199	Shanghai Yitu Technology	yitu	1	2018-02-12	1944	^{190}4136	1	^{199}930	-	^{97}463	-	-	-	
200	Shanghai Yitu Technology	yitu	2	2018-06-21	2077	^{193}4138	1	^{192}870	^{129}5516	^{192}5417	^{77}6101	^{73}13264	^{68}33047	^{13}9.25 $N^{0.9}$
201	Shanghai Yitu Technology	yitu	3	2018-06-21	2077	^{192}4138	1	^{193}871	^{127}5248	^{191}5242	^{78}6286	^{78}19829	^{74}45621	^{61}1.08 $N^{1.1}$
202	Shanghai Yitu Technology	yitu	4	2018-10-30	2119	^{162}2070	1	^{196}910	^{92}1288	^{142}1203	^{61}2440	^{59}5241	^{54}9671	^{46}0.52 $N^{1.0}$
203	Shanghai Yitu Technology	yitu	5	2018-10-30	2043	^{160}2070	1	^{190}861	^{90}1235	^{141}1197	^{62}2508	^{58}5003	^{53}9601	^{42}0.55 $N^{1.0}$

Notes	
1	Configuration size does not capture static data present in libraries. Libraries are not counted because most implementations include common ancillary libraries for image processing (e.g. openCV) or numerical computation (e.g. blas).
2	This multiplier expresses the increase in template size when k images are passed to the template generation function.
3	All durations are measured on Intel®Xeon®CPU E5-2630 v4 @ 2.20GHz processors. Estimates are made by wrapping the API function call in calls to std::chrono::high_resolution_clock which on the machine in (3) counts 1ns clock ticks. Precision is somewhat worse than that however.
4	Search durations are measured as in the prior note. The power-law model in the final column mostly fits the empirical results in Figure 111. However in certain cases the model is not correct and should not be used numerically.

Table 9: Summary of algorithms and properties included in this report. The blue superscripts give ranking for the quantity in that column. Missing search durations, denoted by "-", are absent because those runs were not executed, usually because we did not run on the larger galleries. Caution: The power-law model is sometimes an incorrect model. It is included here only to show broad sublinear behavior, which is flagged in green. The models should not be used for prediction.

MISSES BELOW THRESHOLD, T		ENROL LIFETIME					ENROL MOST RECENT				
FNIR(N, T> 0, R >L)		DATASET: FRVT 2018					DATASET: FRVT 2018				
#	ALGORITHM	N=0.64M	N=1.6M	N=3.0M	N=6.0M	N=12.0M	N=0.64M	N=1.6M	N=3.0M	N=6.0M	N=12.0M
1	3divi-3	^{138}0.3000	^{124}0.3499	^{62}0.3859	^{59}0.4344		^{146}0.3550	^{145}0.4023			
2	3divi-5	^{95}0.1045	^{94}0.1339				^{101}0.1382	^{101}0.1691	^{72}0.1938	^{68}0.2392	^{67}0.3087
3	alchera-0	^{85}0.0852	^{86}0.1105	^{50}0.1361	^{48}0.1913		^{95}0.1128	^{95}0.1405			
4	alchera-3	^{92}0.1018	^{92}0.1296				^{96}0.1205	^{98}0.1590	^{70}0.1891	^{69}0.2467	^{72}0.3628
5	anke-0	^{79}0.0768	^{77}0.0989				^{84}0.0968	^{83}0.1199	^{66}0.1432	^{63}0.1811	^{60}0.2624
6	aware-3	^{84}0.0846	^{78}0.0991	^{47}0.1148	^{43}0.1459		^{94}0.1122	^{93}0.1306	^{67}0.1471	^{62}0.1793	^{53}0.2395
7	aware-5	^{131}0.2628	^{118}0.2984				^{144}0.3459	^{139}0.3729	^{80}0.4094	^{77}0.4615	^{63}0.2637
8	ayonix-0	^{171}0.8262	^{139}0.8490	^{67}0.8640	^{62}0.8809		^{182}0.7795	^{180}0.8114			
9	ayonix-2	^{168}0.7602	^{137}0.8038				^{183}0.7867	^{182}0.8246	^{85}0.8511	^{81}0.8708	^{79}0.8946
10	camvi-3	^{38}0.0281	^{48}0.0509	^{35}0.0680	^{47}0.1871		^{41}0.0413	^{56}0.0736			
11	camvi-4	^{29}0.0257	^{47}0.0505				^{38}0.0393	^{57}0.0741	^{51}0.1008	^{70}0.2532	^{64}0.2731
12	cogent-0	^{51}0.0387	^{45}0.0434	^{29}0.0523	^{26}0.0784	^{13}0.1559	^{52}0.0455	^{45}0.0557	^{40}0.0734	^{43}0.1194	^{40}0.2029
13	cogent-1	^{68}0.0598	^{49}0.0513				^{51}0.0455	^{44}0.0557	^{41}0.0734	^{42}0.1194	^{39}0.2029
14	cogent-2	^{19}0.0220	^{18}0.0299	^{15}0.0390	^{25}0.0703	^{16}0.1595	^{24}0.0356	^{30}0.0475	^{31}0.0655	^{41}0.1185	^{46}0.2241
15	cogent-3	^{30}0.0258	^{27}0.0341	^{24}0.0450	^{29}0.0842	^{25}0.1864	^{27}0.0361	^{36}0.0515	^{42}0.0771	^{50}0.1374	^{56}0.2488
16	cognitec-0	^{91}0.0989	^{90}0.1256				^{103}0.1400	^{99}0.1628	^{71}0.1892	^{66}0.2205	^{66}0.2859
17	cognitec-1	^{67}0.0597	^{68}0.0777	^{41}0.0946	^{40}0.1315	^{38}0.2552	^{77}0.0832	^{77}0.1045	^{59}0.1244	^{55}0.1561	^{51}0.2338
18	cognitec-2	^{41}0.0296	^{39}0.0401	^{28}0.0523	^{31}0.0852	^{34}0.2298	^{46}0.0433	^{46}0.0560	^{35}0.0695	^{33}0.0980	^{36}0.1967
19	cognitec-3	^{39}0.0288	^{38}0.0397	^{27}0.0505	^{28}0.0837	^{32}0.2140	^{44}0.0427	^{43}0.0555	^{32}0.0679	^{31}0.0938	^{29}0.1840
20	dahua-1	^{54}0.0410	^{50}0.0521				^{60}0.0596	^{59}0.0755	^{47}0.0905	^{40}0.1179	^{33}0.1910
21	dermalog-4	^{142}0.3405	^{128}0.3892	^{64}0.4181	^{60}0.4533		^{154}0.4380	^{153}0.4813			
22	dermalog-5	^{63}0.0490	^{62}0.0649				^{74}0.0726	^{71}0.0909	^{55}0.1172	^{58}0.1618	^{59}0.2516
23	dermalog-6	^{36}0.0276	^{37}0.0383				^{42}0.0420	^{41}0.0542	^{34}0.0687	^{37}0.1004	^{28}0.1812
24	everai-0	^{57}0.0460	^{65}0.0676				^{68}0.0681	^{73}0.0921	^{57}0.1223		
25	everai-1	^{28}0.0255	^{34}0.0360				^{33}0.0383	^{37}0.0518	^{33}0.0686		
26	everai-3	^{15}0.0191	^{15}0.0256	^{11}0.0338	^{8}0.0389		^{17}0.0282	^{17}0.0377	^{18}0.0473	^{18}0.0683	^{25}0.1653
27	eyedea-3	^{137}0.2911	^{122}0.3283	^{61}0.3673	^{58}0.4154		^{145}0.3498	^{142}0.3893			
28	glory-1	^{123}0.2160	^{110}0.2447	^{56}0.2618	^{53}0.2884		^{136}0.2790	^{133}0.3067			
29	gorilla-2	^{100}0.1088	^{99}0.1379				^{108}0.1561	^{108}0.1902	^{74}0.2210	^{71}0.2625	^{71}0.3426
30	hik-2	^{101}0.1104	^{98}0.1363	^{51}0.1610	^{49}0.2061	^{41}0.3067	^{89}0.0985	^{88}0.1212			
31	hik-3	^{86}0.0885	^{85}0.1097				^{78}0.0853	^{78}0.1054	^{58}0.1228	^{54}0.1552	^{57}0.2500
32	hik-4	^{83}0.0839	^{83}0.1031	^{48}0.1225	^{46}0.1518	^{39}0.2618	^{76}0.0821	^{74}0.1013	^{56}0.1173	^{53}0.1498	^{58}0.2503
33	hik-5	^{18}0.0218	^{22}0.0308	^{18}0.0397	^{22}0.0661		^{23}0.0339	^{27}0.0467	^{26}0.0593	^{32}0.0967	^{44}0.2164
34	idemia-0	^{70}0.0645	^{69}0.0802	^{42}0.0986	^{39}0.1237	^{26}0.1872	^{81}0.0920	^{81}0.1135	^{62}0.1332	^{59}0.1628	^{45}0.2208
35	idemia-1	^{43}0.0304	^{36}0.0377	^{25}0.0465	^{18}0.0623	^{14}0.1578	^{47}0.0444	^{40}0.0540	^{29}0.0647	^{26}0.0856	^{22}0.1618
36	idemia-2	^{56}0.0453	^{54}0.0564	^{33}0.0668	^{33}0.0896	^{20}0.1706	^{49}0.0449	^{42}0.0543			
37	idemia-3	^{23}0.0238	^{21}0.0308				^{31}0.0373	^{31}0.0497	^{48}0.0927	^{73}0.2887	^{74}0.4442
38	idemia-4	^{20}0.0223	^{16}0.0276	^{10}0.0338	^{11}0.0478	^{11}0.1556	^{19}0.0326	^{19}0.0399	^{17}0.0472	^{17}0.0644	^{26}0.1659
39	idemia-5	^{33}0.0261	^{24}0.0319	^{17}0.0395	^{15}0.0588	^{22}0.1764	^{34}0.0385	^{26}0.0465	^{25}0.0562	^{25}0.0788	^{35}0.1951
40	idemia-6	^{26}0.0253	^{23}0.0316	^{14}0.0383	^{14}0.0581	^{29}0.2046	^{32}0.0377	^{24}0.0458	^{23}0.0550	^{22}0.0760	^{47}0.2242
41	imagus-2	^{164}0.6616	^{135}0.7143	^{66}0.7503	^{61}0.7867		^{177}0.7092	^{176}0.7510			
42	incode-1	^{107}0.1400	^{104}0.1796	^{54}0.2159	^{52}0.2741		^{114}0.1763	^{114}0.2143			
43	incode-3	^{89}0.0949	^{89}0.1227				^{100}0.1349	^{103}0.1703	^{73}0.1986	^{67}0.2378	^{68}0.3157
44	innovatrics-4	^{82}0.0837	^{74}0.0928				^{93}0.1106	^{94}0.1340	^{65}0.1418	^{52}0.1418	^{11}0.1418
45	isystems-0	^{61}0.0485	^{61}0.0633	^{39}0.0795	^{37}0.1057	^{30}0.2072	^{70}0.0707	^{72}0.0912			
46	isystems-1	^{59}0.0480	^{60}0.0627	^{38}0.0784	^{36}0.1054	^{31}0.2081	^{69}0.0702	^{69}0.0903			
47	isystems-2	^{52}0.0394	^{53}0.0545	^{34}0.0679			^{62}0.0612	^{62}0.0814	^{50}0.1006	^{51}0.1405	^{52}0.2374
48	isystems-3	^{42}0.0301	^{41}0.0402	^{31}0.0557	^{32}0.0881	^{28}0.1992	^{53}0.0464	^{52}0.0620	^{45}0.0840	^{46}0.1324	^{54}0.2417
49	lookman-3	^{46}0.0335	^{43}0.0425				^{30}0.0372	^{25}0.0463	^{20}0.0541	^{21}0.0758	^{24}0.1650
50	megvii-0	^{81}0.0822	^{82}0.1023	^{49}0.1228	^{44}0.1489	^{35}0.2348	^{80}0.0895	^{80}0.1086	^{61}0.1287	^{57}0.1606	^{49}0.2288
51	megvii-1						^{58}0.0586	^{58}0.0746	^{46}0.0896	^{47}0.1338	^{65}0.2761
52	microfocus-3	^{179}0.9002	^{143}0.9213	^{69}0.9342			^{188}0.9119	^{187}0.9310			
53	microfocus-5	^{182}0.9679	^{145}0.9835				^{195}0.9733	^{184}0.8361	^{86}0.8563	^{82}0.8760	^{80}0.8958
54	microsoft-0	^{16}0.0208	^{17}0.0292	^{12}0.0361	^{12}0.0536	^{10}0.1502	^{20}0.0329	^{21}0.0443	^{21}0.0544	^{23}0.0767	^{27}0.1733
55	microsoft-1	^{17}0.0214	^{19}0.0299	^{13}0.0373	^{13}0.0542	^{15}0.1585	^{22}0.0339	^{23}0.0449			
56	microsoft-2	^{25}0.0252	^{29}0.0345	^{19}0.0425	^{16}0.0600	^{12}0.1558	^{35}0.0387	^{34}0.0503			
57	microsoft-3	^{14}0.0133	^{14}0.0193				^{16}0.0223	^{16}0.0304	^{16}0.0384	^{15}0.0570	^{20}0.1603
58	microsoft-4	^{10}0.0128	^{11}0.0179	^{8}0.0241	^{9}0.0405	^{17}0.1628	^{13}0.0209	^{13}0.0288	^{15}0.0360	^{13}0.0550	^{18}0.1576
59	microsoft-5	^{9}0.0119	^{9}0.0171	^{7}0.0218	^{7}0.0387	^{18}0.1654	^{12}0.0201	^{12}0.0279	^{12}0.0347	^{12}0.0545	^{15}0.1549
60	microsoft-6	^{5}0.0058	^{5}0.0080	^{5}0.0110	^{6}0.0284	^{19}0.1664	^{5}0.0109	^{5}0.0141	^{5}0.0183	^{5}0.0343	^{13}0.1544
61	nec-0	^{60}0.0483	^{57}0.0604	^{37}0.0726	^{35}0.0989	^{36}0.2378	^{64}0.0662	^{63}0.0815	^{49}0.0961	^{44}0.1199	^{37}0.1994
62	nec-1	^{73}0.0711	^{73}0.0899				^{79}0.0889	^{79}0.1081	^{60}0.1276	^{56}0.1565	^{50}0.2311
63	nec-2	^{2}0.0018	^{2}0.0024	^{2}0.0038	^{4}0.0211	^{2}0.0991	^{1}0.0040	^{2}0.0047	^{2}0.0057	^{2}0.0190	^{2}0.0723
64	nec-3	^{1}0.0018	^{1}0.0021	^{1}0.0026	^{1}0.0113	^{1}0.0788	^{2}0.0040	^{1}0.0044	^{1}0.0049	^{1}0.0095	^{1}0.0580
65	neurotechnology-3	^{159}0.5809	^{134}0.6390				^{172}0.5959	^{172}0.6649	^{84}0.7217	^{80}0.7852	^{78}0.8336
66	neurotechnology-4	^{55}0.0427	^{55}0.0575	^{36}0.0711	^{34}0.0954	^{24}0.1845	^{55}0.0493	^{54}0.0656	^{44}0.0810	^{38}0.1167	^{42}0.2138
67	neurotechnology-5	^{50}0.0384	^{51}0.0527	^{30}0.0546	^{27}0.0811	^{7}0.1366	^{43}0.0422	^{48}0.0564	^{37}0.0705	^{36}0.0988	^{38}0.2014
68	newland-2						^{150}0.4015	^{150}0.4405	^{81}0.4719	^{78}0.5133	
69	noblis-2	^{185}0.9943	^{147}0.9959				^{199}0.9963	^{196}0.9974	^{88}0.9980	^{83}0.9986	
70	ntechlab-0	^{65}0.0518	^{63}0.0666	^{40}0.0850	^{38}0.1158		^{67}0.0677	^{64}0.0830	^{52}0.1029	^{45}0.1306	^{34}0.1948
71	ntechlab-1	^{69}0.0634	^{70}0.0818	^{43}0.1006	^{42}0.1337	^{33}0.2162	^{75}0.0803	^{76}0.1021			
72	ntechlab-3	^{45}0.0329	^{44}0.0434				^{48}0.0445	^{47}0.0561	^{36}0.0699	^{30}0.0933	^{21}0.1609

Table 10: **Identification-mode: Effect of N on FNIR at high threshold.** *Values are threshold-based miss rates i.e. FNIR at FPIR = 0.001 for five enrollment population sizes, N. The left six columns apply for enrollment of a variable number of images per subject. The right six columns apply for enrollment of one image. Missing entries usually apply because another algorithm from the same developer was run instead. Some developers are missing because less accurate algorithms were not run on galleries with* $N \geq 3\,000\,000$. *Throughout blue superscripts indicate the rank of the algorithm for that column.*

MISSES BELOW THRESHOLD, T		ENROL LIFETIME					ENROL MOST RECENT				
FNIR(N, T$>$ 0, R $>$L)		DATASET: FRVT 2018					DATASET: FRVT 2018				
#	ALGORITHM	N=0.64M	N=1.6M	N=3.0M	N=6.0M	N=12.0M	N=0.64M	N=1.6M	N=3.0M	N=6.0M	N=12.0M
73	NTECHLAB-4	^{27}0.0253	^{26}0.0337	^{20}0.0433	^{24}0.0692	^{23}0.1845	^{21}0.0337	^{20}0.0431	^{22}0.0545	^{20}0.0749	^{12}0.1528
74	NTECHLAB-5	^{35}0.0268	^{31}0.0347				^{26}0.0358	^{22}0.0448	^{24}0.0561	^{24}0.0785	^{17}0.1572
75	NTECHLAB-6	^{21}0.0227	^{20}0.0301	^{16}0.0395	^{21}0.0654	^{27}0.1897	^{18}0.0311	^{18}0.0391	^{19}0.0496	^{19}0.0696	^{14}0.1548
76	QUANTASOFT-1	^{184}0.9915	^{146}0.9915				^{173}0.6399	^{170}0.6399	^{83}0.6399		^{76}0.6399
77	RANKONE-0	^{108}0.1485	^{103}0.1788	^{55}0.2210	^{54}0.3260	^{43}0.4758	^{116}0.1899	^{115}0.2192	^{78}0.2635	^{74}0.2992	^{73}0.4301
78	RANKONE-1	^{102}0.1211	^{101}0.1549	^{53}0.1804	^{51}0.2371	^{42}0.3530	^{107}0.1542	^{100}0.1683			
79	RANKONE-2	^{77}0.0744	^{76}0.0943				^{92}0.0998	^{85}0.1200	^{64}0.1382	^{61}0.1744	^{62}0.2636
80	RANKONE-3	^{76}0.0744	^{75}0.0943	^{46}0.1120	^{45}0.1490	^{40}0.2946	^{91}0.0998	^{84}0.1200	^{63}0.1382	^{60}0.1744	^{61}0.2636
81	RANKONE-4	^{105}0.1265	^{100}0.1545				^{109}0.1631	^{109}0.1951	^{75}0.2211		
82	RANKONE-5	^{48}0.0347	^{46}0.0447	^{32}0.0571	^{30}0.0847	^{37}0.2549	^{56}0.0499	^{50}0.0617	^{38}0.0728	^{35}0.0984	^{41}0.2031
83	REALNETWORKS-0	^{119}0.2098	^{112}0.2476	^{58}0.2837			^{120}0.2003	^{119}0.2362			
84	REALNETWORKS-2	^{110}0.1688	^{106}0.2049				^{118}0.1974	^{117}0.2341	^{79}0.2691	^{75}0.3186	^{69}0.3261
85	REMARKAI-2	^{74}0.0731	^{79}0.0991				^{85}0.0971	^{91}0.1264	^{68}0.1495	^{65}0.1928	
86	SENSETIME-0	^{8}0.0118	^{8}0.0165				^{10}0.0184	^{9}0.0234	^{9}0.0296	^{9}0.0427	^{8}0.1287
87	SENSETIME-1	^{11}0.0129	^{10}0.0175				^{11}0.0186	^{11}0.0245	^{11}0.0304	^{11}0.0448	^{9}0.1344
88	SHAMAN-3	^{145}0.3506	^{129}0.3921	^{65}0.4295			^{151}0.4179	^{151}0.4527			
89	SHAMAN-7	^{88}0.0924	^{88}0.1112				^{98}0.1236	^{97}0.1436	^{69}0.1610	^{64}0.1901	^{55}0.2480
90	SIAT-1	^{132}0.2695	^{116}0.2727	^{57}0.2758			^{7}0.0160	^{6}0.0201	^{7}0.0260	^{6}0.0380	^{3}0.1069
91	SIAT-2	^{125}0.2198	^{108}0.2239				^{9}0.0179	^{10}0.0242	^{10}0.0301	^{10}0.0434	^{10}0.1377
92	SMILART-4	^{172}0.8381	^{144}0.9569				^{192}0.9260	^{191}0.9683	^{87}0.9913		
93	SYNESIS-3	^{154}0.4748	^{132}0.5296				^{164}0.5353	^{164}0.5832	^{82}0.6123	^{79}0.6489	^{77}0.6838
94	TEVIAN-4	^{72}0.0685	^{72}0.0878	^{45}0.1032			^{83}0.0952	^{86}0.1201			
95	TEVIAN-5	^{66}0.0518	^{64}0.0667				^{72}0.0717	^{68}0.0898	^{54}0.1094	^{48}0.1338	^{30}0.1873
96	TIGER-0	^{136}0.2859	^{123}0.3361	^{60}0.3659	^{57}0.4139		^{143}0.3452	^{143}0.3921			
97	TIGER-2	^{64}0.0511	^{66}0.0698				^{66}0.0671	^{66}0.0888	^{53}0.1065	^{49}0.1361	^{48}0.2284
98	TONGYITRANS-1	^{71}0.0658	^{71}0.0835	^{44}0.1017	^{41}0.1328		^{57}0.0545	^{55}0.0693			
99	TOSHIBA-0	^{49}0.0374	^{52}0.0529				^{54}0.0488	^{53}0.0648	^{43}0.0809	^{39}0.1170	^{43}0.2140
100	VD-0	^{176}0.8686	^{142}0.9048	^{68}0.9242	^{63}0.9381		^{186}0.8892	^{186}0.9171			
101	VD-1	^{106}0.1312	^{102}0.1654				^{110}0.1664	^{113}0.2036	^{77}0.2372	^{72}0.2759	^{70}0.3314
102	VIGILANTSOLUTIONS-3	^{139}0.3061	^{125}0.3568	^{63}0.3861	^{55}0.3861		^{149}0.3648	^{147}0.4097			
103	VISIONLABS-3	^{31}0.0260	^{30}0.0347	^{23}0.0444	^{23}0.0678		^{39}0.0394	^{35}0.0506	^{28}0.0629	^{29}0.0902	
104	VISIONLABS-4	^{40}0.0294	^{40}0.0402				^{50}0.0452	^{49}0.0604	^{39}0.0733	^{34}0.0982	^{31}0.1893
105	VISIONLABS-5	^{24}0.0250	^{32}0.0353	^{22}0.0441	^{19}0.0628	^{21}0.1727	^{40}0.0396	^{39}0.0531	^{30}0.0654	^{28}0.0878	^{32}0.1894
106	VISIONLABS-6	^{13}0.0131	^{13}0.0185				^{15}0.0211	^{15}0.0289	^{14}0.0359	^{16}0.0571	^{16}0.1572
107	VISIONLABS-7	^{12}0.0131	^{12}0.0185	^{9}0.0242	^{10}0.0412	^{9}0.1495	^{14}0.0211	^{14}0.0289	^{13}0.0359	^{14}0.0569	^{19}0.1576
108	VOCORD-3	^{90}0.0969	^{91}0.1295	^{52}0.1627	^{50}0.2361		^{88}0.0973	^{90}0.1258			
109	VOCORD-5	^{75}0.0735	^{84}0.1076				^{99}0.1261	^{102}0.1697	^{76}0.2327	^{76}0.3286	^{75}0.4628
110	YISHENG-1	^{130}0.2539	^{119}0.3002	^{59}0.3366	^{56}0.3892		^{138}0.3026	^{136}0.3483			
111	YITU-0	^{37}0.0279	^{33}0.0358	^{26}0.0468	^{20}0.0636	^{8}0.1389	^{36}0.0388	^{33}0.0502	^{27}0.0622	^{27}0.0862	^{23}0.1621
112	YITU-1	^{32}0.0261	^{28}0.0341	^{21}0.0434	^{17}0.0611	^{6}0.1361	^{29}0.0366	^{29}0.0472			
113	YITU-2	^{6}0.0096	^{6}0.0133	^{6}0.0174	^{5}0.0274	^{5}0.1180	^{6}0.0156	^{7}0.0204	^{6}0.0258	^{7}0.0382	^{6}0.1241
114	YITU-3	^{7}0.0103	^{7}0.0139				^{8}0.0165	^{8}0.0213	^{8}0.0266	^{8}0.0389	^{7}0.1248
115	YITU-4	^{3}0.0052	^{3}0.0074	^{3}0.0097	^{2}0.0187	^{4}0.1153	^{3}0.0093	^{3}0.0123	^{3}0.0159	^{3}0.0273	^{4}0.1107
116	YITU-5	^{4}0.0057	^{4}0.0076	^{4}0.0100	^{3}0.0188	^{3}0.1111	^{4}0.0101	^{4}0.0128	^{4}0.0163	^{4}0.0294	^{5}0.1118

Table 11: **Identification-mode: Effect of N on FNIR at high threshold.** *Values are threshold-based miss rates i.e.* FNIR *at* FPIR *= 0.001 for five enrollment population sizes, N. The left six columns apply for enrollment of a variable number of images per subject. The right six columns apply for enrollment of one image. Missing entries usually apply because another algorithm from the same developer was run instead. Some developers are missing because less accurate algorithms were not run on galleries with* $N \geq 3\,000\,000$*. Throughout blue superscripts indicate the rank of the algorithm for that column.*

MISSES NOT AT RANK 1		ENROL LIFETIME						ENROL MOST RECENT					
FNIR(N, T= 0, R =1)		DATASET: FRVT 2018						DATASET: FRVT 2018					
#	ALGORITHM	N=0.64M	N=1.6M	N=3.0M	N=6.0M	N=12.0M	aN^b	N=0.64M	N=1.6M	N=3.0M	N=6.0M	N=12.0M	aN^b
1	3DIVI-3	^{140}0.0494	^{123}0.0645	^{61}0.0759	^{57}0.0898		^{89}0.0014 N$^{0.267}$ ^{64}	^{152}0.0680	^{152}0.0857				^{88}0.0023 N$^{0.252}$ ^{98}
2	3DIVI-5	^{85}0.0100	^{86}0.0133				^{45}0.0002 N$^{0.310}$ ^{89}	^{99}0.0163	^{97}0.0202	^{66}0.0236	^{64}0.0279	^{62}0.0327	^{53}0.0007 N$^{0.239}$ ^{89}
3	ALCHERA-0	^{91}0.0106	^{82}0.0121	^{47}0.0135	^{45}0.0170		^{76}0.0006 N$^{0.207}$ ^{44}	^{100}0.0167	^{92}0.0186				^{95}0.0035 N$^{0.117}$ ^{23}
4	ALCHERA-3	^{95}0.0119	^{91}0.0159				^{50}0.0002 N$^{0.312}$ ^{90}	^{66}0.0101	^{72}0.0127	^{56}0.0146	^{56}0.0171	^{55}0.0204	^{31}0.0004 N$^{0.236}$ ^{85}
5	ANKE-0	^{71}0.0077	^{72}0.0100				^{46}0.0002 N$^{0.287}$ ^{79}	^{87}0.0128	^{86}0.0158	^{63}0.0181	^{61}0.0214	^{59}0.0251	^{46}0.0006 N$^{0.231}$ ^{82}
6	AWARE-3	^{108}0.0165	^{101}0.0209	^{52}0.0247	^{50}0.0297		^{70}0.0005 N$^{0.263}$ ^{63}	^{119}0.0264	^{116}0.0332	^{75}0.0387	^{73}0.0456	^{73}0.0532	^{69}0.0011 N$^{0.239}$ ^{90}
7	AWARE-5	^{107}0.0163	^{100}0.0208				^{68}0.0004 N$^{0.270}$ ^{67}	^{121}0.0271	^{117}0.0337	^{76}0.0392	^{74}0.0460	^{66}0.0338	^{103}0.0070 N$^{0.109}$ ^{21}
8	AYONIX-0	^{179}0.4198	^{144}0.4649	^{68}0.4969	^{63}0.5318		^{108}0.1021 N$^{0.106}$ ^{13}	^{193}0.4095	^{191}0.4519				^{113}0.0973 N$^{0.108}$ ^{20}
9	AYONIX-2	^{172}0.2192	^{137}0.2606				^{103}0.0176 N$^{0.189}$ ^{30}	^{187}0.2954	^{186}0.3432	^{86}0.3753	^{82}0.4116	^{79}0.4480	^{111}0.0449 N$^{0.142}$ ^{30}
10	CAMVI-3	^{98}0.0144	^{112}0.0368	^{57}0.0528	^{60}0.1791		^{3}0.0000 N$^{1.076}$ ^{110}	^{114}0.0224	^{140}0.0544				^{2}0.0000 N$^{0.969}$ ^{115}
11	CAMVI-4	^{75}0.0082	^{110}0.0326				^{1}0.0000 N$^{1.500}$ ^{111}	^{91}0.0145	^{137}0.0490	^{81}0.0741	^{81}0.2382	^{78}0.2386	^{1}0.0000 N$^{1.007}$ ^{116}
12	COGENT-0	^{88}0.0103	^{77}0.0106	^{41}0.0109	^{36}0.0114	^{31}0.0122	^{94}0.0047 N$^{0.057}$ ^{6}	^{86}0.0127	^{74}0.0131	^{52}0.0136	^{46}0.0141	^{44}0.0151	^{101}0.0058 N$^{0.058}$ ^{5}
13	COGENT-1	^{87}0.0103	^{76}0.0106				^{98}0.0074 N$^{0.025}$ ^{4}	^{85}0.0127	^{73}0.0131	^{51}0.0136	^{45}0.0141	^{43}0.0151	^{100}0.0058 N$^{0.058}$ ^{4}
14	COGENT-2	^{20}0.0022	^{20}0.0027	^{14}0.0032	^{12}0.0037	^{11}0.0043	^{30}0.0001 N$^{0.232}$ ^{51}	^{27}0.0054	^{26}0.0062	^{22}0.0067	^{20}0.0075	^{19}0.0085	^{55}0.0007 N$^{0.150}$ ^{33}
15	COGENT-3	^{31}0.0032	^{29}0.0037	^{17}0.0042	^{16}0.0048	^{15}0.0056	^{111}13.4494 N$^{-0.467}$ ^{1}	^{29}0.0057	^{27}0.0064	^{24}0.0069	^{22}0.0077	^{20}0.0087	^{60}0.0008 N$^{0.144}$ ^{31}
16	COGNITEC-0	^{99}0.0146	^{96}0.0189				^{29}0.0001 N$^{0.376}$ ^{106}	^{112}0.0221	^{112}0.0278	^{72}0.0323	^{71}0.0378	^{69}0.0443	^{66}0.0010 N$^{0.233}$ ^{83}
17	COGNITEC-1	^{63}0.0069	^{66}0.0089	^{40}0.0106	^{38}0.0128	^{35}0.0154	^{48}0.0002 N$^{0.275}$ ^{70}	^{78}0.0116	^{83}0.0143	^{61}0.0165	^{59}0.0192	^{57}0.0225	^{45}0.0006 N$^{0.226}$ ^{79}
18	COGNITEC-2	^{35}0.0035	^{34}0.0044	^{24}0.0052	^{23}0.0061	^{22}0.0075	^{38}0.0001 N$^{0.254}$ ^{57}	^{46}0.0074	^{42}0.0083	^{34}0.0093	^{32}0.0105	^{31}0.0121	^{57}0.0008 N$^{0.166}$ ^{44}
19	COGNITEC-3	^{42}0.0040	^{39}0.0048	^{26}0.0055	^{25}0.0064	^{23}0.0078	^{61}0.0003 N$^{0.190}$ ^{31}	^{49}0.0078	^{47}0.0088	^{37}0.0098	^{35}0.0111	^{35}0.0126	^{62}0.0009 N$^{0.164}$ ^{41}
20	DAHUA-1	^{40}0.0040	^{40}0.0049				^{44}0.0002 N$^{0.242}$ ^{55}	^{45}0.0074	^{47}0.0089	^{38}0.0102	^{38}0.0115	^{37}0.0135	^{38}0.0005 N$^{0.203}$ ^{62}
21	DERMALOG-4	^{143}0.0759	^{126}0.0961	^{64}0.1105	^{59}0.1260		^{93}0.0037 N$^{0.227}$ ^{49}	^{157}0.1040	^{157}0.1274				^{99}0.0054 N$^{0.221}$ ^{76}
22	DERMALOG-5	^{74}0.0081	^{79}0.0113				^{24}0.0001 N$^{0.353}$ ^{104}	^{90}0.0135	^{89}0.0171	^{64}0.0223	^{69}0.0312	^{71}0.0470	^{30}0.0004 N$^{0.260}$ ^{100}
23	DERMALOG-6	^{55}0.0055	^{48}0.0060				^{90}0.0015 N$^{0.095}$ ^{9}	^{63}0.0095	^{56}0.0102	^{42}0.0107	^{37}0.0115	^{33}0.0125	^{92}0.0027 N$^{0.092}$ ^{14}
24	EVERAI-0	^{61}0.0065	^{93}0.0166				^{2}0.0000 N$^{1.029}$ ^{109}	^{69}0.0102	^{99}0.0209	^{74}0.0348			^{3}0.0000 N$^{0.795}$ ^{114}
25	EVERAI-1	^{21}0.0022	^{21}0.0027				^{37}0.0001 N$^{0.222}$ ^{48}	^{20}0.0047	^{20}0.0056	^{20}0.0061			^{42}0.0005 N$^{0.166}$ ^{42}
26	EVERAI-3	^{16}0.0020	^{16}0.0023	^{11}0.0026	^{11}0.0028		^{69}0.0004 N$^{0.113}$ ^{14}	^{14}0.0041	^{15}0.0047	^{18}0.0052	^{17}0.0059	^{16}0.0066	^{36}0.0005 N$^{0.160}$ ^{39}
27	EYEDEA-3	^{139}0.0480	^{122}0.0613	^{60}0.0717	^{56}0.0831		^{91}0.0018 N$^{0.246}$ ^{56}	^{150}0.0663	^{151}0.0824				^{93}0.0028 N$^{0.238}$ ^{87}
28	GLORY-1	^{149}0.0818	^{125}0.0932	^{62}0.1007	^{58}0.1091		^{102}0.0147 N$^{0.129}$ ^{16}	^{162}0.1154	^{159}0.1291				^{109}0.0223 N$^{0.123}$ ^{26}
29	GORILLA-2	^{86}0.0102	^{87}0.0137				^{41}0.0001 N$^{0.321}$ ^{98}	^{101}0.0170	^{100}0.0220	^{70}0.0261	^{68}0.0311	^{67}0.0375	^{35}0.0005 N$^{0.269}$ ^{106}
30	HIK-2	^{104}0.0155	^{94}0.0185	^{50}0.0208	^{48}0.0240	^{42}0.0272	^{86}0.0012 N$^{0.193}$ ^{34}	^{92}0.0147	^{90}0.0172				^{78}0.0015 N$^{0.173}$ ^{47}
31	HIK-3	^{77}0.0085	^{78}0.0107				^{56}0.0003 N$^{0.255}$ ^{59}	^{77}0.0115	^{82}0.0141	^{60}0.0164	^{60}0.0194	^{58}0.0228	^{39}0.0005 N$^{0.235}$ ^{84}
32	HIK-4	^{76}0.0083	^{75}0.0104	^{44}0.0121	^{41}0.0146	^{36}0.0177	^{54}0.0003 N$^{0.260}$ ^{62}	^{76}0.0112	^{80}0.0138	^{59}0.0159	^{58}0.0188	^{56}0.0220	^{41}0.0005 N$^{0.230}$ ^{81}
33	HIK-5	^{26}0.0026	^{25}0.0034	^{16}0.0040	^{17}0.0049		^{51}0.0002 N$^{0.199}$ ^{39}	^{30}0.0057	^{29}0.0067	^{26}0.0075	^{26}0.0087	^{26}0.0103	^{28}0.0004 N$^{0.202}$ ^{60}
34	IDEMIA-0	^{48}0.0048	^{52}0.0063	^{31}0.0076	^{29}0.0095	^{27}0.0116	^{27}0.0001 N$^{0.304}$ ^{84}	^{61}0.0093	^{61}0.0113	^{49}0.0131	^{49}0.0153	^{49}0.0182	^{32}0.0004 N$^{0.227}$ ^{80}
35	IDEMIA-1	^{51}0.0049	^{53}0.0065	^{33}0.0080	^{31}0.0100	^{33}0.0124	^{22}0.0001 N$^{0.320}$ ^{97}	^{64}0.0096	^{65}0.0116	^{50}0.0135	^{53}0.0162	^{53}0.0194	^{27}0.0004 N$^{0.243}$ ^{94}
36	IDEMIA-2	^{70}0.0075	^{70}0.0099	^{43}0.0119	^{43}0.0149	^{39}0.0183	^{39}0.0001 N$^{0.304}$ ^{86}	^{72}0.0105	^{71}0.0126				^{58}0.0008 N$^{0.194}$ ^{55}
37	IDEMIA-3	^{44}0.0041	^{45}0.0054				^{26}0.0001 N$^{0.294}$ ^{82}	^{50}0.0080	^{54}0.0095	^{43}0.0110	^{43}0.0127	^{41}0.0148	^{34}0.0005 N$^{0.212}$ ^{70}
38	IDEMIA-4	^{45}0.0042	^{45}0.0052	^{27}0.0061	^{26}0.0074	^{25}0.0088	^{40}0.0001 N$^{0.257}$ ^{60}	^{51}0.0080	^{50}0.0092	^{41}0.0106	^{41}0.0124	^{40}0.0143	^{43}0.0005 N$^{0.202}$ ^{61}
39	IDEMIA-5	^{47}0.0047	^{50}0.0062	^{29}0.0073	^{28}0.0089	^{26}0.0107	^{36}0.0001 N$^{0.280}$ ^{72}	^{59}0.0090	^{59}0.0107	^{47}0.0123	^{47}0.0144	^{47}0.0169	^{37}0.0005 N$^{0.217}$ ^{74}
40	IDEMIA-6	^{56}0.0055	^{57}0.0071	^{34}0.0083	^{32}0.0100	^{30}0.0119	^{43}0.0001 N$^{0.270}$ ^{66}	^{68}0.0102	^{69}0.0122	^{55}0.0139	^{52}0.0161	^{52}0.0187	^{49}0.0006 N$^{0.209}$ ^{69}
41	IMAGUS-2	^{162}0.1470	^{133}0.1833	^{65}0.2086	^{61}0.2379		^{99}0.0083 N$^{0.215}$ ^{45}	^{176}0.1838	^{177}0.2223				^{106}0.0115 N$^{0.208}$ ^{67}
42	INCODE-1	^{83}0.0098	^{84}0.0131	^{54}0.0286	^{53}0.0466		^{4}0.0000 N$^{0.729}$ ^{108}	^{95}0.0151	^{93}0.0190				^{44}0.0005 N$^{0.250}$ ^{96}
43	INCODE-3	^{62}0.0067	^{65}0.0088				^{35}0.0001 N$^{0.308}$ ^{88}	^{80}0.0121	^{85}0.0153	^{62}0.0178	^{62}0.0215	^{60}0.0258	^{29}0.0004 N$^{0.257}$ ^{99}
44	INNOVATRICS-4	^{65}0.0070	^{61}0.0081				^{81}0.0008 N$^{0.162}$ ^{21}	^{79}0.0120	^{84}0.0149	^{58}0.0158	^{50}0.0158	^{45}0.0158	^{96}0.0040 N$^{0.088}$ ^{12}
45	ISYSTEMS-0	^{68}0.0074	^{64}0.0085	^{38}0.0095	^{35}0.0105	^{29}0.0118	^{82}0.0009 N$^{0.160}$ ^{20}	^{82}0.0122	^{77}0.0136				^{90}0.0025 N$^{0.119}$ ^{25}
46	ISYSTEMS-1	^{69}0.0074	^{63}0.0085	^{37}0.0094	^{34}0.0105	^{28}0.0118	^{83}0.0009 N$^{0.158}$ ^{19}	^{81}0.0122	^{76}0.0136				^{91}0.0025 N$^{0.118}$ ^{24}
47	ISYSTEMS-2	^{39}0.0039	^{37}0.0046	^{23}0.0052			^{66}0.0004 N$^{0.175}$ ^{26}	^{48}0.0076	^{44}0.0088	^{36}0.0096	^{34}0.0108	^{32}0.0121	^{64}0.0009 N$^{0.156}$ ^{35}
48	ISYSTEMS-3	^{33}0.0035	^{32}0.0040	^{20}0.0044	^{18}0.0050	^{16}0.0057	^{65}0.0004 N$^{0.166}$ ^{23}	^{40}0.0069	^{37}0.0075	^{30}0.0081	^{27}0.0090	^{25}0.0100	^{75}0.0012 N$^{0.129}$ ^{28}
49	LOOKMAN-3	^{78}0.0086	^{67}0.0089				^{95}0.0049 N$^{0.042}$ ^{5}	^{74}0.0109	^{62}0.0114	^{45}0.0117	^{40}0.0123	^{36}0.0131	^{97}0.0049 N$^{0.059}$ ^{8}
50	MEGVII-0	^{67}0.0072	^{71}0.0099	^{45}0.0123	^{44}0.0150	^{38}0.0182	^{32}0.0001 N$^{0.317}$ ^{94}	^{47}0.0075	^{51}0.0094	^{44}0.0111	^{44}0.0134	^{46}0.0162	^{14}0.0002 N$^{0.264}$ ^{103}
51	MEGVII-1						-	^{83}0.0124	^{78}0.0137	^{57}0.0148	^{54}0.0163	^{50}0.0182	^{87}0.0021 N$^{0.131}$ ^{29}
52	MICROFOCUS-3	^{181}0.4791	^{146}0.5389	^{69}0.5771			^{107}0.0951 N$^{0.121}$ ^{15}	^{195}0.5417	^{194}0.5953				^{114}0.1370 N$^{0.103}$ ^{19}
53	MICROFOCUS-5	^{176}0.3155	^{141}0.3701				^{104}0.0307 N$^{0.174}$ ^{25}	^{190}0.3716	^{189}0.4257	^{87}0.4624	^{83}0.5013	^{80}0.5404	^{112}0.0684 N$^{0.127}$ ^{27}
54	MICROSOFT-0	^{18}0.0021	^{19}0.0026	^{13}0.0031	^{14}0.0040	^{13}0.0048	^{16}0.0000 N$^{0.280}$ ^{73}	^{23}0.0051	^{23}0.0058	^{21}0.0066	^{21}0.0077	^{22}0.0090	^{25}0.0003 N$^{0.199}$ ^{57}
55	MICROSOFT-1	^{17}0.0020	^{18}0.0026	^{12}0.0031	^{13}0.0038	^{12}0.0047	^{14}0.0000 N$^{0.286}$ ^{78}	^{21}0.0049	^{21}0.0056				^{47}0.0006 N$^{0.158}$ ^{38}
56	MICROSOFT-2	^{22}0.0023	^{23}0.0029	^{15}0.0035	^{15}0.0042	^{14}0.0051	^{19}0.0001 N$^{0.272}$ ^{69}	^{26}0.0052	^{25}0.0061				^{40}0.0005 N$^{0.174}$ ^{48}
57	MICROSOFT-3	^{2}0.0009	^{4}0.0011				^{12}0.0000 N$^{0.255}$ ^{58}	^{3}0.0028	^{4}0.0032	^{5}0.0035	^{5}0.0039	^{4}0.0045	^{23}0.0003 N$^{0.166}$ ^{43}
58	MICROSOFT-4	^{1}0.0008	^{1}0.0010	^{3}0.0013	^{4}0.0015	^{4}0.0019	^{9}0.0000 N$^{0.285}$ ^{76}	^{2}0.0027	^{2}0.0031	^{3}0.0034	^{3}0.0038	^{3}0.0045	^{17}0.0003 N$^{0.174}$ ^{49}
59	MICROSOFT-5	^{4}0.0010	^{5}0.0013	^{5}0.0015	^{6}0.0019	^{7}0.0025	^{8}0.0000 N$^{0.304}$ ^{85}	^{4}0.0028	^{5}0.0033	^{7}0.0037	^{8}0.0044	^{8}0.0052	^{8}0.0002 N$^{0.215}$ ^{72}
60	MICROSOFT-6	^{5}0.0010	^{7}0.0014	^{7}0.0016	^{8}0.0020	^{9}0.0026	^{6}0.0000 N$^{0.317}$ ^{95}	^{5}0.0029	^{8}0.0033	^{8}0.0039	^{10}0.0045	^{9}0.0053	^{12}0.0002 N$^{0.206}$ ^{66}
61	NEC-0	^{82}0.0097	^{83}0.0127	^{48}0.0154	^{46}0.0185	^{40}0.0223	^{53}0.0002 N$^{0.284}$ ^{75}	^{96}0.0157	^{94}0.0196	^{65}0.0229	^{63}0.0270	^{61}0.0320	^{48}0.0006 N$^{0.243}$ ^{93}
62	NEC-1	^{97}0.0136	^{92}0.0164				^{85}0.0009 N$^{0.202}$ ^{42}	^{108}0.0206	^{106}0.0235	^{69}0.0259	^{67}0.0292	^{63}0.0329	^{89}0.0024 N$^{0.160}$ ^{40}
63	NEC-2	^{6}0.0010	^{3}0.0011	^{1}0.0012	^{1}0.0012	^{1}0.0014	^{57}0.0003 N$^{0.096}$ ^{11}	^{1}0.0026	^{1}0.0028	^{1}0.0029	^{1}0.0030	^{1}0.0031	^{74}0.0012 N$^{0.059}$ ^{7}
64	NEC-3	^{7}0.0012	^{6}0.0013	^{4}0.0014	^{3}0.0014	^{2}0.0016	^{73}0.0005 N$^{0.061}$ ^{7}	^{8}0.0030	^{3}0.0031	^{2}0.0032	^{2}0.0034	^{2}0.0035	^{81}0.0016 N$^{0.048}$ ^{2}
65	NEUROTECHNOLOGY-3	^{106}0.0161	^{98}0.0199				^{79}0.0007 N$^{0.234}$ ^{52}	^{107}0.0204	^{109}0.0250	^{71}0.0288	^{70}0.0331	^{68}0.0386	^{70}0.0011 N$^{0.216}$ ^{73}
66	NEUROTECHNOLOGY-4	^{52}0.0049	^{47}0.0058	^{28}0.0065	^{27}0.0075	^{24}0.0087	^{63}0.0004 N$^{0.195}$ ^{36}	^{43}0.0072	^{40}0.0082	^{33}0.0090	^{31}0.0100	^{30}0.0114	^{63}0.0009 N$^{0.156}$ ^{34}
67	NEUROTECHNOLOGY-5	^{34}0.0035	^{33}0.0042	^{19}0.0043	^{20}0.0053	^{17}0.0061	^{59}0.0003 N$^{0.184}$ ^{28}	^{34}0.0061	^{31}0.0068	^{25}0.0074	^{24}0.0082	^{23}0.0094	^{61}0.0008 N$^{0.149}$ ^{32}
68	NEWLAND-2						-	^{151}0.0671	^{150}0.0811	^{82}0.0913	^{78}0.1038		^{98}0.0050 N$^{0.195}$ ^{56}
69	NOBLIS-2	^{157}0.1261	^{132}0.1565				^{96}0.0054 N$^{0.236}$ ^{53}	^{167}0.1509	^{169}0.1816	^{84}0.2040	^{80}0.2377		^{105}0.0102 N$^{0.201}$ ^{59}
70	NTECHLAB-0	^{57}0.0056	^{59}0.0077	^{36}0.0094	^{37}0.0114	^{34}0.0139	^{25}0.0001 N$^{0.323}$ ^{99}	^{60}0.0092	^{63}0.0115	^{54}0.0137	^{55}0.0164	^{54}0.0196	^{19}0.0003 N$^{0.261}$ ^{101}
71	NTECHLAB-1	^{66}0.0070	^{69}0.0097	^{42}0.0119	^{40}0.0146	^{37}0.0179	^{31}0.0001 N$^{0.317}$ ^{96}	^{73}0.0108	^{81}0.0139				^{18}0.0003 N$^{0.278}$ ^{108}
72	NTECHLAB-3	^{37}0.0037	^{42}0.0051				^{13}0.0000 N$^{0.351}$ ^{103}	^{38}0.0065	^{41}0.0082	^{35}0.0096	^{36}0.0115	^{38}0.0135	^{15}0.0002 N$^{0.251}$ ^{97}

Table 12: **Investigation-mode: Effect of N on FNIR at rank 1** *For five enrollment population sizes, N, with T = 0 and FPIR = 1. The left five columns apply for consolidated enrollment of a variable number of lifetime images from each subject. The right five columns apply for enrollment of one recent image. Missing entries usually apply because another algorithm from the same developer was run instead. Some developers are missing because less accurate algorithms were not run on galleries with $N >$ 1 600 000. Throughout blue superscripts indicate the rank of the algorithm for that column, and yellow highlighting indicates the most accurate value. Caution: The Power-low models are mostly intended to draw attention to the kind of behavior, not as a model to be used for prediction.*

MISSES NOT AT RANK 1		ENROL LIFETIME						ENROL MOST RECENT					
FNIR(N, T= 0, R =1)		DATASET: FRVT 2018						DATASET: FRVT 2018					
#	ALGORITHM	N=0.64M	N=1.6M	N=3.0M	N=6.0M	N=12.0M	aN^b	N=0.64M	N=1.6M	N=3.0M	N=6.0M	N=12.0M	aN^b
73	NTECHLAB-4	[30] 0.0030	[31] 0.0040	[21] 0.0049	[22] 0.0060	[21] 0.0075	[15] 0.0000 $N^{0.315}$ [93]	[28] 0.0056	[33] 0.0068	[29] 0.0078	[28] 0.0092	[28] 0.0107	[20] 0.0003 $N^{0.220}$ [75]
74	NTECHLAB-5	[29] 0.0028	[30] 0.0039				[10] 0.0000 $N^{0.365}$ [105]	[24] 0.0051	[28] 0.0064	[28] 0.0076	[30] 0.0092	[29] 0.0112	[7] 0.0001 $N^{0.266}$ [104]
75	NTECHLAB-6	[24] 0.0024	[26] 0.0034	[18] 0.0042	[19] 0.0052	[18] 0.0066	[11] 0.0000 $N^{0.346}$ [102]	[19] 0.0047	[24] 0.0059	[23] 0.0069	[23] 0.0081	[24] 0.0098	[10] 0.0002 $N^{0.250}$ [95]
76	QUANTASOFT-1	[188] 0.9857	[149] 0.9857				-	[182] 0.2198	[176] 0.2198	[85] 0.2198		[76] 0.2198	[115] 0.2198 $N^{0.000}$ [1]
77	RANKONE-0	[122] 0.0255	[108] 0.0319	[55] 0.0366	[52] 0.0425	[44] 0.0486	[88] 0.0014 $N^{0.220}$ [47]	[137] 0.0375	[133] 0.0455	[80] 0.0514	[76] 0.0564	[75] 0.0654	[94] 0.0032 $N^{0.186}$ [51]
78	RANKONE-1	[102] 0.0152	[97] 0.0194	[51] 0.0224	[49] 0.0260	[43] 0.0302	[77] 0.0007 $N^{0.232}$ [50]	[115] 0.0226	[108] 0.0247				[102] 0.0062 $N^{0.097}$ [16]
79	RANKONE-2	[94] 0.0117	[89] 0.0149				[62] 0.0003 $N^{0.268}$ [65]	[106] 0.0181	[102] 0.0221	[68] 0.0250	[66] 0.0288	[65] 0.0330	[72] 0.0012 $N^{0.204}$ [65]
80	RANKONE-3	[93] 0.0117	[88] 0.0149	[49] 0.0172	[47] 0.0200	[41] 0.0236	[71] 0.0005 $N^{0.237}$ [54]	[105] 0.0181	[101] 0.0221	[67] 0.0250	[65] 0.0288	[64] 0.0330	[71] 0.0012 $N^{0.204}$ [64]
81	RANKONE-4	[119] 0.0246	[107] 0.0318				[74] 0.0006 $N^{0.282}$ [74]	[132] 0.0351	[132] 0.0441	[79] 0.0508			[77] 0.0014 $N^{0.239}$ [91]
82	RANKONE-5	[59] 0.0058	[58] 0.0072	[35] 0.0086	[33] 0.0103	[32] 0.0122	[49] 0.0002 $N^{0.258}$ [61]	[67] 0.0102	[68] 0.0120	[53] 0.0136	[51] 0.0158	[51] 0.0182	[54] 0.0007 $N^{0.201}$ [58]
83	REALNETWORKS-0	[131] 0.0337	[115] 0.0443	[56] 0.0527			[78] 0.0007 $N^{0.290}$ [80]	[127] 0.0330	[131] 0.0426				[56] 0.0008 $N^{0.280}$ [110]
84	REALNETWORKS-2	[117] 0.0240	[109] 0.0320				[64] 0.0004 $N^{0.313}$ [91]	[125] 0.0323	[125] 0.0418	[78] 0.0494	[77] 0.0587	[74] 0.0604	[82] 0.0017 $N^{0.223}$ [77]
85	REMARKAI-2	[46] 0.0047	[51] 0.0062				[23] 0.0001 $N^{0.314}$ [92]	[56] 0.0085	[58] 0.0105	[46] 0.0122	[48] 0.0145		[26] 0.0004 $N^{0.237}$ [86]
86	SENSETIME-0	[13] 0.0016	[13] 0.0018				-	[17] 0.0046	[16] 0.0048	[17] 0.0050	[14] 0.0053	[13] 0.0057	[84] 0.0018 $N^{0.071}$ [9]
87	SENSETIME-1	[12] 0.0016	[11] 0.0018				-	[16] 0.0046	[17] 0.0048	[15] 0.0050	[15] 0.0053	[14] 0.0062	[76] 0.0012 $N^{0.095}$ [15]
88	SHAMAN-3	[148] 0.0808	[127] 0.0969	[63] 0.1091			[97] 0.0060 $N^{0.195}$ [37]	[159] 0.1074	[155] 0.1266				[104] 0.0097 $N^{0.180}$ [50]
89	SHAMAN-7	[125] 0.0290	[105] 0.0310				[101] 0.0106 $N^{0.075}$ [8]	[139] 0.0397	[128] 0.0422	[77] 0.0442	[75] 0.0468	[72] 0.0499	[107] 0.0139 $N^{0.078}$ [10]
90	SIAT-1	[174] 0.2638	[138] 0.2639	[66] 0.2640			[110] 0.2618 $N^{0.001}$ [3]	[11] 0.0037	[10] 0.0039	[10] 0.0041	[9] 0.0044	[6] 0.0049	[65] 0.0010 $N^{0.098}$ [17]
91	SIAT-2	[171] 0.2127	[136] 0.2128				[109] 0.2115 $N^{0.000}$ [2]	[12] 0.0037	[11] 0.0040	[11] 0.0042	[11] 0.0045	[5] 0.0049	[67] 0.0011 $N^{0.092}$ [13]
92	SMILART-4	[186] 0.8189	[147] 0.9531				[106] 0.0894 $N^{0.166}$ [22]	[199] 0.9176	[198] 0.9649	[88] 0.9908			[116] 0.4706 $N^{0.050}$ [3]
93	SYNESIS-3	[154] 0.1133	[131] 0.1350				[100] 0.0088 $N^{0.191}$ [32]	[166] 0.1478	[167] 0.1721	[83] 0.1897	[79] 0.2108	[77] 0.2338	[108] 0.0184 $N^{0.156}$ [36]
94	TEVIAN-4	[58] 0.0058	[60] 0.0080	[39] 0.0097			[18] 0.0001 $N^{0.341}$ [101]	[71] 0.0105	[75] 0.0134				[24] 0.0003 $N^{0.264}$ [102]
95	TEVIAN-5	[43] 0.0040	[44] 0.0053				[21] 0.0001 $N^{0.307}$ [87]	[44] 0.0074	[48] 0.0092	[39] 0.0104	[42] 0.0125	[42] 0.0151	[22] 0.0003 $N^{0.240}$ [92]
96	TIGER-0	[134] 0.0364	[117] 0.0480	[58] 0.0565	[55] 0.0678		[84] 0.0009 $N^{0.278}$ [71]	[143] 0.0494	[144] 0.0638				[73] 0.0012 $N^{0.279}$ [109]
97	TIGER-2	[32] 0.0034	[35] 0.0044				[20] 0.0001 $N^{0.295}$ [83]	[35] 0.0063	[39] 0.0075	[32] 0.0088	[33] 0.0107	[34] 0.0126	[16] 0.0003 $N^{0.239}$ [88]
98	TONGYITRANS-1	[81] 0.0096	[80] 0.0114	[46] 0.0127	[42] 0.0148		[80] 0.0007 $N^{0.193}$ [33]	[52] 0.0080	[52] 0.0095				[50] 0.0006 $N^{0.189}$ [54]
99	TOSHIBA-0	[25] 0.0026	[24] 0.0033				[17] 0.0001 $N^{0.285}$ [77]	[32] 0.0058	[32] 0.0068	[27] 0.0076	[25] 0.0085	[48] 0.0178	[5] 0.0001 $N^{0.337}$ [112]
100	VD-0	[178] 0.3583	[143] 0.4303	[67] 0.4776	[62] 0.5281		[105] 0.0355 $N^{0.174}$ [24]	[192] 0.4073	[192] 0.4751				[110] 0.0431 $N^{0.168}$ [45]
101	VD-1	[113] 0.0184	[102] 0.0221				[87] 0.0012 $N^{0.201}$ [41]	[118] 0.0256	[115] 0.0302	[73] 0.0341	[72] 0.0389	[70] 0.0443	[85] 0.0021 $N^{0.188}$ [53]
102	VIGILANTSOLUTIONS-3	[136] 0.0410	[121] 0.0549	[59] 0.0654	[54] 0.0654		[92] 0.0023 $N^{0.219}$ [46]	[148] 0.0561	[148] 0.0719				[79] 0.0015 $N^{0.271}$ [107]
103	VISIONLABS-3	[36] 0.0037	[41] 0.0050	[30] 0.0076	[39] 0.0130		[5] 0.0000 $N^{0.563}$ [107]	[42] 0.0070	[46] 0.0089	[48] 0.0124	[57] 0.0185		[4] 0.0000 $N^{0.434}$ [113]
104	VISIONLABS-4	[14] 0.0016	[14] 0.0020				[34] 0.0001 $N^{0.203}$ [43]	[13] 0.0037	[13] 0.0044	[14] 0.0049	[19] 0.0062	[21] 0.0088	[6] 0.0001 $N^{0.282}$ [111]
105	VISIONLABS-5	[11] 0.0015	[12] 0.0018	[9] 0.0020	[10] 0.0028	[10] 0.0040	[7] 0.0000 $N^{0.332}$ [100]	[9] 0.0035	[12] 0.0041	[12] 0.0046	[16] 0.0054	[17] 0.0068	[11] 0.0002 $N^{0.223}$ [78]
106	VISIONLABS-6	[10] 0.0013	[9] 0.0015				[52] 0.0002 $N^{0.142}$ [18]	[7] 0.0030	[7] 0.0033	[6] 0.0037	[7] 0.0044	[12] 0.0057	[9] 0.0002 $N^{0.214}$ [71]
107	VISIONLABS-7	[8] 0.0013	[8] 0.0014	[6] 0.0016	[5] 0.0018	[5] 0.0022	[33] 0.0001 $N^{0.183}$ [27]	[6] 0.0030	[6] 0.0033	[4] 0.0035	[4] 0.0039	[7] 0.0050	[21] 0.0003 $N^{0.169}$ [46]
108	VOCORD-3	[54] 0.0053	[55] 0.0067	[32] 0.0080	[30] 0.0096		[42] 0.0001 $N^{0.271}$ [68]	[41] 0.0070	[43] 0.0085				[33] 0.0005 $N^{0.204}$ [63]
109	VOCORD-5	[49] 0.0048	[46] 0.0057				[67] 0.0004 $N^{0.187}$ [29]	[54] 0.0081	[49] 0.0092	[40] 0.0104	[39] 0.0120	[39] 0.0140	[51] 0.0006 $N^{0.188}$ [52]
110	YISHENG-1	[103] 0.0155	[99] 0.0208	[53] 0.0248	[51] 0.0298		[60] 0.0003 $N^{0.294}$ [81]	[116] 0.0227	[114] 0.0290				[52] 0.0006 $N^{0.266}$ [105]
111	YITU-0	[41] 0.0040	[38] 0.0047	[25] 0.0053	[24] 0.0061	[20] 0.0071	[55] 0.0003 $N^{0.200}$ [40]	[39] 0.0066	[36] 0.0074	[31] 0.0082	[29] 0.0092	[27] 0.0103	[59] 0.0008 $N^{0.156}$ [37]
112	YITU-1	[38] 0.0039	[36] 0.0046	[22] 0.0051	[21] 0.0059	[19] 0.0069	[58] 0.0003 $N^{0.194}$ [35]	[37] 0.0065	[35] 0.0072				[80] 0.0015 $N^{0.110}$ [22]
113	YITU-2	[9] 0.0013	[10] 0.0015	[8] 0.0017	[7] 0.0019	[6] 0.0023	[28] 0.0001 $N^{0.196}$ [38]	[15] 0.0041	[14] 0.0044	[13] 0.0047	[12] 0.0050	[11] 0.0055	[68] 0.0011 $N^{0.099}$ [18]
114	YITU-3	[19] 0.0021	[17] 0.0023				[75] 0.0006 $N^{0.098}$ [12]	[25] 0.0052	[19] 0.0054	[19] 0.0057	[18] 0.0061	[15] 0.0065	[83] 0.0017 $N^{0.081}$ [11]
115	YITU-4	[3] 0.0010	[2] 0.0011	[2] 0.0012	[2] 0.0014	[3] 0.0019	[47] 0.0002 $N^{0.130}$ [17]	[10] 0.0036	[9] 0.0037	[9] 0.0040	[6] 0.0042	[18] 0.0072	[13] 0.0002 $N^{0.208}$ [68]
116	YITU-5	[15] 0.0019	[15] 0.0020	[10] 0.0021	[9] 0.0023	[8] 0.0025	[72] 0.0005 $N^{0.096}$ [10]	[18] 0.0047	[18] 0.0048	[16] 0.0050	[13] 0.0052	[10] 0.0055	[86] 0.0021 $N^{0.058}$ [6]

Table 13: **Investigation-mode: Effect of N on FNIR at rank 1** *For five enrollment population sizes, N, with T = 0 and FPIR = 1. The left five columns apply for consolidated enrollment of a variable number of lifetime images from each subject. The right five columns apply for enrollment of one recent image. Missing entries usually apply because another algorithm from the same developer was run instead. Some developers are missing because less accurate algorithms were not run on galleries with $N >$ 1 600 000. Throughout blue superscripts indicate the rank of the algorithm for that column, and yellow highlighting indicates the most accurate value. Caution: The Power-low models are mostly intended to draw attention to the kind of behavior, not as a model to be used for prediction.*

MISSES NOT AT RANK 50		ENROL LIFETIME						ENROL MOST RECENT					
FNIR(N, T= 0, R =50)		DATASET: FRVT 2018						DATASET: FRVT 2018					
#	ALGORITHM	N=0.64M	N=1.6M	N=3.0M	N=6.0M	N=12.0M	aN^b	N=0.64M	N=1.6M	N=3.0M	N=6.0M	N=12.0M	aN^b
1	3DIVI-3	^{127}0.0103	^{116}0.0151	^{59}0.0192	^{55}0.0241		^{30}0.0001 $N^{0.382}$ ^{100}	^{136}0.0159	^{138}0.0217				^{11}0.0002 $N^{0.343}$ ^{106}
2	3DIVI-5	^{79}0.0030	^{77}0.0037				^{52}0.0001 $N^{0.237}$ ^{67}	^{91}0.0065	^{92}0.0074	^{62}0.0083	^{62}0.0094	^{60}0.0107	^{53}0.0007 $N^{0.169}$ ^{71}
3	ALCHERA-0	^{115}0.0073	^{99}0.0076	^{52}0.0079	^{49}0.0101		^{90}0.0012 $N^{0.133}$ ^{38}	^{128}0.0125	^{121}0.0129				^{109}0.0079 $N^{0.034}$ ^{13}
4	ALCHERA-3	^{78}0.0030	^{80}0.0040				^{22}0.0000 $N^{0.309}$ ^{84}	^{57}0.0047	^{64}0.0052	^{46}0.0056	^{49}0.0063	^{45}0.0070	^{62}0.0008 $N^{0.136}$ ^{60}
5	ANKE-0	^{65}0.0024	^{71}0.0030				^{48}0.0001 $N^{0.234}$ ^{65}	^{83}0.0057	^{81}0.0065	^{59}0.0072	^{57}0.0081	^{54}0.0092	^{49}0.0006 $N^{0.164}$ ^{68}
6	AWARE-3	^{93}0.0039	^{89}0.0050	^{48}0.0061	^{47}0.0077		^{38}0.0001 $N^{0.299}$ ^{81}	^{106}0.0081	^{113}0.0101	^{71}0.0118	^{69}0.0139	^{71}0.0170	^{27}0.0003 $N^{0.248}$ ^{94}
7	AWARE-5	^{94}0.0041	^{92}0.0053				^{51}0.0001 $N^{0.263}$ ^{76}	^{112}0.0088	^{115}0.0108	^{73}0.0127	^{72}0.0154	^{61}0.0115	^{79}0.0017 $N^{0.128}$ ^{54}
8	AYONIX-0	^{177}0.1723	^{143}0.2142	^{67}0.2467	^{63}0.2850		^{105}0.0085 $N^{0.225}$ ^{62}	^{193}0.1967	^{192}0.2402				^{111}0.0107 $N^{0.218}$ ^{87}
9	AYONIX-2	^{168}0.0646	^{135}0.0873				^{85}0.0008 $N^{0.329}$ ^{90}	^{186}0.0974	^{186}0.1298	^{86}0.1547	^{81}0.1850	^{78}0.2171	^{91}0.0026 $N^{0.273}$ ^{99}
10	CAMVI-3	^{134}0.0142	^{126}0.0367	^{63}0.0527	^{61}0.1789		^{4}0.0000 $N^{1.080}$ ^{108}	^{144}0.0221	^{160}0.0541				^{3}0.0000 $N^{0.980}$ ^{115}
11	CAMVI-4	^{122}0.0078	^{124}0.0323				^{1}0.0000 $N^{1.545}$ ^{111}	^{133}0.0137	^{157}0.0485	^{83}0.0736	^{82}0.2380	^{79}0.2383	^{1}0.0000 $N^{1.024}$ ^{116}
12	COGENT-0	^{55}0.0021	^{53}0.0024	^{31}0.0027	^{31}0.0031	^{33}0.0045	^{33}0.0001 $N^{0.253}$ ^{73}	^{59}0.0047	^{54}0.0050	^{41}0.0054	^{48}0.0062	^{63}0.0122	^{10}0.0001 $N^{0.288}$ ^{102}
13	COGENT-1	^{54}0.0021	^{52}0.0024				^{60}0.0002 $N^{0.189}$ ^{54}	^{58}0.0047	^{53}0.0050	^{40}0.0054	^{47}0.0062	^{62}0.0122	^{9}0.0001 $N^{0.288}$ ^{101}
14	COGENT-2	^{24}0.0011	^{27}0.0013	^{17}0.0014	^{17}0.0016	^{14}0.0017	^{63}0.0002 $N^{0.137}$ ^{40}	^{37}0.0038	^{36}0.0041	^{29}0.0042	^{28}0.0044	^{23}0.0047	^{75}0.0016 $N^{0.066}$ ^{32}
15	COGENT-3	^{35}0.0014	^{31}0.0016	^{19}0.0018	^{19}0.0020	^{17}0.0023	^{111}35.4798 $N^{-0.578}$ ^{1}	^{38}0.0040	^{40}0.0042	^{32}0.0044	^{30}0.0046	^{26}0.0048	^{77}0.0017 $N^{0.065}$ ^{30}
16	COGNITEC-0	^{92}0.0039	^{87}0.0050				^{6}0.0000 $N^{0.599}$ ^{106}	^{100}0.0076	^{103}0.0092	^{69}0.0104	^{68}0.0123	^{68}0.0148	^{39}0.0004 $N^{0.218}$ ^{86}
17	COGNITEC-1	^{67}0.0024	^{66}0.0028	^{39}0.0032	^{37}0.0037	^{32}0.0044	^{61}0.0002 $N^{0.200}$ ^{55}	^{81}0.0056	^{76}0.0060	^{57}0.0066	^{55}0.0072	^{51}0.0081	^{65}0.0010 $N^{0.128}$ ^{55}
18	COGNITEC-2	^{49}0.0020	^{43}0.0021	^{24}0.0023	^{22}0.0025	^{19}0.0027	^{74}0.0004 $N^{0.113}$ ^{33}	^{68}0.0049	^{63}0.0052	^{42}0.0054	^{38}0.0056	^{35}0.0060	^{86}0.0021 $N^{0.063}$ ^{28}
19	COGNITEC-3	^{61}0.0023	^{54}0.0025	^{29}0.0026	^{26}0.0028	^{22}0.0031	^{81}0.0007 $N^{0.086}$ ^{25}	^{75}0.0053	^{71}0.0056	^{49}0.0057	^{42}0.0060	^{40}0.0063	^{90}0.0025 $N^{0.057}$ ^{24}
20	DAHUA-1	^{53}0.0021	^{48}0.0022				^{78}0.0005 $N^{0.099}$ ^{30}	^{56}0.0046	^{50}0.0049	^{37}0.0051	^{36}0.0054	^{32}0.0058	^{73}0.0015 $N^{0.085}$ ^{40}
21	DERMALOG-4	^{139}0.0186	^{121}0.0272	^{61}0.0340	^{58}0.0427		^{55}0.0001 $N^{0.372}$ ^{98}	^{149}0.0262	^{153}0.0365				^{14}0.0002 $N^{0.363}$ ^{108}
22	DERMALOG-5	^{112}0.0066	^{107}0.0092				^{24}0.0001 $N^{0.362}$ ^{95}	^{125}0.0113	^{125}0.0142	^{78}0.0192	^{76}0.0275	^{75}0.0427	^{37}0.0004 $N^{0.248}$ ^{95}
23	DERMALOG-6	^{100}0.0046	^{84}0.0047				^{100}0.0035 $N^{0.020}$ ^{7}	^{105}0.0080	^{94}0.0081	^{63}0.0083	^{60}0.0085	^{52}0.0087	^{106}0.0053 $N^{0.030}$ ^{10}
24	EVERAI-0	^{104}0.0050	^{115}0.0150				^{3}0.0000 $N^{1.185}$ ^{109}	^{101}0.0077	^{135}0.0182	^{79}0.0317			^{2}0.0000 $N^{0.919}$ ^{114}
25	EVERAI-1	^{30}0.0013	^{29}0.0014				^{69}0.0004 $N^{0.096}$ ^{29}	^{25}0.0031	^{28}0.0033	^{21}0.0034			^{70}0.0012 $N^{0.070}$ ^{35}
26	EVERAI-3	^{28}0.0012	^{28}0.0013	^{16}0.0014	^{14}0.0014		^{79}0.0006 $N^{0.057}$ ^{16}	^{21}0.0029	^{16}0.0030	^{14}0.0032	^{15}0.0034	^{12}0.0035	^{69}0.0012 $N^{0.065}$ ^{31}
27	EYEDEA-3	^{130}0.0113	^{117}0.0160	^{60}0.0209	^{56}0.0252		^{44}0.0001 $N^{0.364}$ ^{96}	^{140}0.0175	^{139}0.0236				^{19}0.0002 $N^{0.326}$ ^{104}
28	GLORY-1	^{158}0.0415	^{129}0.0490	^{64}0.0539	^{59}0.0600		^{102}0.0047 $N^{0.164}$ ^{45}	^{173}0.0604	^{171}0.0698				^{108}0.0073 $N^{0.158}$ ^{65}
29	GORILLA-2	^{59}0.0023	^{70}0.0029				^{20}0.0000 $N^{0.289}$ ^{78}	^{70}0.0050	^{77}0.0061	^{58}0.0070	^{58}0.0084	^{56}0.0102	^{15}0.0002 $N^{0.238}$ ^{92}
30	HIK-2	^{125}0.0084	^{106}0.0090	^{53}0.0097	^{50}0.0106	^{43}0.0118	^{96}0.0018 $N^{0.115}$ ^{34}	^{111}0.0087	^{104}0.0093				^{98}0.0035 $N^{0.068}$ ^{34}
31	HIK-3	^{58}0.0023	^{64}0.0028				^{47}0.0001 $N^{0.230}$ ^{64}	^{48}0.0044	^{57}0.0051	^{50}0.0058	^{51}0.0066	^{47}0.0076	^{34}0.0003 $N^{0.189}$ ^{78}
32	HIK-4	^{64}0.0023	^{68}0.0028	^{40}0.0033	^{38}0.0039	^{35}0.0048	^{43}0.0001 $N^{0.246}$ ^{69}	^{53}0.0045	^{58}0.0051	^{51}0.0058	^{50}0.0065	^{46}0.0076	^{38}0.0004 $N^{0.175}$ ^{73}
33	HIK-5	^{13}0.0009	^{17}0.0011	^{13}0.0012	^{15}0.0014		^{56}0.0001 $N^{0.140}$ ^{42}	^{23}0.0029	^{25}0.0033	^{22}0.0035	^{20}0.0038	^{17}0.0042	^{45}0.0006 $N^{0.122}$ ^{52}
34	IDEMIA-0	^{39}0.0016	^{42}0.0019	^{25}0.0023	^{24}0.0026	^{23}0.0031	^{41}0.0001 $N^{0.226}$ ^{63}	^{55}0.0045	^{55}0.0051	^{44}0.0055	^{44}0.0060	^{44}0.0067	^{61}0.0008 $N^{0.134}$ ^{58}
35	IDEMIA-1	^{45}0.0019	^{51}0.0024	^{38}0.0029	^{36}0.0036	^{34}0.0046	^{17}0.0000 $N^{0.307}$ ^{83}	^{67}0.0049	^{74}0.0058	^{56}0.0065	^{56}0.0076	^{53}0.0089	^{33}0.0003 $N^{0.201}$ ^{83}
36	IDEMIA-2	^{82}0.0031	^{79}0.0040	^{43}0.0048	^{43}0.0058	^{40}0.0074	^{31}0.0001 $N^{0.290}$ ^{79}	^{90}0.0061	^{87}0.0069				^{66}0.0010 $N^{0.135}$ ^{59}
37	IDEMIA-3	^{46}0.0019	^{46}0.0022				^{64}0.0002 $N^{0.175}$ ^{48}	^{64}0.0049	^{65}0.0053	^{47}0.0057	^{46}0.0062	^{43}0.0067	^{67}0.0011 $N^{0.109}$ ^{49}
38	IDEMIA-4	^{37}0.0015	^{36}0.0017	^{21}0.0020	^{21}0.0023	^{20}0.0028	^{45}0.0001 $N^{0.207}$ ^{56}	^{46}0.0043	^{45}0.0046	^{36}0.0051	^{37}0.0055	^{39}0.0062	^{63}0.0008 $N^{0.121}$ ^{51}
39	IDEMIA-5	^{44}0.0018	^{49}0.0023	^{28}0.0026	^{34}0.0033	^{31}0.0042	^{18}0.0000 $N^{0.289}$ ^{77}	^{61}0.0048	^{70}0.0056	^{54}0.0062	^{54}0.0070	^{50}0.0080	^{40}0.0005 $N^{0.175}$ ^{72}
40	IDEMIA-6	^{57}0.0022	^{65}0.0028	^{41}0.0034	^{39}0.0043	^{36}0.0055	^{37}0.0001 $N^{0.258}$ ^{74}	^{76}0.0054	^{78}0.0062	^{60}0.0072	^{59}0.0084	^{57}0.0102	^{25}0.0003 $N^{0.220}$ ^{88}
41	IMAGUS-2	^{155}0.0348	^{130}0.0510	^{65}0.0641	^{60}0.0804		^{67}0.0002 $N^{0.375}$ ^{99}	^{166}0.0468	^{166}0.0657				^{32}0.0003 $N^{0.371}$ ^{109}
42	INCODE-1	^{71}0.0026	^{74}0.0033	^{58}0.0167	^{57}0.0323		^{2}0.0000 $N^{1.217}$ ^{110}	^{78}0.0055	^{79}0.0063				^{55}0.0007 $N^{0.153}$ ^{64}
43	INCODE-3	^{42}0.0017	^{44}0.0021				^{28}0.0001 $N^{0.251}$ ^{70}	^{50}0.0044	^{61}0.0052	^{48}0.0057	^{52}0.0067	^{49}0.0078	^{31}0.0003 $N^{0.194}$ ^{82}
44	INNOVATRICS-4	^{50}0.0020	^{47}0.0022				^{73}0.0004 $N^{0.118}$ ^{35}	^{72}0.0052	^{73}0.0058	^{53}0.0061	^{45}0.0061	^{38}0.0061	^{92}0.0026 $N^{0.054}$ ^{22}
45	ISYSTEMS-0	^{101}0.0048	^{88}0.0050	^{45}0.0053	^{42}0.0056	^{39}0.0060	^{94}0.0017 $N^{0.076}$ ^{21}	^{108}0.0086	^{102}0.0089				^{103}0.0048 $N^{0.044}$ ^{15}
46	ISYSTEMS-1	^{102}0.0048	^{90}0.0050	^{44}0.0053	^{41}0.0056	^{38}0.0060	^{95}0.0017 $N^{0.075}$ ^{20}	^{109}0.0086	^{101}0.0089				^{104}0.0049 $N^{0.041}$ ^{14}
47	ISYSTEMS-2	^{74}0.0026	^{62}0.0027	^{35}0.0029			^{89}0.0012 $N^{0.061}$ ^{17}	^{77}0.0054	^{72}0.0056	^{52}0.0058	^{43}0.0060	^{41}0.0063	^{93}0.0027 $N^{0.051}$ ^{20}
48	ISYSTEMS-3	^{69}0.0025	^{60}0.0026	^{30}0.0027	^{25}0.0028	^{21}0.0030	^{91}0.0012 $N^{0.053}$ ^{13}	^{73}0.0052	^{66}0.0054	^{43}0.0055	^{39}0.0057	^{33}0.0059	^{94}0.0028 $N^{0.046}$ ^{18}
49	LOOKMAN-3	^{118}0.0075	^{100}0.0077				^{103}0.0060 $N^{0.017}$ ^{6}	^{119}0.0099	^{112}0.0100	^{68}0.0101	^{64}0.0102	^{58}0.0104	^{110}0.0079 $N^{0.016}$ ^{3}
50	MEGVII-0	^{27}0.0012	^{40}0.0019	^{26}0.0025	^{33}0.0032	^{30}0.0041	^{7}0.0000 $N^{0.422}$ ^{103}	^{12}0.0026	^{20}0.0031	^{20}0.0034	^{23}0.0039	^{24}0.0048	^{12}0.0002 $N^{0.204}$ ^{84}
51	MEGVII-1						-	^{116}0.0091	^{106}0.0094	^{64}0.0097	^{63}0.0101	^{59}0.0106	^{102}0.0044 $N^{0.053}$ ^{21}
52	MICROFOCUS-3	^{179}0.2047	^{145}0.2625	^{69}0.3017			^{104}0.0070 $N^{0.252}$ ^{71}	^{195}0.2518	^{194}0.3113				^{112}0.0114 $N^{0.232}$ ^{91}
53	MICROFOCUS-5	^{174}0.1040	^{140}0.1422				^{86}0.0011 $N^{0.341}$ ^{93}	^{190}0.1322	^{190}0.1744	^{87}0.2066	^{83}0.2445	^{80}0.2829	^{101}0.0042 $N^{0.260}$ ^{96}
54	MICROSOFT-0	^{8}0.0008	^{12}0.0010	^{11}0.0011	^{11}0.0012	^{10}0.0014	^{42}0.0001 $N^{0.174}$ ^{47}	^{18}0.0028	^{19}0.0031	^{15}0.0032	^{17}0.0035	^{14}0.0037	^{58}0.0007 $N^{0.101}$ ^{45}
55	MICROSOFT-1	^{9}0.0008	^{10}0.0009	^{10}0.0011	^{10}0.0012	^{11}0.0014	^{39}0.0001 $N^{0.177}$ ^{50}	^{15}0.0028	^{15}0.0030				^{60}0.0007 $N^{0.098}$ ^{43}
56	MICROSOFT-2	^{11}0.0008	^{11}0.0010	^{9}0.0011	^{12}0.0012	^{12}0.0014	^{36}0.0001 $N^{0.186}$ ^{52}	^{20}0.0029	^{21}0.0032				^{59}0.0007 $N^{0.101}$ ^{46}
57	MICROSOFT-3	^{2}0.0004	^{4}0.0004				^{23}0.0001 $N^{0.153}$ ^{43}	^{4}0.0018	^{4}0.0019	^{4}0.0021	^{4}0.0022	^{3}0.0023	^{52}0.0006 $N^{0.078}$ ^{38}
58	MICROSOFT-4	^{1}0.0004	^{1}0.0004	^{1}0.0005	^{1}0.0005	^{1}0.0006	^{27}0.0001 $N^{0.140}$ ^{41}	^{3}0.0018	^{3}0.0019	^{3}0.0020	^{2}0.0021	^{2}0.0022	^{54}0.0007 $N^{0.070}$ ^{36}
59	MICROSOFT-5	^{3}0.0004	^{3}0.0004	^{3}0.0005	^{2}0.0005	^{2}0.0006	^{34}0.0001 $N^{0.134}$ ^{39}	^{2}0.0018	^{1}0.0018	^{1}0.0019	^{1}0.0020	^{1}0.0021	^{56}0.0007 $N^{0.067}$ ^{33}
60	MICROSOFT-6	^{4}0.0004	^{2}0.0004	^{2}0.0005	^{3}0.0006	^{3}0.0006	^{54}0.0001 $N^{0.085}$ ^{23}	^{1}0.0018	^{2}0.0019	^{2}0.0019	^{3}0.0021	^{4}0.0023	^{41}0.0005 $N^{0.091}$ ^{41}
61	NEC-0	^{60}0.0023	^{73}0.0030	^{42}0.0038	^{40}0.0047	^{37}0.0059	^{15}0.0000 $N^{0.324}$ ^{87}	^{79}0.0055	^{80}0.0064	^{61}0.0074	^{61}0.0085	^{55}0.0100	^{35}0.0003 $N^{0.205}$ ^{85}
62	NEC-1	^{119}0.0076	^{102}0.0080				^{101}0.0038 $N^{0.051}$ ^{12}	^{131}0.0135	^{122}0.0138	^{74}0.0142	^{70}0.0147	^{69}0.0154	^{107}0.0073 $N^{0.046}$ ^{16}
63	NEC-2	^{10}0.0008	^{8}0.0008	^{6}0.0009	^{5}0.0009	^{4}0.0009	^{75}0.0004 $N^{0.046}$ ^{11}	^{7}0.0022	^{5}0.0023	^{5}0.0023	^{5}0.0024	^{5}0.0025	^{72}0.0014 $N^{0.034}$ ^{12}
64	NEC-3	^{22}0.0011	^{20}0.0011	^{12}0.0011	^{9}0.0011	^{8}0.0011	^{82}0.0008 $N^{0.026}$ ^{9}	^{13}0.0026	^{12}0.0027	^{10}0.0028	^{7}0.0028	^{6}0.0029	^{81}0.0019 $N^{0.026}$ ^{5}
65	NEUROTECHNOLOGY-3	^{90}0.0038	^{91}0.0051				^{21}0.0000 $N^{0.326}$ ^{89}	^{93}0.0068	^{97}0.0083	^{65}0.0097	^{67}0.0116	^{67}0.0137	^{23}0.0003 $N^{0.243}$ ^{93}
66	NEUROTECHNOLOGY-4	^{51}0.0020	^{50}0.0024	^{32}0.0027	^{30}0.0031	^{27}0.0035	^{59}0.0002 $N^{0.189}$ ^{53}	^{60}0.0048	^{56}0.0051	^{39}0.0054	^{40}0.0057	^{37}0.0060	^{76}0.0016 $N^{0.081}$ ^{39}
67	NEUROTECHNOLOGY-5	^{40}0.0017	^{39}0.0018	^{20}0.0019	^{20}0.0021	^{16}0.0023	^{72}0.0004 $N^{0.105}$ ^{32}	^{51}0.0045	^{48}0.0047	^{35}0.0048	^{32}0.0050	^{29}0.0053	^{85}0.0021 $N^{0.055}$ ^{23}
68	NEWLAND-2						-	^{146}0.0235	^{144}0.0288	^{80}0.0332	^{78}0.0391		^{68}0.0011 $N^{0.227}$ ^{90}
69	NOBLIS-2	^{156}0.0366	^{131}0.0520				^{66}0.0002 $N^{0.383}$ ^{101}	^{162}0.0403	^{162}0.0560	^{82}0.0682	^{79}0.0940		^{24}0.0003 $N^{0.372}$ ^{110}
70	NTECHLAB-0	^{31}0.0013	^{32}0.0016	^{22}0.0021	^{23}0.0026	^{24}0.0032	^{12}0.0000 $N^{0.320}$ ^{85}	^{29}0.0033	^{31}0.0039	^{30}0.0043	^{34}0.0051	^{31}0.0058	^{22}0.0002 $N^{0.193}$ ^{81}
71	NTECHLAB-1	^{32}0.0013	^{38}0.0018	^{23}0.0022	^{27}0.0029	^{28}0.0038	^{9}0.0000 $N^{0.366}$ ^{97}	^{31}0.0034	^{35}0.0040				^{30}0.0003 $N^{0.177}$ ^{74}
72	NTECHLAB-3	^{21}0.0010	^{23}0.0012				^{25}0.0001 $N^{0.219}$ ^{59}	^{19}0.0028	^{23}0.0032	^{23}0.0035	^{22}0.0039	^{20}0.0044	^{36}0.0004 $N^{0.149}$ ^{63}

Table 14: **Investigation-mode: Effect of N on FNIR at rank 50** *For five enrollment population sizes, N, with T = 0 and FPIR = 1. The left five columns apply for consolidated enrollment of a variable number of lifetime images from each subject. The right five columns apply for enrollment of one recent image. Missing entries usually apply because another algorithm from the same developer was run instead. Some developers are missing because less accurate algorithms were not run on galleries with $N >$ 1 600 000. Throughout blue superscripts indicate the rank of the algorithm for that column, and yellow highlighting indicates the most accurate value. Caution: The Power-low models are mostly intended to draw attention to the kind of behavior, not as a model to be used for prediction.*

MISSES NOT AT RANK 50		ENROL LIFETIME						ENROL MOST RECENT					
FNIR(N, T= 0, R =50)		DATASET: FRVT 2018						DATASET: FRVT 2018					
#	ALGORITHM	N=0.64M	N=1.6M	N=3.0M	N=6.0M	N=12.0M	aN^b	N=0.64M	N=1.6M	N=3.0M	N=6.0M	N=12.0M	aN^b
73	NTECHLAB-4	[15] 0.0009	[15] 0.0010	[14] 0.0012	[13] 0.0014	[13] 0.0016	[26] 0.0001 $N^{0.208}$ [58]	[14] 0.0027	[13] 0.0030	[16] 0.0032	[16] 0.0035	[15] 0.0039	[43] 0.0005 $N^{0.120}$ [50]
74	NTECHLAB-5	[6] 0.0007	[7] 0.0008				[14] 0.0000 $N^{0.237}$ [66]	[6] 0.0021	[8] 0.0025	[8] 0.0027	[9] 0.0031	[11] 0.0035	[20] 0.0002 $N^{0.168}$ [69]
75	NTECHLAB-6	[5] 0.0006	[5] 0.0008	[5] 0.0008	[7] 0.0010	[9] 0.0012	[13] 0.0000 $N^{0.244}$ [68]	[5] 0.0021	[6] 0.0023	[7] 0.0026	[8] 0.0028	[7] 0.0032	[26] 0.0003 $N^{0.147}$ [62]
76	QUANTASOFT-1	[188] 0.9843	[149] 0.9843				-	[188] 0.1140	[184] 0.1140	[85] 0.1140		[77] 0.1140	[115] 0.1140 $N^{0.000}$ [1]
77	RANKONE-0	[116] 0.0074	[109] 0.0100	[55] 0.0120	[53] 0.0146	[44] 0.0176	[57] 0.0001 $N^{0.297}$ [80]	[130] 0.0127	[129] 0.0159	[77] 0.0185	[75] 0.0206	[73] 0.0252	[48] 0.0006 $N^{0.226}$ [89]
78	RANKONE-1	[96] 0.0042	[94] 0.0055	[51] 0.0067	[48] 0.0082	[42] 0.0100	[40] 0.0001 $N^{0.300}$ [82]	[104] 0.0078	[98] 0.0086				[83] 0.0020 $N^{0.103}$ [48]
79	RANKONE-2	[89] 0.0037	[85] 0.0047				[53] 0.0001 $N^{0.253}$ [72]	[98] 0.0075	[100] 0.0087	[67] 0.0098	[66] 0.0111	[66] 0.0128	[51] 0.0006 $N^{0.184}$ [77]
80	RANKONE-3	[88] 0.0037	[83] 0.0047	[46] 0.0055	[44] 0.0067	[41] 0.0079	[50] 0.0001 $N^{0.258}$ [75]	[97] 0.0075	[99] 0.0087	[66] 0.0098	[65] 0.0111	[65] 0.0128	[50] 0.0006 $N^{0.184}$ [76]
81	RANKONE-4	[107] 0.0058	[101] 0.0079				[35] 0.0001 $N^{0.335}$ [91]	[118] 0.0099	[120] 0.0128	[75] 0.0153			[18] 0.0002 $N^{0.284}$ [100]
82	RANKONE-5	[56] 0.0021	[55] 0.0025	[36] 0.0029	[35] 0.0034	[29] 0.0040	[49] 0.0001 $N^{0.220}$ [60]	[74] 0.0053	[75] 0.0058	[55] 0.0063	[53] 0.0069	[48] 0.0077	[64] 0.0009 $N^{0.129}$ [56]
83	REALNETWORKS-0	[108] 0.0059	[104] 0.0083	[54] 0.0108			[16] 0.0000 $N^{0.393}$ [102]	[103] 0.0077	[110] 0.0098				[17] 0.0002 $N^{0.267}$ [98]
84	REALNETWORKS-2	[95] 0.0042	[96] 0.0061				[10] 0.0000 $N^{0.423}$ [104]	[99] 0.0075	[108] 0.0098	[72] 0.0119	[71] 0.0149	[70] 0.0155	[21] 0.0002 $N^{0.262}$ [97]
85	REMARKAI-2	[34] 0.0013	[33] 0.0016				[32] 0.0001 $N^{0.224}$ [61]	[36] 0.0038	[39] 0.0042	[33] 0.0046	[33] 0.0050		[57] 0.0007 $N^{0.125}$ [53]
86	SENSETIME-0	[29] 0.0012	[26] 0.0013				-	[41] 0.0041	[38] 0.0041	[28] 0.0042	[25] 0.0043	[19] 0.0044	[95] 0.0028 $N^{0.026}$ [4]
87	SENSETIME-1	[26] 0.0011	[22] 0.0012				-	[40] 0.0040	[37] 0.0041	[27] 0.0041	[24] 0.0042	[25] 0.0048	[80] 0.0018 $N^{0.057}$ [25]
88	SHAMAN-3	[152] 0.0344	[127] 0.0404	[62] 0.0452			[99] 0.0032 $N^{0.177}$ [49]	[167] 0.0468	[161] 0.0544				[105] 0.0053 $N^{0.163}$ [67]
89	SHAMAN-7	[147] 0.0243	[120] 0.0248				[107] 0.0183 $N^{0.021}$ [8]	[160] 0.0334	[149] 0.0339	[81] 0.0344	[77] 0.0352	[74] 0.0362	[113] 0.0230 $N^{0.028}$ [7]
90	SIAT-1	[183] 0.2635	[146] 0.2635	[68] 0.2636			[110] 0.2626 $N^{0.000}$ [2]	[22] 0.0029	[14] 0.0030	[13] 0.0031	[11] 0.0032	[9] 0.0033	[74] 0.0016 $N^{0.046}$ [17]
91	SIAT-2	[181] 0.2124	[142] 0.2124				[109] 0.2116 $N^{0.000}$ [3]	[26] 0.0031	[22] 0.0032	[17] 0.0032	[13] 0.0033	[10] 0.0034	[84] 0.0020 $N^{0.032}$ [11]
92	SMILART-4	[186] 0.8160	[148] 0.9522				[108] 0.0859 $N^{0.168}$ [46]	[200] 0.9159	[199] 0.9638	[88] 0.9906			[116] 0.4632 $N^{0.051}$ [19]
93	SYNESIS-3	[165] 0.0582	[132] 0.0632				[106] 0.0174 $N^{0.090}$ [28]	[179] 0.0851	[175] 0.0891	[84] 0.0942	[80] 0.1020	[76] 0.1126	[114] 0.0231 $N^{0.096}$ [42]
94	TEVIAN-4	[47] 0.0019	[45] 0.0022	[27] 0.0025			[58] 0.0002 $N^{0.185}$ [51]	[42] 0.0041	[44] 0.0046				[47] 0.0006 $N^{0.143}$ [61]
95	TEVIAN-5	[36] 0.0014	[34] 0.0017				[62] 0.0002 $N^{0.160}$ [44]	[30] 0.0034	[30] 0.0037	[25] 0.0041	[27] 0.0044	[28] 0.0050	[44] 0.0006 $N^{0.134}$ [57]
96	TIGER-0	[109] 0.0061	[108] 0.0097	[56] 0.0125	[54] 0.0164		[11] 0.0000 $N^{0.444}$ [105]	[117] 0.0098	[123] 0.0139				[7] 0.0001 $N^{0.384}$ [112]
97	TIGER-2	[18] 0.0010	[21] 0.0012				[29] 0.0001 $N^{0.208}$ [57]	[17] 0.0028	[18] 0.0030	[19] 0.0034	[19] 0.0038	[22] 0.0045	[29] 0.0003 $N^{0.161}$ [66]
98	TONGYITRANS-1	[106] 0.0057	[95] 0.0060	[49] 0.0062	[45] 0.0067		[97] 0.0020 $N^{0.076}$ [22]	[65] 0.0049	[59] 0.0052				[88] 0.0022 $N^{0.061}$ [27]
99	TOSHIBA-0	[23] 0.0011	[24] 0.0012				[65] 0.0002 $N^{0.126}$ [37]	[34] 0.0037	[33] 0.0039	[26] 0.0041	[26] 0.0043	[64] 0.0127	[5] 0.0000 $N^{0.350}$ [107]
100	VD-0	[173] 0.1006	[139] 0.1421	[66] 0.1752	[62] 0.2147		[87] 0.0011 $N^{0.340}$ [92]	[189] 0.1248	[189] 0.1699				[71] 0.0014 $N^{0.336}$ [105]
101	VD-1	[126] 0.0098	[110] 0.0105				[98] 0.0031 $N^{0.085}$ [24]	[134] 0.0145	[128] 0.0155	[76] 0.0166	[74] 0.0179	[72] 0.0196	[99] 0.0036 $N^{0.103}$ [47]
102	VIGILANTSOLUTIONS-3	[114] 0.0072	[111] 0.0110	[57] 0.0143	[52] 0.0143		[46] 0.0001 $N^{0.322}$ [86]	[127] 0.0118	[131] 0.0166				[8] 0.0001 $N^{0.373}$ [111]
103	VISIONLABS-3	[80] 0.0030	[82] 0.0042	[50] 0.0066	[51] 0.0119		[5] 0.0000 $N^{0.612}$ [107]	[87] 0.0057	[90] 0.0073	[70] 0.0106	[73] 0.0166		[4] 0.0000 $N^{0.481}$ [113]
104	VISIONLABS-4	[20] 0.0010	[19] 0.0011				[68] 0.0002 $N^{0.103}$ [31]	[11] 0.0025	[11] 0.0027	[12] 0.0030	[21] 0.0039	[34] 0.0059	[6] 0.0000 $N^{0.290}$ [103]
105	VISIONLABS-5	[17] 0.0009	[14] 0.0010	[15] 0.0012	[16] 0.0016	[18] 0.0026	[8] 0.0000 $N^{0.341}$ [94]	[10] 0.0025	[10] 0.0026	[11] 0.0029	[14] 0.0033	[18] 0.0044	[13] 0.0002 $N^{0.192}$ [80]
106	VISIONLABS-6	[19] 0.0010	[16] 0.0010				[77] 0.0005 $N^{0.056}$ [15]	[9] 0.0023	[9] 0.0025	[9] 0.0027	[10] 0.0031	[16] 0.0040	[16] 0.0002 $N^{0.177}$ [75]
107	VISIONLABS-7	[16] 0.0009	[13] 0.0010	[8] 0.0010	[8] 0.0011	[7] 0.0011	[70] 0.0004 $N^{0.070}$ [19]	[8] 0.0023	[7] 0.0024	[6] 0.0025	[6] 0.0025	[8] 0.0032	[46] 0.0006 $N^{0.098}$ [44]
108	VOCORD-3	[63] 0.0023	[56] 0.0025	[33] 0.0028	[28] 0.0031		[76] 0.0004 $N^{0.123}$ [36]	[39] 0.0040	[41] 0.0042				[78] 0.0017 $N^{0.063}$ [29]
109	VOCORD-5	[75] 0.0027	[69] 0.0029				[92] 0.0013 $N^{0.056}$ [14]	[71] 0.0051	[68] 0.0054	[45] 0.0056	[41] 0.0060	[42] 0.0064	[82] 0.0019 $N^{0.074}$ [37]
110	YISHENG-1	[84] 0.0035	[86] 0.0047	[47] 0.0058	[46] 0.0072		[19] 0.0000 $N^{0.325}$ [88]	[95] 0.0069	[95] 0.0082				[42] 0.0005 $N^{0.191}$ [79]
111	YITU-0	[72] 0.0026	[63] 0.0027	[37] 0.0029	[32] 0.0031	[26] 0.0034	[84] 0.0008 $N^{0.090}$ [26]	[63] 0.0048	[52] 0.0049	[38] 0.0052	[35] 0.0054	[30] 0.0057	[87] 0.0021 $N^{0.060}$ [26]
112	YITU-1	[70] 0.0026	[61] 0.0027	[34] 0.0029	[29] 0.0031	[25] 0.0034	[83] 0.0008 $N^{0.090}$ [27]	[62] 0.0048	[51] 0.0049				[97] 0.0033 $N^{0.029}$ [9]
113	YITU-2	[12] 0.0008	[9] 0.0009	[7] 0.0009	[6] 0.0010	[5] 0.0010	[71] 0.0004 $N^{0.063}$ [18]	[32] 0.0034	[29] 0.0035	[24] 0.0036	[18] 0.0036	[13] 0.0037	[89] 0.0024 $N^{0.027}$ [6]
114	YITU-3	[43] 0.0018	[37] 0.0018				[88] 0.0011 $N^{0.036}$ [10]	[54] 0.0045	[46] 0.0047	[34] 0.0047	[31] 0.0048	[27] 0.0049	[96] 0.0031 $N^{0.029}$ [8]
115	YITU-4	[7] 0.0008	[6] 0.0008	[4] 0.0008	[4] 0.0008	[6] 0.0011	[80] 0.0006 $N^{0.015}$ [4]	[28] 0.0032	[24] 0.0033	[18] 0.0033	[12] 0.0033	[36] 0.0060	[28] 0.0003 $N^{0.168}$ [70]
116	YITU-5	[41] 0.0017	[35] 0.0017	[18] 0.0017	[18] 0.0017	[15] 0.0018	[93] 0.0014 $N^{0.015}$ [5]	[47] 0.0044	[42] 0.0044	[31] 0.0044	[29] 0.0044	[21] 0.0045	[100] 0.0039 $N^{0.008}$ [2]

Table 15: **Investigation-mode: Effect of N on FNIR at rank 50** *For five enrollment population sizes, N, with T = 0 and FPIR = 1. The left five columns apply for consolidated enrollment of a variable number of lifetime images from each subject. The right five columns apply for enrollment of one recent image. Missing entries usually apply because another algorithm from the same developer was run instead. Some developers are missing because less accurate algorithms were not run on galleries with $N > 1\,600\,000$. Throughout blue superscripts indicate the rank of the algorithm for that column, and yellow highlighting indicates the most accurate value. Caution: The Power-low models are mostly intended to draw attention to the kind of behavior, not as a model to be used for prediction.*

MISSES OUTSIDE RANK R		RESOURCE USAGE		ENROLL LIFETIME CONSOLIDATED = 1.6M				ENROL MOST RECENT, N = 1.6M			
FNIR(N, T=0, R)		TEMPLATE		FRVT 2018 MUGSHOTS							
#	ALGORITHM	BYTES	MSEC	R=1	R=10	R=50	WORK-10	R=1	R=10	R=50	WORK-10
1	3DIVI-0	[184]4096	[90]426				[199]10.000	[118]0.0344	[118]0.0344	[118]0.0344	[117]1.190
2	3DIVI-1	[195]4224	[94]428				[188]10.000	[119]0.0375	[119]0.0375	[119]0.0375	[123]1.233
3	3DIVI-2	[49]528	[92]428				[179]10.000	[124]0.0404	[124]0.0404	[124]0.0404	[129]1.259
4	3DIVI-3	[42]512	[130]625	[123]0.0645	[123]0.0645	[123]0.0645	[121]1.345	[152]0.0857	[152]0.0857	[152]0.0857	[148]1.469
5	3DIVI-4	[177]4096	[131]628	[85]0.0133	[85]0.0133	[85]0.0133	[82]1.069	[96]0.0201	[96]0.0201	[96]0.0201	[94]1.115
6	3DIVI-5	[182]4096	[139]653	[86]0.0133	[86]0.0133	[86]0.0133	[81]1.069	[97]0.0202	[97]0.0202	[97]0.0202	[95]1.116
7	3DIVI-6	[48]528	[138]653	[95]0.0186	[95]0.0186	[95]0.0186	[101]1.127	[110]0.0265	[110]0.0265	[110]0.0265	[115]1.186
8	ALCHERA-0	[111]2048	[42]263	[82]0.0121	[82]0.0121	[82]0.0121	[87]1.085	[92]0.0186	[92]0.0186	[92]0.0186	[104]1.138
9	ALCHERA-1	[120]2048	[8]66	[148]0.9824	[148]0.9824	[148]0.9824	[148]9.748	[199]0.9869	[199]0.9869	[199]0.9869	[199]9.812
10	ALCHERA-2	[131]2048	[16]115	[124]0.0914	[124]0.0914	[124]0.0914	[125]1.552	[153]0.0973	[153]0.0973	[153]0.0973	[152]1.567
11	ALCHERA-3	[128]2048	[117]548	[91]0.0159	[91]0.0159	[91]0.0159	[88]1.086	[72]0.0127	[72]0.0127	[72]0.0127	[66]1.074
12	ANKE-0	[165]2072	[96]431	[72]0.0100	[72]0.0100	[72]0.0100	[68]1.055	[86]0.0158	[86]0.0158	[86]0.0158	[80]1.095
13	ANKE-1	[164]2072	[97]433	[73]0.0101	[73]0.0101	[73]0.0101	[69]1.055	[87]0.0158	[87]0.0158	[87]0.0158	[82]1.096
14	AWARE-0	[100]1564	[140]653				[192]10.000	[145]0.0639	[145]0.0639	[145]0.0639	[147]1.439
15	AWARE-1	[99]1564	[136]651				[183]10.000	[141]0.0587	[141]0.0587	[141]0.0587	[143]1.382
16	AWARE-2	[167]2076	[197]912				[184]10.000	[142]0.0600	[142]0.0600	[142]0.0600	[145]1.416
17	AWARE-3	[166]2076	[163]716	[101]0.0209	[101]0.0209	[101]0.0209	[99]1.110	[116]0.0332	[116]0.0332	[116]0.0332	[116]1.186
18	AWARE-4	[2]92	[160]712	[119]0.0529	[119]0.0529	[119]0.0529	[115]1.275	[147]0.0704	[147]0.0704	[147]0.0704	[141]1.378
19	AWARE-5	[173]3100	[182]827	[100]0.0208	[100]0.0208	[100]0.0208	[98]1.110	[117]0.0337	[117]0.0337	[117]0.0337	[118]1.191
20	AWARE-6	[3]124	[175]818	[120]0.0538	[120]0.0538	[120]0.0538	[117]1.286	[149]0.0722	[149]0.0722	[149]0.0722	[144]1.394
21	AYONIX-0	[81]1036	[1]10	[144]0.4649	[144]0.4649	[144]0.4649	[144]4.268	[191]0.4519	[191]0.4519	[191]0.4519	[192]4.304
22	AYONIX-1	[82]1036	[3]12	[140]0.3364	[140]0.3364	[140]0.3364	[139]3.073	[187]0.3432	[187]0.3432	[187]0.3432	[186]3.244
23	AYONIX-2	[77]1036	[2]11	[137]0.2606	[137]0.2606	[137]0.2606	[136]2.620	[186]0.3432	[186]0.3432	[186]0.3432	[187]3.244
24	CAMVI-1	[62]1024	[24]177				[156]10.000	[179]0.2267	[179]0.2267	[179]0.2267	[176]2.419
25	CAMVI-2	[71]1024	[172]774				[173]10.000	[160]0.1292	[160]0.1292	[160]0.1292	[159]1.781
26	CAMVI-3	[73]1024	[158]707	[112]0.0368	[112]0.0368	[112]0.0368	[119]1.330	[140]0.0544	[140]0.0544	[140]0.0544	[150]1.488
27	CAMVI-4	[69]1024	[165]718	[110]0.0326	[110]0.0326	[110]0.0326	[118]1.291	[137]0.0490	[137]0.0490	[137]0.0490	[146]1.438
28	CAMVI-5	[66]1024	[170]769	[116]0.0458	[116]0.0458	[116]0.0458	[123]1.410	[146]0.0673	[146]0.0673	[146]0.0673	[153]1.602
29	COGENT-0	[46]525	[118]551	[77]0.0106	[77]0.0106	[77]0.0106	[76]1.062	[74]0.0131	[74]0.0131	[74]0.0131	[91]1.111
30	COGENT-1	[45]525	[119]552	[76]0.0106	[76]0.0106	[76]0.0106	[77]1.062	[73]0.0131	[73]0.0131	[73]0.0131	[90]1.111
31	COGENT-2	[84]1043	[203]987	[20]0.0027	[20]0.0027	[20]0.0027	[22]1.017	[26]0.0062	[26]0.0062	[26]0.0062	[30]1.045
32	COGENT-3	[83]1043	[202]960	[29]0.0037	[29]0.0037	[29]0.0037	[32]1.024	[27]0.0064	[27]0.0064	[27]0.0064	[35]1.047
33	COGNITEC-0	[154]2052	[23]176	[96]0.0189	[96]0.0189	[96]0.0189	[93]1.103	[112]0.0278	[112]0.0278	[112]0.0278	[111]1.160
34	COGNITEC-1	[150]2052	[28]202	[66]0.0089	[66]0.0089	[66]0.0089	[64]1.048	[83]0.0143	[83]0.0143	[83]0.0143	[76]1.086
35	COGNITEC-2	[157]2052	[34]227	[34]0.0044	[34]0.0044	[34]0.0044	[35]1.027	[42]0.0083	[42]0.0083	[42]0.0083	[46]1.059
36	COGNITEC-3	[148]2052	[52]297	[39]0.0048	[39]0.0048	[39]0.0048	[40]1.031	[45]0.0088	[45]0.0088	[45]0.0088	[52]1.062
37	DAHUA-0	[144]2048	[72]378	[56]0.0070	[56]0.0070	[56]0.0070	[62]1.047	[64]0.0115	[64]0.0115	[64]0.0115	[73]1.082
38	DAHUA-1	[134]2048	[68]371	[40]0.0049	[40]0.0049	[40]0.0049	[39]1.030	[47]0.0089	[47]0.0089	[47]0.0089	[45]1.058
39	DERMALOG-0	[5]128	[64]344				[170]10.000	[161]0.1309	[161]0.1309	[161]0.1309	[158]1.778
40	DERMALOG-1	[7]128	[22]171				[200]10.000	[163]0.1563	[163]0.1563	[163]0.1563	[163]1.945
41	DERMALOG-2	[23]256	[65]344				[175]10.000	[162]0.1377	[162]0.1377	[162]0.1377	[161]1.817
42	DERMALOG-3	[8]128	[31]211	[128]0.0970	[128]0.0970	[128]0.0970	[127]1.566	[158]0.1281	[158]0.1281	[158]0.1281	[157]1.752
43	DERMALOG-4	[4]128	[29]208	[126]0.0961	[126]0.0961	[126]0.0961	[126]1.561	[157]0.1274	[157]0.1274	[157]0.1274	[156]1.748
44	DERMALOG-5	[6]128	[109]532	[79]0.0113	[79]0.0113	[79]0.0113	[91]1.089	[89]0.0171	[89]0.0171	[89]0.0171	[103]1.137
45	DERMALOG-6	[15]256	[105]514	[48]0.0060	[48]0.0060	[48]0.0060	[63]1.047	[56]0.0102	[56]0.0102	[56]0.0102	[72]1.081
46	EVERAI-0	[124]2048	[99]438	[93]0.0166	[93]0.0166	[93]0.0166	[103]1.141	[99]0.0209	[99]0.0209	[99]0.0209	[112]1.174
47	EVERAI-1	[115]2048	[125]590	[21]0.0027	[21]0.0027	[21]0.0027	[21]1.017	[20]0.0056	[20]0.0056	[20]0.0056	[19]1.038
48	EVERAI-2	[139]2048	[71]377	[22]0.0029	[22]0.0029	[22]0.0029	[26]1.018	[22]0.0058	[22]0.0058	[22]0.0058	[21]1.039
49	EVERAI-3	[110]2048	[167]735	[16]0.0023	[16]0.0023	[16]0.0023	[17]1.015	[15]0.0047	[15]0.0047	[15]0.0047	[14]1.034
50	EYEDEA-0	[194]4152	[89]424				[154]10.000	[184]0.3000	[184]0.3000	[184]0.3000	[184]2.864
51	EYEDEA-1	[80]1036	[56]311				[185]10.000	[172]0.1981	[172]0.1981	[172]0.1981	[171]2.226
52	EYEDEA-2	[78]1036	[95]429				[162]10.000	[173]0.2000	[173]0.2000	[173]0.2000	[172]2.246
53	EYEDEA-3	[79]1036	[73]385	[122]0.0613	[122]0.0613	[122]0.0613	[120]1.343	[151]0.0824	[151]0.0824	[151]0.0824	[149]1.470
54	GLORY-0	[33]418	[18]160	[130]0.1335	[130]0.1335	[130]0.1335	[131]1.965	[168]0.1803	[168]0.1803	[168]0.1803	[173]2.318
55	GLORY-1	[103]1726	[81]405	[125]0.0932	[125]0.0932	[125]0.0932	[129]1.656	[159]0.1291	[159]0.1291	[159]0.1291	[162]1.925
56	GORILLA-0	[202]8300	[91]427				[172]10.000				[200]10.000
57	GORILLA-1	[170]2156	[21]169	[114]0.0414	[114]0.0414	[114]0.0414	[110]1.211	[143]0.0627	[143]0.0627	[143]0.0627	[136]1.331
58	GORILLA-2	[87]1132	[62]341	[87]0.0137	[87]0.0137	[87]0.0137	[80]1.067	[100]0.0220	[100]0.0220	[100]0.0220	[96]1.116
59	GORILLA-3	[169]2156	[124]563	[103]0.0245	[103]0.0245	[103]0.0245	[97]1.110	[121]0.0384	[121]0.0384	[121]0.0384	[114]1.178
60	HBINNO-0	[44]520	[43]265				[164]10.000	[183]0.2746	[183]0.2746	[183]0.2746	[183]2.743
61	HIK-0	[105]1808	[194]875				[151]10.000	[107]0.0236	[107]0.0236	[107]0.0236	[113]1.176
62	HIK-1	[107]1808	[178]820				[196]10.000	[91]0.0173	[91]0.0173	[91]0.0173	[97]1.116
63	HIK-2	[106]1808	[176]820	[94]0.0185	[94]0.0185	[94]0.0185	[100]1.119	[90]0.0172	[90]0.0172	[90]0.0172	[93]1.115
64	HIK-3	[90]1408	[132]633	[78]0.0107	[78]0.0107	[78]0.0107	[72]1.057	[82]0.0141	[82]0.0141	[82]0.0141	[74]1.082
65	HIK-4	[88]1152	[104]510	[75]0.0104	[75]0.0104	[75]0.0104	[70]1.055	[80]0.0138	[80]0.0138	[80]0.0138	[70]1.081
66	HIK-5	[89]1408	[129]619	[25]0.0034	[25]0.0034	[25]0.0034	[25]1.018	[29]0.0067	[29]0.0067	[29]0.0067	[27]1.043
67	HIK-6	[91]1408	[126]610	[27]0.0034	[27]0.0034	[27]0.0034	[24]1.018	[30]0.0067	[30]0.0067	[30]0.0067	[28]1.043
68	IDEMIA-0	[31]364	[85]416	[52]0.0063	[52]0.0063	[52]0.0063	[47]1.034	[61]0.0113	[61]0.0113	[61]0.0113	[61]1.070
69	IDEMIA-1	[32]364	[88]417	[53]0.0065	[53]0.0065	[53]0.0065	[49]1.035	[65]0.0116	[65]0.0116	[65]0.0116	[63]1.072
70	IDEMIA-2	[30]364	[87]417	[70]0.0099	[70]0.0099	[70]0.0099	[71]1.056	[71]0.0126	[71]0.0126	[71]0.0126	[71]1.081
71	IDEMIA-3	[50]528	[149]689	[45]0.0054	[45]0.0054	[45]0.0054	[45]1.033	[54]0.0095	[54]0.0095	[54]0.0095	[57]1.066
72	IDEMIA-4	[47]528	[147]669	[43]0.0052	[43]0.0052	[43]0.0052	[38]1.029	[50]0.0092	[50]0.0092	[50]0.0092	[49]1.061

Table 16: **Rank-based accuracy for the FRVT 2018 mugshot sets**. *In columns 3 and 4 are template size and template generation duration. Thereafter values are rank-based FNIR with T = 0 and FPIR = 1. This is appropriate to investigational uses but not those with higher volumes where candidates from all searches would need review. Columns 5 - 9 show FRVT 2018 accuracy for various ranks for galleries unenrolled with all lifetime images. Column 10 is a workload statistic, a small value shows an algorithm front-loads mates into the first 10 candidates. The last four columns gives analogous results for enrollment only of the most recent image - see Figure 8. Throughout, blue superscripts indicate the rank of the algorithm for that column, and the best value is highlighted in yellow.*

MISSES OUTSIDE RANK R		RESOURCE USAGE		ENROLL LIFETIME CONSOLIDATED = 1.6M				ENROL MOST RECENT, N = 1.6M			
FNIR(N, T=0, R)		TEMPLATE		FRVT 2018 MUGSHOTS							
#	ALGORITHM	BYTES	MSEC	R=1	R=10	R=50	WORK-10	R=1	R=10	R=50	WORK-10
73	IDEMIA-5	[29] 352	[70] 374	[50] 0.0062	[50] 0.0062	[50] 0.0062	[46] 1.034	[59] 0.0107	[59] 0.0107	[59] 0.0107	[58] 1.068
74	IDEMIA-6	[28] 352	[69] 373	[57] 0.0071	[57] 0.0071	[57] 0.0071	[55] 1.039	[69] 0.0122	[69] 0.0122	[69] 0.0122	[67] 1.075
75	IMAGUS-0	[43] 512	[5] 43				[198] 10.000	[185] 0.3054	[185] 0.3054	[185] 0.3054	[185] 2.977
76	IMAGUS-2	[37] 512	[9] 76	[133] 0.1833	[133] 0.1833	[133] 0.1833	[133] 2.070	[177] 0.2223	[177] 0.2223	[177] 0.2223	[174] 2.329
77	IMAGUS-3	[41] 512	[7] 57	[139] 0.3008	[139] 0.3008	[139] 0.3008	[138] 2.951	[188] 0.3576	[188] 0.3576	[188] 0.3576	[188] 3.380
78	INCODE-0	[67] 1024	[26] 190	[113] 0.0376	[113] 0.0376	[113] 0.0376	[109] 1.201	[139] 0.0515	[139] 0.0515	[139] 0.0515	[132] 1.285
79	INCODE-1	[127] 2048	[151] 690	[84] 0.0131	[84] 0.0131	[84] 0.0131	[78] 1.066	[93] 0.0190	[93] 0.0190	[93] 0.0190	[88] 1.106
80	INCODE-2	[122] 2048	[49] 291	[81] 0.0120	[81] 0.0120	[81] 0.0120	[75] 1.060	[98] 0.0203	[98] 0.0203	[98] 0.0203	[92] 1.113
81	INCODE-3	[117] 2048	[155] 704	[65] 0.0088	[65] 0.0088	[65] 0.0088	[60] 1.044	[85] 0.0153	[85] 0.0153	[85] 0.0153	[75] 1.086
82	INNOVATRICS-0	[54] 530	[100] 455				[186] 10.000	[127] 0.0421	[127] 0.0421	[127] 0.0421	[125] 1.234
83	INNOVATRICS-1	[52] 530	[58] 316				[182] 10.000	[126] 0.0421	[126] 0.0421	[126] 0.0421	[124] 1.234
84	INNOVATRICS-2	[53] 530	[41] 255	[118] 0.0499	[118] 0.0499	[118] 0.0499	[122] 1.354	[136] 0.0475	[136] 0.0475	[136] 0.0475	[140] 1.343
85	INNOVATRICS-3	[51] 530	[40] 255	[104] 0.0301	[104] 0.0301	[104] 0.0301	[104] 1.147	[113] 0.0287	[113] 0.0287	[113] 0.0287	[108] 1.151
86	INNOVATRICS-4	[85] 1076	[83] 406	[61] 0.0081	[61] 0.0081	[61] 0.0081	[59] 1.042	[84] 0.0149	[84] 0.0149	[84] 0.0149	[77] 1.087
87	ISYSTEMS-0	[141] 2048	[33] 222	[64] 0.0085	[64] 0.0085	[64] 0.0085	[74] 1.059	[77] 0.0136	[77] 0.0136	[77] 0.0136	[83] 1.098
88	ISYSTEMS-1	[64] 1024	[32] 222	[63] 0.0085	[63] 0.0085	[63] 0.0085	[73] 1.058	[76] 0.0136	[76] 0.0136	[76] 0.0136	[84] 1.098
89	ISYSTEMS-2	[137] 2048	[59] 316	[37] 0.0046	[37] 0.0046	[37] 0.0046	[44] 1.032	[44] 0.0088	[44] 0.0088	[44] 0.0088	[53] 1.062
90	ISYSTEMS-3	[113] 2048	[189] 856	[32] 0.0040	[32] 0.0040	[32] 0.0040	[37] 1.029	[37] 0.0075	[37] 0.0075	[37] 0.0075	[43] 1.057
91	LOOKMAN-3	[26] 292	[63] 342	[67] 0.0089	[67] 0.0089	[67] 0.0089	[85] 1.074	[62] 0.0114	[62] 0.0114	[62] 0.0114	[79] 1.095
92	LOOKMAN-4	[55] 548	[60] 325	[68] 0.0091	[68] 0.0091	[68] 0.0091	[86] 1.074	[66] 0.0117	[66] 0.0117	[66] 0.0117	[81] 1.096
93	MEGVII-0	[118] 2048	[174] 794	[71] 0.0099	[71] 0.0099	[71] 0.0099	[65] 1.048	[51] 0.0094	[51] 0.0094	[51] 0.0094	[39] 1.052
94	MEGVII-1	[178] 4096	[137] 652				[159] 10.000	[78] 0.0137	[78] 0.0137	[78] 0.0137	[86] 1.102
95	MEGVII-2	[180] 4096	[143] 656				[176] 10.000	[79] 0.0137	[79] 0.0137	[79] 0.0137	[87] 1.102
96	MICROFOCUS-0	[18] 256	[106] 525				[168] 10.000	[195] 0.5972	[195] 0.5972	[195] 0.5972	[195] 5.397
97	MICROFOCUS-1	[24] 256	[107] 527				[180] 10.000	[196] 0.5972	[196] 0.5972	[196] 0.5972	[196] 5.398
98	MICROFOCUS-2	[22] 256	[108] 529				[174] 10.000	[197] 0.6272	[197] 0.6272	[197] 0.6272	[197] 5.839
99	MICROFOCUS-3	[21] 256	[46] 269	[146] 0.5389	[146] 0.5389	[146] 0.5389	[146] 4.849	[194] 0.5953	[194] 0.5953	[194] 0.5953	[194] 5.373
100	MICROFOCUS-4	[20] 256	[47] 270	[145] 0.5191	[145] 0.5191	[145] 0.5191	[145] 4.688	[193] 0.5775	[193] 0.5775	[193] 0.5775	[193] 5.212
101	MICROFOCUS-5	[16] 256	[45] 266	[141] 0.3701	[141] 0.3701	[141] 0.3701	[141] 3.437	[189] 0.4257	[189] 0.4257	[189] 0.4257	[189] 3.877
102	MICROFOCUS-6	[17] 256	[44] 265	[142] 0.3732	[142] 0.3732	[142] 0.3732	[142] 3.453	[190] 0.4283	[190] 0.4283	[190] 0.4283	[190] 3.897
103	MICROSOFT-0	[36] 512	[48] 283	[19] 0.0026	[19] 0.0026	[19] 0.0026	[16] 1.015	[23] 0.0058	[23] 0.0058	[23] 0.0058	[20] 1.038
104	MICROSOFT-1	[74] 1024	[66] 349	[18] 0.0026	[18] 0.0026	[18] 0.0026	[15] 1.015	[21] 0.0056	[21] 0.0056	[21] 0.0056	[18] 1.038
105	MICROSOFT-2	[63] 1024	[120] 555	[23] 0.0029	[23] 0.0029	[23] 0.0029	[20] 1.016	[25] 0.0061	[25] 0.0061	[25] 0.0061	[25] 1.041
106	MICROSOFT-3	[72] 1024	[80] 404	[4] 0.0011	[4] 0.0011	[4] 0.0011	[2] 1.007	[4] 0.0032	[4] 0.0032	[4] 0.0032	[3] 1.022
107	MICROSOFT-4	[123] 2048	[171] 773	[1] 0.0010	[1] 0.0010	[1] 0.0010	[1] 1.006	[2] 0.0031	[2] 0.0031	[2] 0.0031	[2] 1.022
108	MICROSOFT-5	[70] 1024	[148] 673	[5] 0.0013	[5] 0.0013	[5] 0.0013	[3] 1.007	[5] 0.0033	[5] 0.0033	[5] 0.0033	[1] 1.021
109	MICROSOFT-6	[68] 1024	[152] 695	[7] 0.0014	[7] 0.0014	[7] 0.0014	[4] 1.007	[8] 0.0033	[8] 0.0033	[8] 0.0033	[4] 1.023
110	NEC-0	[172] 2592	[10] 82	[83] 0.0127	[83] 0.0127	[83] 0.0127	[79] 1.066	[94] 0.0196	[94] 0.0196	[94] 0.0196	[89] 1.110
111	NEC-1	[171] 2592	[11] 88	[92] 0.0164	[92] 0.0164	[92] 0.0164	[92] 1.101	[106] 0.0235	[106] 0.0235	[106] 0.0235	[110] 1.158
112	NEC-2	[101] 1616	[141] 653	[3] 0.0011	[3] 0.0011	[3] 0.0011	[6] 1.009	[1] 0.0028	[1] 0.0028	[1] 0.0028	[5] 1.023
113	NEC-3	[102] 1712	[150] 690	[6] 0.0013	[6] 0.0013	[6] 0.0013	[9] 1.011	[3] 0.0031	[3] 0.0031	[3] 0.0031	[8] 1.026
114	NEUROTECHNOLOGY-0	[197] 5214	[154] 702				[171] 10.000	[138] 0.0497	[138] 0.0497	[138] 0.0497	[131] 1.278
115	NEUROTECHNOLOGY-1	[199] 5214	[145] 661				[195] 10.000	[135] 0.0467	[135] 0.0467	[135] 0.0467	[128] 1.250
116	NEUROTECHNOLOGY-2	[198] 5214	[144] 658				[193] 10.000	[134] 0.0465	[134] 0.0465	[134] 0.0465	[127] 1.249
117	NEUROTECHNOLOGY-3	[136] 2048	[116] 547	[98] 0.0199	[98] 0.0199	[98] 0.0199	[95] 1.108	[109] 0.0250	[109] 0.0250	[109] 0.0250	[106] 1.148
118	NEUROTECHNOLOGY-4	[142] 2048	[115] 543	[47] 0.0058	[47] 0.0058	[47] 0.0058	[52] 1.037	[40] 0.0082	[40] 0.0082	[40] 0.0082	[44] 1.058
119	NEUROTECHNOLOGY-5	[19] 256	[84] 412	[33] 0.0042	[33] 0.0042	[33] 0.0042	[34] 1.026	[31] 0.0068	[31] 0.0068	[31] 0.0068	[37] 1.050
120	NEUROTECHNOLOGY-6	[13] 256	[169] 746	[90] 0.0153	[90] 0.0153	[90] 0.0153	[83] 1.070	[95] 0.0201	[95] 0.0201	[95] 0.0201	[85] 1.102
121	NEWLAND-2	[116] 2048	[191] 868				[157] 10.000	[150] 0.0811	[150] 0.0811	[150] 0.0811	[151] 1.491
122	NOBLIS-1	[140] 2048	[30] 211	[135] 0.2049	[135] 0.2049	[135] 0.2049	[135] 2.390	[181] 0.2512	[181] 0.2512	[181] 0.2512	[181] 2.698
123	NOBLIS-2	[200] 6144	[110] 535	[132] 0.1565	[132] 0.1565	[132] 0.1565	[132] 1.967	[169] 0.1816	[169] 0.1816	[169] 0.1816	[166] 2.098
124	NTECHLAB-0	[196] 4442	[166] 730	[59] 0.0077	[59] 0.0077	[59] 0.0077	[53] 1.038	[63] 0.0115	[63] 0.0115	[63] 0.0115	[55] 1.064
125	NTECHLAB-1	[104] 1736	[82] 405	[69] 0.0097	[69] 0.0097	[69] 0.0097	[61] 1.046	[81] 0.0139	[81] 0.0139	[81] 0.0139	[65] 1.074
126	NTECHLAB-3	[174] 3484	[184] 831	[42] 0.0051	[42] 0.0051	[42] 0.0051	[33] 1.024	[41] 0.0082	[41] 0.0082	[41] 0.0082	[34] 1.047
127	NTECHLAB-4	[175] 3484	[198] 929	[31] 0.0040	[31] 0.0040	[31] 0.0040	[29] 1.019	[33] 0.0068	[33] 0.0068	[33] 0.0068	[24] 1.041
128	NTECHLAB-5	[108] 1940	[164] 717	[30] 0.0039	[30] 0.0039	[30] 0.0039	[27] 1.018	[28] 0.0064	[28] 0.0064	[28] 0.0064	[17] 1.037
129	NTECHLAB-6	[109] 1940	[187] 841	[26] 0.0034	[26] 0.0034	[26] 0.0034	[18] 1.015	[24] 0.0059	[24] 0.0059	[24] 0.0059	[15] 1.034
130	QUANTASOFT-1	[125] 2048	[76] 396	[149] 0.9857	[149] 0.9857	[149] 0.9857	[149] 9.866	[176] 0.2198	[176] 0.2198	[176] 0.2198	[180] 2.559
131	RANKONE-0	[12] 228	[6] 50	[108] 0.0319	[108] 0.0319	[108] 0.0319	[108] 1.188	[133] 0.0455	[133] 0.0455	[133] 0.0455	[130] 1.275
132	RANKONE-1	[27] 324	[17] 136	[97] 0.0194	[97] 0.0194	[97] 0.0194	[96] 1.109	[108] 0.0247	[108] 0.0247	[108] 0.0247	[105] 1.145
133	RANKONE-2	[11] 133	[14] 113	[89] 0.0149	[89] 0.0149	[89] 0.0149	[90] 1.086	[102] 0.0221	[102] 0.0221	[102] 0.0221	[102] 1.135
134	RANKONE-3	[9] 133	[15] 114	[88] 0.0149	[88] 0.0149	[88] 0.0149	[89] 1.086	[101] 0.0221	[101] 0.0221	[101] 0.0221	[101] 1.135
135	RANKONE-4	[1] 85	[4] 36	[107] 0.0318	[107] 0.0318	[107] 0.0318	[107] 1.171	[132] 0.0441	[132] 0.0441	[132] 0.0441	[126] 1.249
136	RANKONE-5	[10] 133	[12] 94	[58] 0.0072	[58] 0.0072	[58] 0.0072	[58] 1.042	[68] 0.0120	[68] 0.0120	[68] 0.0120	[69] 1.078
137	REALNETWORKS-0	[185] 4100	[38] 244	[115] 0.0443	[115] 0.0443	[115] 0.0443	[111] 1.222	[131] 0.0426	[131] 0.0426	[131] 0.0426	[122] 1.222
138	REALNETWORKS-1	[186] 4104	[37] 243	[111] 0.0329	[111] 0.0329	[111] 0.0329	[106] 1.163	[130] 0.0426	[130] 0.0426	[130] 0.0426	[121] 1.222
139	REALNETWORKS-2	[189] 4104	[39] 245	[109] 0.0320	[109] 0.0320	[109] 0.0320	[105] 1.159	[125] 0.0418	[125] 0.0418	[125] 0.0418	[120] 1.217
140	REMARKAI-0	[135] 2048	[128] 615	[54] 0.0065	[54] 0.0065	[54] 0.0065	[48] 1.034	[60] 0.0109	[60] 0.0109	[60] 0.0109	[56] 1.065
141	REMARKAI-2	[143] 2048	[98] 434	[51] 0.0062	[51] 0.0062	[51] 0.0062	[42] 1.031	[58] 0.0105	[58] 0.0105	[58] 0.0105	[48] 1.061
142	SENSETIME-0	[188] 4104	[162] 715	[13] 0.0018	[13] 0.0018	[13] 0.0018	[14] 1.014	[16] 0.0048	[16] 0.0048	[16] 0.0048	[23] 1.040
143	SENSETIME-1	[187] 4104	[142] 656	[11] 0.0018	[11] 0.0018	[11] 0.0018	[13] 1.013	[17] 0.0048	[17] 0.0048	[17] 0.0048	[22] 1.040
144	SHAMAN-0	[179] 4096	[113] 538				[161] 10.000	[165] 0.1707	[165] 0.1707	[165] 0.1707	[165] 2.092

Table 17: **Rank-based accuracy for the FRVT 2018 mugshot sets**. *In columns 3 and 4 are template size and template generation duration. Thereafter values are rank-based FNIR with T = 0 and FPIR = 1. This is appropriate to investigational uses but not those with higher volumes where candidates from all searches would need review. Columns 5 - 9 show FRVT 2018 accuracy for various ranks for galleries unenrolled with all lifetime images. Column 10 is a workload statistic, a small value shows an algorithm front-loads mates into the first 10 candidates. The last four columns gives analogous results for enrollment only of the most recent image - see Figure 8. Throughout, blue superscripts indicate the rank of the algorithm for that column, and the best value is highlighted in yellow.*

MISSES OUTSIDE RANK R		RESOURCE USAGE		ENROLL LIFETIME CONSOLIDATED = 1.6M				ENROL MOST RECENT, N = 1.6M			
FNIR(N, T=0, R)		TEMPLATE		FRVT 2018 MUGSHOTS							
#	ALGORITHM	BYTES	MSEC	R=1	R=10	R=50	WORK-10	R=1	R=10	R=50	WORK-10
145	SHAMAN-1	^{183}4096	^{121}557				^{190}10.000	^{166}0.1718	^{166}0.1718	^{166}0.1718	^{164}2.078
146	SHAMAN-2	^{201}8192	^{122}557				^{194}10.000	^{182}0.2620	^{182}0.2620	^{182}0.2620	^{182}2.710
147	SHAMAN-3	^{121}2048	^{156}704	^{127}0.0969	^{127}0.0969	^{127}0.0969	^{128}1.613	^{155}0.1266	^{155}0.1266	^{155}0.1266	^{160}1.811
148	SHAMAN-4	^{130}2048	^{135}642	^{134}0.1867	^{134}0.1867	^{134}0.1867	^{134}2.163	^{178}0.2242	^{178}0.2242	^{178}0.2242	^{177}2.431
149	SHAMAN-6	^{145}2048	^{157}706	^{106}0.0312	^{106}0.0312	^{106}0.0312	^{114}1.249	^{129}0.0424	^{129}0.0424	^{129}0.0424	^{139}1.339
150	SHAMAN-7	^{114}2048	^{159}709	^{105}0.0310	^{105}0.0310	^{105}0.0310	^{113}1.248	^{128}0.0422	^{128}0.0422	^{128}0.0422	^{138}1.337
151	SIAT-0	^{86}1096	^{67}358				^{197}10.000	^{55}0.0101	^{55}0.0101	^{55}0.0101	^{47}1.059
152	SIAT-1	^{149}2052	^{188}842	^{138}0.2639	^{138}0.2639	^{138}0.2639	^{140}3.373	^{10}0.0039	^{10}0.0039	^{10}0.0039	^{11}1.031
153	SIAT-2	^{153}2052	^{195}906	^{136}0.2128	^{136}0.2128	^{136}0.2128	^{137}2.913	^{11}0.0040	^{11}0.0040	^{11}0.0040	^{13}1.032
154	SMILART-0	^{75}1024	^{20}168				^{191}10.000	^{170}0.1931	^{170}0.1931	^{170}0.1931	^{169}2.204
155	SMILART-1	^{65}1024	^{146}662				^{165}10.000	^{175}0.2188	^{175}0.2188	^{175}0.2188	^{178}2.435
156	SMILART-2	^{61}1024	^{123}560				^{155}10.000	^{171}0.1946	^{171}0.1946	^{171}0.1946	^{168}2.196
157	SMILART-4	^{38}512	^{19}167	^{147}0.9531	^{147}0.9531	^{147}0.9531	^{147}9.573	^{198}0.9649	^{198}0.9649	^{198}0.9649	^{198}9.679
158	SMILART-5	^{126}2048	^{103}464				^{178}10.000				^{201}10.000
159	SYNESIS-0	^{35}512	^{36}237				^{152}10.000	^{164}0.1621	^{164}0.1621	^{164}0.1621	^{175}2.380
160	SYNESIS-3	^{181}4096	^{13}103	^{131}0.1350	^{131}0.1350	^{131}0.1350	^{130}1.868	^{167}0.1721	^{167}0.1721	^{167}0.1721	^{167}2.140
161	TEVIAN-0	^{112}2048	^{75}394				^{153}10.000	^{104}0.0225	^{104}0.0225	^{104}0.0225	^{99}1.122
162	TEVIAN-1	^{146}2048	^{79}398				^{203}10.000	^{105}0.0225	^{105}0.0225	^{105}0.0225	^{100}1.122
163	TEVIAN-2	^{119}2048	^{77}397				^{167}10.000	^{103}0.0224	^{103}0.0224	^{103}0.0224	^{98}1.121
164	TEVIAN-3	^{129}2048	^{55}300	^{74}0.0102	^{74}0.0102	^{74}0.0102	^{67}1.052	^{88}0.0169	^{88}0.0169	^{88}0.0169	^{78}1.093
165	TEVIAN-4	^{138}2048	^{53}299	^{60}0.0080	^{60}0.0080	^{60}0.0080	^{56}1.041	^{75}0.0134	^{75}0.0134	^{75}0.0134	^{68}1.076
166	TEVIAN-5	^{132}2048	^{86}416	^{44}0.0053	^{44}0.0053	^{44}0.0053	^{36}1.028	^{48}0.0092	^{48}0.0092	^{48}0.0092	^{41}1.054
167	TIGER-0	^{155}2052	^{93}428	^{117}0.0480	^{117}0.0480	^{117}0.0480	^{112}1.247	^{144}0.0638	^{144}0.0638	^{144}0.0638	^{137}1.334
168	TIGER-1	^{156}2052	^{78}398				^{189}10.000				^{202}10.000
169	TIGER-2	^{152}2052	^{102}464	^{35}0.0044	^{35}0.0044	^{35}0.0044	^{31}1.023	^{39}0.0075	^{39}0.0075	^{39}0.0075	^{32}1.046
170	TIGER-3	^{147}2052	^{101}464				^{158}10.000	^{38}0.0075	^{38}0.0075	^{38}0.0075	^{33}1.046
171	TONGYITRANS-0	^{162}2070	^{27}190	^{49}0.0060	^{49}0.0060	^{49}0.0060	^{50}1.036	^{53}0.0095	^{53}0.0095	^{53}0.0095	^{50}1.062
172	TONGYITRANS-1	^{160}2070	^{25}189	^{80}0.0114	^{80}0.0114	^{80}0.0114	^{84}1.073	^{52}0.0095	^{52}0.0095	^{52}0.0095	^{51}1.062
173	TOSHIBA-0	^{98}1548	^{199}930	^{24}0.0033	^{24}0.0033	^{24}0.0033	^{28}1.018	^{32}0.0068	^{32}0.0068	^{32}0.0068	^{31}1.046
174	TOSHIBA-1	^{159}2060	^{201}931	^{28}0.0035	^{28}0.0035	^{28}0.0035	^{30}1.019	^{34}0.0071	^{34}0.0071	^{34}0.0071	^{36}1.047
175	VD-0	^{76}1028	^{61}337	^{143}0.4303	^{143}0.4303	^{143}0.4303	^{143}3.703	^{192}0.4751	^{192}0.4751	^{192}0.4751	^{191}4.074
176	VD-1	^{151}2052	^{153}695	^{102}0.0221	^{102}0.0221	^{102}0.0221	^{102}1.140	^{115}0.0302	^{115}0.0302	^{115}0.0302	^{119}1.197
177	VIGILANTSOLUTIONS-0	^{93}1544	^{180}823				^{166}10.000	^{154}0.1254	^{154}0.1254	^{154}0.1254	^{154}1.712
178	VIGILANTSOLUTIONS-1	^{158}2056	^{168}739				^{202}10.000	^{174}0.2038	^{174}0.2038	^{174}0.2038	^{170}2.210
179	VIGILANTSOLUTIONS-2	^{95}1544	^{177}820				^{177}10.000	^{180}0.2387	^{180}0.2387	^{180}0.2387	^{179}2.555
180	VIGILANTSOLUTIONS-3	^{97}1544	^{185}832	^{121}0.0549	^{121}0.0549	^{121}0.0549	^{116}1.280	^{148}0.0719	^{148}0.0719	^{148}0.0719	^{142}1.378
181	VIGILANTSOLUTIONS-4	^{92}1544	^{183}830	^{129}0.0993	^{129}0.0993	^{129}0.0993	^{124}1.549	^{156}0.1272	^{156}0.1272	^{156}0.1272	^{155}1.721
182	VIGILANTSOLUTIONS-5	^{94}1544	^{173}778				^{169}10.000	^{67}0.0118	^{67}0.0118	^{67}0.0118	^{60}1.069
183	VIGILANTSOLUTIONS-6	^{96}1544	^{186}834				^{181}10.000	^{70}0.0125	^{70}0.0125	^{70}0.0125	^{64}1.072
184	VISIONLABS-3	^{14}256	^{35}228	^{41}0.0050	^{41}0.0050	^{41}0.0050	^{57}1.041	^{46}0.0089	^{46}0.0089	^{46}0.0089	^{62}1.072
185	VISIONLABS-4	^{25}256	^{57}315	^{14}0.0020	^{14}0.0020	^{14}0.0020	^{12}1.013	^{13}0.0044	^{13}0.0044	^{13}0.0044	^{10}1.031
186	VISIONLABS-5	^{34}512	^{54}300	^{12}0.0018	^{12}0.0018	^{12}0.0018	^{11}1.012	^{12}0.0041	^{12}0.0041	^{12}0.0041	^{9}1.029
187	VISIONLABS-6	^{40}512	^{50}292	^{9}0.0015	^{9}0.0015	^{9}0.0015	^{10}1.011	^{7}0.0033	^{7}0.0033	^{7}0.0033	^{7}1.025
188	VISIONLABS-7	^{39}512	^{51}293	^{8}0.0014	^{8}0.0014	^{8}0.0014	^{8}1.010	^{6}0.0033	^{6}0.0033	^{6}0.0033	^{6}1.025
189	VOCORD-0	^{57}608	^{112}536				^{160}10.000	^{123}0.0403	^{123}0.0403	^{123}0.0403	^{135}1.301
190	VOCORD-1	^{56}608	^{111}536				^{150}10.000	^{122}0.0402	^{122}0.0402	^{122}0.0402	^{134}1.299
191	VOCORD-2	^{133}2048	^{134}635				^{187}10.000	^{120}0.0382	^{120}0.0382	^{120}0.0382	^{133}1.290
192	VOCORD-3	^{60}896	^{161}714	^{55}0.0067	^{55}0.0067	^{55}0.0067	^{54}1.038	^{43}0.0085	^{43}0.0085	^{43}0.0085	^{42}1.054
193	VOCORD-4	^{59}896	^{114}538	^{62}0.0084	^{62}0.0084	^{62}0.0084	^{66}1.051	^{57}0.0102	^{57}0.0102	^{57}0.0102	^{59}1.068
194	VOCORD-5	^{58}768	^{179}822	^{46}0.0057	^{46}0.0057	^{46}0.0057	^{51}1.036	^{49}0.0092	^{49}0.0092	^{49}0.0092	^{54}1.063
195	VOCORD-6	^{203}10240	^{181}825				^{201}10.000	^{203}1.0000	^{203}1.0000	^{203}1.0000	^{203}10.000
196	YISHENG-0	^{168}2108	^{127}615				^{163}10.000	^{111}0.0268	^{111}0.0268	^{111}0.0268	^{107}1.149
197	YISHENG-1	^{176}3704	^{74}387	^{99}0.0208	^{99}0.0208	^{99}0.0208	^{94}1.105	^{114}0.0290	^{114}0.0290	^{114}0.0290	^{109}1.156
198	YITU-0	^{191}4136	^{133}633	^{38}0.0047	^{38}0.0047	^{38}0.0047	^{43}1.031	^{36}0.0074	^{36}0.0074	^{36}0.0074	^{40}1.053
199	YITU-1	^{190}4136	^{200}930	^{36}0.0046	^{36}0.0046	^{36}0.0046	^{41}1.031	^{35}0.0072	^{35}0.0072	^{35}0.0072	^{38}1.052
200	YITU-2	^{193}4138	^{192}870	^{10}0.0015	^{10}0.0015	^{10}0.0015	^{7}1.010	^{14}0.0044	^{14}0.0044	^{14}0.0044	^{16}1.035
201	YITU-3	^{192}4138	^{193}871	^{17}0.0023	^{17}0.0023	^{17}0.0023	^{23}1.018	^{19}0.0054	^{19}0.0054	^{19}0.0054	^{29}1.044
202	YITU-4	^{163}2070	^{196}910	^{2}0.0011	^{2}0.0011	^{2}0.0011	^{5}1.008	^{9}0.0037	^{9}0.0037	^{9}0.0037	^{12}1.031
203	YITU-5	^{161}2070	^{190}861	^{15}0.0020	^{15}0.0020	^{15}0.0020	^{19}1.016	^{18}0.0048	^{18}0.0048	^{18}0.0048	^{26}1.041

Table 18: **Rank-based accuracy for the FRVT 2018 mugshot sets**. *In columns 3 and 4 are template size and template generation duration. Thereafter values are rank-based FNIR with T = 0 and FPIR = 1. This is appropriate to investigational uses but not those with higher volumes where candidates from all searches would need review. Columns 5 - 9 show FRVT 2018 accuracy for various ranks for galleries unenrolled with all lifetime images. Column 10 is a workload statistic, a small value shows an algorithm front-loads mates into the first 10 candidates. The last four columns gives analogous results for enrollment only of the most recent image - see Figure 8. Throughout, blue superscripts indicate the rank of the algorithm for that column, and the best value is highlighted in yellow.*

MISSES BELOW THRESHOLD, T		ENROL MOST RECENT MUGSHOT, N = 1.6M								
FNIR(N, T> 0, R >L)		DATASET: FRVT 2018 MUGSHOTS			DATASET: WEBCAM PROBES			DATASET: PROFILE PROBES		
#	ALGORITHM	FPIR=0.001	FPIR=0.01	FPIR=0.1	FPIR=0.001	FPIR=0.01	FPIR=0.1	FPIR=0.001	FPIR=0.01	FPIR=0.1
1	3DIVI-0	[126] 0.256	[134] 0.160	[135] 0.086	[115] 0.425	[117] 0.302	[115] 0.180			
2	3DIVI-1	[125] 0.256	[135] 0.160	[136] 0.087						
3	3DIVI-2	[121] 0.255	[136] 0.164	[137] 0.089						
4	3DIVI-3	[145] 0.402	[152] 0.284	[152] 0.168	[131] 0.626	[133] 0.497	[129] 0.343			
5	3DIVI-4	[105] 0.171	[107] 0.096	[101] 0.047	[108] 0.343	[108] 0.237	[109] 0.138			
6	3DIVI-5	[101] 0.169	[106] 0.095	[102] 0.047	[106] 0.339	[107] 0.234	[108] 0.137	[20] 0.995	[25] 0.987	[28] 0.961
7	3DIVI-6	[104] 0.170	[110] 0.098	[107] 0.051	[107] 0.342	[109] 0.238	[110] 0.142			
8	ALCHERA-0	[95] 0.140	[94] 0.073	[91] 0.035	[77] 0.216	[78] 0.146	[79] 0.087			
9	ALCHERA-1	[198] 0.999	[198] 0.999	[199] 0.995	[169] 1.000	[169] 1.000	[161] 1.000			
10	ALCHERA-2	[156] 0.490	[155] 0.304	[154] 0.184	[128] 0.591	[127] 0.442	[126] 0.295			
11	ALCHERA-3	[98] 0.159	[95] 0.073	[84] 0.030	[84] 0.239	[82] 0.152	[74] 0.081	[28] 0.999	[27] 0.993	[22] 0.921
12	ANKE-0	[83] 0.120	[89] 0.065	[87] 0.033	[79] 0.220	[80] 0.151	[82] 0.088	[18] 0.991	[24] 0.985	[29] 0.972
13	ANKE-1	[89] 0.122	[88] 0.065	[88] 0.033	[78] 0.220	[81] 0.151	[81] 0.088			
14	AWARE-0	[194] 0.983	[126] 0.128	[133] 0.085	[143] 0.817	[111] 0.253	[114] 0.178			
15	AWARE-1	[195] 0.996	[125] 0.127	[132] 0.081						
16	AWARE-2	[192] 0.977	[122] 0.120	[130] 0.078						
17	AWARE-3	[93] 0.131	[100] 0.085	[108] 0.051	[99] 0.298	[100] 0.204	[107] 0.132			
18	AWARE-4	[127] 0.271	[139] 0.177	[144] 0.107	[123] 0.509	[125] 0.375	[124] 0.253			
19	AWARE-5	[139] 0.373	[103] 0.088	[105] 0.050	[87] 0.253	[85] 0.163	[86] 0.099	[30] 1.000	[33] 0.999	[33] 0.998
20	AWARE-6	[128] 0.278	[140] 0.178	[146] 0.109	[112] 0.398	[115] 0.283	[116] 0.188			
21	AYONIX-0	[180] 0.811	[187] 0.725	[190] 0.598	[152] 0.939	[154] 0.892	[155] 0.802			
22	AYONIX-1	[183] 0.825	[185] 0.702	[188] 0.526	[148] 0.920	[150] 0.845	[151] 0.703			
23	AYONIX-2	[182] 0.825	[186] 0.702	[187] 0.526	[149] 0.920	[149] 0.845	[150] 0.702			
24	CAMVI-1	[173] 0.684	[178] 0.549	[178] 0.375	[140] 0.770	[144] 0.648	[144] 0.488			
25	CAMVI-2	[160] 0.537	[164] 0.402	[161] 0.242						
26	CAMVI-3	[56] 0.074	[83] 0.060	[115] 0.055	[46] 0.132	[69] 0.108	[85] 0.094			
27	CAMVI-4	[57] 0.074	[79] 0.056	[104] 0.050	[48] 0.136	[58] 0.100	[75] 0.083	[26] 0.999	[30] 0.994	[15] 0.816
28	CAMVI-5	[75] 0.102	[99] 0.078	[123] 0.069	[73] 0.179	[75] 0.132	[94] 0.110			
29	COGENT-0	[45] 0.056	[52] 0.032	[61] 0.020	[51] 0.140	[62] 0.100	[71] 0.069			
30	COGENT-1	[44] 0.056	[51] 0.032	[60] 0.020	[50] 0.140	[61] 0.100	[70] 0.069			
31	COGENT-2	[30] 0.047	[19] 0.020	[21] 0.010	[24] 0.098	[25] 0.063	[28] 0.036	[22] 0.997	[26] 0.993	[31] 0.983
32	COGENT-3	[36] 0.051	[18] 0.018	[19] 0.009	[20] 0.095	[23] 0.061	[29] 0.037			
33	COGNITEC-0	[99] 0.163	[108] 0.098	[111] 0.053	[100] 0.303	[98] 0.200	[97] 0.115			
34	COGNITEC-1	[77] 0.105	[77] 0.055	[78] 0.027	[82] 0.230	[77] 0.135	[72] 0.071			
35	COGNITEC-2	[46] 0.056	[42] 0.027	[39] 0.014	[72] 0.178	[64] 0.101	[53] 0.050	[31] 1.000	[15] 0.947	[23] 0.936
36	COGNITEC-3	[43] 0.055	[44] 0.028	[41] 0.014	[65] 0.162	[59] 0.100	[51] 0.050			
37	DAHUA-0	[67] 0.089	[70] 0.047	[68] 0.022	[47] 0.135	[47] 0.083	[45] 0.046			
38	DAHUA-1	[59] 0.075	[58] 0.039	[55] 0.018	[41] 0.122	[40] 0.075	[39] 0.042	[10] 0.953	[10] 0.862	[13] 0.679
39	DERMALOG-0	[155] 0.488	[159] 0.364	[160] 0.233	[135] 0.657	[139] 0.528	[134] 0.362			
40	DERMALOG-1	[158] 0.528	[165] 0.405	[165] 0.268						
41	DERMALOG-2	[157] 0.503	[161] 0.378	[162] 0.244						
42	DERMALOG-3	[154] 0.484	[158] 0.362	[158] 0.231	[133] 0.655	[138] 0.526	[133] 0.361			
43	DERMALOG-4	[153] 0.481	[157] 0.360	[157] 0.230	[134] 0.657	[136] 0.526	[132] 0.359			
44	DERMALOG-5	[71] 0.091	[64] 0.045	[74] 0.024	[57] 0.154	[56] 0.096	[58] 0.057			
45	DERMALOG-6	[41] 0.054	[45] 0.028	[44] 0.015	[27] 0.105	[29] 0.067	[33] 0.039	[8] 0.948	[9] 0.856	[10] 0.642
46	EVERAI-0	[73] 0.092	[73] 0.047	[80] 0.028	[67] 0.170	[60] 0.100	[61] 0.060			
47	EVERAI-1	[37] 0.052	[27] 0.023	[22] 0.010	[43] 0.128	[36] 0.074	[32] 0.039			
48	EVERAI-2	[38] 0.053	[34] 0.025	[27] 0.011	[40] 0.119	[41] 0.076	[36] 0.041			
49	EVERAI-3	[17] 0.038	[17] 0.018	[17] 0.008	[21] 0.096	[21] 0.060	[22] 0.034	[14] 0.979	[6] 0.535	[4] 0.247
50	EYEDEA-0	[181] 0.812	[184] 0.679	[184] 0.484	[147] 0.914	[147] 0.783	[147] 0.619			
51	EYEDEA-1	[168] 0.632	[169] 0.480	[172] 0.335						
52	EYEDEA-2	[178] 0.794	[172] 0.490	[174] 0.338						
53	EYEDEA-3	[142] 0.389	[150] 0.267	[150] 0.160	[125] 0.543	[126] 0.404	[125] 0.264			
54	GLORY-0	[138] 0.369	[154] 0.297	[159] 0.233	[126] 0.547	[130] 0.470	[138] 0.390			
55	GLORY-1	[133] 0.307	[147] 0.238	[153] 0.179	[124] 0.537	[128] 0.448	[130] 0.352			
56	GORILLA-0									
57	GORILLA-1	[146] 0.408	[148] 0.248	[147] 0.136	[118] 0.453	[119] 0.314	[118] 0.191			
58	GORILLA-2	[108] 0.190	[114] 0.108	[106] 0.051	[92] 0.268	[90] 0.170	[84] 0.093			
59	GORILLA-3	[135] 0.326	[133] 0.160	[124] 0.074	[117] 0.434	[110] 0.247	[105] 0.131			
60	HBINNO-0	[177] 0.766	[182] 0.632	[183] 0.458						
61	HIK-0	[82] 0.114	[93] 0.070	[95] 0.040	[58] 0.155	[66] 0.103	[64] 0.061			
62	HIK-1	[87] 0.120	[91] 0.067	[90] 0.034						
63	HIK-2	[88] 0.121	[92] 0.067	[89] 0.034						
64	HIK-3	[78] 0.105	[82] 0.060	[85] 0.030	[60] 0.158	[67] 0.105	[63] 0.061			
65	HIK-4	[74] 0.101	[80] 0.056	[82] 0.029	[56] 0.153	[63] 0.101	[59] 0.059			
66	HIK-5	[27] 0.047	[23] 0.022	[29] 0.011	[11] 0.077	[11] 0.048	[15] 0.028	[27] 0.999	[29] 0.994	[12] 0.662
67	HIK-6	[32] 0.050	[26] 0.022	[28] 0.011	[12] 0.086	[14] 0.052	[16] 0.029	[32] 1.000	[32] 0.997	[11] 0.645
68	IDEMIA-0	[81] 0.114	[85] 0.062	[81] 0.029	[85] 0.240	[83] 0.156	[78] 0.085			
69	IDEMIA-1	[40] 0.054	[50] 0.031	[54] 0.018						
70	IDEMIA-2	[42] 0.054	[53] 0.032	[56] 0.019						
71	IDEMIA-3	[31] 0.050	[32] 0.024	[40] 0.014	[66] 0.165	[43] 0.079	[54] 0.050			
72	IDEMIA-4	[19] 0.040	[31] 0.024	[42] 0.014	[39] 0.118	[42] 0.079	[52] 0.050	[11] 0.969	[17] 0.962	[26] 0.952

Table 19: ***Threshold-based accuracy****. Values are FNIR(N, T, L) with N = 1.6 million with thresholds set to produce FPIR = 0.001, 0.01, and 0.1 in non-mate searches. Columns 3-5 apply to FRVT-2018 mugshots: Columns 6-8 show the corresponding FNIR values for webcam images searched against the FRVT-2018 mugshot gallery. Finally, the three rightmost columns show FNIR for profile view images searched against the FRVT-2018 frontal gallery. Throughout blue superscripts indicate the rank of the algorithm for that column. Caution: The Power-low models are mostly intended to draw attention to the kind of behavior, not as a model to be used for prediction.*

MISSES BELOW THRESHOLD, T		ENROL MOST RECENT MUGSHOT, N = 1.6M								
FNIR(N, T> 0, R >L)		DATASET: FRVT 2018 MUGSHOTS			DATASET: WEBCAM PROBES			DATASET: PROFILE PROBES		
#	ALGORITHM	FPIR=0.001	FPIR=0.01	FPIR=0.1	FPIR=0.001	FPIR=0.01	FPIR=0.1	FPIR=0.001	FPIR=0.01	FPIR=0.1
73	IDEMIA-5	^{26}0.047	^{46}0.028	^{49}0.017	^{55}0.150	^{65}0.102	^{69}0.065	^{12}0.974	^{19}0.968	^{27}0.960
74	IDEMIA-6	^{24}0.046	^{43}0.028	^{51}0.018	^{81}0.226	^{84}0.161	^{93}0.108			
75	IMAGUS-0	^{175}0.734	^{181}0.608	^{182}0.453	^{145}0.872	^{146}0.779	^{148}0.635			
76	IMAGUS-2	^{176}0.751	^{179}0.566	^{179}0.377	^{142}0.816	^{143}0.645	^{142}0.460			
77	IMAGUS-3	^{179}0.808	^{183}0.670	^{186}0.512	^{146}0.909	^{148}0.809	^{149}0.667			
78	INCODE-0	^{134}0.313	^{144}0.201	^{143}0.107	^{114}0.420	^{118}0.304	^{117}0.191			
79	INCODE-1	^{114}0.214	^{115}0.114	^{103}0.050	^{96}0.296	^{96}0.198	^{95}0.110			
80	INCODE-2	^{107}0.186	^{112}0.102	^{100}0.046	^{93}0.269	^{91}0.176	^{87}0.100			
81	INCODE-3	^{103}0.170	^{101}0.086	^{94}0.037	^{90}0.264	^{87}0.164	^{80}0.087			
82	INNOVATRICS-0	^{124}0.255	^{138}0.165	^{139}0.089	^{109}0.361	^{112}0.258	^{113}0.159			
83	INNOVATRICS-1	^{123}0.255	^{137}0.165	^{138}0.089						
84	INNOVATRICS-2	^{120}0.237	^{132}0.142	^{131}0.079	^{101}0.310	^{102}0.209	^{101}0.126			
85	INNOVATRICS-3	^{116}0.224	^{128}0.134	^{122}0.068	^{97}0.297	^{99}0.203	^{98}0.116			
86	INNOVATRICS-4	^{94}0.134	^{98}0.076	^{93}0.035	^{80}0.222	^{79}0.149	^{77}0.085	^{13}0.977	^{18}0.966	^{24}0.945
87	ISYSTEMS-0	^{72}0.091	^{69}0.047	^{72}0.023	^{69}0.173	^{70}0.110	^{67}0.065			
88	ISYSTEMS-1	^{69}0.090	^{67}0.047	^{71}0.023						
89	ISYSTEMS-2	^{62}0.081	^{55}0.035	^{46}0.015	^{42}0.126	^{45}0.080	^{46}0.046			
90	ISYSTEMS-3	^{52}0.062	^{40}0.027	^{36}0.012	^{30}0.107	^{31}0.068	^{31}0.039	^{29}1.000	^{31}0.995	^{21}0.913
91	LOOKMAN-3	^{25}0.046	^{41}0.027	^{50}0.017	^{33}0.112	^{46}0.082	^{57}0.057			
92	LOOKMAN-4	^{28}0.047	^{39}0.027	^{47}0.016	^{29}0.105	^{38}0.075	^{56}0.052	^{16}0.980	^{22}0.978	^{30}0.977
93	MEGVII-0	^{80}0.109	^{81}0.058	^{77}0.025	^{35}0.116	^{30}0.067	^{23}0.034			
94	MEGVII-1	^{58}0.075	^{57}0.039	^{67}0.022	^{23}0.097	^{22}0.061	^{21}0.033			
95	MEGVII-2	^{61}0.080	^{59}0.039	^{65}0.022	^{22}0.096	^{20}0.059	^{20}0.033	^{23}0.997	^{8}0.698	^{7}0.429
96	MICROFOCUS-0	^{188}0.933	^{192}0.867	^{194}0.749	^{158}0.985	^{157}0.950	^{158}0.877			
97	MICROFOCUS-1	^{189}0.933	^{193}0.867	^{195}0.749						
98	MICROFOCUS-2	^{190}0.934	^{194}0.870	^{196}0.758						
99	MICROFOCUS-3	^{187}0.931	^{191}0.866	^{193}0.748	^{157}0.979	^{156}0.948	^{157}0.876			
100	MICROFOCUS-4	^{197}0.999	^{199}0.999	^{198}0.994	^{155}0.975	^{155}0.940	^{156}0.862			
101	MICROFOCUS-5	^{184}0.836	^{189}0.736	^{189}0.588	^{151}0.928	^{152}0.865	^{154}0.748			
102	MICROFOCUS-6	^{193}0.978	^{195}0.963	^{191}0.641	^{150}0.923	^{151}0.858	^{153}0.739			
103	MICROSOFT-0	^{21}0.044	^{22}0.022	^{25}0.010	^{34}0.115	^{33}0.071	^{34}0.040			
104	MICROSOFT-1	^{23}0.045	^{24}0.022	^{26}0.011						
105	MICROSOFT-2	^{34}0.050	^{36}0.026	^{34}0.012						
106	MICROSOFT-3	^{16}0.030	^{16}0.014	^{12}0.006	^{17}0.091	^{18}0.056	^{14}0.028			
107	MICROSOFT-4	^{13}0.029	^{15}0.013	^{10}0.005	^{13}0.087	^{15}0.053	^{13}0.026			
108	MICROSOFT-5	^{12}0.028	^{12}0.012	^{7}0.005	^{10}0.070	^{9}0.041	^{7}0.021	^{2}0.338	^{2}0.188	^{2}0.123
109	MICROSOFT-6	^{5}0.014	^{5}0.008	^{3}0.004	^{5}0.037	^{5}0.024	^{4}0.016	^{1}0.203	^{1}0.148	^{1}0.109
110	NEC-0	^{63}0.082	^{74}0.049	^{83}0.029	^{52}0.140	^{52}0.093	^{60}0.059			
111	NEC-1	^{79}0.108	^{87}0.063	^{92}0.035	^{75}0.197	^{76}0.133	^{76}0.083			
112	NEC-2	^{2}0.005	^{1}0.004	^{1}0.003	^{2}0.020	^{2}0.013	^{1}0.010			
113	NEC-3	^{1}0.004	^{2}0.004	^{2}0.003	^{1}0.017	^{1}0.013	^{2}0.011	^{5}0.664	^{5}0.479	^{6}0.340
114	NEUROTECHNOLOGY-0	^{129}0.295	^{143}0.196	^{145}0.108	^{119}0.465	^{120}0.317	^{120}0.196			
115	NEUROTECHNOLOGY-1	^{131}0.299	^{142}0.195	^{142}0.105						
116	NEUROTECHNOLOGY-2	^{132}0.299	^{141}0.195	^{141}0.105						
117	NEUROTECHNOLOGY-3	^{172}0.665	^{111}0.101	^{110}0.052	^{91}0.266	^{86}0.164	^{83}0.088			
118	NEUROTECHNOLOGY-4	^{54}0.066	^{48}0.030	^{43}0.014	^{36}0.117	^{34}0.073	^{35}0.040			
119	NEUROTECHNOLOGY-5	^{48}0.056	^{35}0.025	^{33}0.012	^{44}0.130	^{37}0.074	^{40}0.042	^{21}0.996	^{23}0.982	^{25}0.948
120	NEUROTECHNOLOGY-6	^{122}0.255	^{123}0.124	^{109}0.051	^{113}0.418	^{101}0.206	^{88}0.103			
121	NEWLAND-2	^{150}0.441	^{153}0.296	^{149}0.157	^{120}0.466	^{122}0.335	^{122}0.213			
122	NOBLIS-1	^{199}1.000	^{197}0.992	^{180}0.419	^{199}1.000	^{199}1.000	^{160}1.000			
123	NOBLIS-2	^{196}0.997	^{173}0.490	^{169}0.309	^{166}1.000	^{166}1.000	^{146}0.565	^{33}1.000	^{34}1.000	^{34}1.000
124	NTECHLAB-0	^{64}0.083	^{72}0.047	^{69}0.023	^{64}0.162	^{68}0.105	^{62}0.061			
125	NTECHLAB-1	^{76}0.102	^{78}0.056	^{79}0.027						
126	NTECHLAB-3	^{47}0.056	^{49}0.030	^{45}0.015	^{37}0.118	^{39}0.075	^{41}0.043			
127	NTECHLAB-4	^{20}0.043	^{29}0.024	^{32}0.012	^{28}0.105	^{28}0.065	^{27}0.036			
128	NTECHLAB-5	^{22}0.045	^{30}0.024	^{31}0.012	^{26}0.102	^{26}0.063	^{25}0.034			
129	NTECHLAB-6	^{18}0.039	^{20}0.021	^{23}0.010	^{19}0.094	^{19}0.059	^{18}0.032	^{4}0.566	^{4}0.443	^{5}0.317
130	QUANTASOFT-1	^{170}0.640	^{175}0.494	^{173}0.335						
131	RANKONE-0	^{115}0.219	^{127}0.129	^{129}0.078	^{111}0.391	^{116}0.291	^{119}0.195			
132	RANKONE-1	^{100}0.168	^{102}0.087	^{98}0.043						
133	RANKONE-2	^{85}0.120	^{97}0.073	^{97}0.042	^{89}0.261	^{95}0.190	^{100}0.126			
134	RANKONE-3	^{84}0.120	^{96}0.073	^{96}0.042	^{88}0.255	^{93}0.187	^{99}0.122			
135	RANKONE-4	^{109}0.195	^{124}0.126	^{125}0.076	^{116}0.426	^{121}0.324	^{123}0.221			
136	RANKONE-5	^{50}0.062	^{56}0.036	^{62}0.021	^{70}0.173	^{72}0.119	^{73}0.074	^{24}0.998	^{28}0.994	^{32}0.988
137	REALNETWORKS-0	^{119}0.236	^{131}0.140	^{128}0.077	^{104}0.319	^{104}0.209	^{103}0.129			
138	REALNETWORKS-1	^{118}0.236	^{130}0.140	^{127}0.077	^{103}0.319	^{103}0.209	^{102}0.129			
139	REALNETWORKS-2	^{117}0.234	^{129}0.139	^{126}0.077	^{102}0.315	^{105}0.209	^{104}0.129			
140	REMARKAI-0	^{92}0.130	^{86}0.062	^{76}0.025	^{76}0.203	^{74}0.123	^{66}0.064			
141	REMARKAI-2	^{91}0.126	^{84}0.061	^{75}0.024	^{74}0.196	^{73}0.122	^{65}0.063	^{15}0.980	^{16}0.958	^{18}0.878
142	SENSETIME-0	^{9}0.023	^{10}0.012	^{14}0.007	^{8}0.063	^{8}0.040	^{9}0.025	^{124}1.000	^{20}0.971	^{16}0.844
143	SENSETIME-1	^{11}0.025	^{11}0.012	^{15}0.007	^{9}0.064	^{10}0.041	^{11}0.025			
144	SHAMAN-0	^{152}0.474	^{160}0.370	^{164}0.259	^{130}0.621	^{134}0.507	^{136}0.375			

Table 20: ***Threshold-based accuracy****. Values are FNIR(N, T, L) with N = 1.6 million with thresholds set to produce FPIR = 0.001, 0.01, and 0.1 in non-mate searches. Columns 3-5 apply to FRVT-2018 mugshots: Columns 6-8 show the corresponding FNIR values for webcam images searched against the FRVT-2018 mugshot gallery. Finally, the three rightmost columns show FNIR for profile view images searched against the FRVT-2018 frontal gallery. Throughout blue superscripts indicate the rank of the algorithm for that column. Caution: The Power-low models are mostly intended to draw attention to the kind of behavior, not as a model to be used for prediction.*

MISSES BELOW THRESHOLD, T		ENROL MOST RECENT MUGSHOT, N = 1.6M								
FNIR(N, T> 0, R >L)		DATASET: FRVT 2018 MUGSHOTS			DATASET: WEBCAM PROBES			DATASET: PROFILE PROBES		
#	ALGORITHM	FPIR=0.001	FPIR=0.01	FPIR=0.1	FPIR=0.001	FPIR=0.01	FPIR=0.1	FPIR=0.001	FPIR=0.01	FPIR=0.1
145	SHAMAN-1	[159]0.532	[166]0.406	[167]0.274						
146	SHAMAN-2	[174]0.700	[180]0.582	[181]0.424						
147	SHAMAN-3	[151]0.453	[156]0.348	[156]0.225	[129]0.597	[131]0.472	[127]0.317			
148	SHAMAN-4	[165]0.616	[171]0.490	[176]0.344	[139]0.754	[142]0.639	[143]0.480			
149	SHAMAN-6	[96]0.143	[105]0.095	[119]0.060	[83]0.237	[88]0.168	[92]0.108	[9]0.952	[14]0.935	[20]0.905
150	SHAMAN-7	[97]0.144	[104]0.094	[118]0.060	[86]0.240	[89]0.169	[90]0.107			
151	SIAT-0	[70]0.091	[68]0.047	[64]0.022	[31]0.107	[27]0.064	[26]0.035			
152	SIAT-1	[6]0.020	[6]0.009	[6]0.005	[110]0.365	[123]0.348	[128]0.337			
153	SIAT-2	[10]0.024	[7]0.009	[5]0.005	[121]0.478	[129]0.460	[141]0.451			
154	SMILART-0	[166]0.620	[170]0.486	[170]0.322						
155	SMILART-1	[171]0.641	[177]0.505	[175]0.342						
156	SMILART-2	[167]0.629	[174]0.492	[171]0.325						
157	SMILART-4	[191]0.968	[196]0.965	[197]0.964	[156]0.976	[158]0.973	[159]0.973			
158	SMILART-5									
159	SYNESIS-0	[163]0.554	[162]0.378	[155]0.213	[138]0.734	[141]0.598	[140]0.431			
160	SYNESIS-3	[164]0.583	[168]0.444	[168]0.294	[132]0.646	[135]0.524	[135]0.372			
161	TEVIAN-0	[111]0.203	[117]0.114	[113]0.054	[105]0.331	[106]0.227	[106]0.132			
162	TEVIAN-1	[112]0.203	[118]0.114	[114]0.054						
163	TEVIAN-2	[110]0.202	[116]0.114	[112]0.054						
164	TEVIAN-3	[106]0.180	[109]0.098	[99]0.044	[98]0.298	[97]0.198	[96]0.113			
165	TEVIAN-4	[86]0.120	[90]0.066	[86]0.031	[71]0.176	[71]0.115	[68]0.065			
166	TEVIAN-5	[68]0.090	[71]0.047	[66]0.022	[53]0.144	[49]0.089	[50]0.049	[7]0.910	[7]0.661	[8]0.483
167	TIGER-0	[143]0.392	[149]0.263	[148]0.142	[122]0.500	[124]0.366	[121]0.211			
168	TIGER-1				[127]0.580	[132]0.487	[139]0.396			
169	TIGER-2	[66]0.089	[61]0.042	[53]0.018	[62]0.158	[55]0.095	[49]0.048	[25]0.998	[12]0.927	[9]0.503
170	TIGER-3	[65]0.089	[62]0.042	[52]0.018	[61]0.158	[54]0.095	[48]0.048			
171	TONGYITRANS-0	[60]0.077	[60]0.041	[57]0.019	[32]0.112	[32]0.069	[30]0.038			
172	TONGYITRANS-1	[55]0.069	[54]0.035	[48]0.016	[25]0.101	[24]0.062	[24]0.034			
173	TOSHIBA-0	[53]0.065	[47]0.029	[37]0.013	[38]0.118	[35]0.074	[38]0.041	[17]0.988	[21]0.971	[19]0.899
174	TOSHIBA-1	[51]0.062	[21]0.021	[24]0.010	[18]0.092	[16]0.054	[19]0.032			
175	VD-0	[186]0.917	[190]0.828	[192]0.668	[153]0.946	[153]0.871	[152]0.725			
176	VD-1	[113]0.204	[121]0.118	[117]0.059	[94]0.281	[94]0.188	[89]0.106			
177	VIGILANTSOLUTIONS-0	[161]0.539	[163]0.394	[163]0.247	[137]0.695	[140]0.557	[137]0.389			
178	VIGILANTSOLUTIONS-1	[169]0.637	[176]0.502	[177]0.348						
179	VIGILANTSOLUTIONS-2	[185]0.876	[188]0.731	[185]0.489						
180	VIGILANTSOLUTIONS-3	[147]0.410	[151]0.283	[151]0.163	[136]0.660	[137]0.526	[131]0.356			
181	VIGILANTSOLUTIONS-4	[162]0.550	[167]0.424	[166]0.268	[144]0.817	[145]0.709	[145]0.523			
182	VIGILANTSOLUTIONS-5	[149]0.433	[63]0.045	[70]0.023						
183	VIGILANTSOLUTIONS-6	[148]0.426	[65]0.046	[73]0.023						
184	VISIONLABS-3	[35]0.051	[37]0.026	[38]0.013	[49]0.137	[50]0.091	[55]0.051			
185	VISIONLABS-4	[49]0.060	[38]0.026	[20]0.010	[63]0.159	[57]0.097	[43]0.045			
186	VISIONLABS-5	[39]0.053	[25]0.022	[18]0.008	[54]0.147	[48]0.087	[37]0.041			
187	VISIONLABS-6	[15]0.029	[14]0.012	[11]0.005	[16]0.090	[13]0.051	[12]0.025			
188	VISIONLABS-7	[14]0.029	[13]0.012	[9]0.005	[15]0.090	[12]0.051	[10]0.025	[3]0.461	[3]0.322	[3]0.198
189	VOCORD-0	[144]0.399	[120]0.116	[121]0.062	[95]0.285	[92]0.181	[91]0.108			
190	VOCORD-1	[130]0.299	[119]0.116	[120]0.062						
191	VOCORD-2	[137]0.366	[113]0.107	[116]0.057						
192	VOCORD-3	[90]0.126	[75]0.050	[59]0.020	[59]0.155	[53]0.093	[47]0.048			
193	VOCORD-4	[140]0.378	[76]0.054	[63]0.021	[68]0.173	[51]0.093	[44]0.046			
194	VOCORD-5	[102]0.170	[66]0.046	[58]0.019	[45]0.130	[44]0.080	[42]0.043	[19]0.992	[13]0.929	[14]0.787
195	VOCORD-6	[203]1.000	[203]1.000	[203]1.000	[201]1.000	[201]1.000	[201]1.000			
196	YISHENG-0	[141]0.380	[146]0.209	[134]0.086	[154]0.974	[114]0.275	[112]0.146			
197	YISHENG-1	[136]0.348	[145]0.208	[140]0.090	[141]0.808	[113]0.269	[111]0.144			
198	YITU-0	[33]0.050	[33]0.025	[35]0.012	[14]0.090	[17]0.054	[17]0.030			
199	YITU-1	[29]0.047	[28]0.023	[30]0.011						
200	YITU-2	[7]0.020	[8]0.011	[13]0.006	[6]0.049	[6]0.028	[5]0.016			
201	YITU-3	[8]0.021	[9]0.011	[16]0.007	[7]0.052	[7]0.033	[8]0.021			
202	YITU-4	[3]0.012	[3]0.007	[4]0.004	[3]0.027	[3]0.017	[3]0.011	[6]0.902	[11]0.875	[17]0.845
203	YITU-5	[4]0.013	[4]0.007	[8]0.005	[4]0.032	[4]0.023	[6]0.017			

Table 21: **Threshold-based accuracy**. *Values are FNIR(N, T, L) with N = 1.6 million with thresholds set to produce FPIR = 0.001, 0.01, and 0.1 in non-mate searches. Columns 3-5 apply to FRVT-2018 mugshots: Columns 6-8 show the corresponding FNIR values for webcam images searched against the FRVT-2018 mugshot gallery. Finally, the three rightmost columns show FNIR for profile view images searched against the FRVT-2018 frontal gallery. Throughout blue superscripts indicate the rank of the algorithm for that column. Caution: The Power-low models are mostly intended to draw attention to the kind of behavior, not as a model to be used for prediction.*

		INVESTIGATION MODE				IDENTIFICATION MODE				FAILURE TO EXTRACT			
		RANK ONE MISS RATE, FNIR(N, 0, 1)				HIGH T → FPIR = 0.01, FNIR(N, T, L)				FEATURES			
		N=1.6M	N=1.6M	N=1.6M	N=1.1M	N=1.6M	N=1.6M	N=1.6M	N=1.1M	N=1.6M	N=1.6M	N=1.6M	N=1.1M
#	ALGORITHM	FRVT-18	WEBCAM	PROFILE	WILD	FRVT-18	WEBCAM	PROFILE	WILD^{+}	FRVT-18	WEBCAM	PROFILE	WILD
1	3DIVI-0	^{118}0.034	^{111}0.086		^{59}0.071	^{134}0.160	^{117}0.302		^{63}0.095	0.003	0.007		0.013
2	3DIVI-1	^{119}0.038			^{62}0.074	^{135}0.160			^{64}0.095	0.003			0.013
3	3DIVI-2	^{124}0.040			^{64}0.076	^{136}0.164			^{65}0.096	0.003			0.013
4	3DIVI-3	^{152}0.086	^{129}0.206		^{81}0.094	^{152}0.284	^{133}0.497		^{85}0.136	0.002	0.005		0.009
5	3DIVI-4	^{96}0.020	^{96}0.062			^{107}0.096	^{108}0.237			0.002	0.005		
6	3DIVI-5	^{97}0.020	^{95}0.062	^{23}0.894	^{32}0.052	^{106}0.095	^{107}0.234	^{25}0.987	^{42}0.069	0.002	0.005	0.442	0.004
7	3DIVI-6	^{110}0.027	^{105}0.074		^{38}0.060	^{110}0.098	^{109}0.238		^{45}0.072	0.002	0.005		0.004
8	ALCHERA-0	^{92}0.019	^{84}0.047		^{77}0.092	^{94}0.073	^{78}0.146		^{55}0.089	0.006	0.014		0.030
9	ALCHERA-1	^{199}0.987	^{163}1.000			^{198}0.999	^{169}1.000			0.006	0.013		
10	ALCHERA-2	^{153}0.097	^{126}0.166		^{84}0.098	^{155}0.304	^{127}0.442		^{84}0.135	0.001	0.002		0.012
11	ALCHERA-3	^{72}0.013	^{64}0.035	^{15}0.629	^{46}0.064	^{95}0.073	^{82}0.152	^{27}0.993	^{40}0.067	0.001	0.002	0.106	0.012
12	ANKE-0	^{86}0.016	^{67}0.038	^{24}0.897	^{112}0.289	^{89}0.065	^{80}0.151	^{24}0.985		0.000	0.001	0.080	0.001
13	ANKE-1	^{87}0.016	^{66}0.038		^{111}0.284	^{88}0.065	^{81}0.151			0.000	0.001		0.001
14	AWARE-0	^{145}0.064	^{122}0.138		^{125}0.588	^{126}0.128	^{111}0.253		^{123}0.587	0.006	0.054		0.143
15	AWARE-1	^{141}0.059			^{124}0.580	^{125}0.127			^{121}0.580	0.006			0.143
16	AWARE-2	^{142}0.060				^{122}0.120				0.006			0.143
17	AWARE-3	^{116}0.033	^{112}0.090		^{122}0.503	^{100}0.085	^{100}0.204		^{118}0.505	0.004	0.003		0.014
18	AWARE-4	^{147}0.070	^{128}0.176			^{139}0.177	^{125}0.375			0.003	0.003		
19	AWARE-5	^{117}0.034	^{98}0.067	^{33}0.979	^{123}0.509	^{103}0.088	^{85}0.163	^{33}0.999	^{119}0.508	0.001	0.002	0.189	0.002
20	AWARE-6	^{149}0.072	^{121}0.128			^{140}0.178	^{115}0.283			0.001	0.002		
21	AYONIX-0	^{191}0.452	^{157}0.685		^{120}0.400	^{187}0.725	^{154}0.892		^{122}0.586	0.010	0.031		0.068
22	AYONIX-1	^{187}0.343	^{152}0.527		^{117}0.334	^{185}0.702	^{150}0.845		^{120}0.555	0.010	0.031		0.066
23	AYONIX-2	^{186}0.343	^{153}0.527			^{186}0.702	^{149}0.845			0.010	0.031		
24	CAMVI-1	^{179}0.227	^{143}0.337		^{96}0.148	^{178}0.549	^{144}0.648		^{95}0.196	0.005	0.009		0.058
25	CAMVI-2	^{160}0.129			^{91}0.130	^{164}0.402			^{90}0.157	0.005			0.058
26	CAMVI-3	^{140}0.054	^{113}0.090		^{94}0.139	^{83}0.060	^{69}0.108		^{77}0.130	0.006	0.013		0.074
27	CAMVI-4	^{137}0.049	^{107}0.077	^{16}0.640	^{136}1.000	^{79}0.056	^{58}0.100	^{30}0.994	^{134}1.000	0.000	0.000	0.000	0.000
28	CAMVI-5	^{146}0.067	^{117}0.103		^{157}1.000	^{99}0.078	^{75}0.132		^{156}1.000	0.000	0.000		0.001
29	COGENT-0	^{74}0.013	^{82}0.046		^{78}0.093	^{52}0.032	^{62}0.100		^{72}0.110	0.000	0.000		0.000
30	COGENT-1	^{73}0.013	^{81}0.046			^{51}0.032	^{61}0.100			0.000	0.000		
31	COGENT-2	^{26}0.006	^{27}0.020	^{25}0.901	^{21}0.045	^{19}0.020	^{25}0.063	^{26}0.993	^{23}0.051	0.000	0.000	0.000	0.000
32	COGENT-3	^{27}0.006	^{33}0.021		^{33}0.053	^{18}0.018	^{23}0.061		^{32}0.063	0.000	0.000		0.000
33	COGNITEC-0	^{112}0.028	^{92}0.059			^{108}0.098	^{98}0.200			0.003	0.002		
34	COGNITEC-1	^{83}0.014	^{62}0.034		^{61}0.074	^{77}0.055	^{77}0.135		^{46}0.072	0.003	0.002		0.025
35	COGNITEC-2	^{42}0.008	^{49}0.025	^{29}0.941	^{50}0.065	^{42}0.027	^{64}0.101	^{15}0.947	^{28}0.061	0.003	0.002	0.924	0.021
36	COGNITEC-3	^{45}0.009	^{48}0.025		^{29}0.051	^{44}0.028	^{59}0.100		^{19}0.049	0.004	0.002		0.012
37	DAHUA-0	^{64}0.012	^{51}0.026			^{70}0.047	^{47}0.083			0.004	0.003		
38	DAHUA-1	^{47}0.009	^{44}0.024	^{14}0.590	^{4}0.038	^{58}0.039	^{40}0.075	^{10}0.862	^{8}0.043	0.002	0.002	0.346	0.001
39	DERMALOG-0	^{161}0.131	^{133}0.218		^{63}0.075	^{159}0.364	^{139}0.528		^{69}0.104	0.003	0.002		0.020
40	DERMALOG-1	^{163}0.156			^{75}0.089	^{165}0.405			^{81}0.131	0.003			0.020
41	DERMALOG-2	^{162}0.138			^{66}0.076	^{161}0.378			^{70}0.105	0.003			0.020
42	DERMALOG-3	^{158}0.128	^{132}0.217			^{158}0.362	^{138}0.526			0.002	0.002		
43	DERMALOG-4	^{157}0.127	^{131}0.215		^{53}0.066	^{157}0.360	^{136}0.526		^{61}0.095	0.001	0.002		0.013
44	DERMALOG-5	^{89}0.017	^{65}0.037		^{52}0.066	^{64}0.045	^{56}0.096		^{38}0.066	0.001	0.002		0.013
45	DERMALOG-6	^{56}0.010	^{47}0.024	^{13}0.517	^{35}0.056	^{45}0.028	^{29}0.067	^{9}0.856	^{26}0.054	0.003	0.006	0.181	0.014
46	EVERAI-0	^{99}0.021	^{69}0.038			^{73}0.047	^{60}0.100			0.000	0.000		
47	EVERAI-1	^{20}0.006	^{28}0.020		^{129}0.928	^{27}0.023	^{36}0.074		^{127}0.927	0.000	0.000		0.000
48	EVERAI-2	^{22}0.006	^{35}0.022		^{113}0.302	^{34}0.025	^{41}0.076		^{108}0.308	0.000	0.000		0.001
49	EVERAI-3	^{15}0.005	^{24}0.019	^{4}0.154	^{5}0.038	^{17}0.018	^{21}0.060	^{6}0.535	^{11}0.044	0.000	0.000	0.032	0.001
50	EYEDEA-0	^{184}0.300	^{147}0.443		^{92}0.131	^{184}0.679	^{147}0.783		^{103}0.249	0.001	0.003		0.008
51	EYEDEA-1	^{172}0.198			^{60}0.072	^{169}0.480			^{80}0.131	0.001			0.008
52	EYEDEA-2	^{173}0.200			^{57}0.070	^{172}0.490			^{78}0.130	0.000			0.005
53	EYEDEA-3	^{151}0.082	^{124}0.148		^{48}0.064	^{150}0.267	^{126}0.404		^{56}0.091	0.001	0.003		0.008
54	GLORY-0	^{168}0.180	^{140}0.320			^{154}0.297	^{130}0.470			0.011	0.013		
55	GLORY-1	^{159}0.129	^{137}0.267		^{114}0.315	^{147}0.238	^{128}0.448		^{110}0.353	0.011	0.013		0.114
56	GORILLA-0				^{133}0.994				^{131}0.994	0.001			0.008
57	GORILLA-1	^{143}0.063	^{114}0.095		^{37}0.057	^{148}0.248	^{119}0.314		^{48}0.076	0.001	0.001		0.007
58	GORILLA-2	^{100}0.022	^{79}0.044		^{19}0.045	^{114}0.108	^{90}0.170		^{20}0.049	0.001	0.001		0.006
59	GORILLA-3	^{121}0.038	^{101}0.070		^{56}0.069	^{133}0.160	^{110}0.247		^{51}0.080	0.001	0.001		0.007
60	HBINNO-0	^{183}0.275			^{118}0.335	^{182}0.632			^{112}0.411	0.007			0.151
61	HIK-0	^{107}0.024	^{60}0.033		^{97}0.153	^{93}0.070	^{66}0.103		^{89}0.155	0.010	0.004		0.027
62	HIK-1	^{91}0.017			^{101}0.162	^{91}0.067			^{92}0.166	0.003			0.013
63	HIK-2	^{90}0.017			^{83}0.094	^{92}0.067			^{68}0.103	0.001			0.008
64	HIK-3	^{82}0.014	^{53}0.027			^{82}0.060	^{67}0.105			0.000	0.000		
65	HIK-4	^{80}0.014	^{52}0.027		^{42}0.062	^{80}0.056	^{63}0.101		^{47}0.075	0.000	0.000		0.008
66	HIK-5	^{29}0.007	^{16}0.017	^{10}0.371		^{23}0.022	^{11}0.048	^{29}0.994		0.000	0.000	0.000	0.001
67	HIK-6	^{30}0.007	^{15}0.017	^{11}0.371	^{135}1.000	^{26}0.022	^{14}0.052	^{32}0.997	^{133}1.000	0.000	0.000	0.000	0.001
68	IDEMIA-0	^{61}0.011	^{63}0.034		^{104}0.166	^{85}0.062	^{83}0.156		^{107}0.288	0.003	0.000		0.002
69	IDEMIA-1	^{65}0.012			^{99}0.157	^{50}0.031			^{97}0.205	0.003			0.002
70	IDEMIA-2	^{71}0.013			^{107}0.198	^{53}0.032			^{100}0.242	0.005			0.031
71	IDEMIA-3	^{54}0.010	^{61}0.034			^{32}0.024	^{43}0.079			0.000	0.000		
72	IDEMIA-4	^{50}0.009	^{59}0.032	^{27}0.934	^{27}0.051	^{31}0.024	^{42}0.079	^{17}0.962	^{35}0.064	0.000	0.000	0.041	0.003

Table 22: **Miss rates by dataset:** *At left, rank 1 miss rates relevant to investigations; at right, with threshold set to target FPIR = 0.01 for higher volume, low prior, uses. $^{+}$For the WILD set, FPIR = 0.1 Yellow indicates most accurate algorithm. Throughout blue superscripts indicate the rank of the algorithm for that column.*

		INVESTIGATION MODE RANK ONE MISS RATE, FNIR(N, 0, 1)				IDENTIFICATION MODE HIGH T $\rightarrow$ FPIR = 0.01, FNIR(N, T, L)				FAILURE TO EXTRACT FEATURES			
		N=1.6M	N=1.6M	N=1.6M	N=1.1M	N=1.6M	N=1.6M	N=1.6M	N=1.1M	N=1.6M	N=1.6M	N=1.6M	N=1.1M
#	ALGORITHM	FRVT-18	WEBCAM	PROFILE	WILD	FRVT-18	WEBCAM	PROFILE	WILD^{+}	FRVT-18	WEBCAM	PROFILE	WILD
73	IDEMIA-5	^{59}0.011	^{72}0.039	^{30}0.943	^{16}0.044	^{46}0.028	^{65}0.102	^{19}0.968	^{27}0.055	0.000	0.000	0.041	0.000
74	IDEMIA-6	^{69}0.012	^{103}0.072		^{31}0.052	^{43}0.028	^{84}0.161		^{39}0.067	0.000	0.000		0.000
75	IMAGUS-0	^{185}0.305	^{149}0.482		^{109}0.222	^{181}0.608	^{146}0.779		^{109}0.311	0.009	0.013		0.049
76	IMAGUS-2	^{177}0.222	^{138}0.301		^{98}0.154	^{179}0.566	^{143}0.645		^{105}0.252	0.004	0.008		0.023
77	IMAGUS-3	^{188}0.358	^{150}0.513			^{183}0.670	^{148}0.809			0.004	0.008		
78	INCODE-0	^{139}0.051	^{116}0.100			^{144}0.201	^{118}0.304			0.001	0.004		
79	INCODE-1	^{93}0.019	^{83}0.046		^{30}0.052	^{115}0.114	^{96}0.198		^{30}0.062	0.001	0.004		0.009
80	INCODE-2	^{98}0.020	^{85}0.048		^{8}0.039	^{112}0.102	^{91}0.176		^{13}0.045	0.000	0.001		0.001
81	INCODE-3	^{85}0.015	^{74}0.040		^{10}0.039	^{101}0.086	^{87}0.164		^{12}0.044	0.000	0.001		0.001
82	INNOVATRICS-0	^{127}0.042	^{106}0.076		^{105}0.188	^{138}0.165	^{112}0.258		^{101}0.245	0.002	0.008		0.093
83	INNOVATRICS-1	^{126}0.042			^{106}0.193	^{137}0.165			^{99}0.221	0.002			0.093
84	INNOVATRICS-2	^{136}0.048	^{104}0.074			^{132}0.142	^{102}0.209			0.000	0.001		
85	INNOVATRICS-3	^{113}0.029	^{88}0.055		^{58}0.071	^{128}0.134	^{99}0.203		^{52}0.081	0.000	0.001		0.007
86	INNOVATRICS-4	^{84}0.015	^{75}0.040	^{28}0.940	^{55}0.067	^{98}0.076	^{79}0.149	^{18}0.966	^{43}0.071	0.000	0.001	0.046	0.013
87	ISYSTEMS-0	^{77}0.014	^{71}0.038		^{103}0.163	^{69}0.047	^{70}0.110		^{94}0.169	0.003	0.013		0.065
88	ISYSTEMS-1	^{76}0.014			^{102}0.162	^{67}0.047			^{93}0.169	0.003			0.065
89	ISYSTEMS-2	^{44}0.009	^{50}0.026		^{24}0.049	^{55}0.035	^{45}0.080		^{22}0.051	0.002	0.002		0.009
90	ISYSTEMS-3	^{37}0.007	^{42}0.023	^{19}0.718	^{15}0.043	^{40}0.027	^{31}0.068	^{31}0.995	^{10}0.044	0.002	0.002	0.142	0.003
91	LOOKMAN-3	^{62}0.011	^{70}0.038		^{181}1.000	^{41}0.027	^{46}0.082			0.000	0.000		0.000
92	LOOKMAN-4	^{66}0.012	^{73}0.039	^{32}0.978	^{183}1.000	^{39}0.027	^{38}0.075	^{22}0.978		0.000	0.000	0.000	0.000
93	MEGVII-0	^{51}0.009	^{18}0.017		^{41}0.061	^{81}0.058	^{30}0.067		^{60}0.094	0.000	0.000		0.005
94	MEGVII-1	^{78}0.014	^{19}0.017			^{57}0.039	^{22}0.061			0.002	0.000		
95	MEGVII-2	^{79}0.014	^{20}0.017	^{7}0.275		^{59}0.039	^{20}0.059	^{8}0.698		0.002	0.000	0.033	
96	MICROFOCUS-0	^{195}0.597	^{161}0.782		^{115}0.316	^{192}0.867	^{157}0.950		^{115}0.434	0.005	0.030		0.065
97	MICROFOCUS-1	^{196}0.597			^{116}0.316	^{193}0.867			^{116}0.434	0.005			0.065
98	MICROFOCUS-2	^{197}0.627			^{119}0.342	^{194}0.870			^{117}0.447	0.005			0.065
99	MICROFOCUS-3	^{194}0.595	^{160}0.781		^{110}0.279	^{191}0.866	^{156}0.948		^{113}0.412	0.001	0.005		0.014
100	MICROFOCUS-4	^{193}0.577	^{159}0.758			^{199}0.999	^{155}0.940			0.001	0.005		
101	MICROFOCUS-5	^{189}0.426	^{156}0.601		^{100}0.158	^{189}0.736	^{152}0.865		^{106}0.261	0.001	0.005		0.011
102	MICROFOCUS-6	^{190}0.428	^{155}0.583		^{95}0.146	^{195}0.963	^{151}0.858		^{102}0.246	0.001	0.005		0.011
103	MICROSOFT-0	^{23}0.006	^{30}0.021		^{49}0.065	^{22}0.022	^{33}0.071		^{37}0.065	0.000	0.001		0.019
104	MICROSOFT-1	^{21}0.006			^{44}0.062	^{24}0.022			^{29}0.061	0.000			0.019
105	MICROSOFT-2	^{25}0.006			^{45}0.063	^{36}0.026			^{34}0.063	0.000			0.019
106	MICROSOFT-3	^{4}0.003	^{8}0.012			^{16}0.014	^{18}0.056			0.000	0.001		
107	MICROSOFT-4	^{2}0.003	^{7}0.012		^{9}0.039	^{15}0.013	^{15}0.053		^{9}0.043	0.000	0.001		0.004
108	MICROSOFT-5	^{5}0.003	^{5}0.011	^{1}0.087	^{2}0.033	^{12}0.012	^{9}0.041	^{2}0.188	^{4}0.041	0.000	0.001	0.049	0.000
109	MICROSOFT-6	^{8}0.003	^{6}0.011	^{2}0.089		^{5}0.008	^{5}0.024	^{1}0.148		0.000	0.001	0.049	
110	NEC-0	^{94}0.020	^{77}0.041		^{134}0.999	^{74}0.049	^{52}0.093		^{132}0.999	0.001	0.002		0.064
111	NEC-1	^{106}0.024	^{89}0.056			^{87}0.063	^{76}0.133			0.005	0.003		
112	NEC-2	^{1}0.003	^{2}0.009		^{80}0.093	^{1}0.004	^{2}0.013		^{71}0.107	0.000	0.001		0.025
113	NEC-3	^{3}0.003	^{3}0.010	^{6}0.272	^{74}0.088	^{2}0.004	^{1}0.013	^{5}0.479	^{58}0.092	0.000	0.001	0.041	0.025
114	NEUROTECHNOLOGY-0	^{138}0.050	^{118}0.104		^{137}1.000	^{143}0.196	^{120}0.317		^{135}1.000	0.004	0.022		0.091
115	NEUROTECHNOLOGY-1	^{135}0.047			^{130}0.954	^{142}0.195			^{128}0.953	0.001			0.028
116	NEUROTECHNOLOGY-2	^{134}0.047			^{131}0.983	^{141}0.195			^{129}0.983	0.001			0.028
117	NEUROTECHNOLOGY-3	^{109}0.025	^{78}0.042			^{111}0.101	^{86}0.164			0.000	0.001		
118	NEUROTECHNOLOGY-4	^{40}0.008	^{26}0.020		^{76}0.090	^{48}0.030	^{34}0.073		^{74}0.122	0.000	0.001		0.007
119	NEUROTECHNOLOGY-5	^{31}0.007	^{46}0.024	^{22}0.854	^{121}0.408	^{35}0.025	^{37}0.074	^{23}0.982	^{114}0.415	0.000	0.000	0.030	0.000
120	NEUROTECHNOLOGY-6	^{95}0.020	^{80}0.045		^{25}0.050	^{123}0.124	^{101}0.206		^{36}0.065	0.000	0.000		0.001
121	NEWLAND-2	^{150}0.081	^{119}0.117			^{153}0.296	^{122}0.335			0.007	0.012		
122	NOBLIS-1	^{181}0.251	^{151}0.522		^{127}0.734	^{197}0.992	^{199}1.000		^{124}0.744	0.000	0.000		0.000
123	NOBLIS-2	^{169}0.182	^{146}0.392	^{31}0.971		^{173}0.490	^{166}1.000	^{34}1.000		0.000	0.000	0.000	
124	NTECHLAB-0	^{63}0.012	^{58}0.031		^{12}0.041	^{72}0.047	^{68}0.105		^{7}0.043	0.000	0.001		0.005
125	NTECHLAB-1	^{81}0.014			^{20}0.045	^{78}0.056			^{21}0.049	0.000			0.005
126	NTECHLAB-3	^{41}0.008	^{39}0.023			^{49}0.030	^{39}0.075			0.000	0.000		
127	NTECHLAB-4	^{33}0.007	^{23}0.019		^{14}0.043	^{29}0.024	^{28}0.065		^{18}0.048	0.000	0.000		0.003
128	NTECHLAB-5	^{28}0.006	^{21}0.018		^{7}0.038	^{30}0.024	^{26}0.063		^{6}0.042	0.000	0.000		0.000
129	NTECHLAB-6	^{24}0.006	^{17}0.017	^{5}0.208	^{6}0.038	^{20}0.021	^{19}0.059	^{4}0.443	^{5}0.042	0.000	0.000	0.040	0.000
130	QUANTASOFT-1	^{176}0.220	^{158}0.727		^{126}0.620	^{175}0.494			^{125}0.760	0.000	0.000		0.000
131	RANKONE-0	^{133}0.045	^{120}0.117		^{89}0.114	^{127}0.129	^{116}0.291		^{91}0.161	0.000	0.000		0.000
132	RANKONE-1	^{108}0.025			^{68}0.077	^{102}0.087			^{67}0.102	0.000			0.000
133	RANKONE-2	^{102}0.022	^{102}0.071			^{97}0.073	^{95}0.190			0.000	0.000		
134	RANKONE-3	^{101}0.022	^{99}0.068		^{69}0.078	^{96}0.073	^{93}0.187		^{62}0.095	0.000	0.000		0.000
135	RANKONE-4	^{132}0.044	^{123}0.141		^{82}0.094	^{124}0.126	^{121}0.324		^{75}0.126	0.000	0.000		0.000
136	RANKONE-5	^{68}0.012	^{76}0.041	^{34}0.981	^{39}0.061	^{56}0.036	^{72}0.119	^{28}0.994	^{41}0.068	0.000	0.000	0.489	0.000
137	REALNETWORKS-0	^{131}0.043	^{110}0.078		^{65}0.076	^{131}0.140	^{104}0.209		^{53}0.084	0.001	0.000		0.004
138	REALNETWORKS-1	^{130}0.043	^{109}0.078			^{130}0.140	^{103}0.209			0.001	0.000		
139	REALNETWORKS-2	^{125}0.042	^{108}0.078		^{132}0.992	^{129}0.139	^{105}0.209		^{130}0.992	0.001	0.000		0.000
140	REMARKAI-0	^{60}0.011	^{57}0.030			^{86}0.062	^{74}0.123			0.000	0.001		
141	REMARKAI-2	^{58}0.010	^{55}0.029	^{18}0.708	^{23}0.046	^{84}0.061	^{73}0.122	^{16}0.958	^{25}0.052	0.000	0.001	0.017	0.000
142	SENSETIME-0	^{16}0.005	^{13}0.016	^{12}0.446		^{10}0.012	^{8}0.040	^{20}0.971		0.004	0.000	0.042	0.000
143	SENSETIME-1	^{17}0.005	^{12}0.016		^{3}0.038	^{11}0.012	^{10}0.041		^{1}-0.796	0.004	0.000		0.000
144	SHAMAN-0	^{165}0.171	^{136}0.262		^{90}0.115	^{160}0.370	^{134}0.507		^{86}0.146	0.020	0.011		0.043

Table 23: **Miss rates by dataset:** *At left, rank 1 miss rates relevant to investigations; at right, with threshold set to target FPIR = 0.01 for higher volume, low prior, uses. $^{+}$For the WILD set, FPIR = 0.1 Yellow indicates most accurate algorithm. Throughout blue superscripts indicate the rank of the algorithm for that column.*

		INVESTIGATION MODE				IDENTIFICATION MODE				FAILURE TO EXTRACT			
		RANK ONE MISS RATE, FNIR(N, 0, 1)				HIGH T → FPIR = 0.01, FNIR(N, T, L)				FEATURES			
		N=1.6M	N=1.6M	N=1.6M	N=1.1M	N=1.6M	N=1.6M	N=1.6M	N=1.1M	N=1.6M	N=1.6M	N=1.6M	N=1.1M
#	ALGORITHM	FRVT-18	WEBCAM	PROFILE	WILD	FRVT-18	WEBCAM	PROFILE	WILD^{+}	FRVT-18	WEBCAM	PROFILE	WILD
145	SHAMAN-1	^{166}0.172			^{88}0.113	^{166}0.406			^{88}0.153	0.020			0.043
146	SHAMAN-2	^{182}0.262			^{93}0.132	^{180}0.582			^{96}0.201	0.020			0.043
147	SHAMAN-3	^{155}0.127	^{127}0.172		^{86}0.109	^{156}0.348	^{131}0.472		^{82}0.132	0.020	0.011		0.043
148	SHAMAN-4	^{178}0.224	^{139}0.319			^{171}0.490	^{142}0.639			0.020	0.011		
149	SHAMAN-6	^{129}0.042	^{91}0.058	^{26}0.910		^{105}0.095	^{88}0.168	^{14}0.935		0.020	0.011	0.869	
150	SHAMAN-7	^{128}0.042	^{90}0.057		^{70}0.078	^{104}0.094	^{89}0.169		^{50}0.079	0.020	0.010		0.029
151	SIAT-0	^{55}0.010	^{32}0.021		^{71}0.078	^{68}0.047	^{27}0.064		^{104}0.250	0.000	0.000		0.008
152	SIAT-1	^{10}0.004	^{142}0.333		^{11}0.040	^{6}0.009	^{123}0.348		^{3}0.041	0.000	0.000		0.003
153	SIAT-2	^{11}0.004	^{148}0.446			^{7}0.009	^{129}0.460			0.000	0.000		
154	SMILART-0	^{170}0.193	^{141}0.325		^{196}1.000	^{170}0.486			^{196}1.000	0.008			0.121
155	SMILART-1	^{175}0.219			^{154}1.000	^{177}0.505			^{153}1.000	0.021			0.006
156	SMILART-2	^{171}0.195			^{145}1.000	^{174}0.492			^{144}1.000	0.000			0.048
157	SMILART-4	^{198}0.965	^{162}0.974		^{128}0.834	^{196}0.965	^{158}0.973		^{126}0.833	0.011	0.013		0.039
158	SMILART-5									0.011	0.013		
159	SYNESIS-0	^{164}0.162	^{145}0.361			^{162}0.378	^{141}0.598			0.002	0.009		0.081
160	SYNESIS-3	^{167}0.172	^{134}0.235			^{168}0.444	^{135}0.524			0.006	0.015		0.042
161	TEVIAN-0	^{104}0.022	^{97}0.066		^{34}0.054	^{117}0.114	^{106}0.227		^{44}0.072	0.002	0.005		0.007
162	TEVIAN-1	^{105}0.022			^{43}0.062	^{118}0.114			^{49}0.078	0.002			0.007
163	TEVIAN-2	^{103}0.022			^{79}0.093	^{116}0.114			^{73}0.118	0.002			0.008
164	TEVIAN-3	^{88}0.017	^{86}0.052			^{109}0.098	^{97}0.198			0.001	0.002		
165	TEVIAN-4	^{75}0.013	^{68}0.038		^{26}0.050	^{90}0.066	^{71}0.115		^{33}0.063	0.001	0.002		0.005
166	TEVIAN-5	^{48}0.009	^{54}0.028	^{8}0.329		^{71}0.047	^{49}0.089	^{7}0.661		0.001	0.002	0.116	
167	TIGER-0	^{144}0.064	^{115}0.095		^{186}1.000	^{149}0.263	^{124}0.366		^{185}1.000	0.000	0.000		0.005
168	TIGER-1		^{144}0.351				^{132}0.487			0.000	0.000		
169	TIGER-2	^{39}0.008	^{41}0.023	^{9}0.355		^{61}0.042	^{55}0.095	^{12}0.927		0.000	0.000	0.056	
170	TIGER-3	^{38}0.008	^{40}0.023			^{62}0.042	^{54}0.095			0.000	0.000		
171	TONGYITRANS-0	^{53}0.010	^{38}0.022			^{60}0.041	^{32}0.069			0.003	0.001		
172	TONGYITRANS-1	^{52}0.010	^{37}0.022		^{87}0.112	^{54}0.035	^{24}0.062		^{83}0.134	0.003	0.001		0.009
173	TOSHIBA-0	^{32}0.007	^{34}0.022	^{17}0.689		^{47}0.029	^{35}0.074	^{21}0.971		0.000	0.000	0.070	0.002
174	TOSHIBA-1	^{34}0.007	^{36}0.022			^{21}0.021	^{16}0.054			0.000	0.000		
175	VD-0	^{192}0.475	^{154}0.551		^{108}0.217	^{190}0.828	^{153}0.871		^{111}0.362	0.011	0.013		0.026
176	VD-1	^{115}0.030	^{87}0.053			^{121}0.118	^{94}0.188			0.005	0.001		0.017
177	VIGILANTSOLUTIONS-0	^{154}0.125	^{130}0.212		^{67}0.076	^{163}0.394	^{140}0.557		^{87}0.152	0.000	0.001		0.003
178	VIGILANTSOLUTIONS-1	^{174}0.204			^{85}0.103	^{176}0.502			^{98}0.209	0.000			0.003
179	VIGILANTSOLUTIONS-2	^{180}0.239			^{47}0.064	^{188}0.731			^{76}0.129	0.000			0.003
180	VIGILANTSOLUTIONS-3	^{148}0.072	^{125}0.151		^{51}0.065	^{151}0.283	^{137}0.526		^{79}0.131	0.000	0.001		0.003
181	VIGILANTSOLUTIONS-4	^{156}0.127	^{135}0.244			^{167}0.424	^{145}0.709			0.000	0.001		
182	VIGILANTSOLUTIONS-5	^{67}0.012				^{63}0.045				0.000	0.001		
183	VIGILANTSOLUTIONS-6	^{70}0.013				^{65}0.046				0.000	0.001		
184	VISIONLABS-3	^{46}0.009	^{56}0.030		^{28}0.051	^{37}0.026	^{50}0.091		^{15}0.046	0.002	0.003		0.014
185	VISIONLABS-4	^{13}0.004	^{25}0.020			^{38}0.026	^{57}0.097			0.001	0.001		
186	VISIONLABS-5	^{12}0.004	^{22}0.019		^{13}0.043	^{25}0.022	^{48}0.087		^{16}0.046	0.001	0.001		0.006
187	VISIONLABS-6	^{7}0.003	^{11}0.015			^{14}0.012	^{13}0.051			0.001	0.001		
188	VISIONLABS-7	^{6}0.003	^{10}0.015	^{3}0.130	^{1}0.033	^{13}0.012	^{12}0.051	^{3}0.322	^{2}0.035	0.001	0.001	0.051	0.001
189	VOCORD-0	^{123}0.040	^{100}0.068			^{120}0.116	^{92}0.181			0.015	0.025		0.019
190	VOCORD-1	^{122}0.040				^{119}0.116				0.015			0.018
191	VOCORD-2	^{120}0.038				^{113}0.107				0.015			0.015
192	VOCORD-3	^{43}0.008	^{45}0.024		^{36}0.057	^{75}0.050	^{53}0.093		^{31}0.062	0.001	0.011		0.006
193	VOCORD-4	^{57}0.010	^{31}0.021			^{76}0.054	^{51}0.093			0.000	0.000		
194	VOCORD-5	^{49}0.009	^{43}0.023	^{20}0.739	^{17}0.044	^{66}0.046	^{44}0.080	^{13}0.929	^{14}0.045	0.001	0.009	0.554	0.003
195	VOCORD-6	^{203}1.000	^{201}1.000			^{203}1.000	^{201}1.000			0.001	0.009		
196	YISHENG-0	^{111}0.027	^{93}0.060		^{54}0.067	^{146}0.209	^{114}0.275		^{66}0.100	0.002	0.005		0.014
197	YISHENG-1	^{114}0.029	^{94}0.060		^{40}0.061	^{145}0.208	^{113}0.269		^{54}0.087	0.002	0.005		0.014
198	YITU-0	^{36}0.007	^{29}0.020		^{73}0.086	^{33}0.025	^{17}0.054		^{59}0.094	0.003	0.001		0.026
199	YITU-1	^{35}0.007			^{72}0.086	^{28}0.023			^{57}0.092	0.003			0.026
200	YITU-2	^{14}0.004	^{4}0.010		^{22}0.046	^{8}0.011	^{6}0.028		^{24}0.051	0.000	0.000		0.000
201	YITU-3	^{19}0.005	^{14}0.016			^{9}0.011	^{7}0.033			0.003	0.001		
202	YITU-4	^{9}0.004	^{1}0.008	^{21}0.831	^{18}0.044	^{3}0.007	^{3}0.017	^{11}0.875	^{17}0.047	0.000	0.000	0.000	0.006
203	YITU-5	^{18}0.005	^{9}0.014			^{4}0.007	^{4}0.023			0.003	0.001		

Table 24: **Miss rates by dataset:** *At left, rank 1 miss rates relevant to investigations; at right, with threshold set to target FPIR = 0.01 for higher volume, low prior, uses. $^{+}$For the WILD set, FPIR = 0.1 Yellow indicates most accurate algorithm. Throughout blue superscripts indicate the rank of the algorithm for that column.*

MISSES OUTSIDE RANK R		MUGSHOT SEARCHES, N = 1.6M IDENTITIES							
		INVESTIGATION MODE, T = 0				IDENTIFICATION MODE, T > 0 FOR FPIR = 0.001			
FNIR(N, T, R)		PROPORTION MATED SEARCHES				PROPORTION MATED SEARCHES			
GALLERY		WITHOUT THE MATE AT RANK 1		WITH NO MATE AT RANK 1	WITH K-TH MATE NOT IN TOP K	WITH THE MATE BELOW THRESHOLD		WITHOUT ANY MATE ABOVE THRESH	WITHOUT ALL MATES ABOVE THRESH
		RECENT	CONSOLIDATED	UNCONSOLIDATED		RECENT	CONSOLIDATED	UNCONSOLIDATED	
1	3DIVI-5	[49] 0.0202	[43] 0.0133	[46] 0.0133	[48] 0.0449	[48] 0.1691	[46] 0.1339	[48] 0.1339	[49] 0.3186
2	3DIVI-6	[52] 0.0265	[46] 0.0186	[51] 0.0172	[47] 0.0410	[51] 0.1705	[47] 0.1345	[49] 0.1350	[48] 0.3160
3	ALCHERA-2	[64] 0.0973	[57] 0.0914	[63] 0.0734	[63] 0.1876	[64] 0.4899	[57] 0.3736	[63] 0.4418	[63] 0.6820
4	ANKE-0	[45] 0.0158	[39] 0.0100	[43] 0.0100	[45] 0.0338	[41] 0.1199	[38] 0.0989	[42] 0.0989	[42] 0.2558
5	ANKE-1	[46] 0.0158	[40] 0.0101	[44] 0.0101	[44] 0.0337	[42] 0.1218	[40] 0.1001	[44] 0.1001	[43] 0.2581
6	AWARE-5	[54] 0.0337	[47] 0.0208	[53] 0.0230	[57] 0.0740	[60] 0.3729	[56] 0.2984	[60] 0.3777	[61] 0.6534
7	AWARE-6	[62] 0.0722	[56] 0.0538	[60] 0.0538	[61] 0.1551	[58] 0.2779	[53] 0.2419	[58] 0.2465	[58] 0.5140
8	AYONIX-1	[70] 0.3432	[62] 0.3364	[67] 0.2841	[68] 0.4764	[68] 0.8247	[61] 0.8533	[66] 0.7935	[66] 0.9037
9	AYONIX-2	[69] 0.3432	[61] 0.2606	[68] 0.2841	[67] 0.4763	[67] 0.8246	[59] 0.8038	[65] 0.7933	[65] 0.9036
10	CAMVI-4	[60] 0.0490	[54] 0.0326	[59] 0.0469	[49] 0.0475	[31] 0.0741	[27] 0.0505	[34] 0.0661	[16] 0.1105
11	CAMVI-5	[61] 0.0673	[55] 0.0458	[62] 0.0633	[56] 0.0638	[40] 0.1020	[36] 0.0727	[40] 0.0922	[29] 0.1513
12	COGENT-2	[14] 0.0062	[12] 0.0027	[12] 0.0027	[12] 0.0086	[19] 0.0475	[12] 0.0299	[19] 0.0391	[20] 0.1275
13	COGENT-3	[15] 0.0064	[18] 0.0037	[13] 0.0029	[13] 0.0091	[21] 0.0515	[17] 0.0341	[27] 0.0450	[28] 0.1448
14	COGNITEC-2	[25] 0.0083	[22] 0.0044	[23] 0.0043	[24] 0.0145	[25] 0.0560	[22] 0.0401	[22] 0.0400	[25] 0.1342
15	COGNITEC-3	[26] 0.0088	[24] 0.0048	[26] 0.0048	[25] 0.0148	[24] 0.0555	[21] 0.0397	[21] 0.0397	[24] 0.1322
16	DAHUA-0	[35] 0.0115	[32] 0.0070	[36] 0.0072	[34] 0.0204	[37] 0.0891	[32] 0.0624	[35] 0.0691	[36] 0.1967
17	DAHUA-1	[27] 0.0089	[25] 0.0049	[27] 0.0052	[27] 0.0173	[33] 0.0755	[28] 0.0521	[30] 0.0577	[33] 0.1738
18	DERMALOG-5	[47] 0.0171	[41] 0.0113	[48] 0.0139	[41] 0.0254	[39] 0.0909	[33] 0.0649	[38] 0.0767	[39] 0.2072
19	DERMALOG-6	[30] 0.0102	[28] 0.0060	[30] 0.0061	[19] 0.0119	[23] 0.0542	[20] 0.0383	[24] 0.0416	[21] 0.1280
20	EVERAI-2	[12] 0.0058	[13] 0.0029	[15] 0.0032	[15] 0.0099	[22] 0.0526	[19] 0.0370	[23] 0.0410	[23] 0.1312
21	EVERAI-3	[8] 0.0047	[11] 0.0023	[11] 0.0024	[11] 0.0073	[11] 0.0377	[11] 0.0256	[11] 0.0285	[11] 0.0978
22	GORILLA-2	[51] 0.0220	[44] 0.0137	[50] 0.0153	[55] 0.0570	[53] 0.1902	[49] 0.1379	[52] 0.1537	[52] 0.3589
23	GORILLA-3	[55] 0.0384	[49] 0.0245	[55] 0.0283	[60] 0.1032	[59] 0.3260	[55] 0.2730	[59] 0.3043	[59] 0.5786
24	HIK-5	[17] 0.0067		[20] 0.0037	[23] 0.0140	[17] 0.0467		[18] 0.0364	[18] 0.1228
25	HIK-6	[18] 0.0067	[16] 0.0034	[19] 0.0037	[22] 0.0140	[20] 0.0500	[16] 0.0324	[20] 0.0392	[22] 0.1310
26	IDEMIA-5	[32] 0.0107	[29] 0.0062	[32] 0.0064	[33] 0.0192	[16] 0.0465	[15] 0.0319	[17] 0.0348	[17] 0.1125
27	IDEMIA-6	[39] 0.0122	[33] 0.0071	[38] 0.0076	[32] 0.0188	[14] 0.0458	[14] 0.0316	[14] 0.0342	[13] 0.1032
28	INCODE-2	[50] 0.0203	[42] 0.0120	[47] 0.0137	[50] 0.0480	[52] 0.1861	[48] 0.1360	[51] 0.1507	[51] 0.3500
29	INCODE-3	[44] 0.0153	[36] 0.0088	[45] 0.0103	[46] 0.0368	[50] 0.1703	[45] 0.1227	[50] 0.1388	[50] 0.3290
30	INNOVATRICS-4	[43] 0.0149	[35] 0.0081	[40] 0.0081	[43] 0.0293	[45] 0.1340	[37] 0.0928	[41] 0.0927	[41] 0.2479
31	ISYSTEMS-3	[22] 0.0075	[20] 0.0040	[22] 0.0041	[16] 0.0106	[29] 0.0620	[23] 0.0402	[28] 0.0500	[30] 0.1519
32	LOOKMAN-3	[34] 0.0114	[37] 0.0089	[34] 0.0067	[17] 0.0109	[15] 0.0463	[25] 0.0425	[13] 0.0338	[12] 0.1015
33	LOOKMAN-4	[36] 0.0117	[38] 0.0091	[35] 0.0072	[21] 0.0134	[18] 0.0472	[24] 0.0417	[15] 0.0346	[14] 0.1086
34	MEGVII-1	[41] 0.0137		[41] 0.0096	[36] 0.0231	[32] 0.0746		[31] 0.0577	[32] 0.1688
35	MEGVII-2	[42] 0.0137		[42] 0.0097	[38] 0.0236	[34] 0.0796		[33] 0.0623	[34] 0.1810
36	MICROFOCUS-5	[71] 0.4257	[63] 0.3701	[69] 0.3701	[69] 0.5522	[69] 0.8361	[63] 0.9835	[67] 0.8139	[67] 0.9189
37	MICROFOCUS-6	[72] 0.4283	[64] 0.3732	[70] 0.3732	[70] 0.5566	[71] 0.9780	[60] 0.8195	[68] 0.8195	[68] 0.9215
38	MICROSOFT-5	[3] 0.0033	[3] 0.0013	[6] 0.0015	[10] 0.0062	[8] 0.0279	[7] 0.0171	[7] 0.0193	[9] 0.0755
39	MICROSOFT-6	[6] 0.0033	[5] 0.0014	[7] 0.0015	[9] 0.0060	[5] 0.0141	[5] 0.0080	[10] 0.0213	[10] 0.0772
40	NEC-2	[1] 0.0028	[2] 0.0011	[1] 0.0008	[1] 0.0019	[2] 0.0047	[2] 0.0024	[1] 0.0021	[2] 0.0086
41	NEC-3	[2] 0.0031	[4] 0.0013	[2] 0.0010	[2] 0.0019	[1] 0.0044	[1] 0.0021	[2] 0.0022	[1] 0.0080
42	NEUROTECHNOLOGY-5	[19] 0.0068	[21] 0.0042	[14] 0.0032	[14] 0.0094	[26] 0.0564	[29] 0.0527	[25] 0.0438	[26] 0.1364
43	NEUROTECHNOLOGY-6	[48] 0.0201	[45] 0.0153	[49] 0.0142	[52] 0.0534	[57] 0.2555	[54] 0.2695	[57] 0.2125	[57] 0.4458
44	NEWLAND-2	[63] 0.0811		[61] 0.0599	[62] 0.1562	[63] 0.4405		[61] 0.3790	[60] 0.6252
45	NOBLIS-1	[68] 0.2512	[60] 0.2049	[65] 0.2032	[65] 0.3631	[73] 0.9996	[66] 0.9998	[72] 0.9994	[72] 0.9997
46	NOBLIS-2	[66] 0.1816	[59] 0.1565	[66] 0.2517	[66] 0.3944	[72] 0.9974	[65] 0.9959	[71] 0.9967	[71] 0.9987
47	NTECHLAB-5	[16] 0.0064	[19] 0.0039	[21] 0.0039	[30] 0.0179	[13] 0.0448	[18] 0.0347	[16] 0.0347	[19] 0.1235
48	NTECHLAB-6	[13] 0.0059	[15] 0.0034	[17] 0.0034	[26] 0.0154	[12] 0.0391	[13] 0.0301	[12] 0.0301	[15] 0.1088
49	QUANTASOFT-1	[67] 0.2198	[66] 0.9857	[71] 0.9426	[71] 0.9502	[66] 0.6399	[64] 0.9915	[69] 0.9640	[70] 0.9801
50	RANKONE-4	[59] 0.0441	[52] 0.0318	[58] 0.0318	[59] 0.0945	[54] 0.1951	[50] 0.1545	[53] 0.1545	[53] 0.3590
51	RANKONE-5	[38] 0.0120	[34] 0.0072	[37] 0.0072	[39] 0.0237	[27] 0.0617	[26] 0.0447	[26] 0.0447	[27] 0.1404
52	REALNETWORKS-2	[56] 0.0418	[53] 0.0320	[54] 0.0268	[58] 0.0903	[56] 0.2341	[52] 0.2049	[56] 0.1775	[56] 0.3949
53	REMARKAI-0	[33] 0.0109	[31] 0.0065	[33] 0.0065	[40] 0.0238	[44] 0.1301	[41] 0.1020	[45] 0.1020	[47] 0.2671
54	REMARKAI-2	[31] 0.0105	[30] 0.0062	[31] 0.0062	[37] 0.0235	[43] 0.1264	[39] 0.0991	[43] 0.0991	[44] 0.2615
55	SENSETIME-0	[9] 0.0048	[9] 0.0018	[9] 0.0018	[4] 0.0037	[6] 0.0234	[6] 0.0165	[5] 0.0168	[5] 0.0603
56	SENSETIME-1	[10] 0.0048	[8] 0.0018	[8] 0.0018	[7] 0.0041	[7] 0.0245	[8] 0.0175	[6] 0.0177	[6] 0.0628
57	SHAMAN-6	[58] 0.0424	[51] 0.0312	[57] 0.0312	[53] 0.0542	[46] 0.1432	[43] 0.1109	[46] 0.1109	[46] 0.2629
58	SHAMAN-7	[57] 0.0422	[50] 0.0310	[56] 0.0310	[51] 0.0529	[47] 0.1436	[44] 0.1112	[47] 0.1112	[45] 0.2624
59	SMILART-4	[73] 0.9649	[65] 0.9531	[72] 0.9722	[72] 0.9738	[70] 0.9683	[62] 0.9569	[70] 0.9740	[69] 0.9781
60	SYNESIS-3	[65] 0.1721	[58] 0.1350	[64] 0.1350	[64] 0.2571	[65] 0.5832	[58] 0.5296	[64] 0.5295	[64] 0.7459
61	TEVIAN-5	[28] 0.0092	[26] 0.0053	[29] 0.0058	[35] 0.0213	[38] 0.0898	[34] 0.0667	[39] 0.0770	[40] 0.2079
62	TIGER-2	[24] 0.0075	[23] 0.0044	[25] 0.0044	[29] 0.0177	[36] 0.0888	[35] 0.0698	[36] 0.0698	[38] 0.2016
63	TIGER-3	[23] 0.0075		[24] 0.0044	[28] 0.0177	[35] 0.0888		[37] 0.0698	[37] 0.2015
64	TOSHIBA-0	[20] 0.0068	[14] 0.0033	[16] 0.0033	[18] 0.0110	[30] 0.0648	[30] 0.0529	[29] 0.0529	[31] 0.1599
65	TOSHIBA-1	[21] 0.0071	[17] 0.0035	[18] 0.0035	[20] 0.0120	[28] 0.0618	[31] 0.0596	[32] 0.0585	[35] 0.1819
66	VD-1	[53] 0.0302	[48] 0.0221	[52] 0.0221	[54] 0.0560	[55] 0.2036	[51] 0.1654	[54] 0.1658	[54] 0.3657
67	VIGILANTSOLUTIONS-5	[37] 0.0118				[62] 0.4327			
68	VIGILANTSOLUTIONS-6	[40] 0.0125		[39] 0.0077	[42] 0.0258	[61] 0.4260		[62] 0.4155	[62] 0.6577
69	VISIONLABS-6	[5] 0.0033	[7] 0.0015	[5] 0.0015	[6] 0.0040	[10] 0.0289	[10] 0.0185	[9] 0.0201	[8] 0.0737
70	VISIONLABS-7	[4] 0.0033	[6] 0.0014	[4] 0.0014	[5] 0.0039	[9] 0.0289	[9] 0.0185	[8] 0.0201	[7] 0.0737
71	VOCORD-5	[29] 0.0092	[27] 0.0057	[28] 0.0054	[31] 0.0182	[49] 0.1697	[42] 0.1076	[55] 0.1717	[55] 0.3775
72	YITU-4	[7] 0.0037	[1] 0.0011	[3] 0.0012	[3] 0.0033	[3] 0.0123	[3] 0.0074	[3] 0.0080	[3] 0.0337
73	YITU-5	[11] 0.0048	[10] 0.0020	[10] 0.0020	[8] 0.0041	[4] 0.0128	[4] 0.0076	[4] 0.0088	[4] 0.0350

Table 25: **Comparing enrollment styles for the FRVT 2018 mugshot sets**. *Consolidated refers to enrollment of all lifetime images in one template Unconsolidated refers to enrollment of those images separately under different identifiers. Columns 3 - 6 values are FNIR at rank 1 and with T = 0. Columns 7 - 10 values are high threshold FNIR. Throughout, blue superscripts indicate the rank of the algorithm for that column, and the best three values are highlighted in yellow and green.*

2019/09/11	FNIR(N, R, T) =	False neg. identification rate	N = Num. enrolled subjects	T = Threshold	$T = 0 \rightarrow$ Investigation
16:09:13	FPIR(N, T) =	False pos. identification rate	R = Num. candidates examined		$T > 0 \rightarrow$ Identification

Figure 19: **[Mugshot Dataset] Error rate reductions in 2018**. *For each* FRVT*2018 participant, the plot shows accuracy gains between Phase 1 (Feb 2018), Phase 2 (Jun 2018) and Phase 3 (Nov 2018) according to two metrics: rank one miss rate, FNIR(N, 1, 0), and high threshold, FNIR(N, L, T), with T set to achieve FPIR = 0.003. The text "Red=" gives the best reduction multiplier for the given metric on the recent enrollment strategy - a smaller value is better.*

FNIR(N, R, T) = False neg. identification rate
FPIR(N, T) = False pos. identification rate
N = Num. enrolled subjects
R = Num. candidates examined
T = Threshold
T = 0 → Investigation
T > 0 → Identification

FNIR(N, R, T) = False neg. identification rate
FPIR(N, T) = False pos. identification rate
N = Num. enrolled subjects
R = Num. candidates examined
T = Threshold
T = 0 → Investigation
T > 0 → Identification

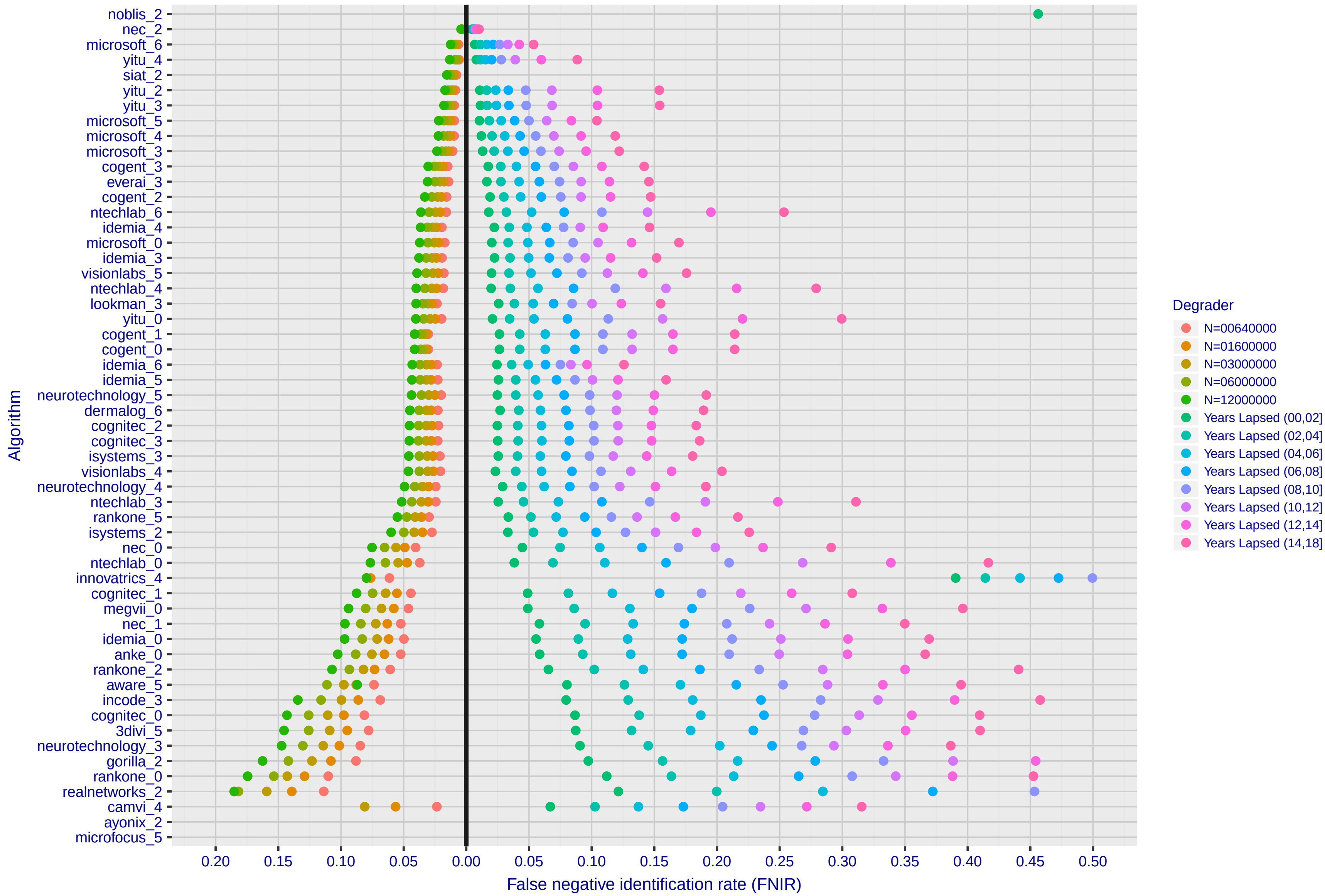

Figure 20: **[FRVT-2018 Mugshot Ageing Dataset] Contrast of ageing and population size dependency.** *The Figure shows, at left, the dependence FNIR(N) for the FRVT-2018, as tabulated in Table 12. At right, is FNIR(N = 3 000 000, ΔT) from Figure 62. Ageing miss rates are computed over all searches binned by number of years between search and initial enrollment. In all cases, FPIR = 0.01.*

This publication is available free of charge from: https://doi.org/10.6028/NIST.IR.8271

FNIR(N, R, T) = False neg. identification rate
FPIR(N, T) = False pos. identification rate
N = Num. enrolled subjects
R = Num. candidates examined
T = Threshold
T = 0 → Investigation
T > 0 → Identification

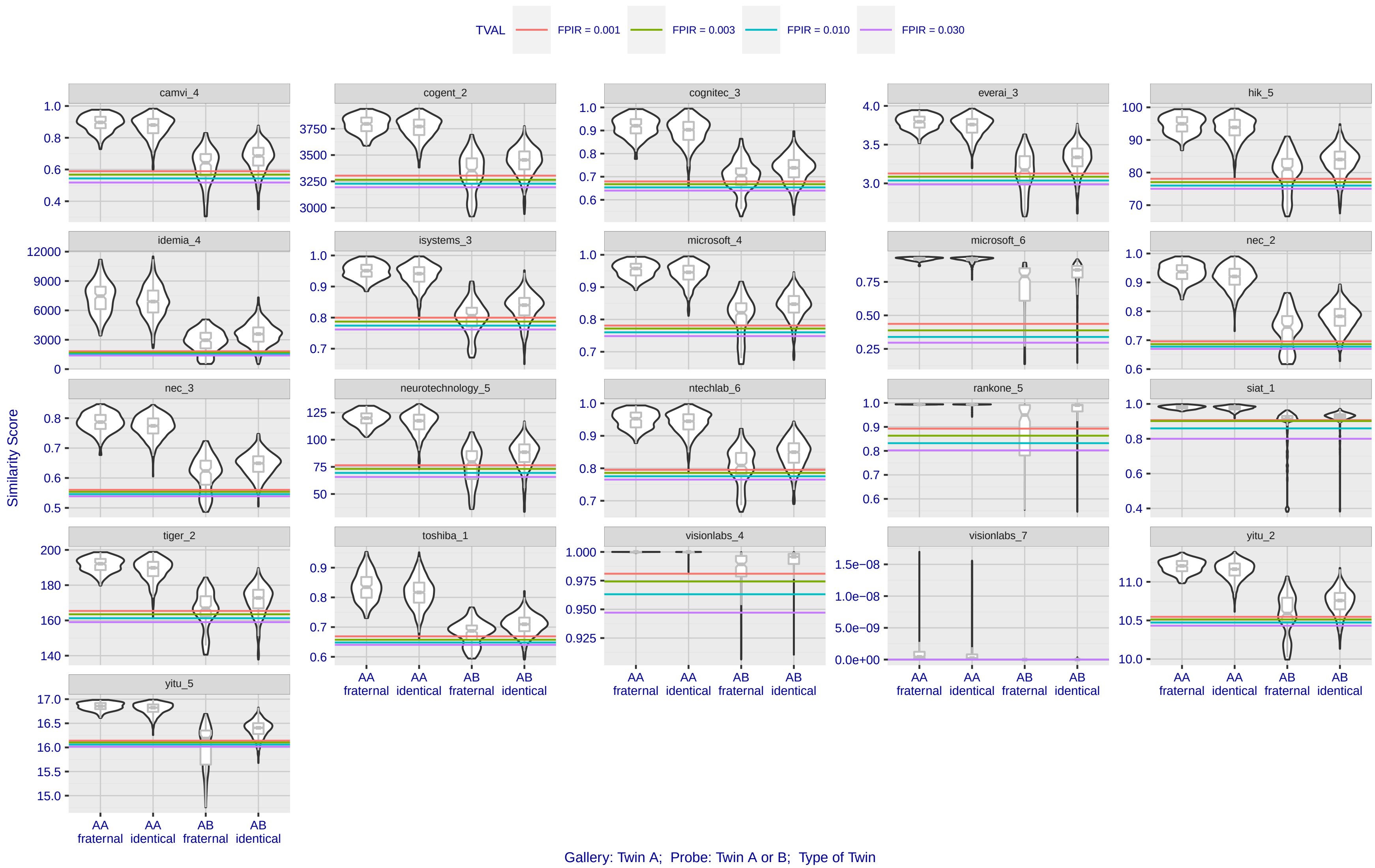

Figure 21: **[Twins Dataset] High scores from twins.** *The Figure shows native similarity scores from searches into a dataset of N = 640 000 background mugshot images plus 104 portrait images, one from each of one of a pair of twins. Two distributions of scores are plotted for each of monozygotic (identical) and dizygotic (fraternal) twins. The first distribution ("AA") shows the mate score from Twin A against their own enrollment. The second ("AB") shows scores from searches of Twin B against the Twin A enrollment: As these are non-mate scores they should be below the various thresholds shown as horizontal lines. That they usually are not is an indication that twins produce very high non-mate scores. Note in theory half of dizygotic (fraternal) twins are different sex. In the sample used here some fraternal twins are correctly rejected.*

Appendices

Appendix A Accuracy on large-population FRVT 2018 mugshots

2019/09/11	FNIR(N, R, T) =	False neg. identification rate	N = Num. enrolled subjects	T = Threshold	$T = 0 \rightarrow$ Investigation
16:09:13	FPIR(N, T) =	False pos. identification rate	R = Num. candidates examined		$T > 0 \rightarrow$ Identification

FNIR(N, R, T) = False neg. identification rate
FPIR(N, T) = False pos. identification rate
N = Num. enrolled subjects
R = Num. candidates examined
T = Threshold
T = 0 → Investigation
T > 0 → Identification

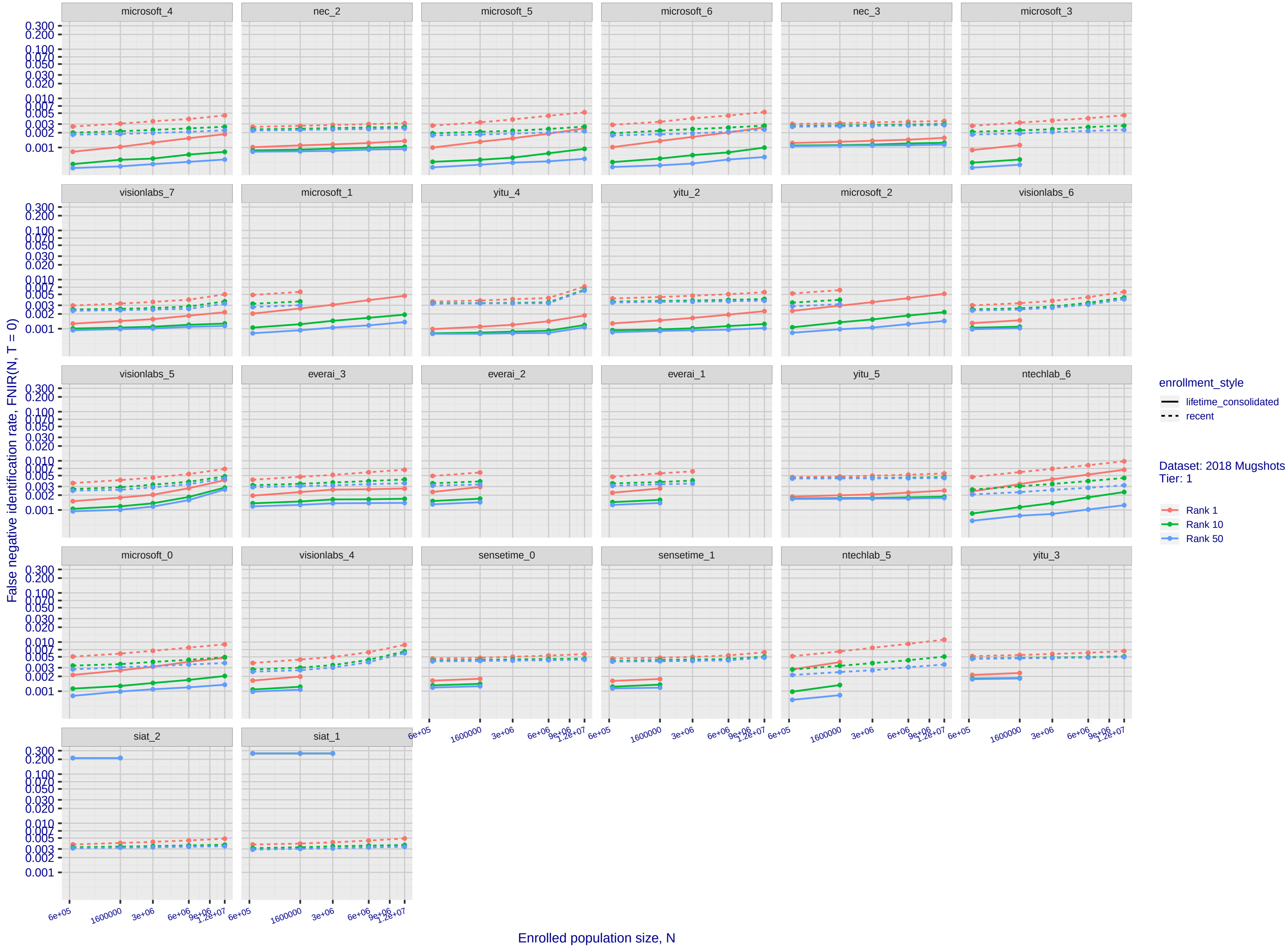

Figure 22: **[FRVT-2018 Mugshot Dataset] Rank-based identification miss rates vs. number of enrolled subjects**. *The figure shows false negative identification rates, FNIR(N, R), across various gallery sizes and ranks 1, 10 and 50. The threshold is set to zero, so this metric rewards even weak scoring rank 1 mates. This also means FPIR = 1, so any search without an enrolled mate will return non-mated candidates. For clarity, results are sorted and reported into tiers spanning multiple pages, the tiering criteria being rank 1 hit rate on a gallery size of 640 000.*

This publication is available free of charge from: https://doi.org/10.6028/NIST.IR.8271

2019/09/11 16:09:13

FNIR(N, R, T) = False neg. identification rate
FPIR(N, T) = False pos. identification rate
N = Num. enrolled subjects
R = Num. candidates examined
T = Threshold
T = 0 → Investigation
T > 0 → Identification

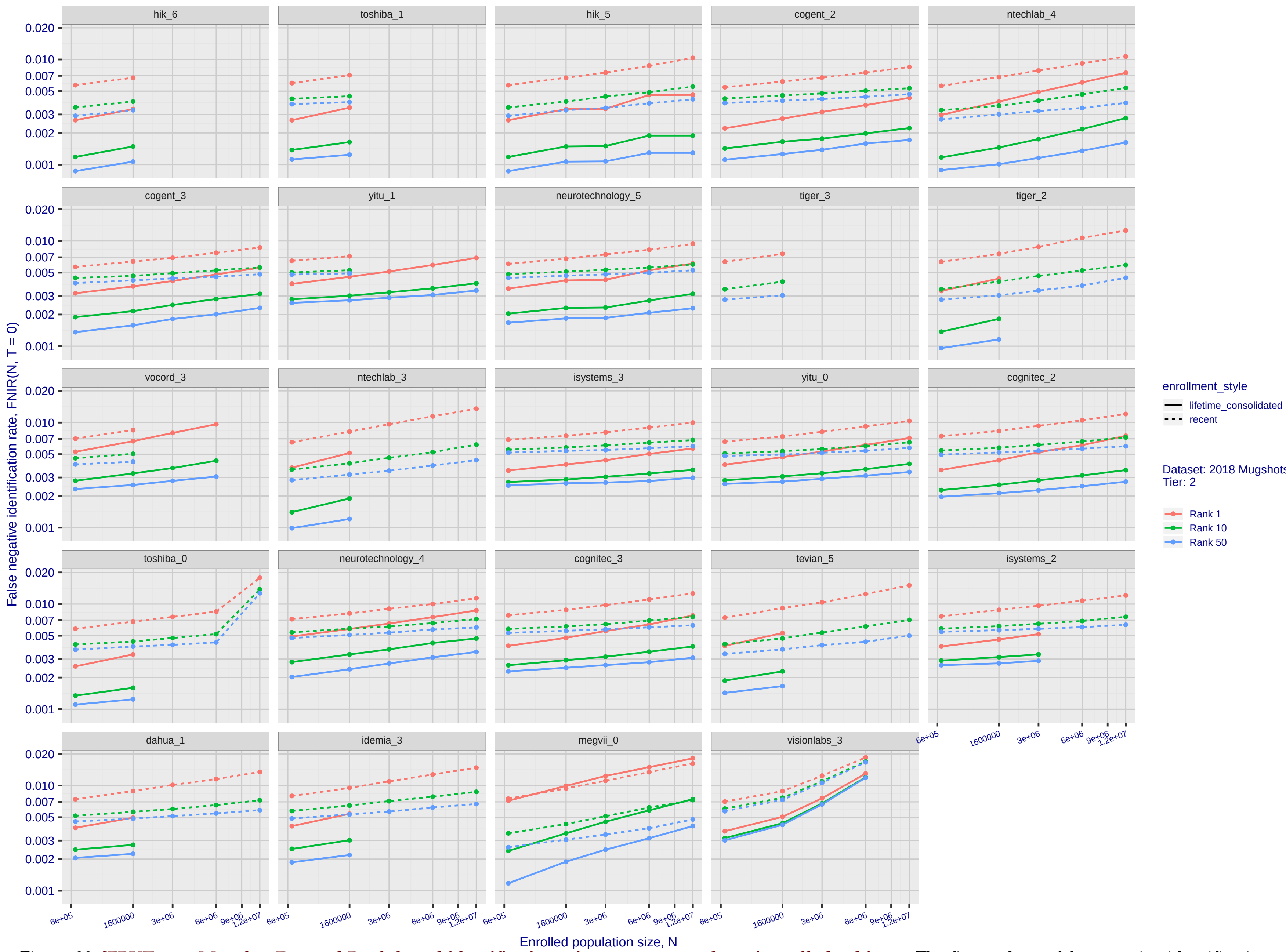

Figure 23: **[FRVT-2018 Mugshot Dataset] Rank-based identification miss rates vs. number of enrolled subjects**. *The figure shows false negative identification rates, FNIR(N, R), across various gallery sizes and ranks 1, 10 and 50. The threshold is set to zero, so this metric rewards even weak scoring rank 1 mates. This also means FPIR = 1, so any search without an enrolled mate will return non-mated candidates. For clarity, results are sorted and reported into tiers spanning multiple pages, the tiering criteria being rank 1 hit rate on a gallery size of 640 000.*

This publication is available free of charge from: https://doi.org/10.6028/NIST.IR.8271

FNIR(N, R, T) = False neg. identification rate
FPIR(N, T) = False pos. identification rate
N = Num. enrolled subjects
R = Num. candidates examined
T = Threshold
T = 0 → Investigation
T > 0 → Identification

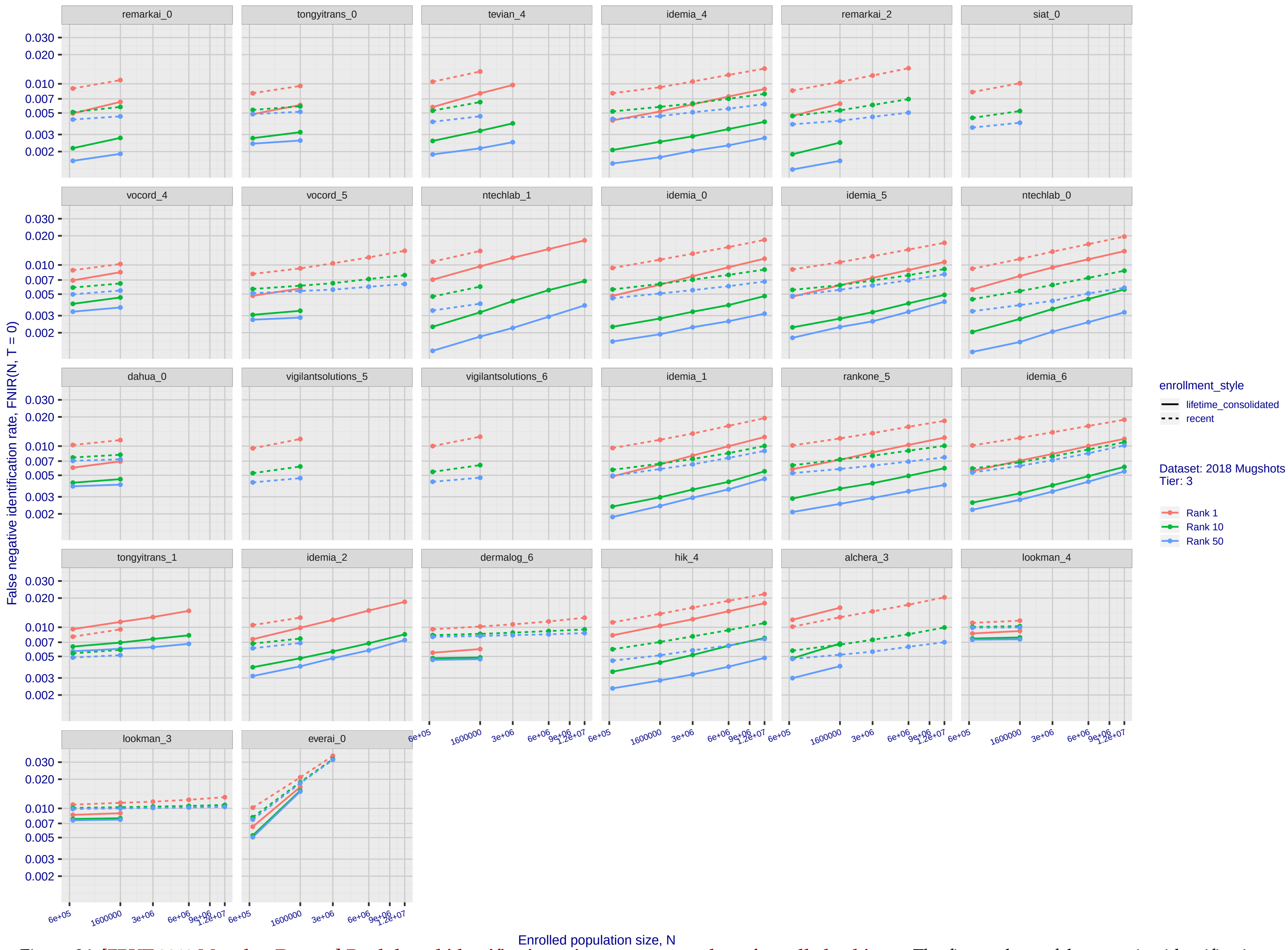

Figure 24: **[FRVT-2018 Mugshot Dataset] Rank-based identification miss rates vs. number of enrolled subjects**. *The figure shows false negative identification rates, FNIR(N, R), across various gallery sizes and ranks 1, 10 and 50. The threshold is set to zero, so this metric rewards even weak scoring rank 1 mates. This also means FPIR = 1, so any search without an enrolled mate will return non-mated candidates. For clarity, results are sorted and reported into tiers spanning multiple pages, the tiering criteria being rank 1 hit rate on a gallery size of 640 000.*

This publication is available free of charge from: https://doi.org/10.6028/NIST.IR.8271

2019/09/11 16:09:13

FNIR(N, R, T) = False neg. identification rate
FPIR(N, T) = False pos. identification rate
N = Num. enrolled subjects
R = Num. candidates examined
T = Threshold
T = 0 → Investigation
T > 0 → Identification

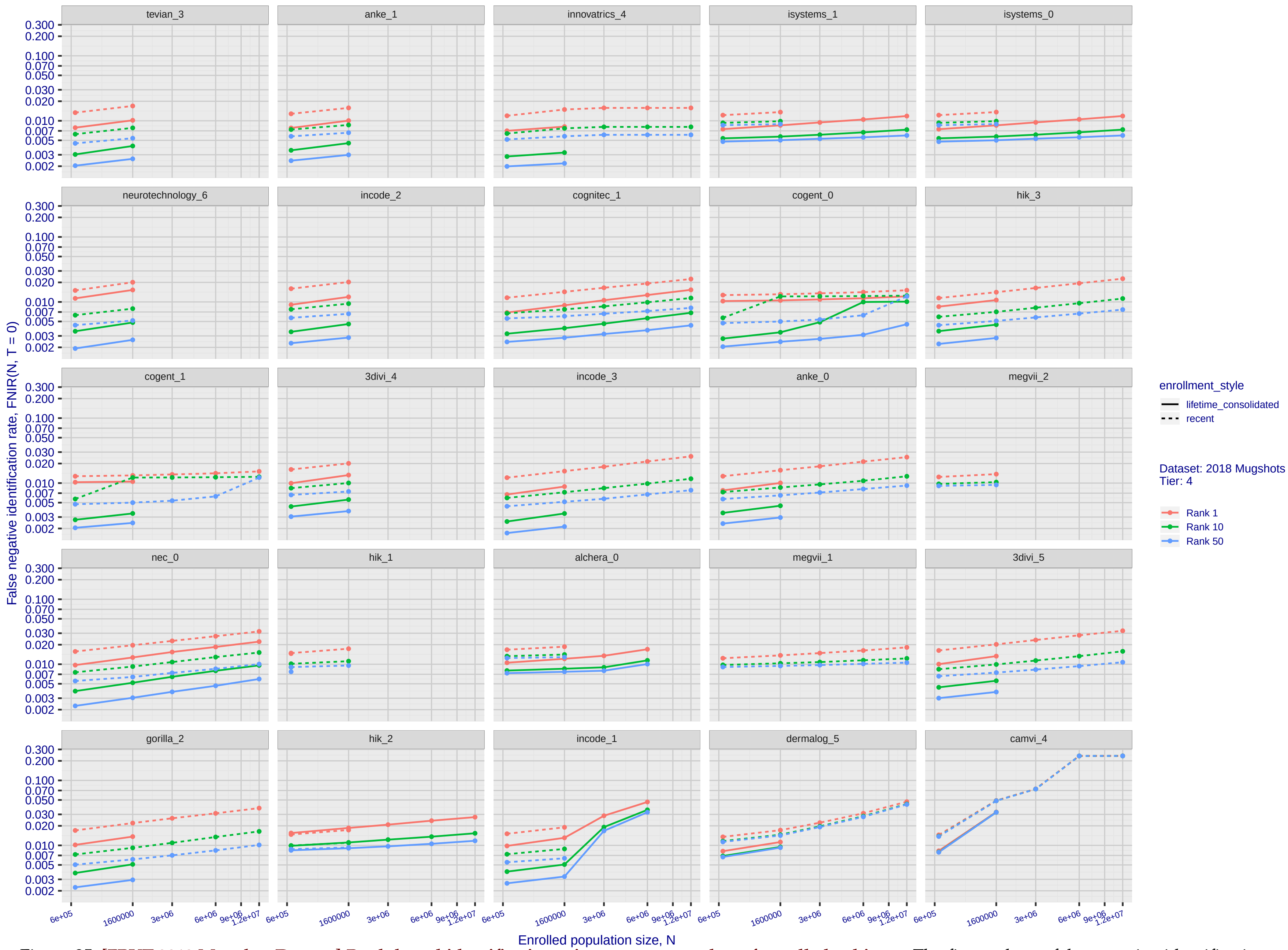

Figure 25: **[FRVT-2018 Mugshot Dataset] Rank-based identification miss rates vs. number of enrolled subjects**. *The figure shows false negative identification rates, FNIR(N, R), across various gallery sizes and ranks 1, 10 and 50. The threshold is set to zero, so this metric rewards even weak scoring rank 1 mates. This also means FPIR = 1, so any search without an enrolled mate will return non-mated candidates. For clarity, results are sorted and reported into tiers spanning multiple pages, the tiering criteria being rank 1 hit rate on a gallery size of 640 000.*

FNIR(N, R, T) = False neg. identification rate
FPIR(N, T) = False pos. identification rate
N = Num. enrolled subjects
R = Num. candidates examined
T = Threshold
T = 0 → Investigation
T > 0 → Identification

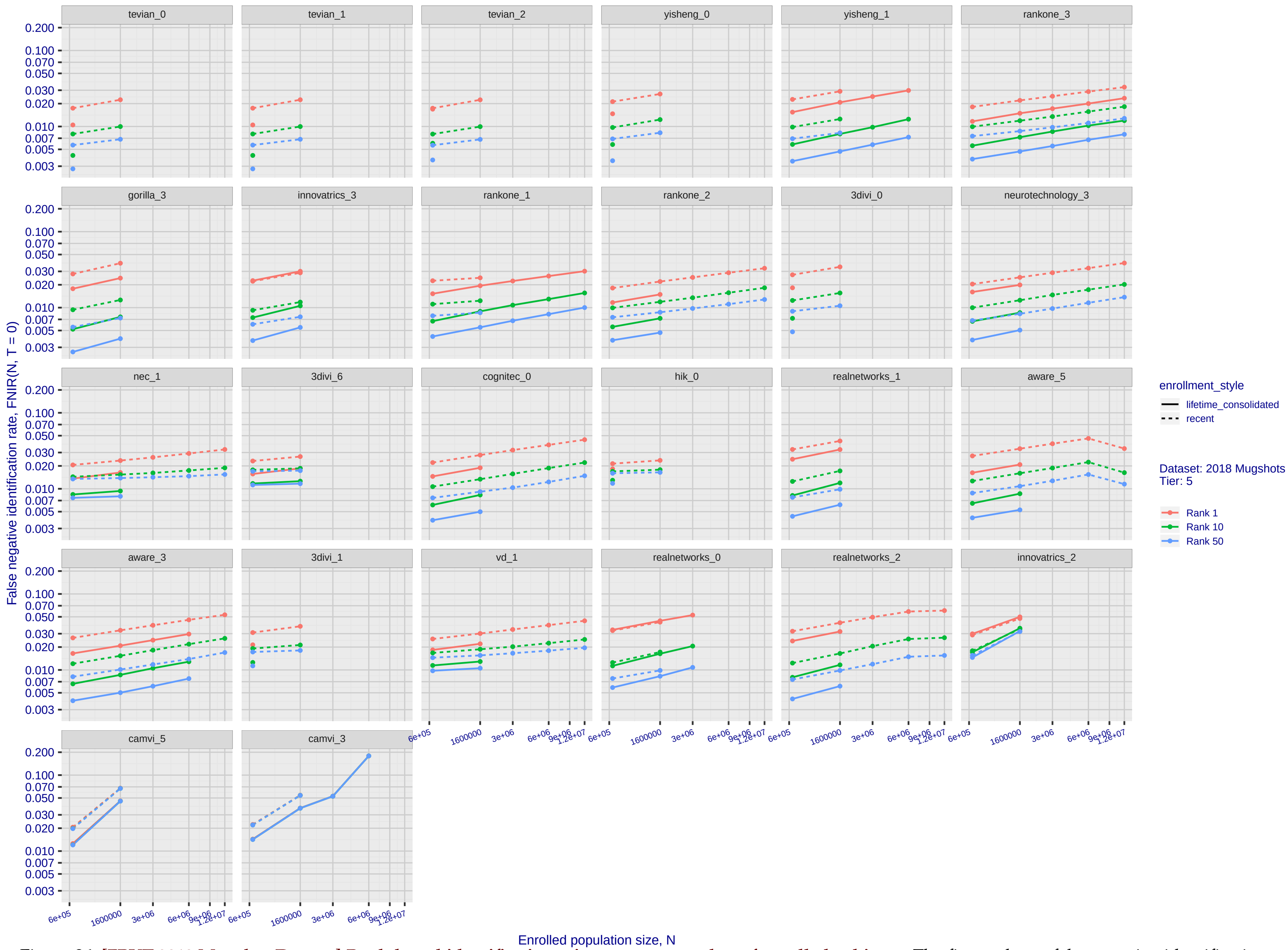

Figure 26: **[FRVT-2018 Mugshot Dataset] Rank-based identification miss rates vs. number of enrolled subjects**. *The figure shows false negative identification rates, FNIR(N, R), across various gallery sizes and ranks 1, 10 and 50. The threshold is set to zero, so this metric rewards even weak scoring rank 1 mates. This also means FPIR = 1, so any search without an enrolled mate will return non-mated candidates. For clarity, results are sorted and reported into tiers spanning multiple pages, the tiering criteria being rank 1 hit rate on a gallery size of 640 000.*

FNIR(N, R, T) = False neg. identification rate
FPIR(N, T) = False pos. identification rate
N = Num. enrolled subjects
R = Num. candidates examined
T = Threshold
T = 0 → Investigation
T > 0 → Identification

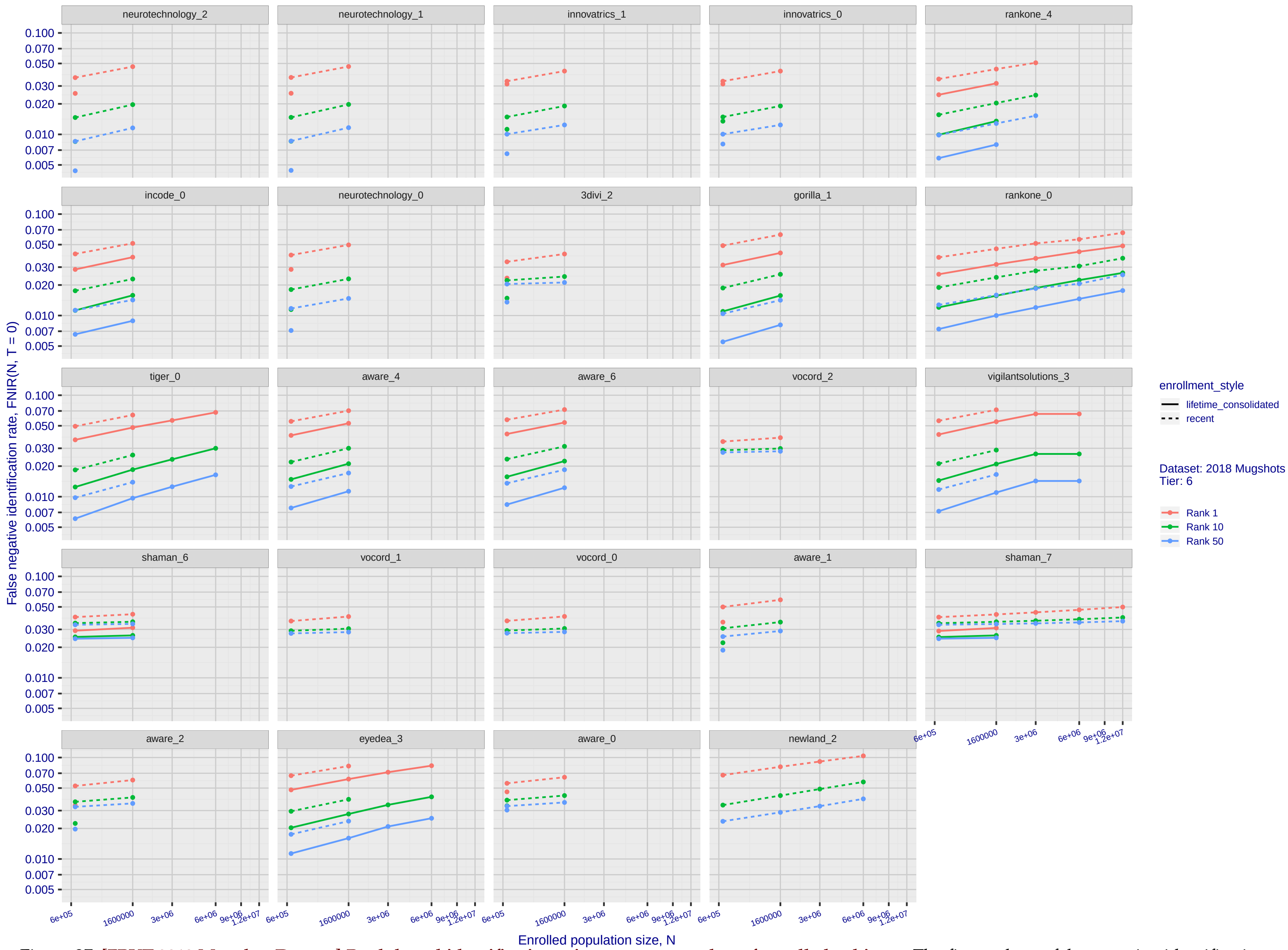

Figure 27: **[FRVT-2018 Mugshot Dataset] Rank-based identification miss rates vs. number of enrolled subjects**. *The figure shows false negative identification rates, FNIR(N, R), across various gallery sizes and ranks 1, 10 and 50. The threshold is set to zero, so this metric rewards even weak scoring rank 1 mates. This also means FPIR = 1, so any search without an enrolled mate will return non-mated candidates. For clarity, results are sorted and reported into tiers spanning multiple pages, the tiering criteria being rank 1 hit rate on a gallery size of 640 000.*

This publication is available free of charge from: https://doi.org/10.6028/NIST.IR.8271

2019/09/11 16:09:13

FNIR(N, R, T) = False neg. identification rate
FPIR(N, T) = False pos. identification rate
N = Num. enrolled subjects
R = Num. candidates examined
T = Threshold
T = 0 → Investigation
T > 0 → Identification

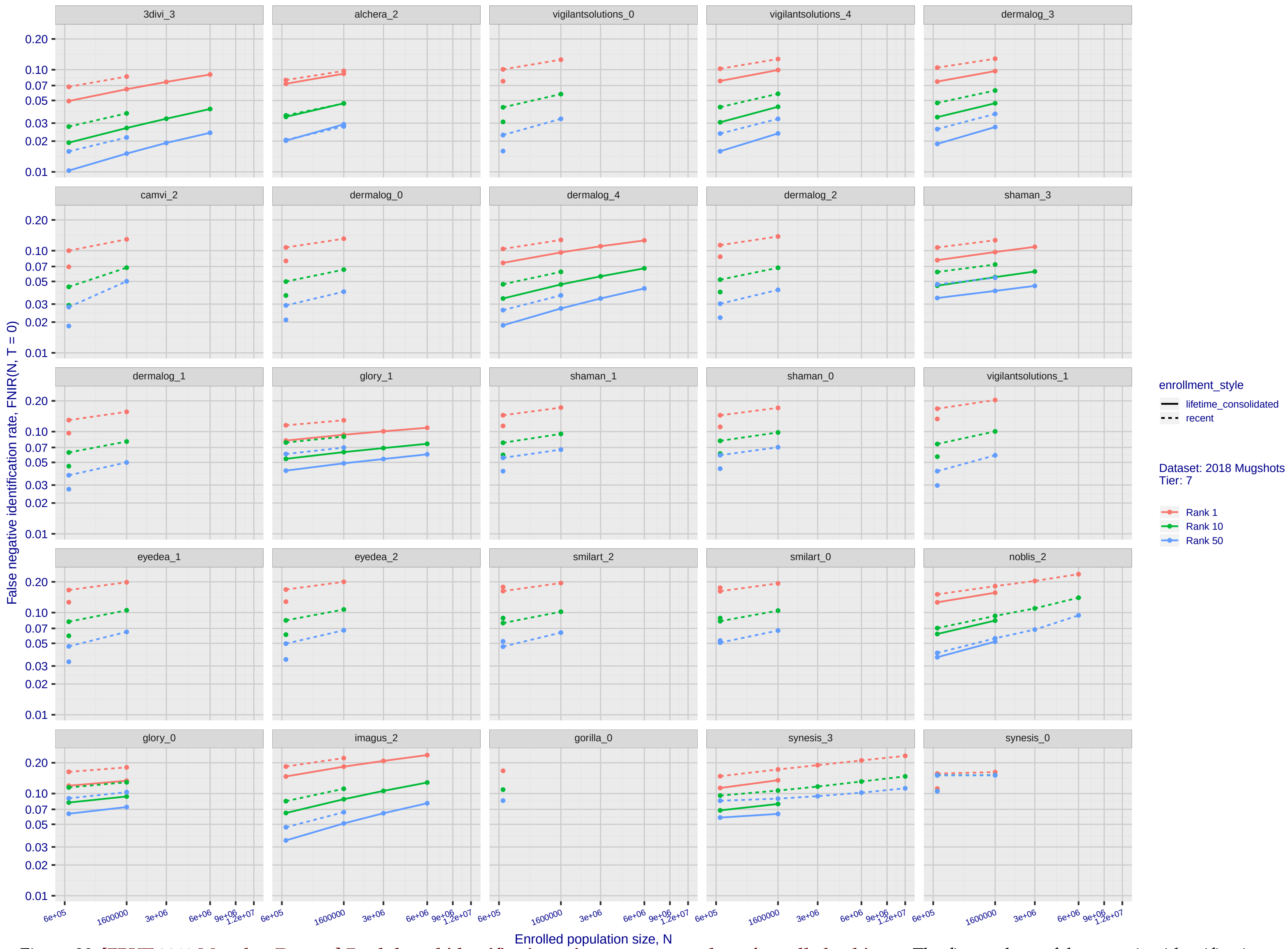

Figure 28: **[FRVT-2018 Mugshot Dataset] Rank-based identification miss rates vs. number of enrolled subjects**. *The figure shows false negative identification rates, FNIR(N, R), across various gallery sizes and ranks 1, 10 and 50. The threshold is set to zero, so this metric rewards even weak scoring rank 1 mates. This also means FPIR = 1, so any search without an enrolled mate will return non-mated candidates. For clarity, results are sorted and reported into tiers spanning multiple pages, the tiering criteria being rank 1 hit rate on a gallery size of 640 000.*

This publication is available free of charge from: https://doi.org/10.6028/NIST.IR.8271

FNIR(N, R, T) = False neg. identification rate
FPIR(N, T) = False pos. identification rate
N = Num. enrolled subjects
R = Num. candidates examined
T = Threshold
T = 0 → Investigation
T > 0 → Identification

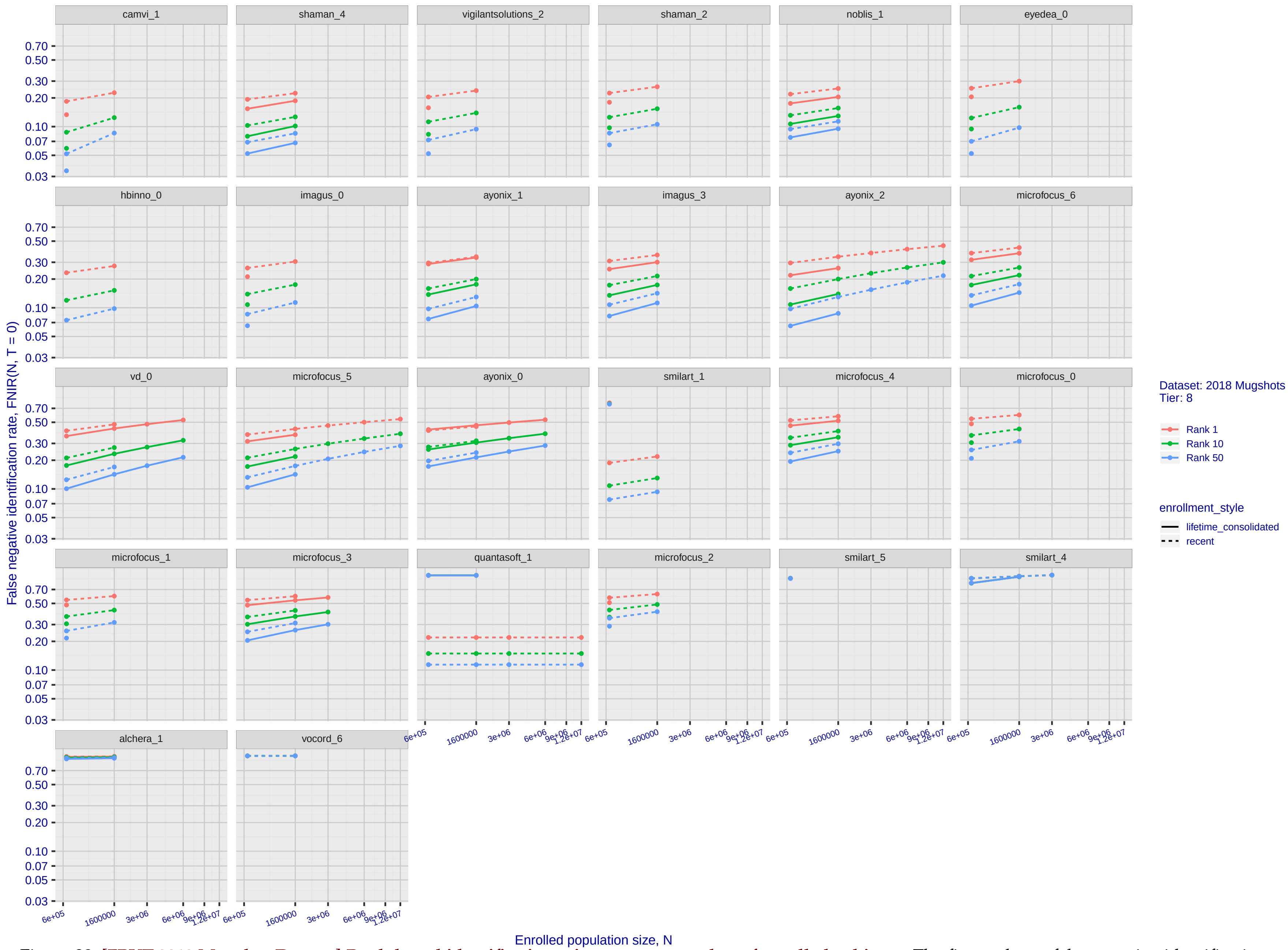

Figure 29: **[FRVT-2018 Mugshot Dataset] Rank-based identification miss rates vs. number of enrolled subjects**. *The figure shows false negative identification rates, FNIR(N, R), across various gallery sizes and ranks 1, 10 and 50. The threshold is set to zero, so this metric rewards even weak scoring rank 1 mates. This also means FPIR = 1, so any search without an enrolled mate will return non-mated candidates. For clarity, results are sorted and reported into tiers spanning multiple pages, the tiering criteria being rank 1 hit rate on a gallery size of 640 000.*

2019/09/11 16:09:13

FNIR(N, R, T) = False neg. identification rate
FPIR(N, T) = False pos. identification rate
N = Num. enrolled subjects
R = Num. candidates examined
T = Threshold
T = 0 → Investigation
T > 0 → Identification

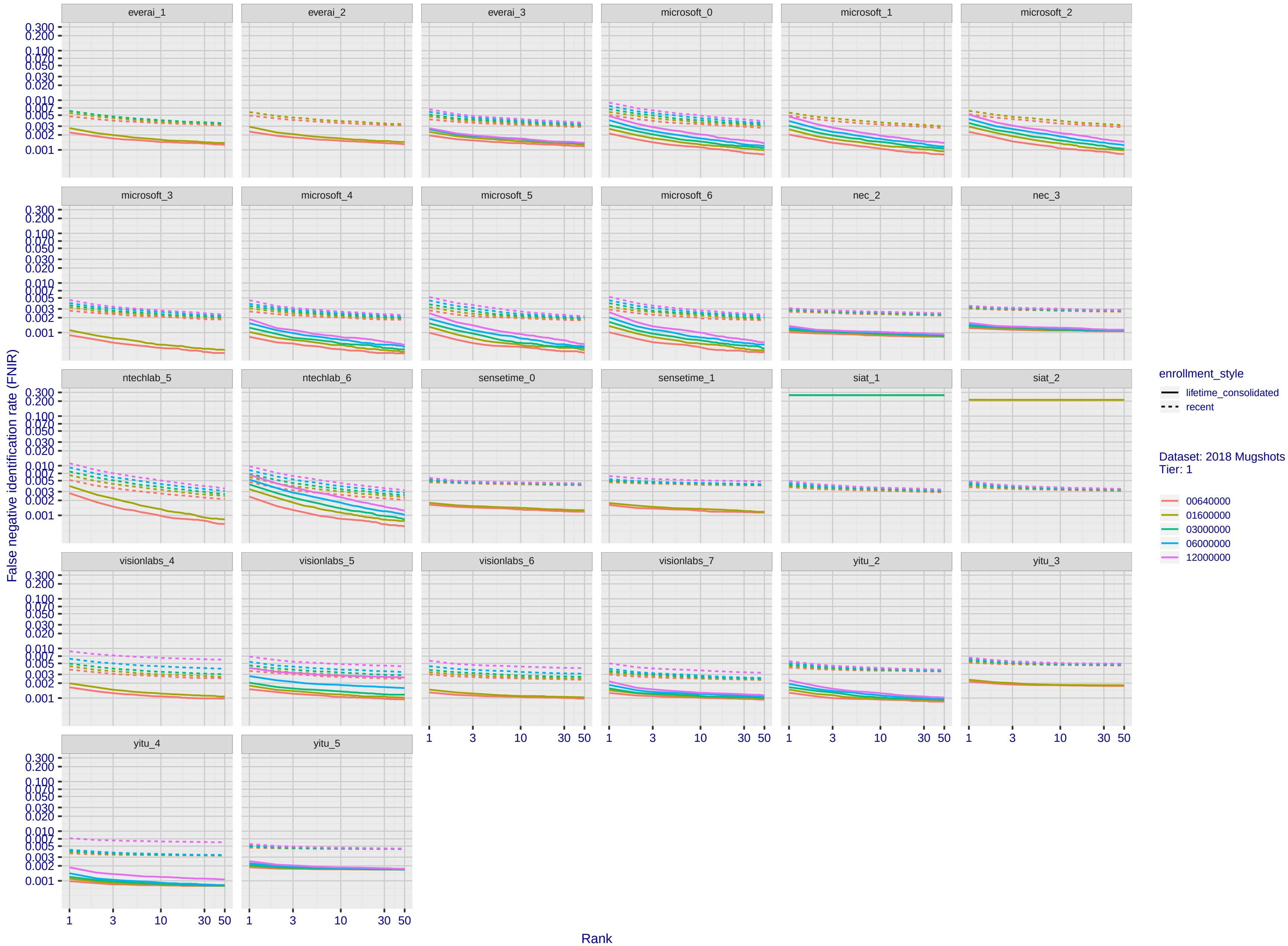

Figure 30: **[FRVT-2018 Mugshot Dataset] Rank-based identification miss rates vs. rank**. *The figure shows false negative identification rates (FNIR) for ranks up to 50. This metric is appropriate to investigational applications where human reviewers will adjudicate sorted candidate lists. Note that with threshold set to zero, FPIR = 1, i.e. any search without an enrolled mate will return non-mated candidates. Results are sorted and reported into tiers for clarity, with the tiering criteria being rank 1 hit rate on a gallery size of N = 640 000 subjects.*

This publication is available free of charge from: https://doi.org/10.6028/NIST.IR.8271

2019/09/11 16:09:13

FNIR(N, R, T) = False neg. identification rate
FPIR(N, T) = False pos. identification rate
N = Num. enrolled subjects
R = Num. candidates examined
T = Threshold
T = 0 → Investigation
T > 0 → Identification

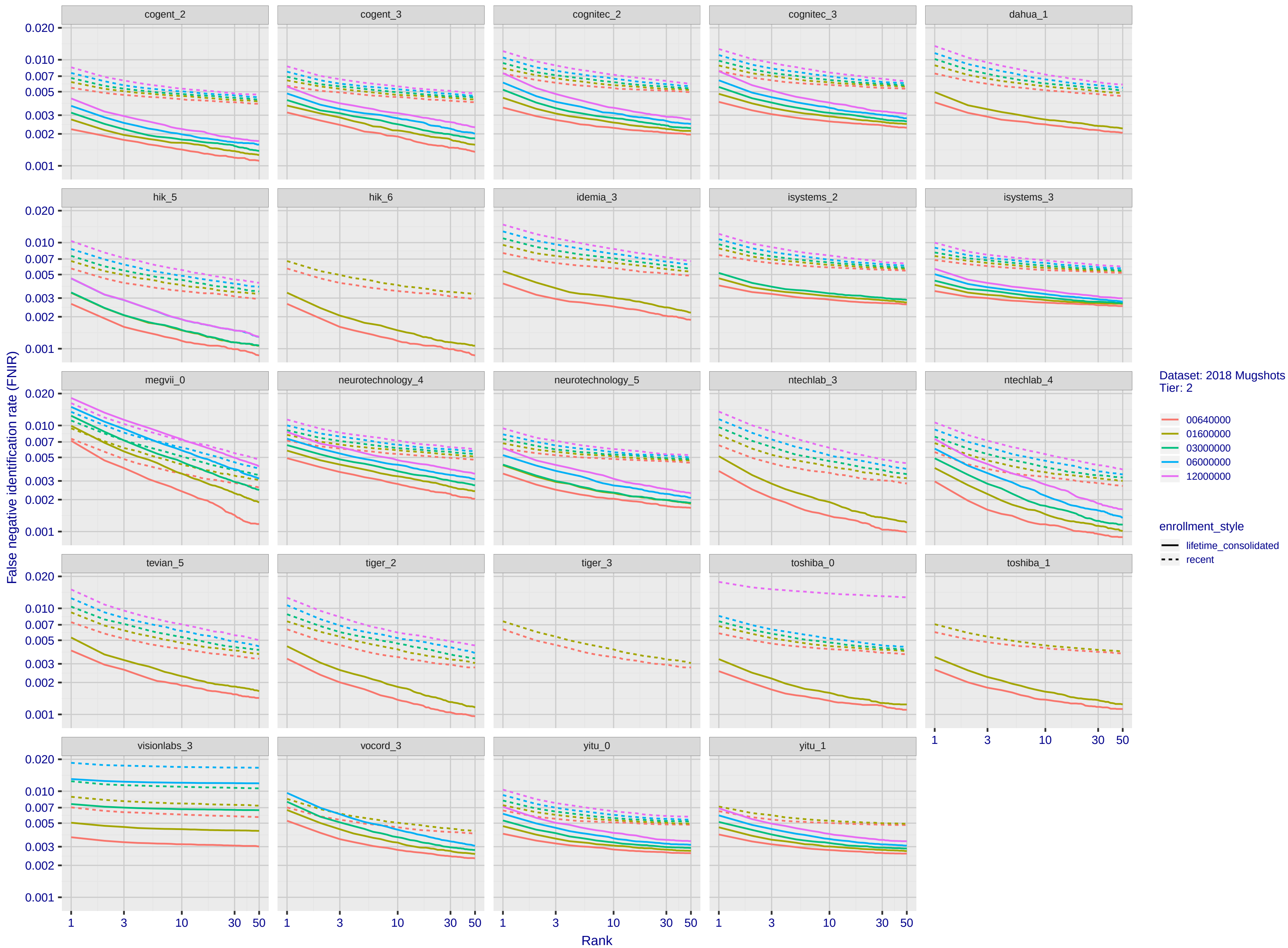

Figure 31: **[FRVT-2018 Mugshot Dataset] Rank-based identification miss rates vs. rank**. *The figure shows false negative identification rates (FNIR) for ranks up to 50. This metric is appropriate to investigational applications where human reviewers will adjudicate sorted candidate lists. Note that with threshold set to zero, FPIR = 1, i.e. any search without an enrolled mate will return non-mated candidates. Results are sorted and reported into tiers for clarity, with the tiering criteria being rank 1 hit rate on a gallery size of N = 640 000 subjects.*

FNIR(N, R, T) = False neg. identification rate
FPIR(N, T) = False pos. identification rate
N = Num. enrolled subjects
R = Num. candidates examined
T = Threshold
T = 0 → Investigation
T > 0 → Identification

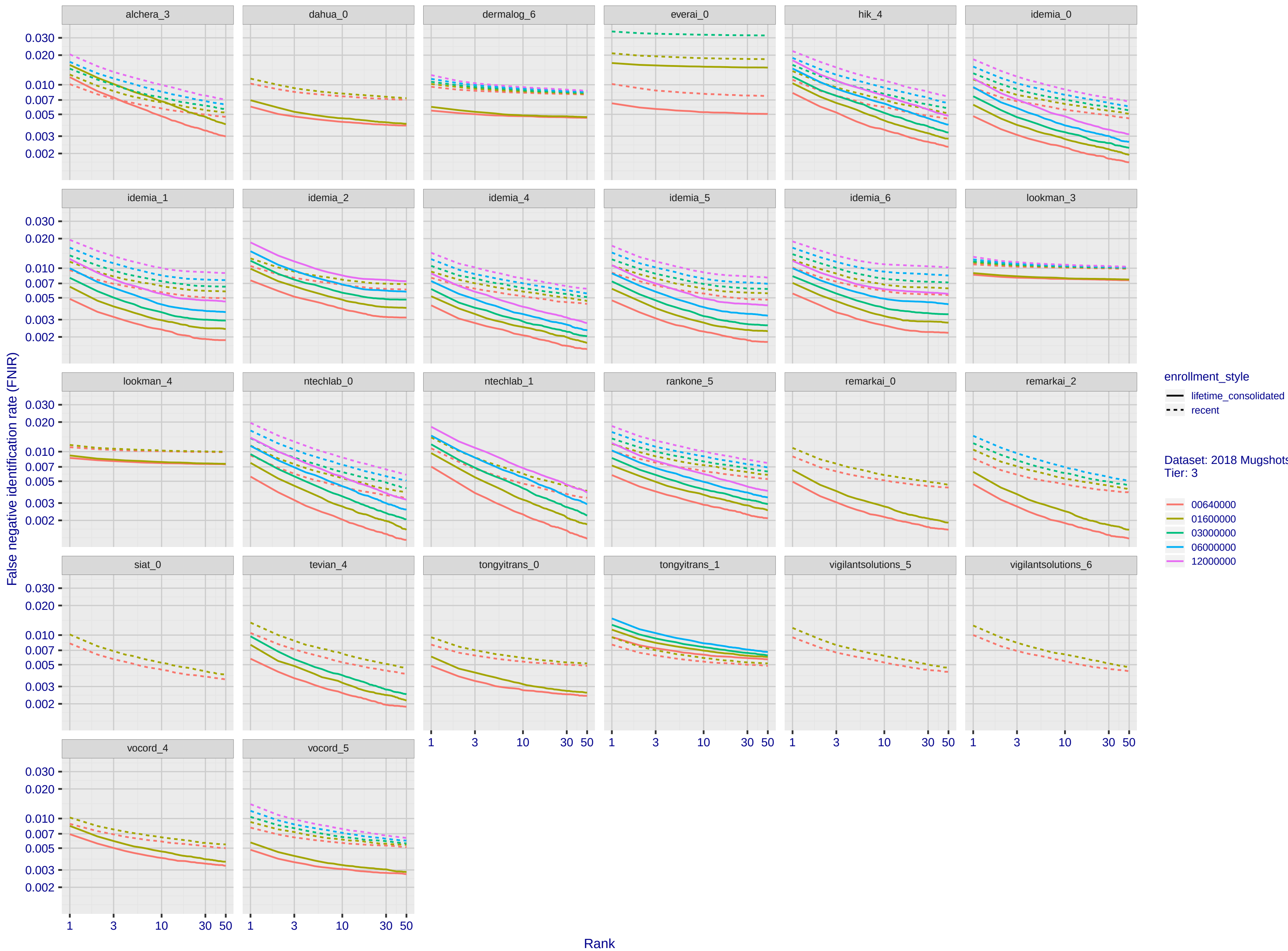

Figure 32: **[FRVT-2018 Mugshot Dataset] Rank-based identification miss rates vs. rank**. *The figure shows false negative identification rates (FNIR) for ranks up to 50. This metric is appropriate to investigational applications where human reviewers will adjudicate sorted candidate lists. Note that with threshold set to zero, FPIR = 1, i.e. any search without an enrolled mate will return non-mated candidates. Results are sorted and reported into tiers for clarity, with the tiering criteria being rank 1 hit rate on a gallery size of N = 640 000 subjects.*

FNIR(N, R, T) = False neg. identification rate
FPIR(N, T) = False pos. identification rate
N = Num. enrolled subjects
R = Num. candidates examined
T = Threshold
T = 0 → Investigation
T > 0 → Identification

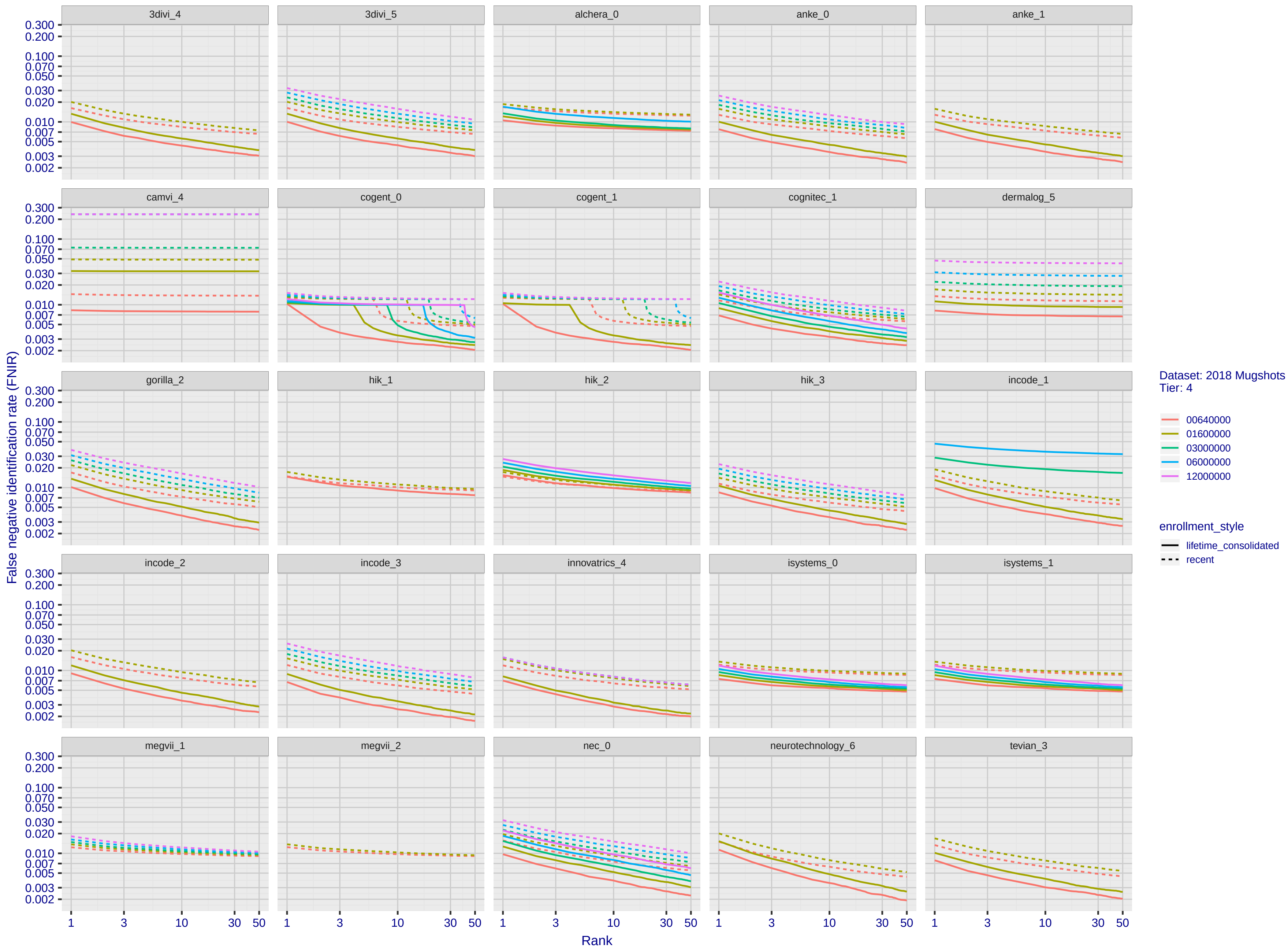

Figure 33: **[FRVT-2018 Mugshot Dataset] Rank-based identification miss rates vs. rank**. *The figure shows false negative identification rates (FNIR) for ranks up to 50. This metric is appropriate to investigational applications where human reviewers will adjudicate sorted candidate lists. Note that with threshold set to zero, FPIR = 1, i.e. any search without an enrolled mate will return non-mated candidates. Results are sorted and reported into tiers for clarity, with the tiering criteria being rank 1 hit rate on a gallery size of N = 640 000 subjects.*

This publication is available free of charge from: https://doi.org/10.6028/NIST.IR.8271

2019/09/11 16:09:13

FNIR(N, R, T) = False neg. identification rate
FPIR(N, T) = False pos. identification rate
N = Num. enrolled subjects
R = Num. candidates examined
T = Threshold
T = 0 → Investigation
T > 0 → Identification

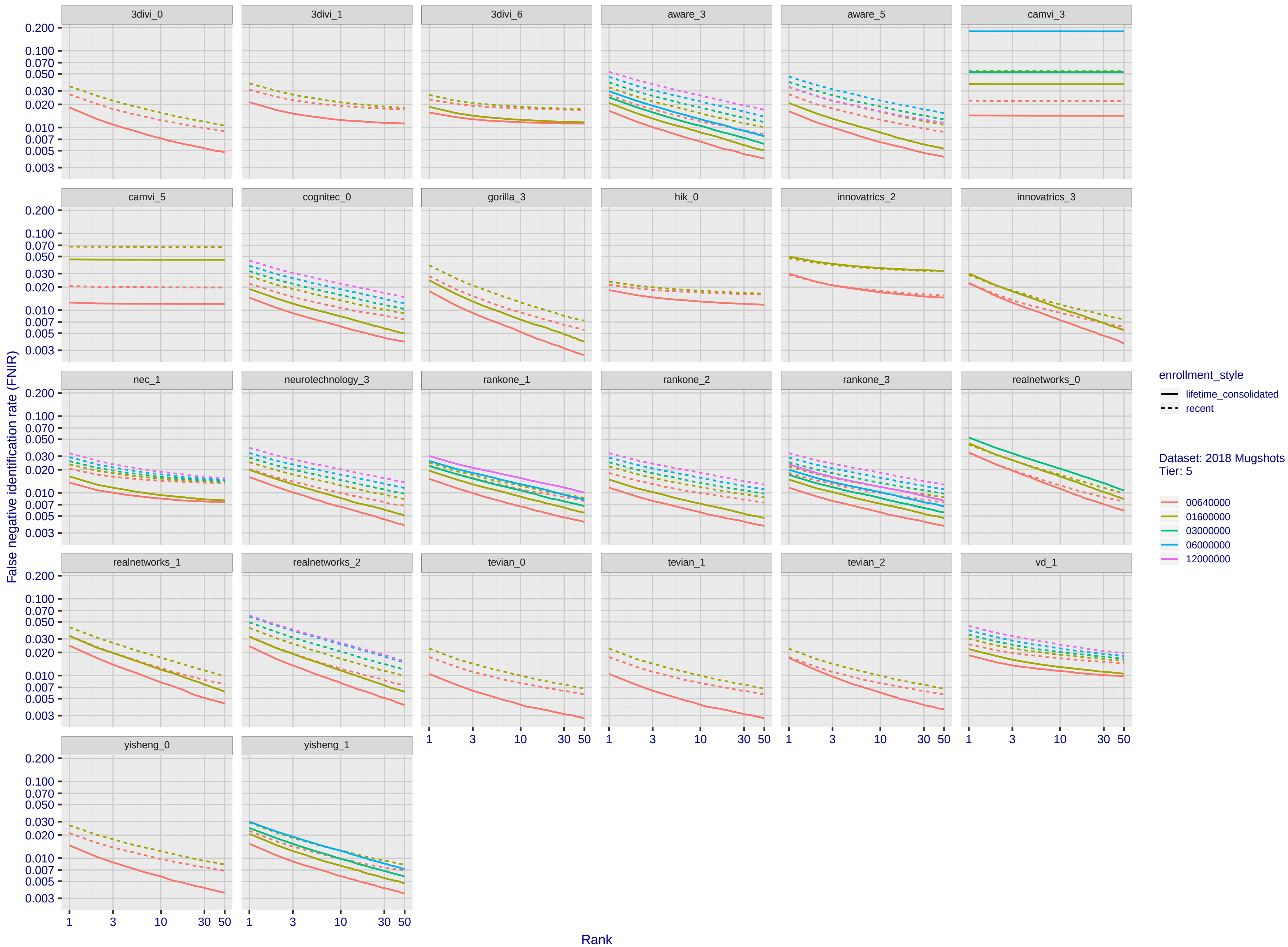

Figure 34: **[FRVT-2018 Mugshot Dataset] Rank-based identification miss rates vs. rank**. *The figure shows false negative identification rates (FNIR) for ranks up to 50. This metric is appropriate to investigational applications where human reviewers will adjudicate sorted candidate lists. Note that with threshold set to zero, FPIR = 1, i.e. any search without an enrolled mate will return non-mated candidates. Results are sorted and reported into tiers for clarity, with the tiering criteria being rank 1 hit rate on a gallery size of N = 640 000 subjects.*

FNIR(N, R, T) = False neg. identification rate
FPIR(N, T) = False pos. identification rate
N = Num. enrolled subjects
R = Num. candidates examined
T = Threshold
T = 0 → Investigation
T > 0 → Identification

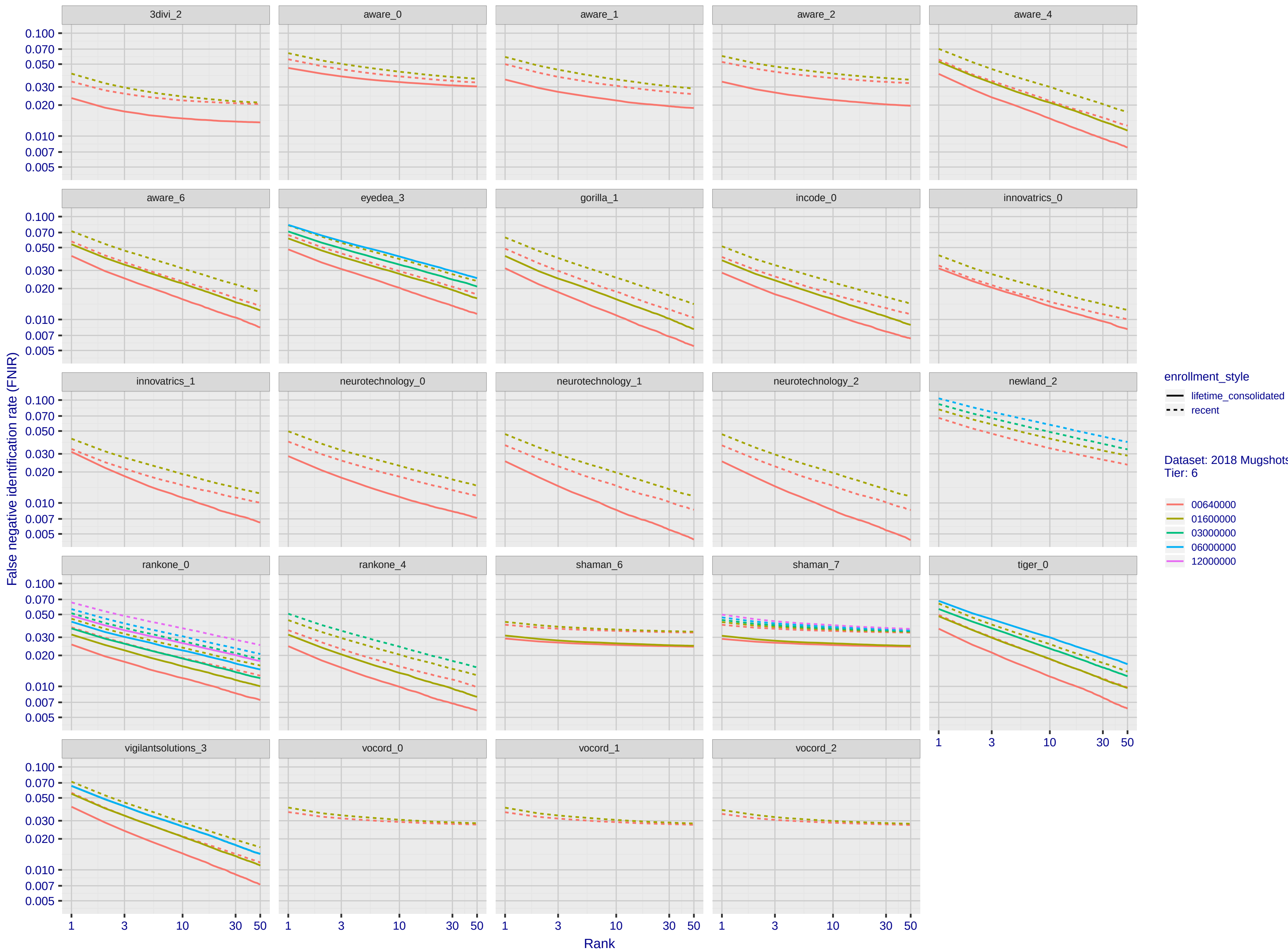

Figure 35: **[FRVT-2018 Mugshot Dataset] Rank-based identification miss rates vs. rank**. *The figure shows false negative identification rates (FNIR) for ranks up to 50. This metric is appropriate to investigational applications where human reviewers will adjudicate sorted candidate lists. Note that with threshold set to zero, FPIR = 1, i.e. any search without an enrolled mate will return non-mated candidates. Results are sorted and reported into tiers for clarity, with the tiering criteria being rank 1 hit rate on a gallery size of N = 640 000 subjects.*

FNIR(N, R, T) = False neg. identification rate
FPIR(N, T) = False pos. identification rate
N = Num. enrolled subjects
R = Num. candidates examined
T = Threshold
T = 0 → Investigation
T > 0 → Identification

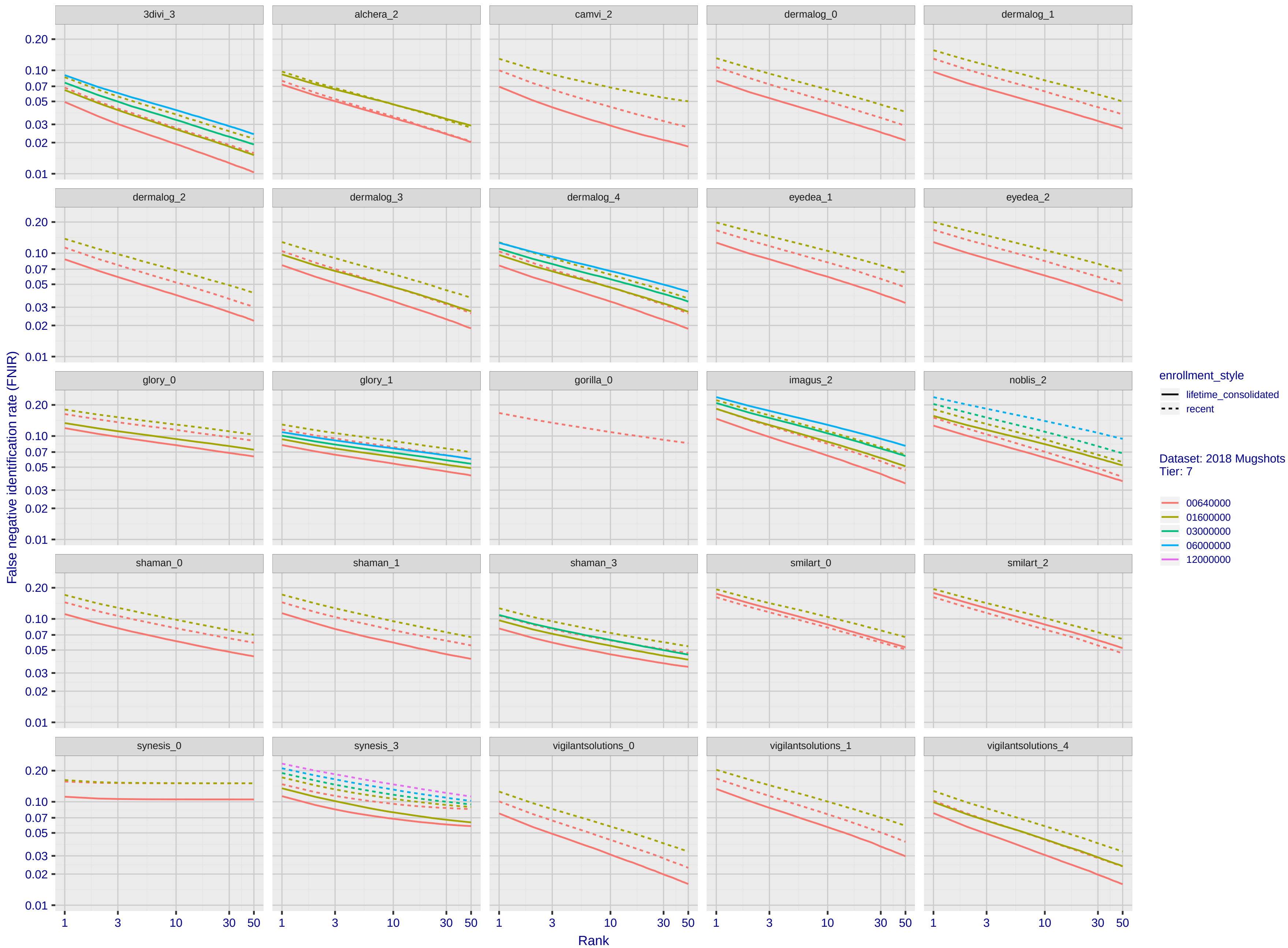

Figure 36: **[FRVT-2018 Mugshot Dataset] Rank-based identification miss rates vs. rank**. *The figure shows false negative identification rates (FNIR) for ranks up to 50. This metric is appropriate to investigational applications where human reviewers will adjudicate sorted candidate lists. Note that with threshold set to zero, FPIR = 1, i.e. any search without an enrolled mate will return non-mated candidates. Results are sorted and reported into tiers for clarity, with the tiering criteria being rank 1 hit rate on a gallery size of N = 640 000 subjects.*

FNIR(N, R, T) = False neg. identification rate
FPIR(N, T) = False pos. identification rate
N = Num. enrolled subjects
R = Num. candidates examined
T = Threshold
T = 0 → Investigation
T > 0 → Identification

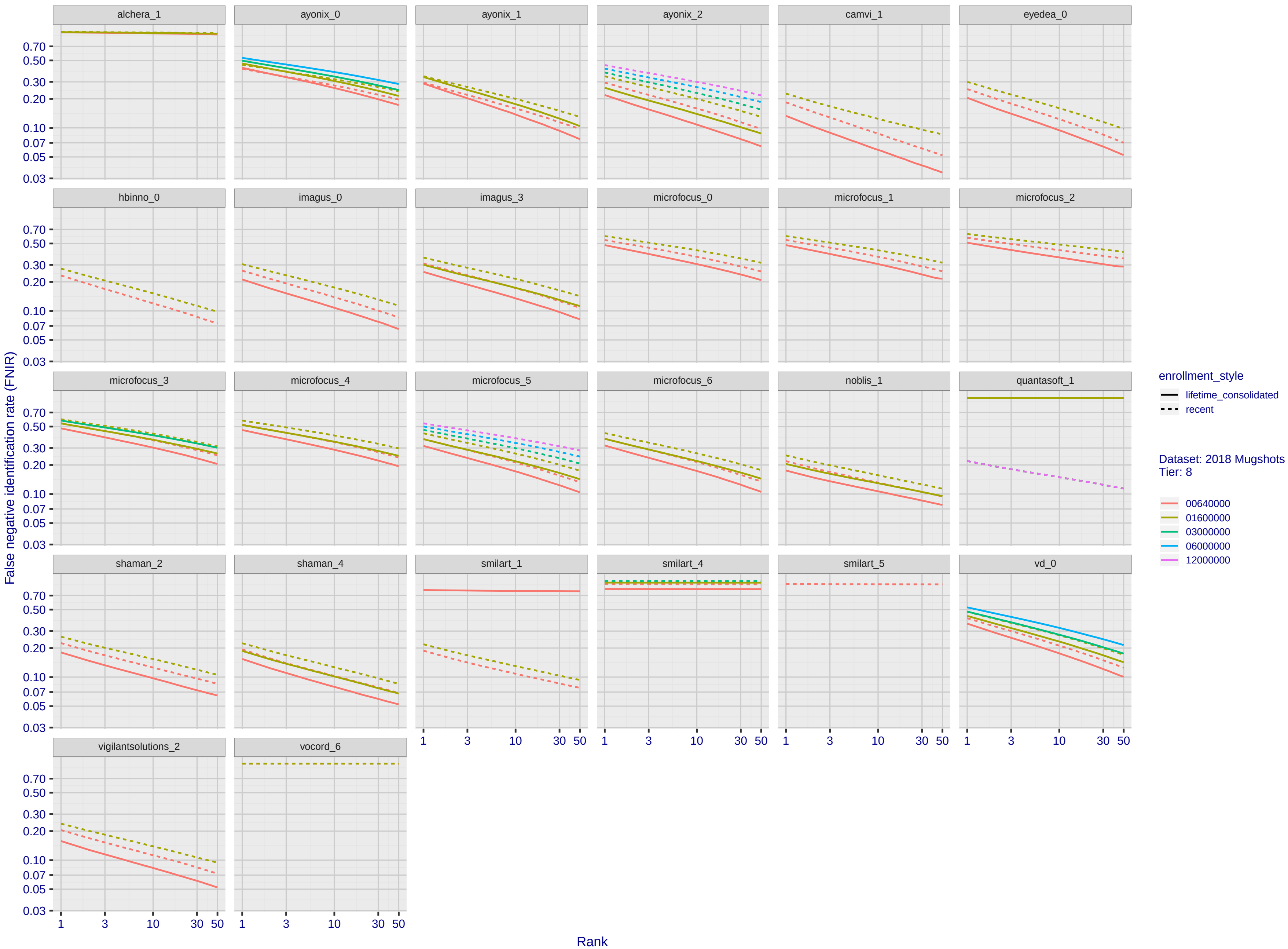

Figure 37: **[FRVT-2018 Mugshot Dataset] Rank-based identification miss rates vs. rank**. *The figure shows false negative identification rates (FNIR) for ranks up to 50. This metric is appropriate to investigational applications where human reviewers will adjudicate sorted candidate lists. Note that with threshold set to zero, FPIR = 1, i.e. any search without an enrolled mate will return non-mated candidates. Results are sorted and reported into tiers for clarity, with the tiering criteria being rank 1 hit rate on a gallery size of N = 640 000 subjects.*

FNIR(N, R, T) = False neg. identification rate
FPIR(N, T) = False pos. identification rate
N = Num. enrolled subjects
R = Num. candidates examined
T = Threshold
T = 0 → Investigation
T > 0 → Identification

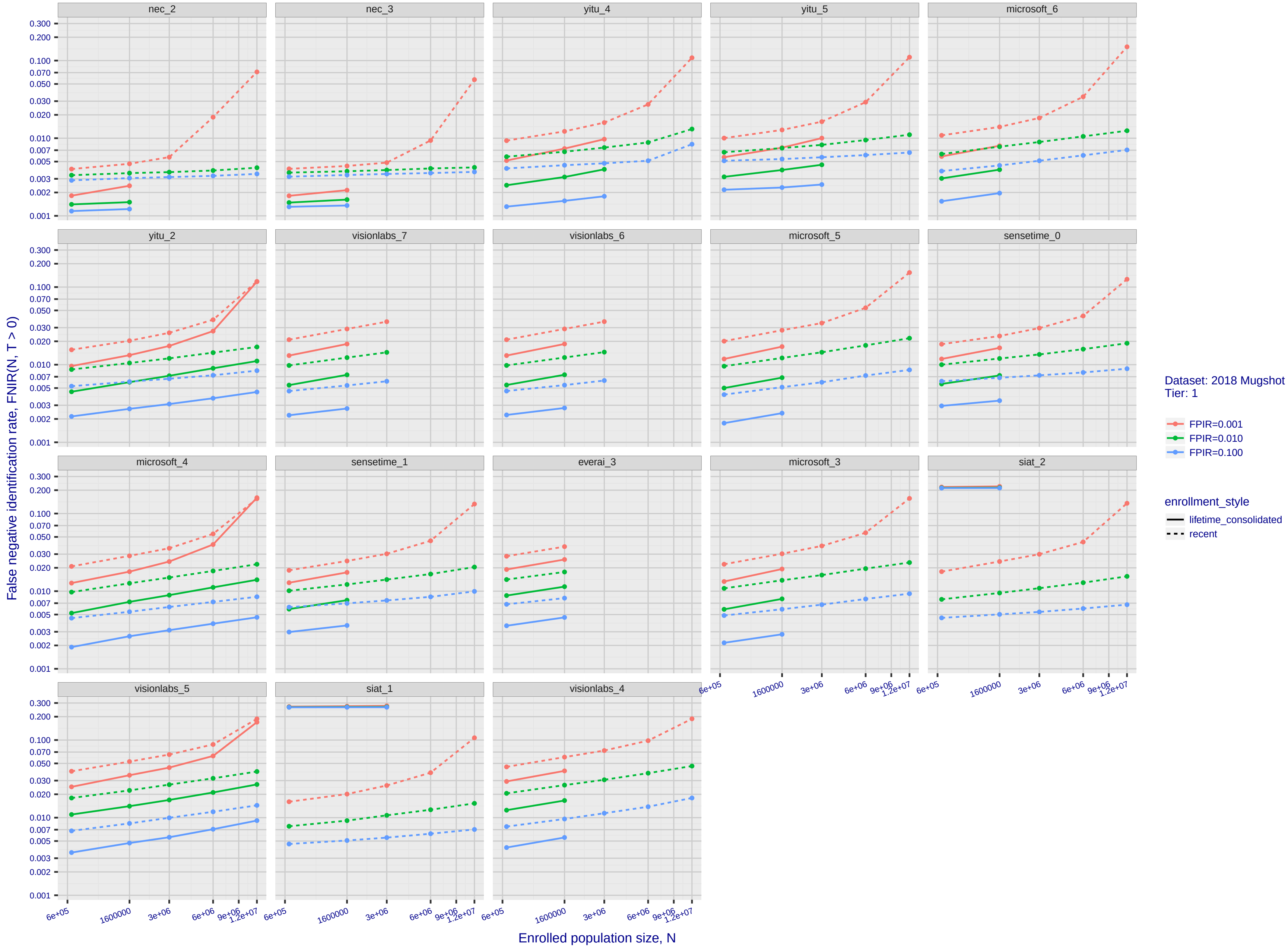

Figure 38: **[FRVT-2018 Mugshot Dataset] Threshold-based identification miss rates vs. number of enrolled subjects**. *The figure shows FNIR(N, T) across various gallery sizes when the threshold is set to achieve the given FPIRs. The rank criterion is irrelevant at high thresholds as mates are always at rank 1. The results are computed from the trials listed in rows 1-10 of Table 5. Less accurate algorithms were not run on large N, so results are missing. For clarity, results are sorted and reported into tiers spanning multiple pages. The tiering criteria is complicated: First paging by FNIR(N_b, 1, 0), then sorting by median FNIR(N_b, T), N_b = 640 000.*

FNIR(N, R, T) = False neg. identification rate
FPIR(N, T) = False pos. identification rate
N = Num. enrolled subjects
R = Num. candidates examined
T = Threshold
T = 0 → Investigation
T > 0 → Identification

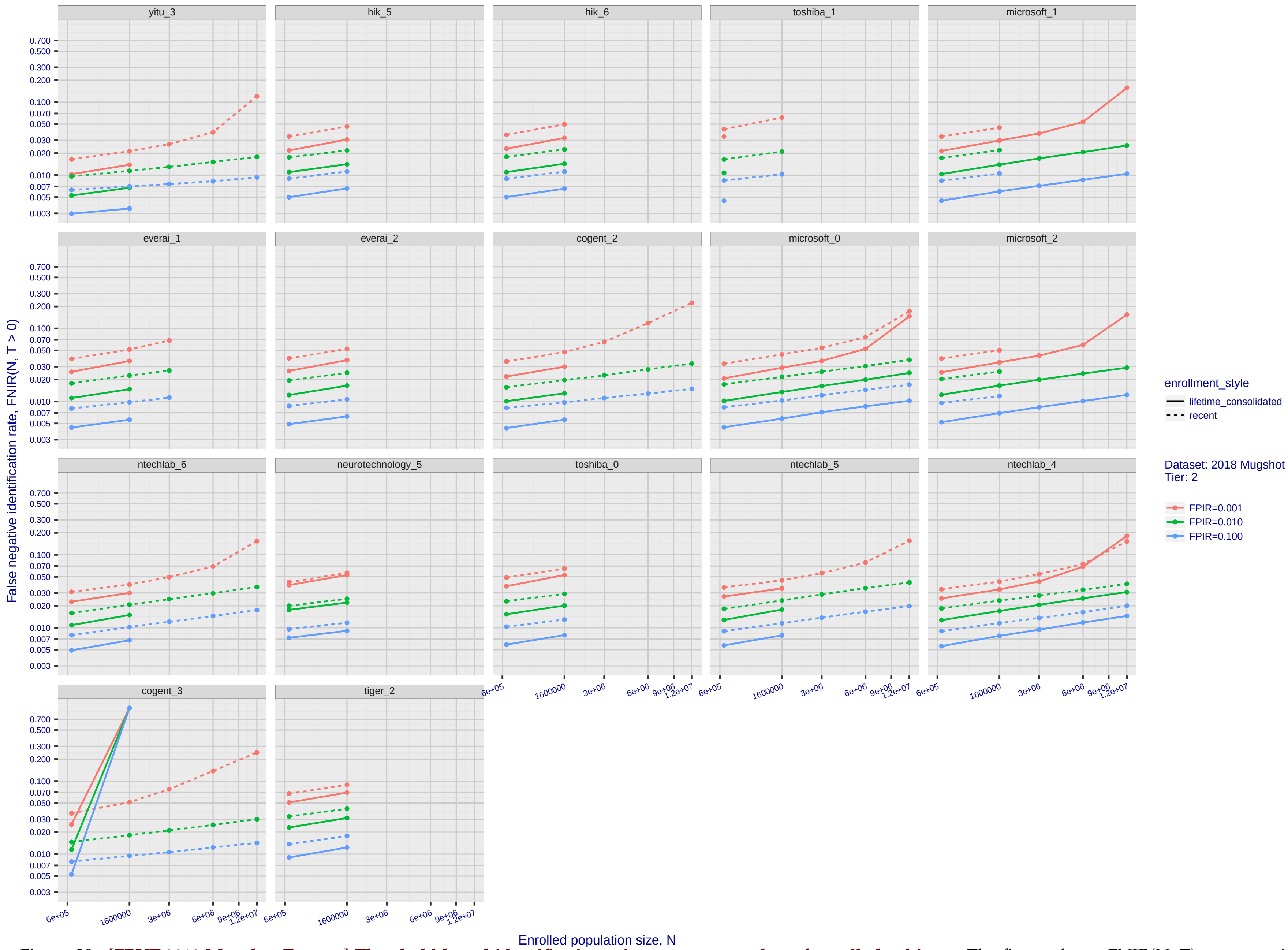

Figure 39: **[FRVT-2018 Mugshot Dataset] Threshold-based identification miss rates vs. number of enrolled subjects**. *The figure shows FNIR(N, T) across various gallery sizes when the threshold is set to achieve the given FPIRs. The rank criterion is irrelevant at high thresholds as mates are always at rank 1. The results are computed from the trials listed in rows 1-10 of Table 5. Less accurate algorithms were not run on large N, so results are missing. For clarity, results are sorted and reported into tiers spanning multiple pages. The tiering criteria is complicated: First paging by FNIR(N_b, 1, 0), then sorting by median FNIR(N_b, T), N_b = 640 000.*

FNIR(N, R, T) = False neg. identification rate
FPIR(N, T) = False pos. identification rate
N = Num. enrolled subjects
R = Num. candidates examined
T = Threshold
T = 0 → Investigation
T > 0 → Identification

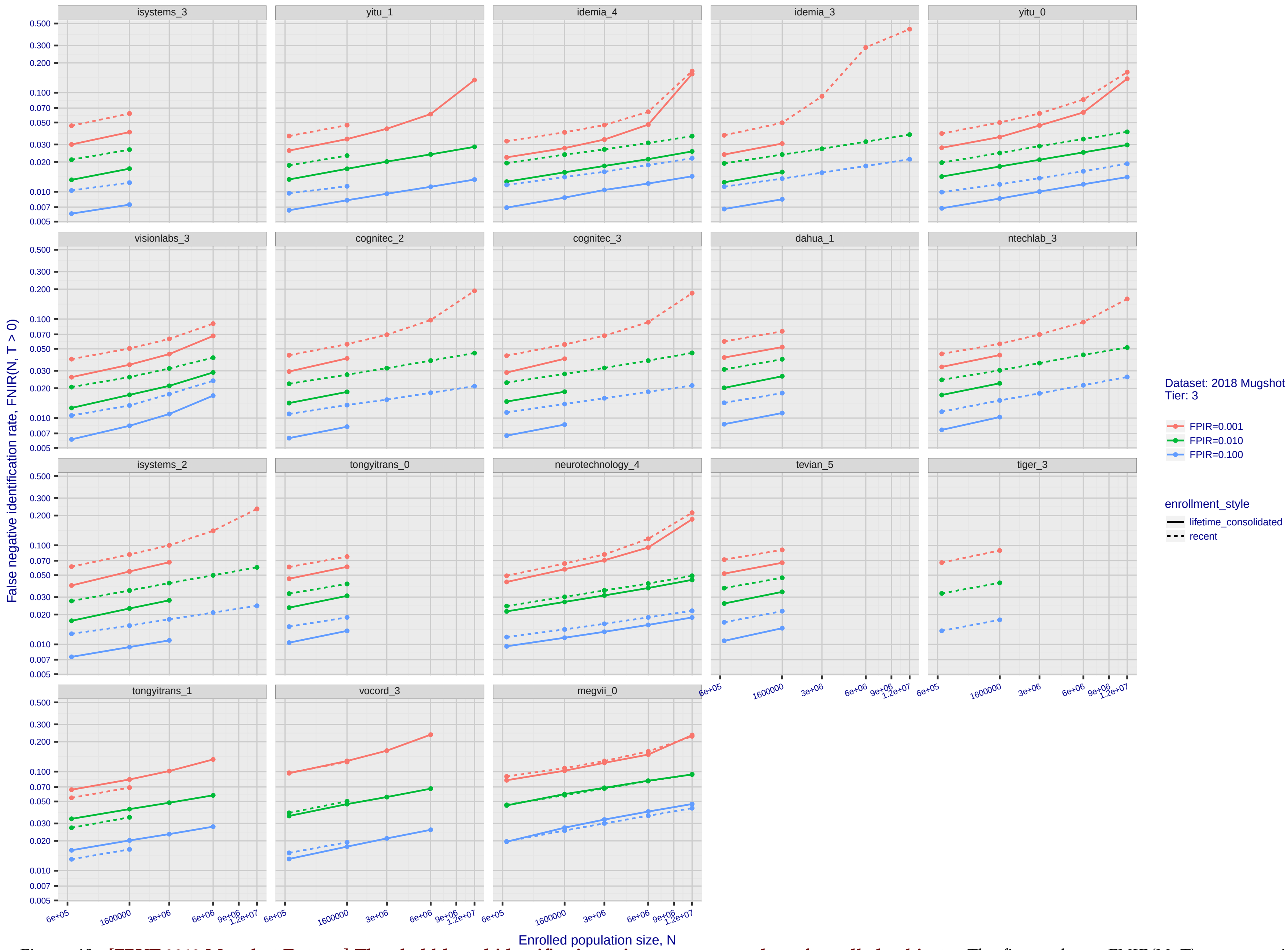

Figure 40: **[FRVT-2018 Mugshot Dataset] Threshold-based identification miss rates vs. number of enrolled subjects**. *The figure shows FNIR(N, T) across various gallery sizes when the threshold is set to achieve the given FPIRs. The rank criterion is irrelevant at high thresholds as mates are always at rank 1. The results are computed from the trials listed in rows 1-10 of Table 5. Less accurate algorithms were not run on large N, so results are missing. For clarity, results are sorted and reported into tiers spanning multiple pages. The tiering criteria is complicated: First paging by FNIR(N_b, 1, 0), then sorting by median FNIR(N_b, T), N_b = 640 000.*

FNIR(N, R, T) = False neg. identification rate
FPIR(N, T) = False pos. identification rate
N = Num. enrolled subjects
R = Num. candidates examined
T = Threshold
T = 0 → Investigation
T > 0 → Identification

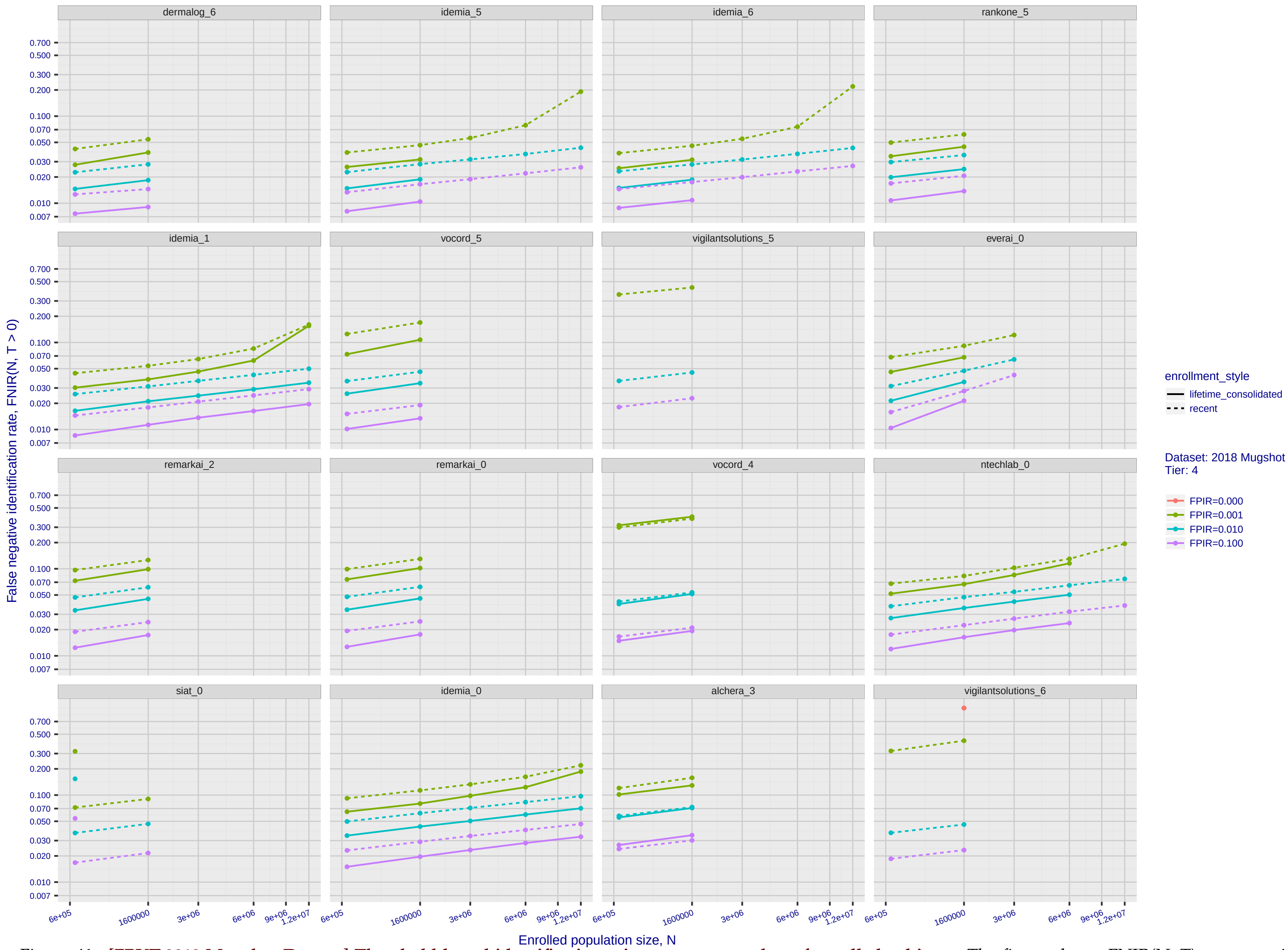

Figure 41: **[FRVT-2018 Mugshot Dataset] Threshold-based identification miss rates vs. number of enrolled subjects**. *The figure shows FNIR(N, T) across various gallery sizes when the threshold is set to achieve the given FPIRs. The rank criterion is irrelevant at high thresholds as mates are always at rank 1. The results are computed from the trials listed in rows 1-10 of Table 5. Less accurate algorithms were not run on large N, so results are missing. For clarity, results are sorted and reported into tiers spanning multiple pages. The tiering criteria is complicated: First paging by FNIR(N_b, 1, 0), then sorting by median FNIR(N_b, T), N_b = 640 000.*

2019/09/11
16:09:13

FNIR(N, R, T) = False neg. identification rate
FPIR(N, T) = False pos. identification rate
N = Num. enrolled subjects
R = Num. candidates examined
T = Threshold
T = 0 → Investigation
T > 0 → Identification

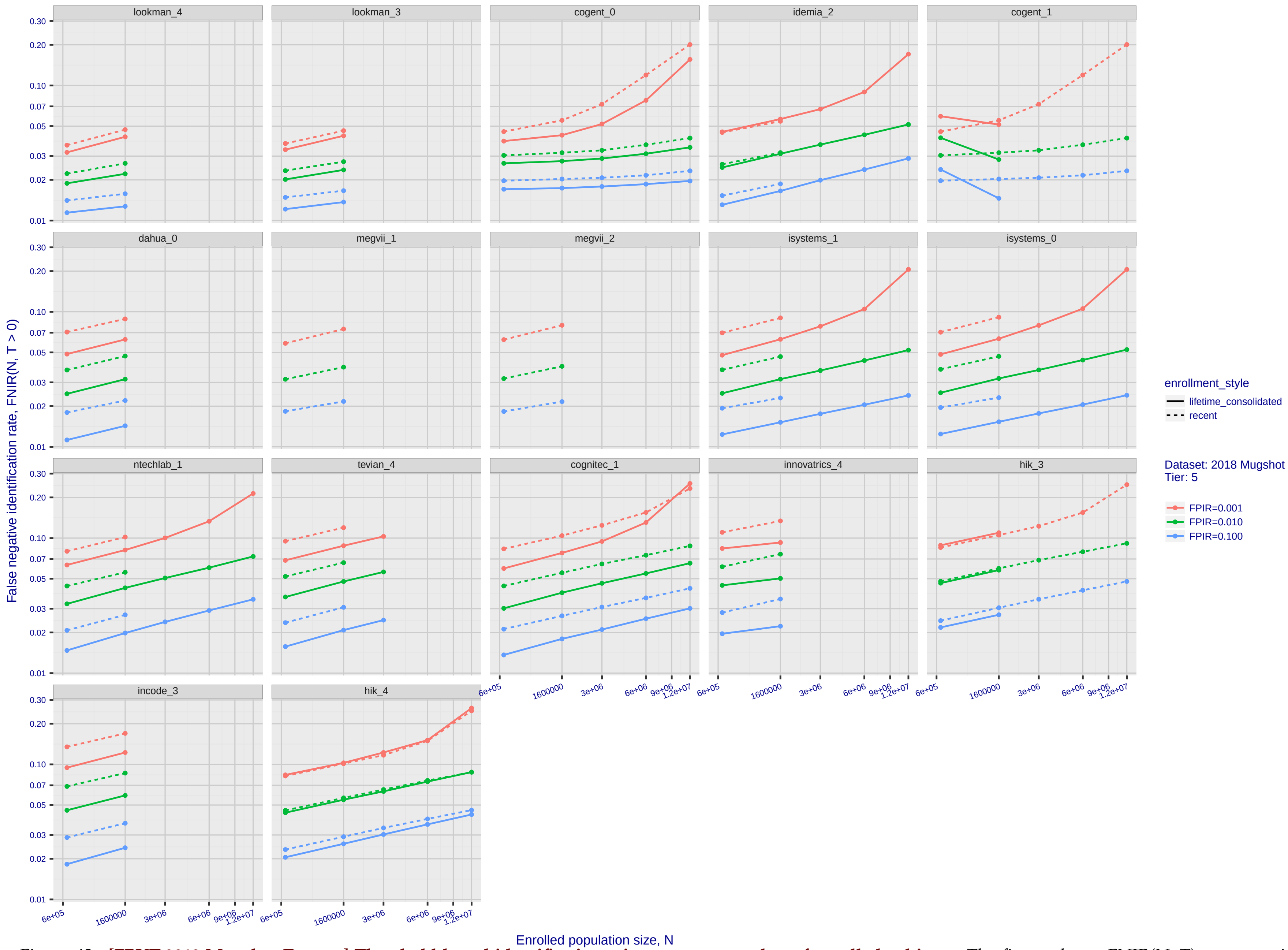

Figure 42: **[FRVT-2018 Mugshot Dataset] Threshold-based identification miss rates vs. number of enrolled subjects**. *The figure shows FNIR(N, T) across various gallery sizes when the threshold is set to achieve the given FPIRs. The rank criterion is irrelevant at high thresholds as mates are always at rank 1. The results are computed from the trials listed in rows 1-10 of Table 5. Less accurate algorithms were not run on large N, so results are missing. For clarity, results are sorted and reported into tiers spanning multiple pages. The tiering criteria is complicated: First paging by FNIR(N_b, 1, 0), then sorting by median FNIR(N_b, T), N_b = 640 000.*

FNIR(N, R, T) = False neg. identification rate
FPIR(N, T) = False pos. identification rate
N = Num. enrolled subjects
R = Num. candidates examined
T = Threshold
T = 0 → Investigation
T > 0 → Identification

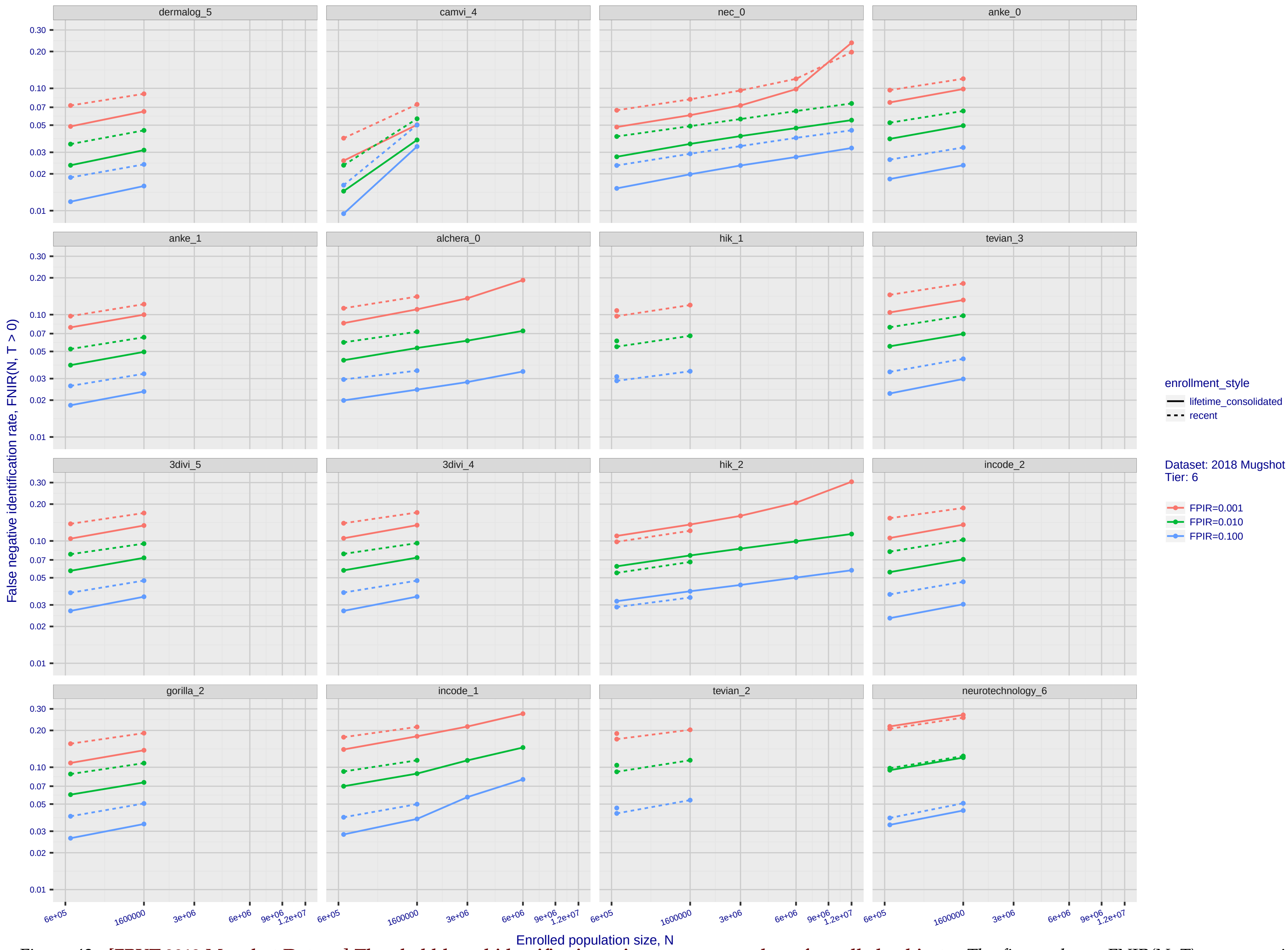

Figure 43: **[FRVT-2018 Mugshot Dataset] Threshold-based identification miss rates vs. number of enrolled subjects**. *The figure shows FNIR(N, T) across various gallery sizes when the threshold is set to achieve the given FPIRs. The rank criterion is irrelevant at high thresholds as mates are always at rank 1. The results are computed from the trials listed in rows 1-10 of Table 5. Less accurate algorithms were not run on large N, so results are missing. For clarity, results are sorted and reported into tiers spanning multiple pages. The tiering criteria is complicated: First paging by FNIR(N_b, 1, 0), then sorting by median FNIR(N_b, T), N_b = 640 000.*

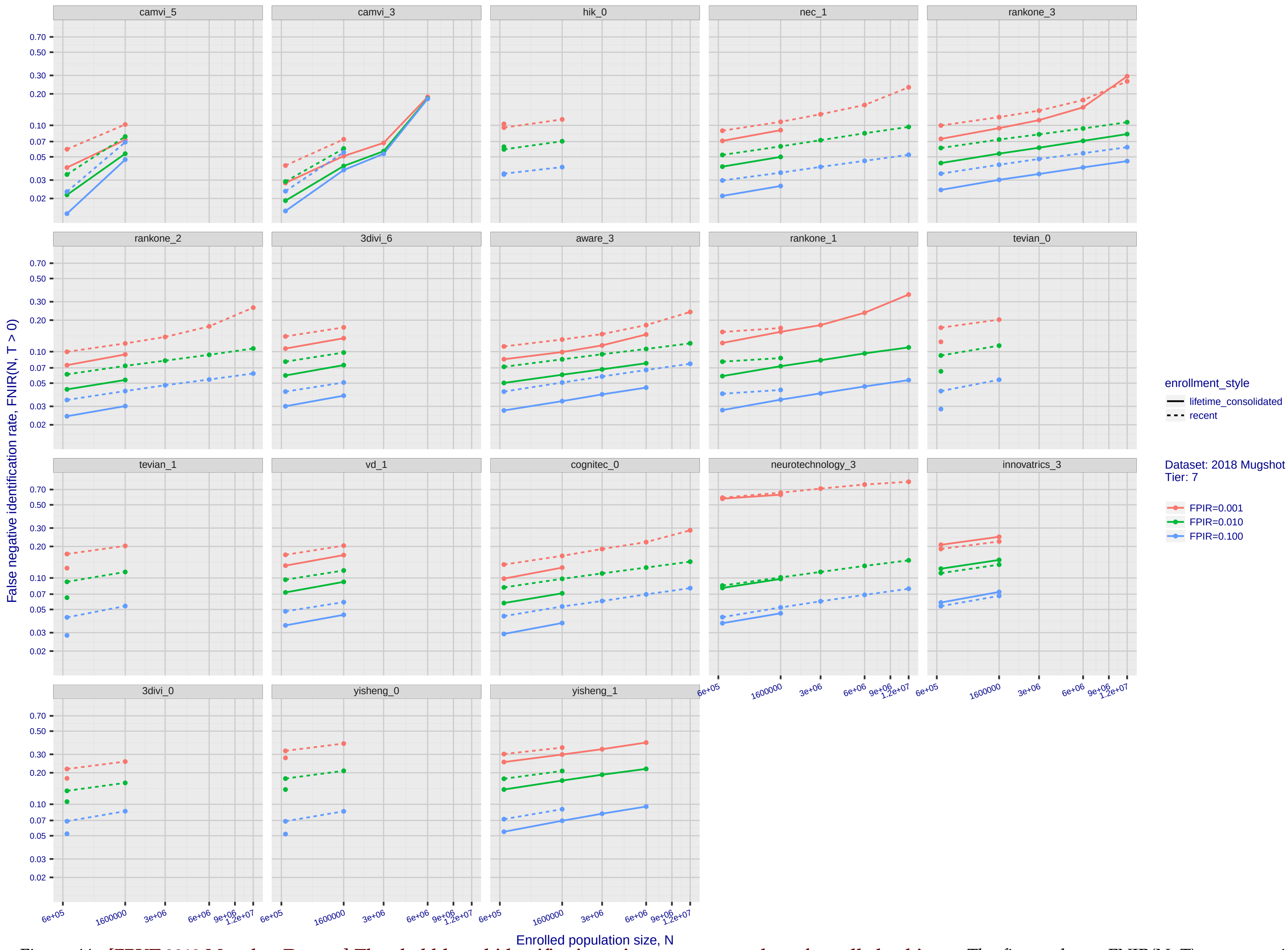

Figure 44: **[FRVT-2018 Mugshot Dataset] Threshold-based identification miss rates vs. number of enrolled subjects**. *The figure shows FNIR(N, T) across various gallery sizes when the threshold is set to achieve the given FPIRs. The rank criterion is irrelevant at high thresholds as mates are always at rank 1. The results are computed from the trials listed in rows 1-10 of Table 5. Less accurate algorithms were not run on large N, so results are missing. For clarity, results are sorted and reported into tiers spanning multiple pages. The tiering criteria is complicated: First paging by FNIR(N_b, 1, 0), then sorting by median FNIR(N_b, T), N_b = 640 000.*

FNIR(N, R, T) = False neg. identification rate
FPIR(N, T) = False pos. identification rate
N = Num. enrolled subjects
R = Num. candidates examined
T = Threshold
T = 0 → Investigation
T > 0 → Identification

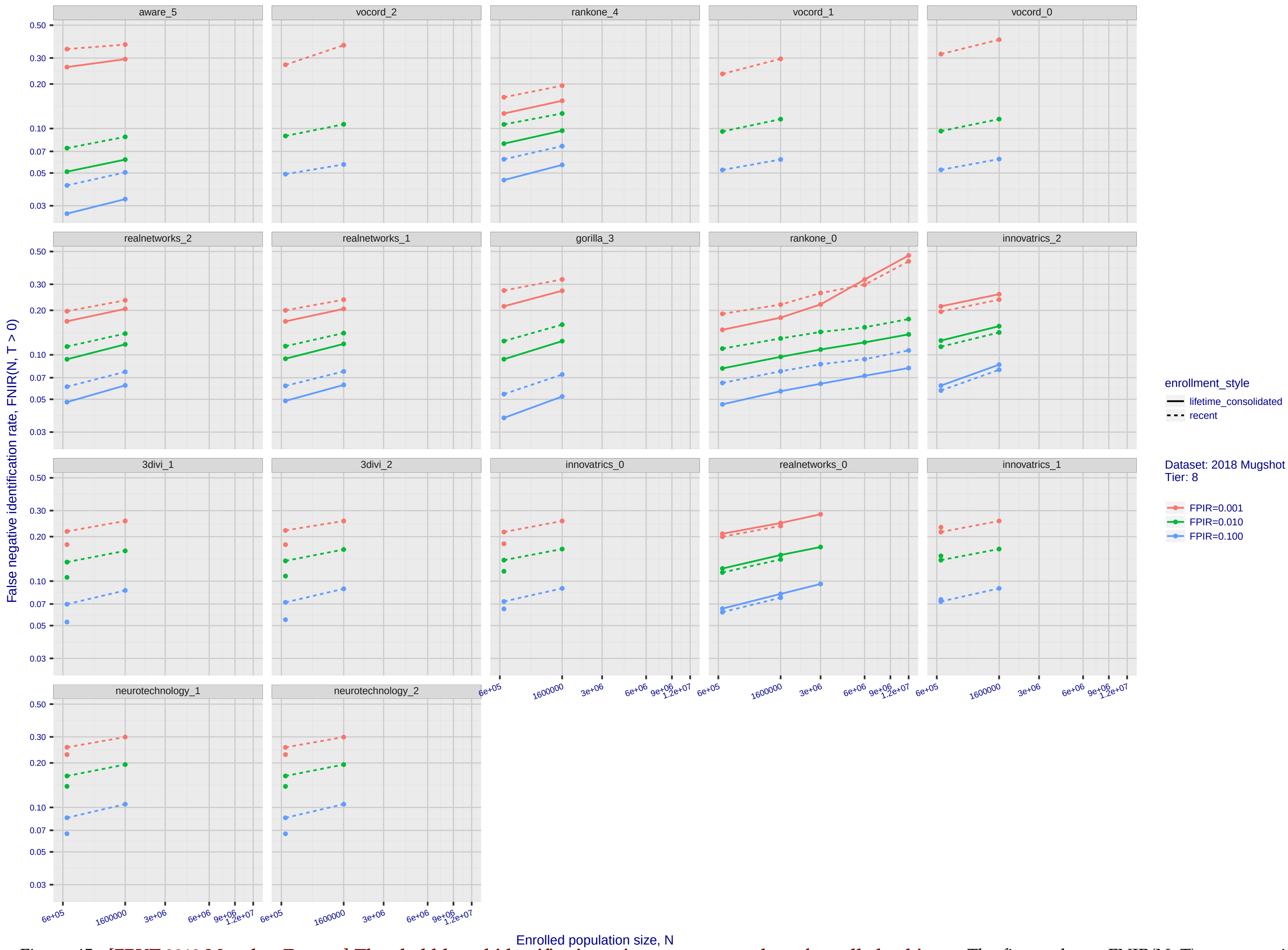

Figure 45: **[FRVT-2018 Mugshot Dataset] Threshold-based identification miss rates vs. number of enrolled subjects**. *The figure shows FNIR(N, T) across various gallery sizes when the threshold is set to achieve the given FPIRs. The rank criterion is irrelevant at high thresholds as mates are always at rank 1. The results are computed from the trials listed in rows 1-10 of Table 5. Less accurate algorithms were not run on large N, so results are missing. For clarity, results are sorted and reported into tiers spanning multiple pages. The tiering criteria is complicated: First paging by FNIR(N_b, 1, 0), then sorting by median FNIR(N_b, T), N_b = 640 000.*

FNIR(N, R, T) = False neg. identification rate
FPIR(N, T) = False pos. identification rate
N = Num. enrolled subjects
R = Num. candidates examined
T = Threshold
T = 0 → Investigation
T > 0 → Identification

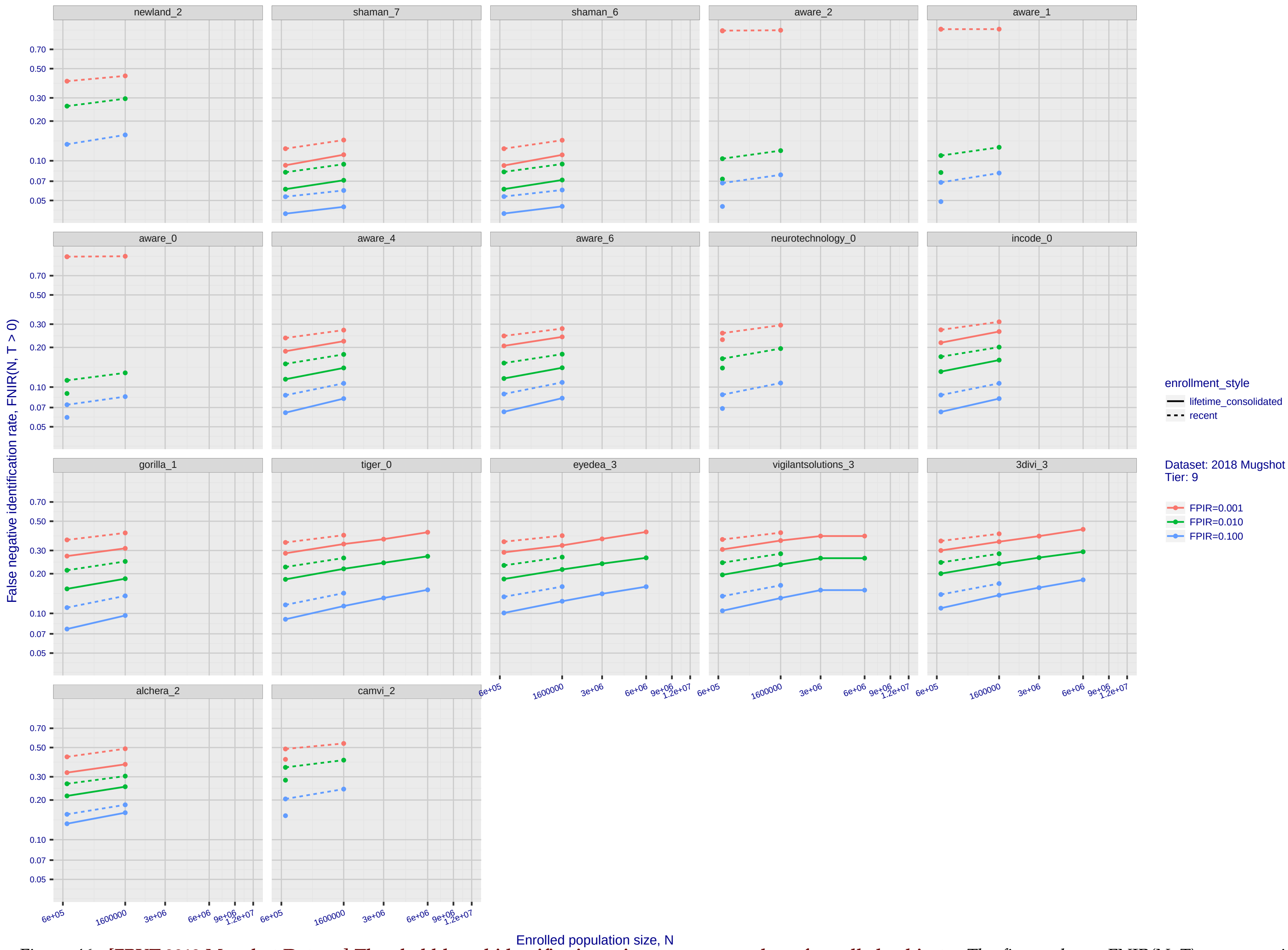

Figure 46: **[FRVT-2018 Mugshot Dataset] Threshold-based identification miss rates vs. number of enrolled subjects**. *The figure shows FNIR(N, T) across various gallery sizes when the threshold is set to achieve the given FPIRs. The rank criterion is irrelevant at high thresholds as mates are always at rank 1. The results are computed from the trials listed in rows 1-10 of Table 5. Less accurate algorithms were not run on large N, so results are missing. For clarity, results are sorted and reported into tiers spanning multiple pages. The tiering criteria is complicated: First paging by FNIR(N_b, 1, 0), then sorting by median FNIR(N_b, T), N_b = 640 000.*

2019/09/11 16:09:13

FNIR(N, R, T) = False neg. identification rate
FPIR(N, T) = False pos. identification rate
N = Num. enrolled subjects
R = Num. candidates examined
T = Threshold
T = 0 → Investigation
T > 0 → Identification

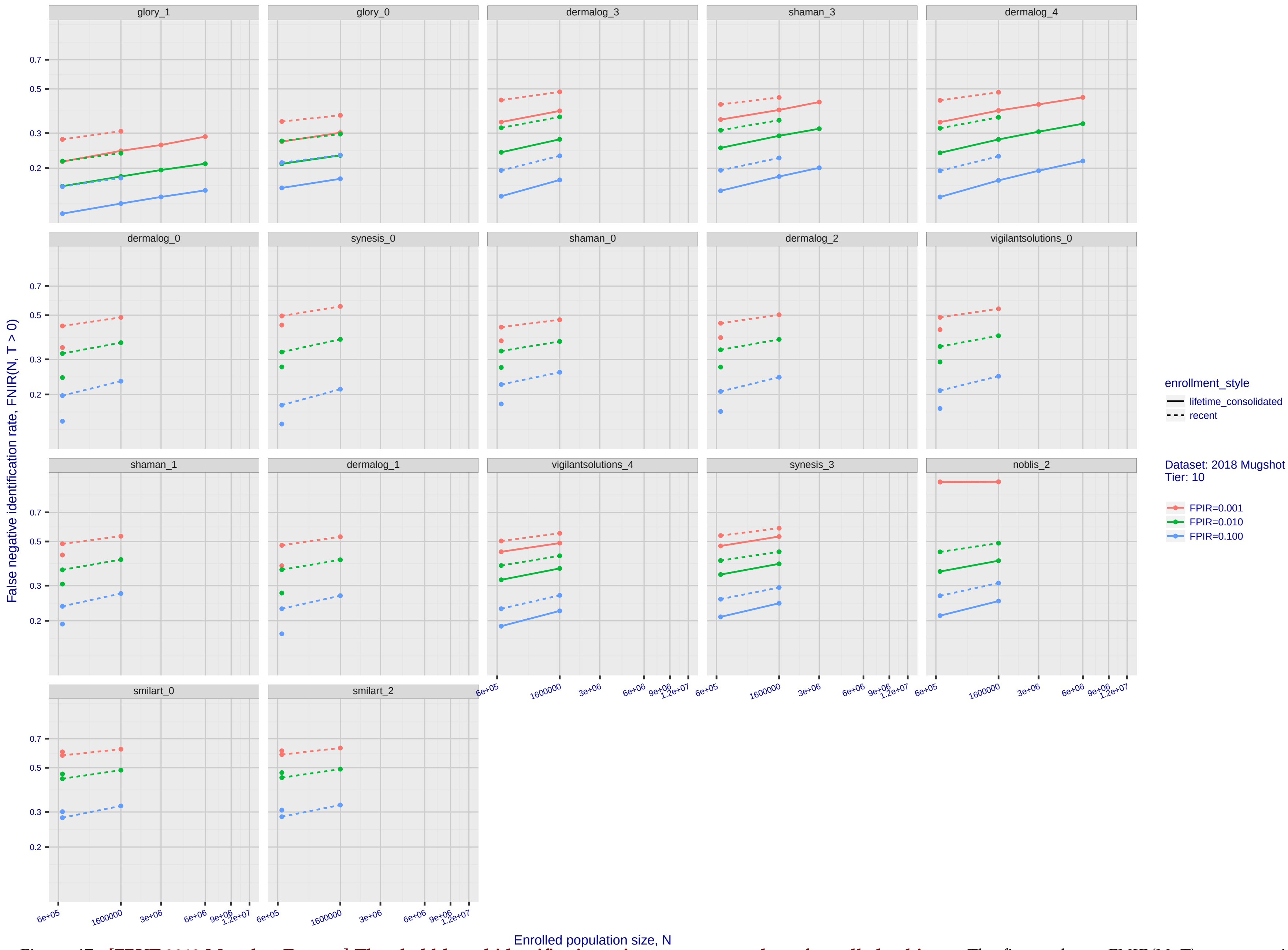

Figure 47: **[FRVT-2018 Mugshot Dataset] Threshold-based identification miss rates vs. number of enrolled subjects**. *The figure shows FNIR(N, T) across various gallery sizes when the threshold is set to achieve the given FPIRs. The rank criterion is irrelevant at high thresholds as mates are always at rank 1. The results are computed from the trials listed in rows 1-10 of Table 5. Less accurate algorithms were not run on large N, so results are missing. For clarity, results are sorted and reported into tiers spanning multiple pages. The tiering criteria is complicated: First paging by FNIR(N_b, 1, 0), then sorting by median FNIR(N_b, T), N_b = 640 000.*

FNIR(N, R, T) = False neg. identification rate N = Num. enrolled subjects T = Threshold T = 0 → Investigation
FPIR(N, T) = False pos. identification rate R = Num. candidates examined T > 0 → Identification

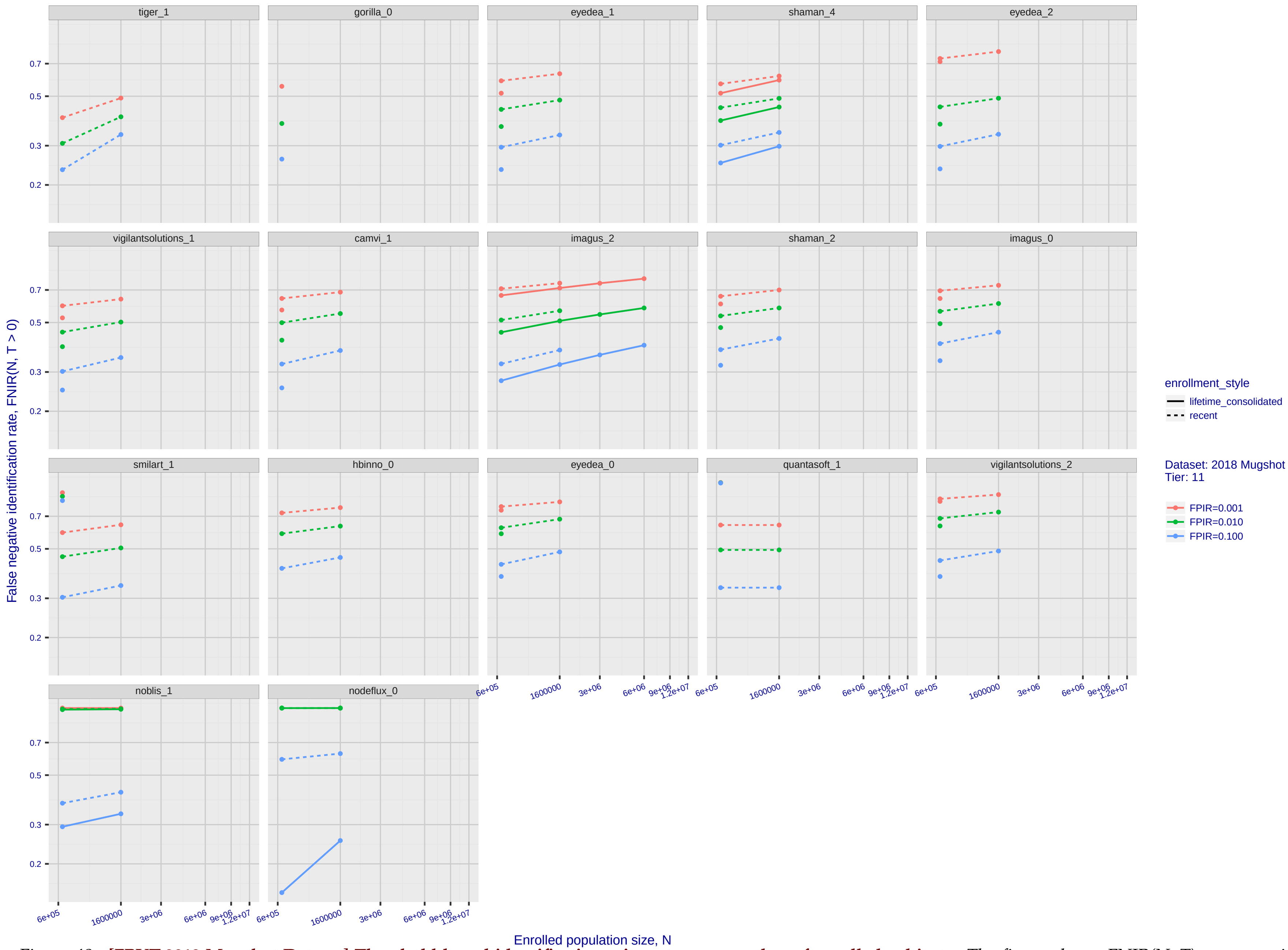

Figure 48: **[FRVT-2018 Mugshot Dataset] Threshold-based identification miss rates vs. number of enrolled subjects**. *The figure shows FNIR(N, T) across various gallery sizes when the threshold is set to achieve the given FPIRs. The rank criterion is irrelevant at high thresholds as mates are always at rank 1. The results are computed from the trials listed in rows 1-10 of Table 5. Less accurate algorithms were not run on large N, so results are missing. For clarity, results are sorted and reported into tiers spanning multiple pages. The tiering criteria is complicated: First paging by FNIR(N_b, 1, 0), then sorting by median FNIR(N_b, T), N_b = 640 000.*

FNIR(N, R, T) = False neg. identification rate
FPIR(N, T) = False pos. identification rate
N = Num. enrolled subjects
R = Num. candidates examined
T = Threshold
T = 0 → Investigation
T > 0 → Identification

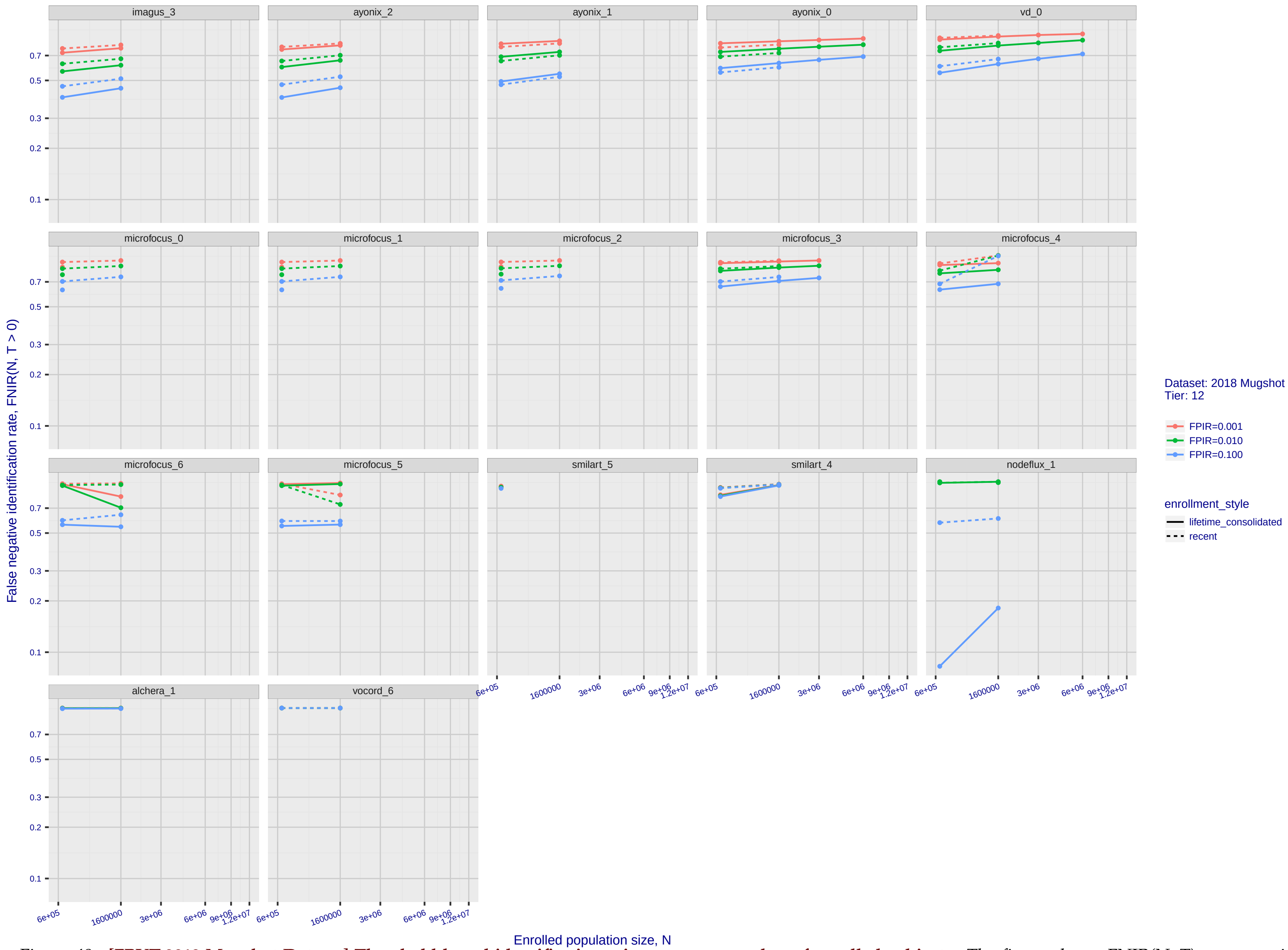

Figure 49: **[FRVT-2018 Mugshot Dataset] Threshold-based identification miss rates vs. number of enrolled subjects**. *The figure shows FNIR(N, T) across various gallery sizes when the threshold is set to achieve the given FPIRs. The rank criterion is irrelevant at high thresholds as mates are always at rank 1. The results are computed from the trials listed in rows 1-10 of Table 5. Less accurate algorithms were not run on large N, so results are missing. For clarity, results are sorted and reported into tiers spanning multiple pages. The tiering criteria is complicated: First paging by FNIR(N_b, 1, 0), then sorting by median FNIR(N_b, T), N_b = 640 000.*

2019/09/11	FNIR(N, R, T) =	False neg. identification rate	N = Num. enrolled subjects	T = Threshold	$T = 0 \rightarrow$ Investigation
16:09:13	FPIR(N, T) =	False pos. identification rate	R = Num. candidates examined		$T > 0 \rightarrow$ Identification

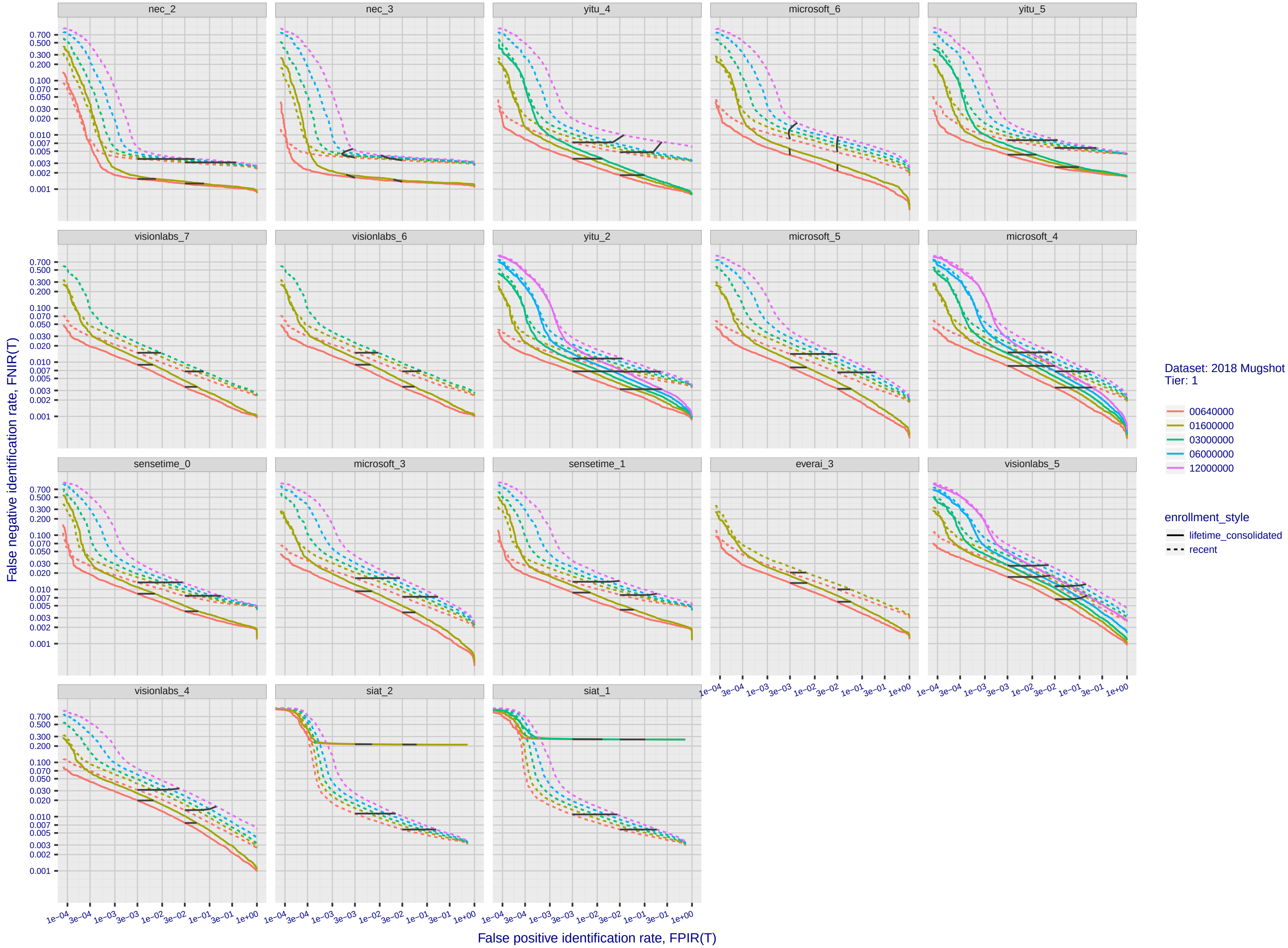

Figure 50: **[FRVT-2018 Mugshot Dataset] Identification miss rates vs. false positive rates**. *The figure shows miss rates FNIR(N, L, T) as a function of FPIR(N, T), with N ranging from 640 000 to 12 000 000 as noted in rows 1-10 of Table 5. These error tradeoff characteristics are useful for applications where a threshold must be elevated to limit false positives, such as when human reviewer labor is not matched to the volume of searches. Dark lines join points of equal threshold: If horizontal, FPIR(T) rises with N, and mate scores are independent of N. Other algorithms adjust scores in an attempt to make FPIR independent of N.*

2019/09/11 16:09:13

FNIR(N, R, T) = False neg. identification rate
FPIR(N, T) = False pos. identification rate
N = Num. enrolled subjects
R = Num. candidates examined
T = Threshold
T = 0 → Investigation
T > 0 → Identification

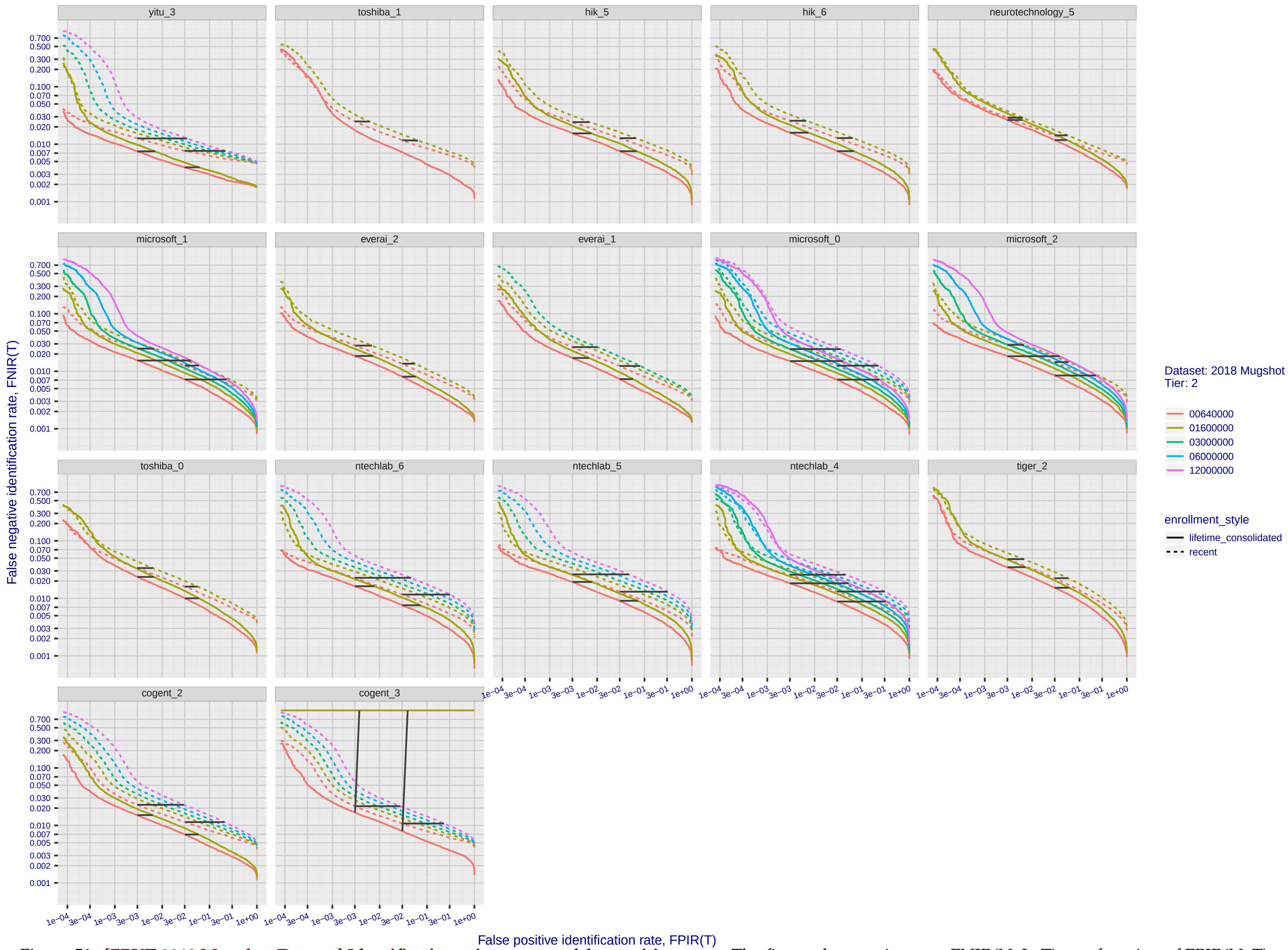

Figure 51: **[FRVT-2018 Mugshot Dataset] Identification miss rates vs. false positive rates**. *The figure shows miss rates FNIR(N, L, T) as a function of FPIR(N, T), with N ranging from 640 000 to 12 000 000 as noted in rows 1-10 of Table 5. These error tradeoff characteristics are useful for applications where a threshold must be elevated to limit false positives, such as when human reviewer labor is not matched to the volume of searches. Dark lines join points of equal threshold: If horizontal, FPIR(T) rises with N, and mate scores are independent of N. Other algorithms adjust scores in an attempt to make FPIR independent of N.*

2019/09/11
16:09:13

FNIR(N, R, T) = False neg. identification rate
FPIR(N, T) = False pos. identification rate
N = Num. enrolled subjects
R = Num. candidates examined
T = Threshold
T = 0 → Investigation
T > 0 → Identification

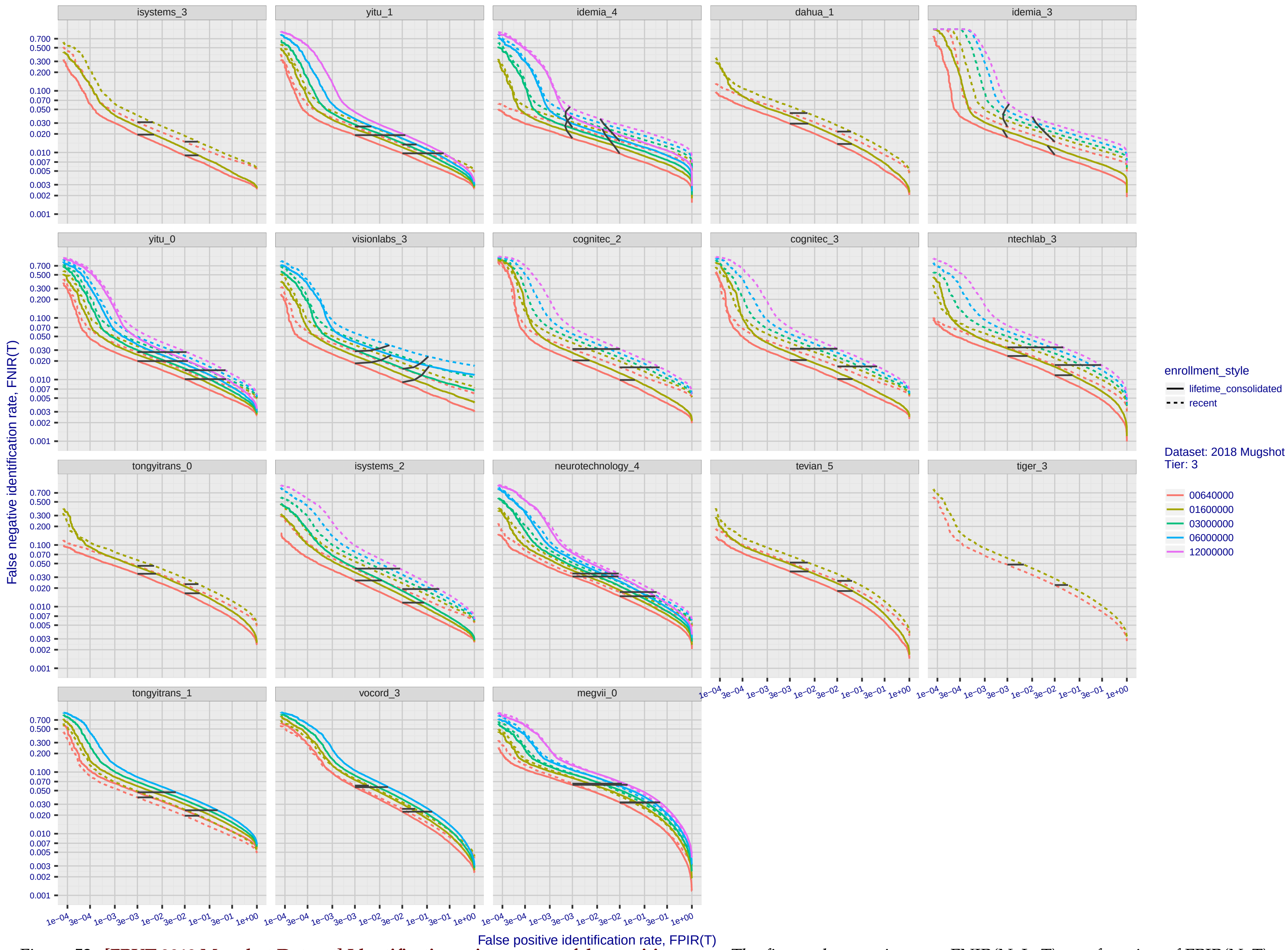

Figure 52: **[FRVT-2018 Mugshot Dataset] Identification miss rates vs. false positive rates**. *The figure shows miss rates FNIR(N, L, T) as a function of FPIR(N, T), with N ranging from 640 000 to 12 000 000 as noted in rows 1-10 of Table 5. These error tradeoff characteristics are useful for applications where a threshold must be elevated to limit false positives, such as when human reviewer labor is not matched to the volume of searches. Dark lines join points of equal threshold: If horizontal, FPIR(T) rises with N, and mate scores are independent of N. Other algorithms adjust scores in an attempt to make FPIR independent of N.*

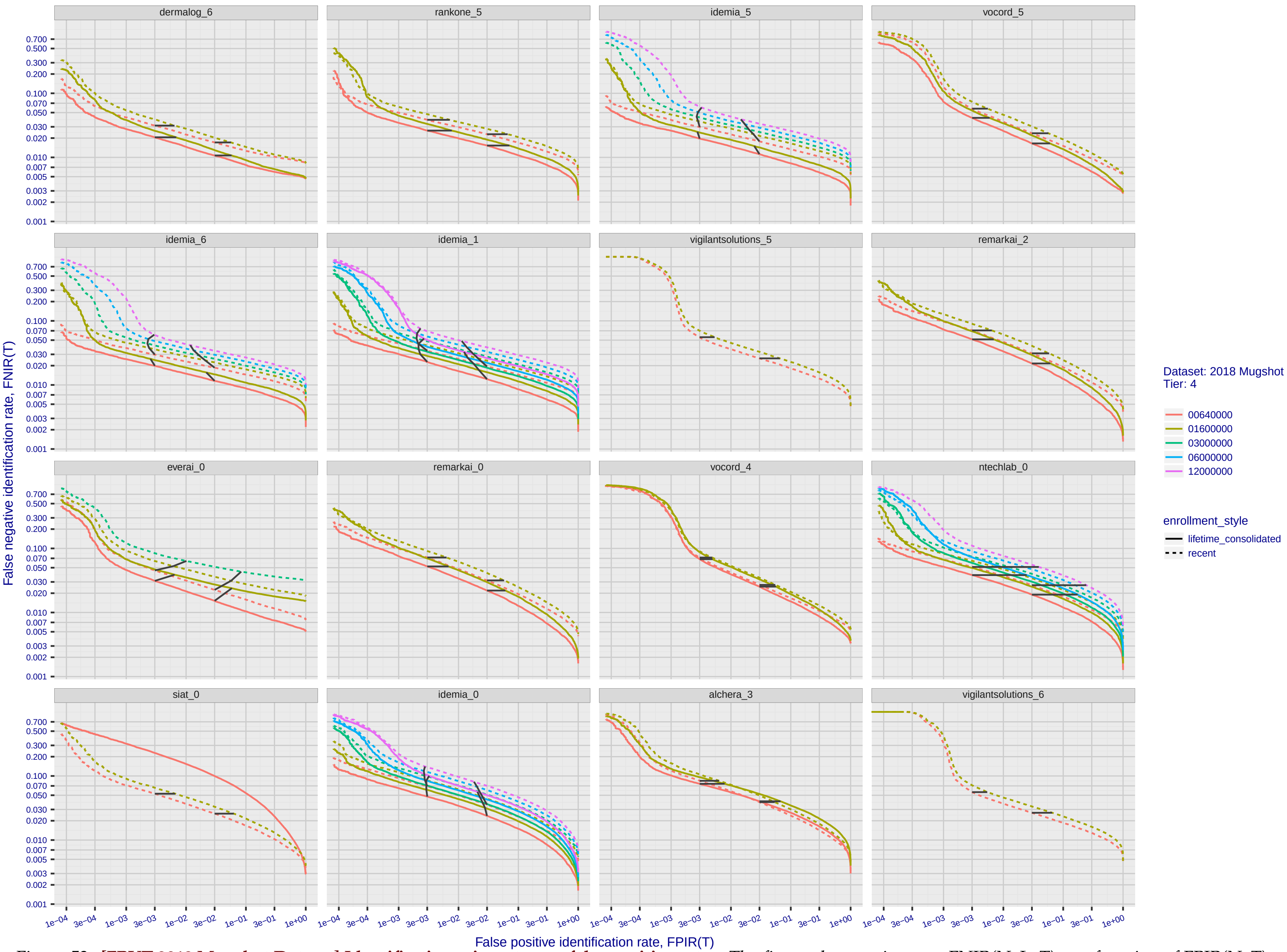

Figure 53: **[FRVT-2018 Mugshot Dataset] Identification miss rates vs. false positive rates**. *The figure shows miss rates FNIR(N, L, T) as a function of FPIR(N, T), with N ranging from 640 000 to 12 000 000 as noted in rows 1-10 of Table 5. These error tradeoff characteristics are useful for applications where a threshold must be elevated to limit false positives, such as when human reviewer labor is not matched to the volume of searches. Dark lines join points of equal threshold: If horizontal, FPIR(T) rises with N, and mate scores are independent of N. Other algorithms adjust scores in an attempt to make FPIR independent of N.*

This publication is available free of charge from: https://doi.org/10.6028/NIST.IR.8271

FNIR(N, R, T) = False neg. identification rate
FPIR(N, T) = False pos. identification rate
N = Num. enrolled subjects
R = Num. candidates examined
T = Threshold
T = 0 → Investigation
T > 0 → Identification

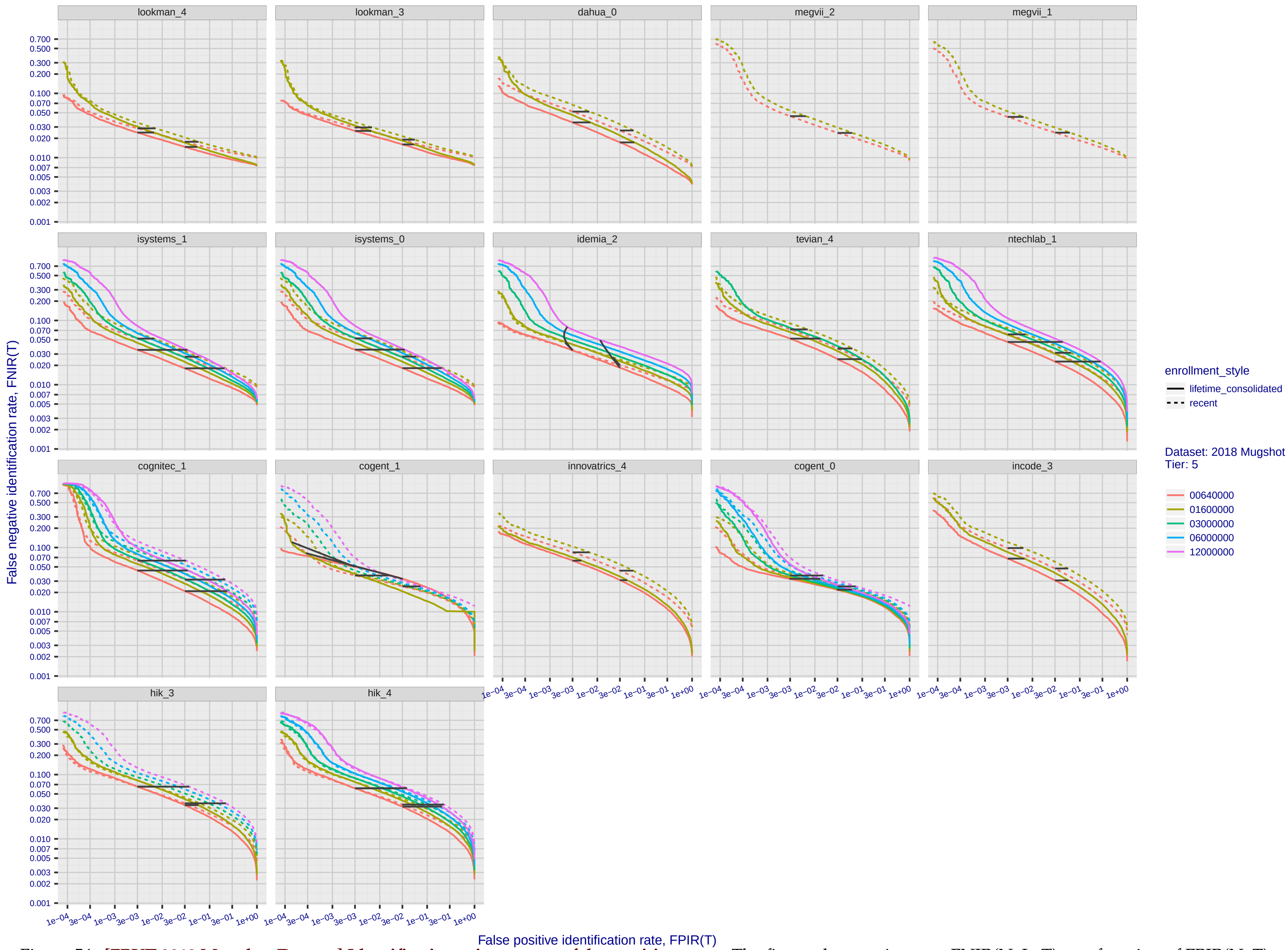

Figure 54: **[FRVT-2018 Mugshot Dataset] Identification miss rates vs. false positive rates**. *The figure shows miss rates FNIR(N, L, T) as a function of FPIR(N, T), with N ranging from 640 000 to 12 000 000 as noted in rows 1-10 of Table 5. These error tradeoff characteristics are useful for applications where a threshold must be elevated to limit false positives, such as when human reviewer labor is not matched to the volume of searches. Dark lines join points of equal threshold: If horizontal, FPIR(T) rises with N, and mate scores are independent of N. Other algorithms adjust scores in an attempt to make FPIR independent of N.*

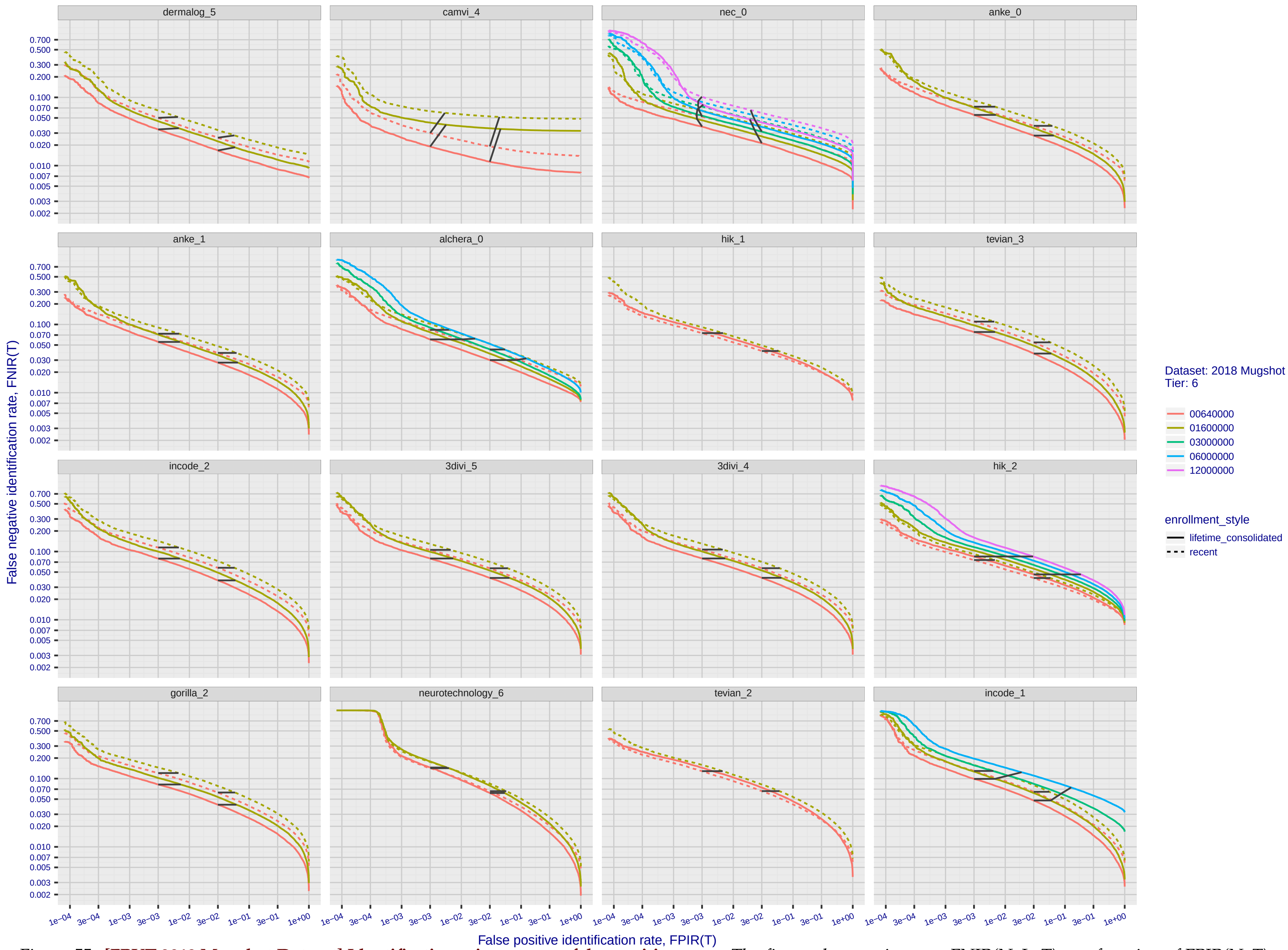

Figure 55: **[FRVT-2018 Mugshot Dataset] Identification miss rates vs. false positive rates**. *The figure shows miss rates FNIR(N, L, T) as a function of FPIR(N, T), with N ranging from 640 000 to 12 000 000 as noted in rows 1-10 of Table 5. These error tradeoff characteristics are useful for applications where a threshold must be elevated to limit false positives, such as when human reviewer labor is not matched to the volume of searches. Dark lines join points of equal threshold: If horizontal, FPIR(T) rises with N, and mate scores are independent of N. Other algorithms adjust scores in an attempt to make FPIR independent of N.*

FNIR(N, R, T) = False neg. identification rate
FPIR(N, T) = False pos. identification rate
N = Num. enrolled subjects
R = Num. candidates examined
T = Threshold
T = 0 → Investigation
T > 0 → Identification

FNIR(N, R, T) = False neg. identification rate
FPIR(N, T) = False pos. identification rate
N = Num. enrolled subjects
R = Num. candidates examined
T = Threshold
T = 0 → Investigation
T > 0 → Identification

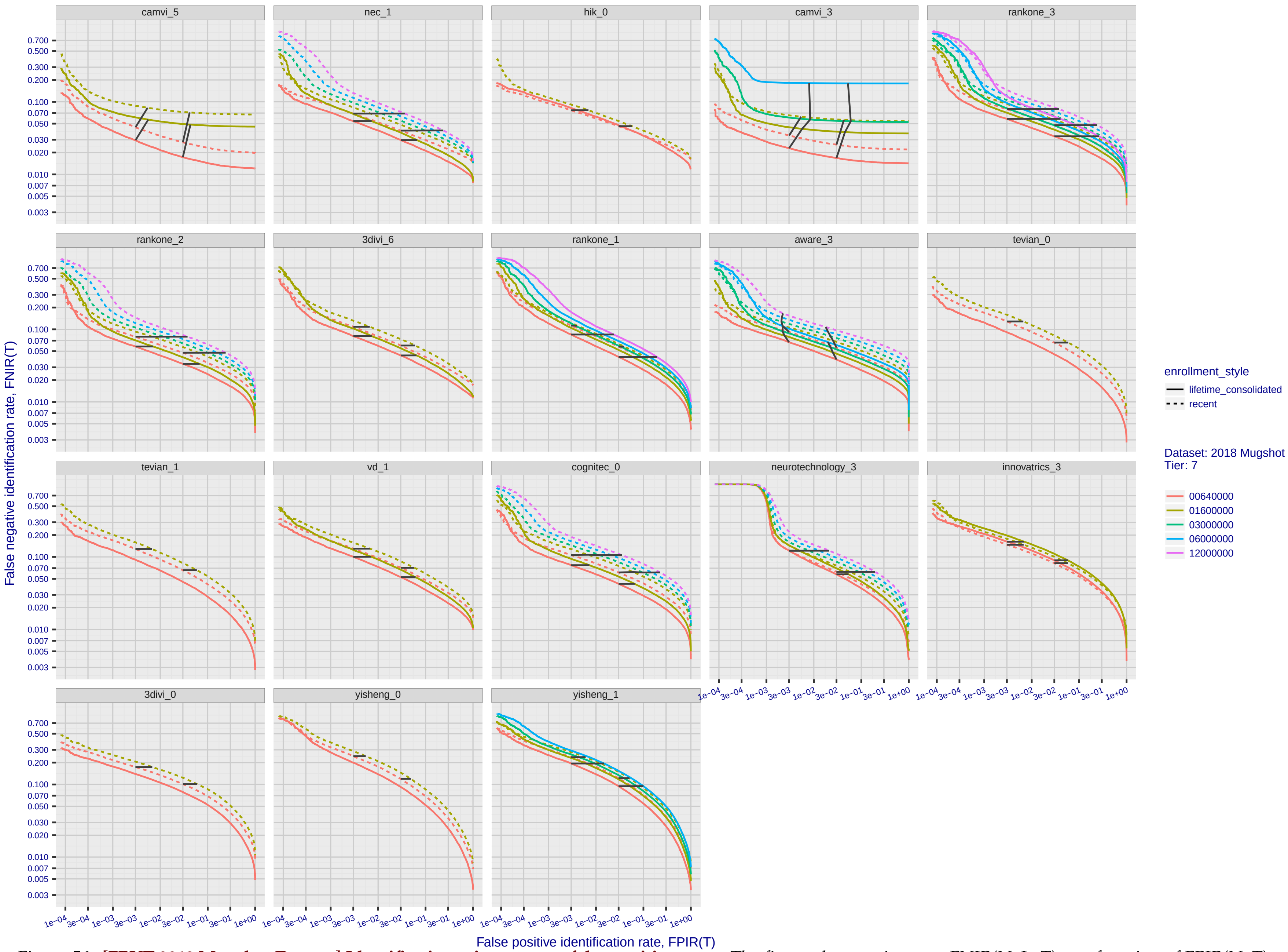

Figure 56: **[FRVT-2018 Mugshot Dataset] Identification miss rates vs. false positive rates**. *The figure shows miss rates FNIR(N, L, T) as a function of FPIR(N, T), with N ranging from 640 000 to 12 000 000 as noted in rows 1-10 of Table 5. These error tradeoff characteristics are useful for applications where a threshold must be elevated to limit false positives, such as when human reviewer labor is not matched to the volume of searches. Dark lines join points of equal threshold: If horizontal, FPIR(T) rises with N, and mate scores are independent of N. Other algorithms adjust scores in an attempt to make FPIR independent of N.*

FNIR(N, R, T) = False neg. identification rate
FPIR(N, T) = False pos. identification rate
N = Num. enrolled subjects
R = Num. candidates examined
T = Threshold
T = 0 → Investigation
T > 0 → Identification

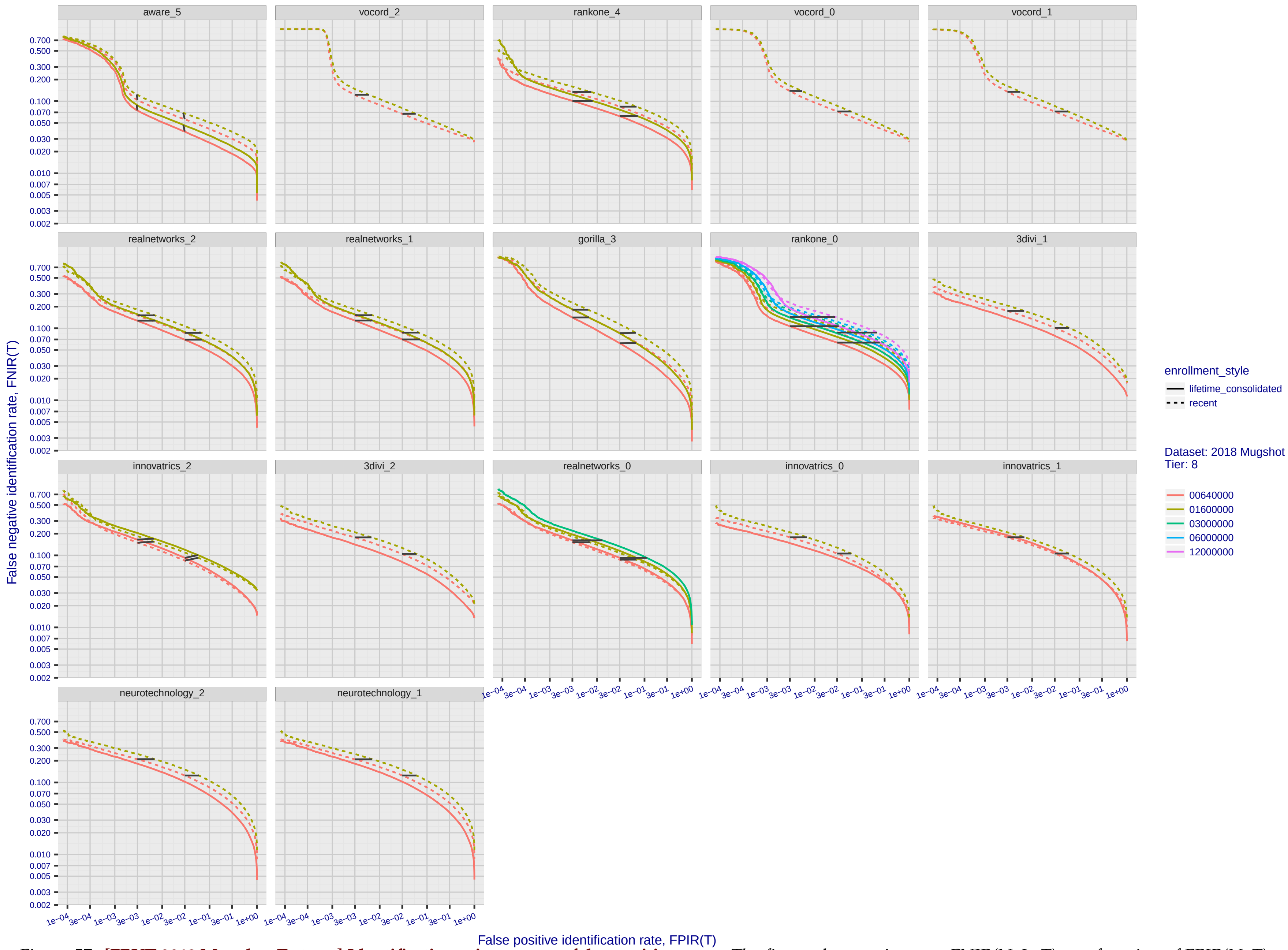

Figure 57: **[FRVT-2018 Mugshot Dataset] Identification miss rates vs. false positive rates**. *The figure shows miss rates FNIR(N, L, T) as a function of FPIR(N, T), with N ranging from 640 000 to 12 000 000 as noted in rows 1-10 of Table 5. These error tradeoff characteristics are useful for applications where a threshold must be elevated to limit false positives, such as when human reviewer labor is not matched to the volume of searches. Dark lines join points of equal threshold: If horizontal, FPIR(T) rises with N, and mate scores are independent of N. Other algorithms adjust scores in an attempt to make FPIR independent of N.*

2019/09/11 16:09:13

FNIR(N, R, T) = False neg. identification rate
FPIR(N, T) = False pos. identification rate
N = Num. enrolled subjects
R = Num. candidates examined
T = Threshold
T = 0 → Investigation
T > 0 → Identification

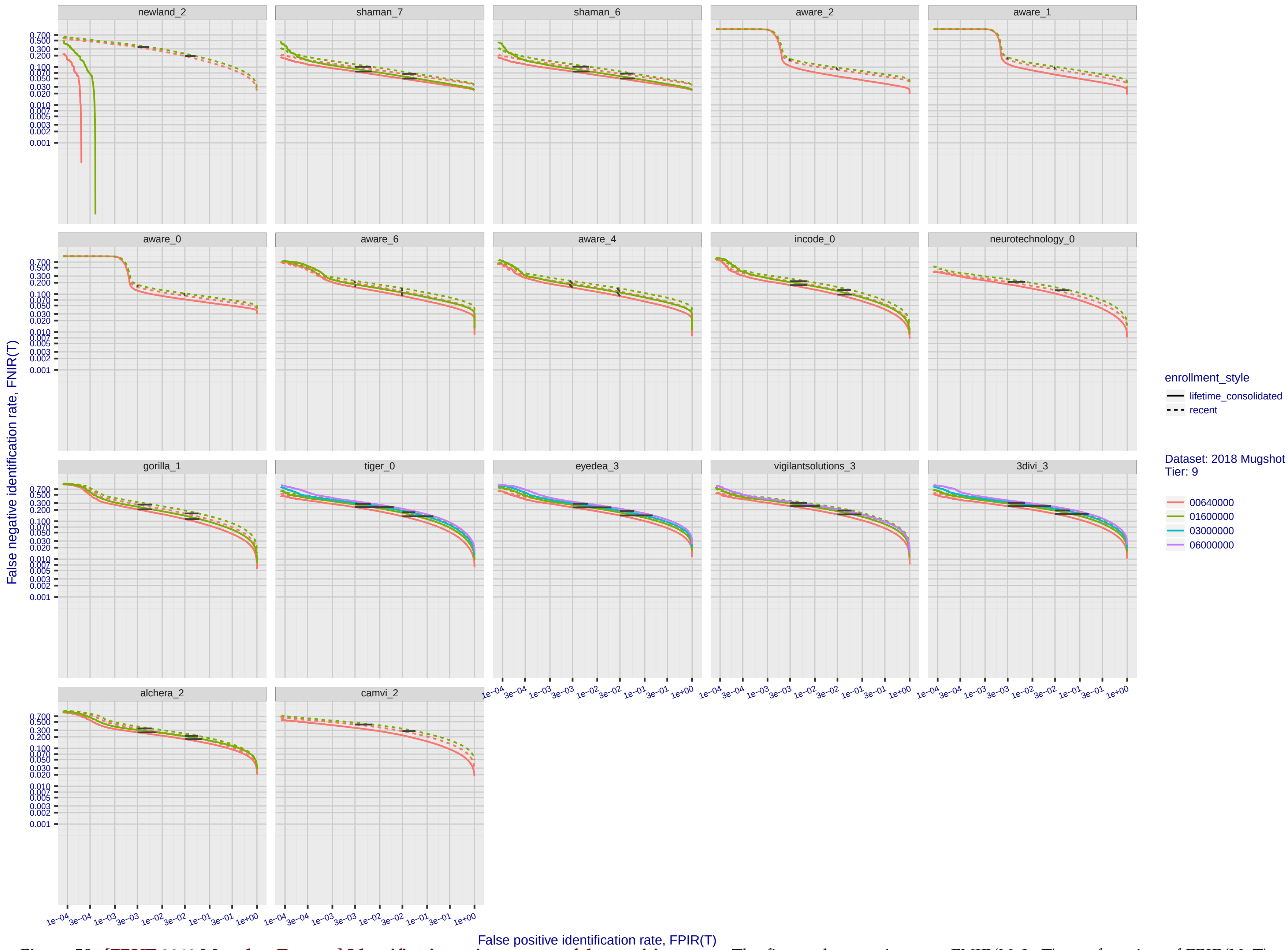

Figure 58: **[FRVT-2018 Mugshot Dataset] Identification miss rates vs. false positive rates**. *The figure shows miss rates FNIR(N, L, T) as a function of FPIR(N, T), with N ranging from 640 000 to 12 000 000 as noted in rows 1-10 of Table 5. These error tradeoff characteristics are useful for applications where a threshold must be elevated to limit false positives, such as when human reviewer labor is not matched to the volume of searches. Dark lines join points of equal threshold: If horizontal, FPIR(T) rises with N, and mate scores are independent of N. Other algorithms adjust scores in an attempt to make FPIR independent of N.*

FNIR(N, R, T) = False neg. identification rate
FPIR(N, T) = False pos. identification rate
N = Num. enrolled subjects
R = Num. candidates examined
T = Threshold
T = 0 → Investigation
T > 0 → Identification

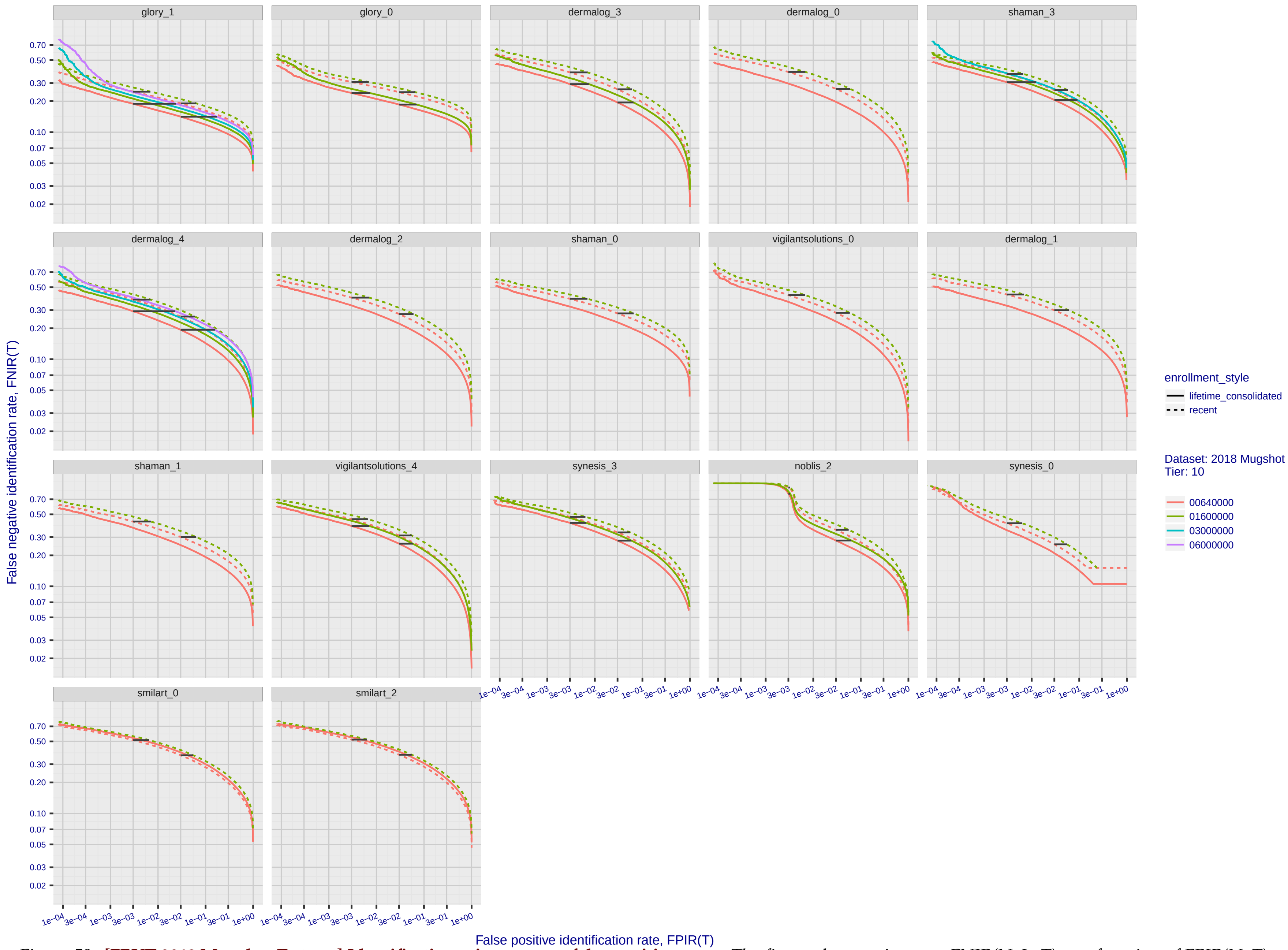

Figure 59: **[FRVT-2018 Mugshot Dataset] Identification miss rates vs. false positive rates**. *The figure shows miss rates FNIR(N, L, T) as a function of FPIR(N, T), with N ranging from 640 000 to 12 000 000 as noted in rows 1-10 of Table 5. These error tradeoff characteristics are useful for applications where a threshold must be elevated to limit false positives, such as when human reviewer labor is not matched to the volume of searches. Dark lines join points of equal threshold: If horizontal, FPIR(T) rises with N, and mate scores are independent of N. Other algorithms adjust scores in an attempt to make FPIR independent of N.*

2019/09/11
16:09:13

FNIR(N, R, T) = False neg. identification rate
FPIR(N, T) = False pos. identification rate
N = Num. enrolled subjects
R = Num. candidates examined
T = Threshold
T = 0 → Investigation
T > 0 → Identification

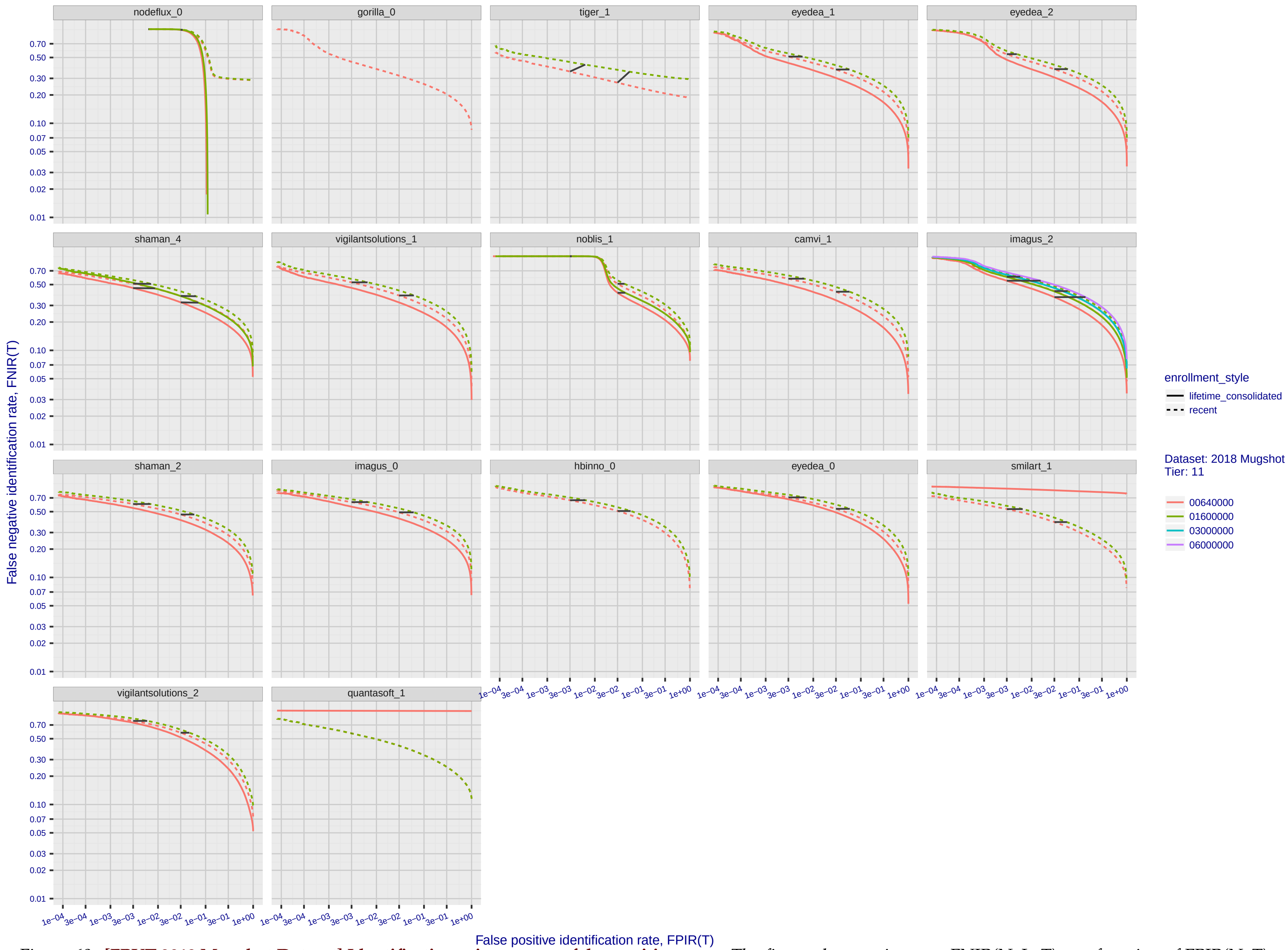

Figure 60: **[FRVT-2018 Mugshot Dataset] Identification miss rates vs. false positive rates**. *The figure shows miss rates FNIR(N, L, T) as a function of FPIR(N, T), with N ranging from 640 000 to 12 000 000 as noted in rows 1-10 of Table 5. These error tradeoff characteristics are useful for applications where a threshold must be elevated to limit false positives, such as when human reviewer labor is not matched to the volume of searches. Dark lines join points of equal threshold: If horizontal, FPIR(T) rises with N, and mate scores are independent of N. Other algorithms adjust scores in an attempt to make FPIR independent of N.*

FNIR(N, R, T) = False neg. identification rate
FPIR(N, T) = False pos. identification rate
N = Num. enrolled subjects
R = Num. candidates examined
T = Threshold
T = 0 → Investigation
T > 0 → Identification

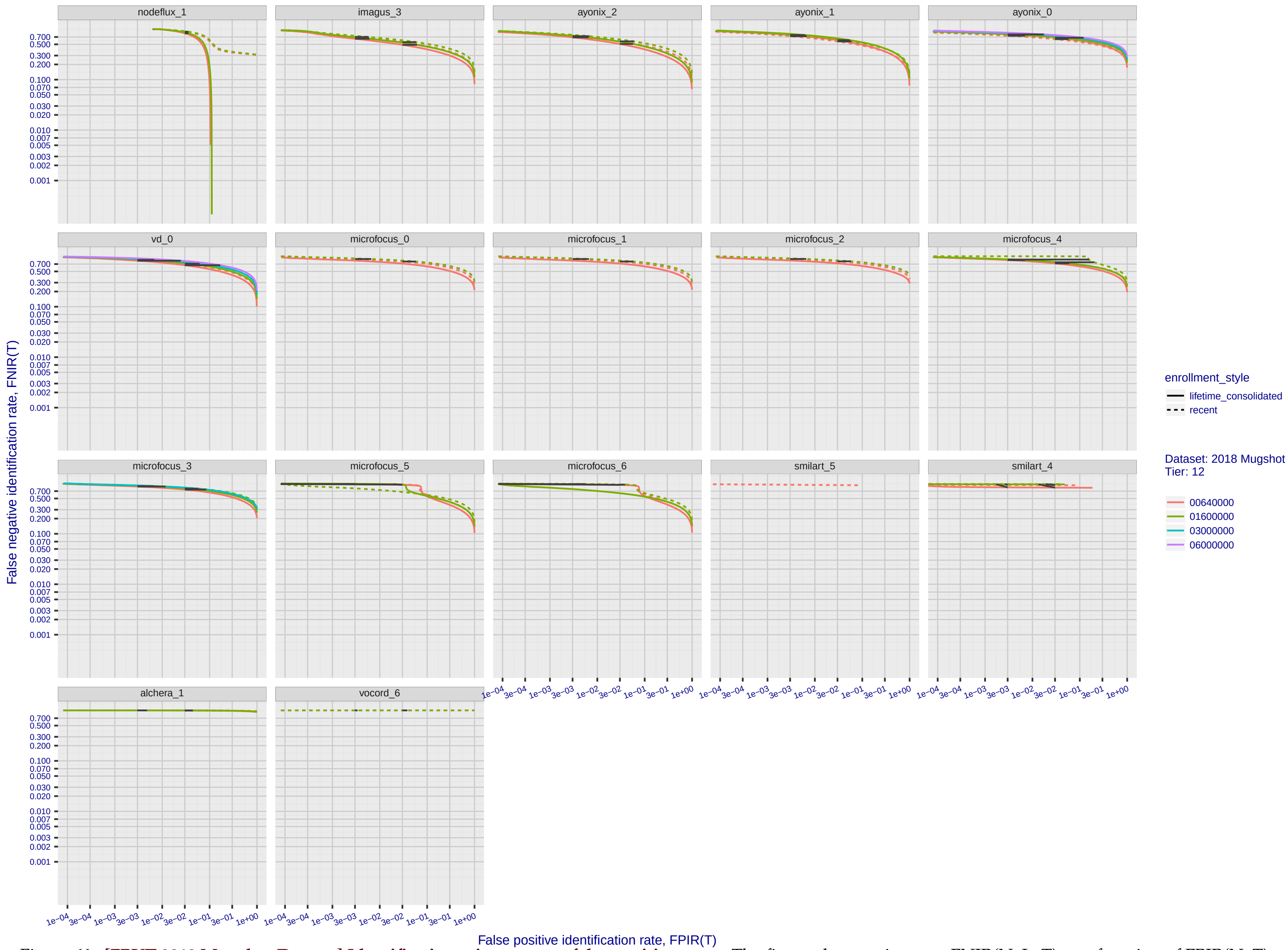

Figure 61: **[FRVT-2018 Mugshot Dataset] Identification miss rates vs. false positive rates**. *The figure shows miss rates FNIR(N, L, T) as a function of FPIR(N, T), with N ranging from 640 000 to 12 000 000 as noted in rows 1-10 of Table 5. These error tradeoff characteristics are useful for applications where a threshold must be elevated to limit false positives, such as when human reviewer labor is not matched to the volume of searches. Dark lines join points of equal threshold: If horizontal, FPIR(T) rises with N, and mate scores are independent of N. Other algorithms adjust scores in an attempt to make FPIR independent of N.*

Appendix B Effect of time-lapse: Accuracy after face ageing

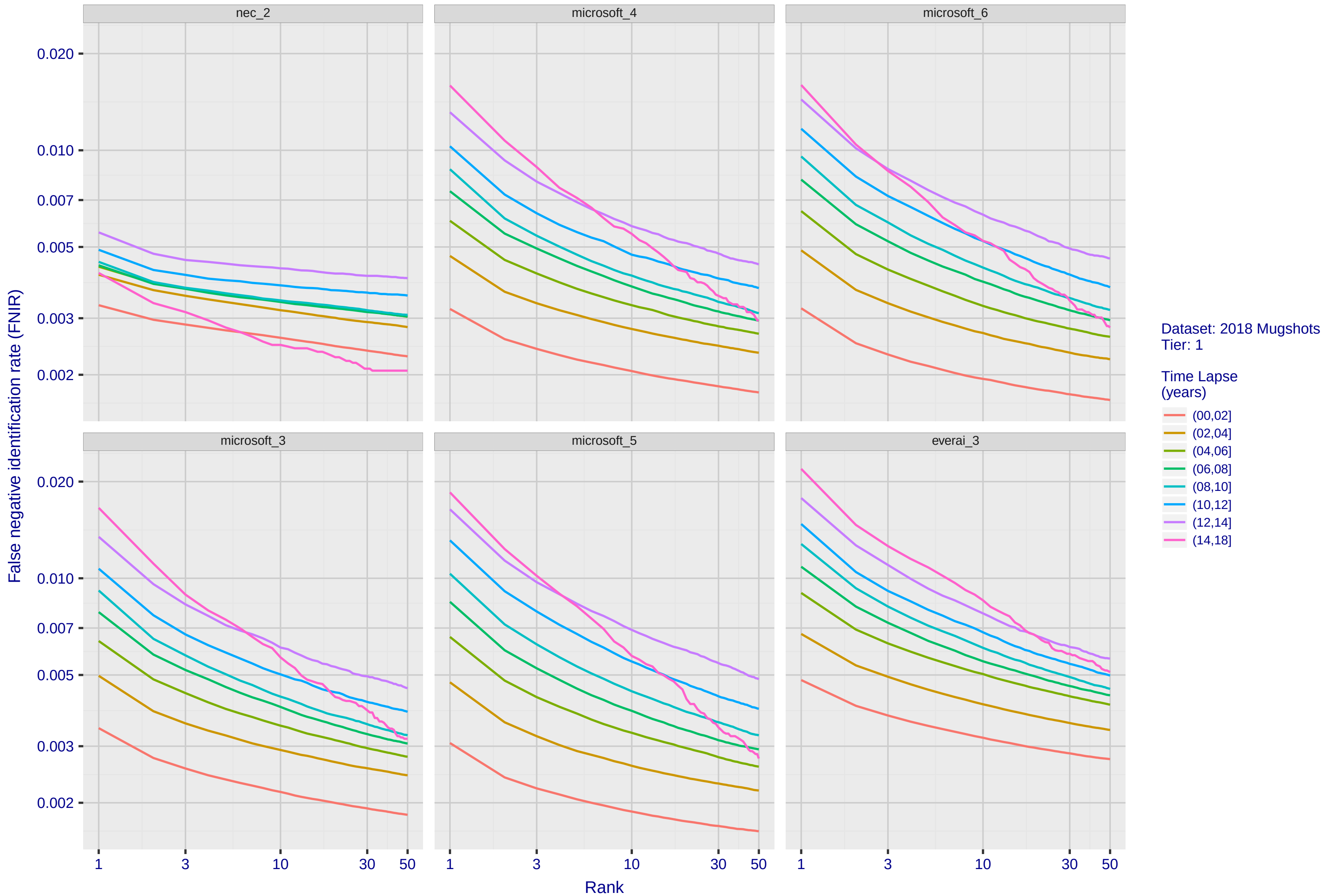

Figure 62: **[FRVT-2018 Mugshot Ageing Dataset] Identification miss rates vs. rank by time-elapsed**. *The oldest image of each individual is enrolled. Thereafter, all more recent images are searched. Miss rates are computed over all searches noted in row 17 of Table 5 and binned by number of years between search and initial enrollment.*

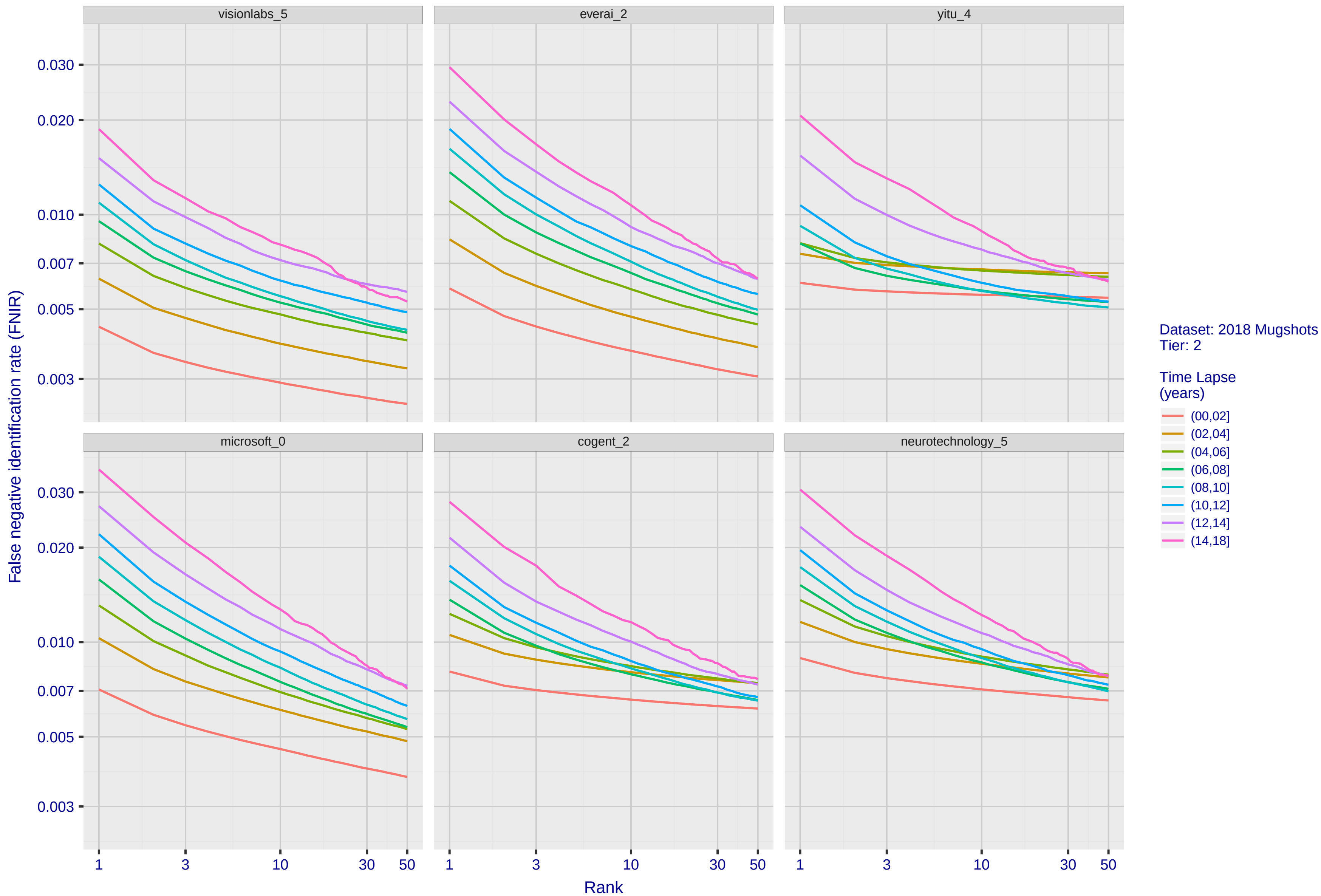

Figure 63: **[FRVT-2018 Mugshot Ageing Dataset] Identification miss rates vs. rank by time-elapsed**. *The oldest image of each individual is enrolled. Thereafter, all more recent images are searched. Miss rates are computed over all searches noted in row 17 of Table 5 and binned by number of years between search and initial enrollment.*

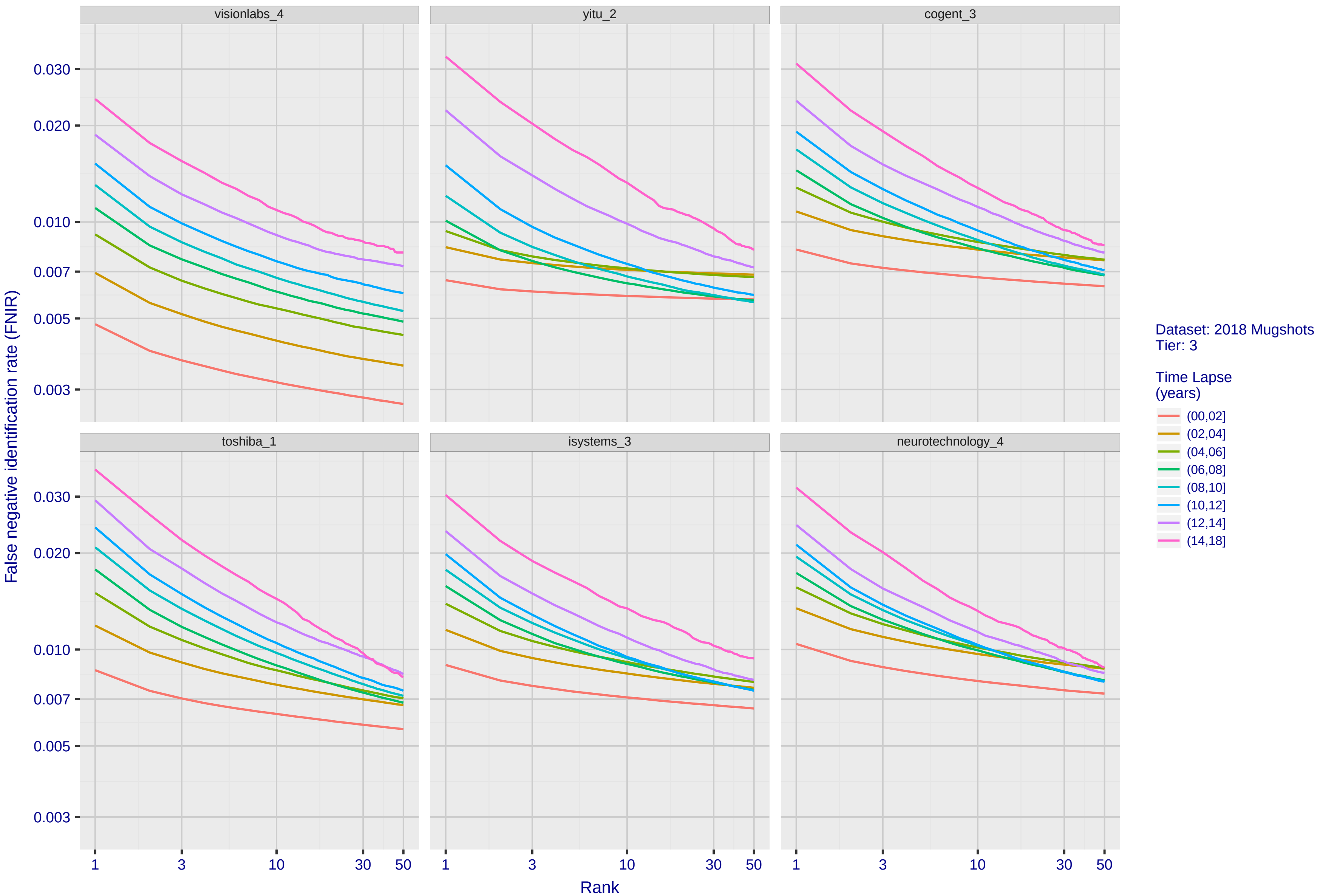

Figure 64: **[FRVT-2018 Mugshot Ageing Dataset] Identification miss rates vs. rank by time-elapsed**. *The oldest image of each individual is enrolled. Thereafter, all more recent images are searched. Miss rates are computed over all searches noted in row 17 of Table 5 and binned by number of years between search and initial enrollment.*

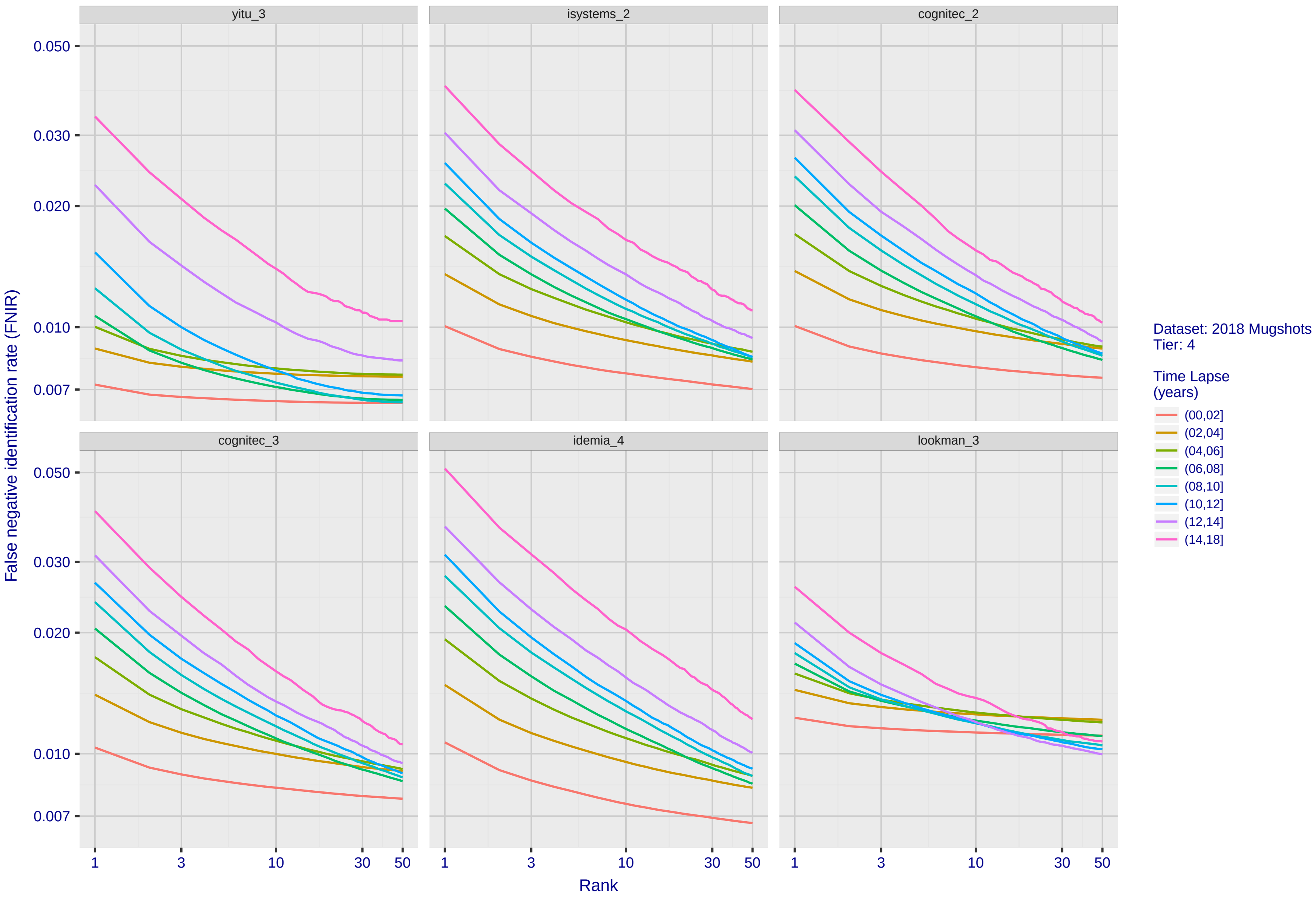

Figure 65: **[FRVT-2018 Mugshot Ageing Dataset] Identification miss rates vs. rank by time-elapsed**. *The oldest image of each individual is enrolled. Thereafter, all more recent images are searched. Miss rates are computed over all searches noted in row 17 of Table 5 and binned by number of years between search and initial enrollment.*

FNIR(N, R, T) = False neg. identification rate
FPIR(N, T) = False pos. identification rate
N = Num. enrolled subjects
R = Num. candidates examined
T = Threshold
T = 0 → Investigation
T > 0 → Identification

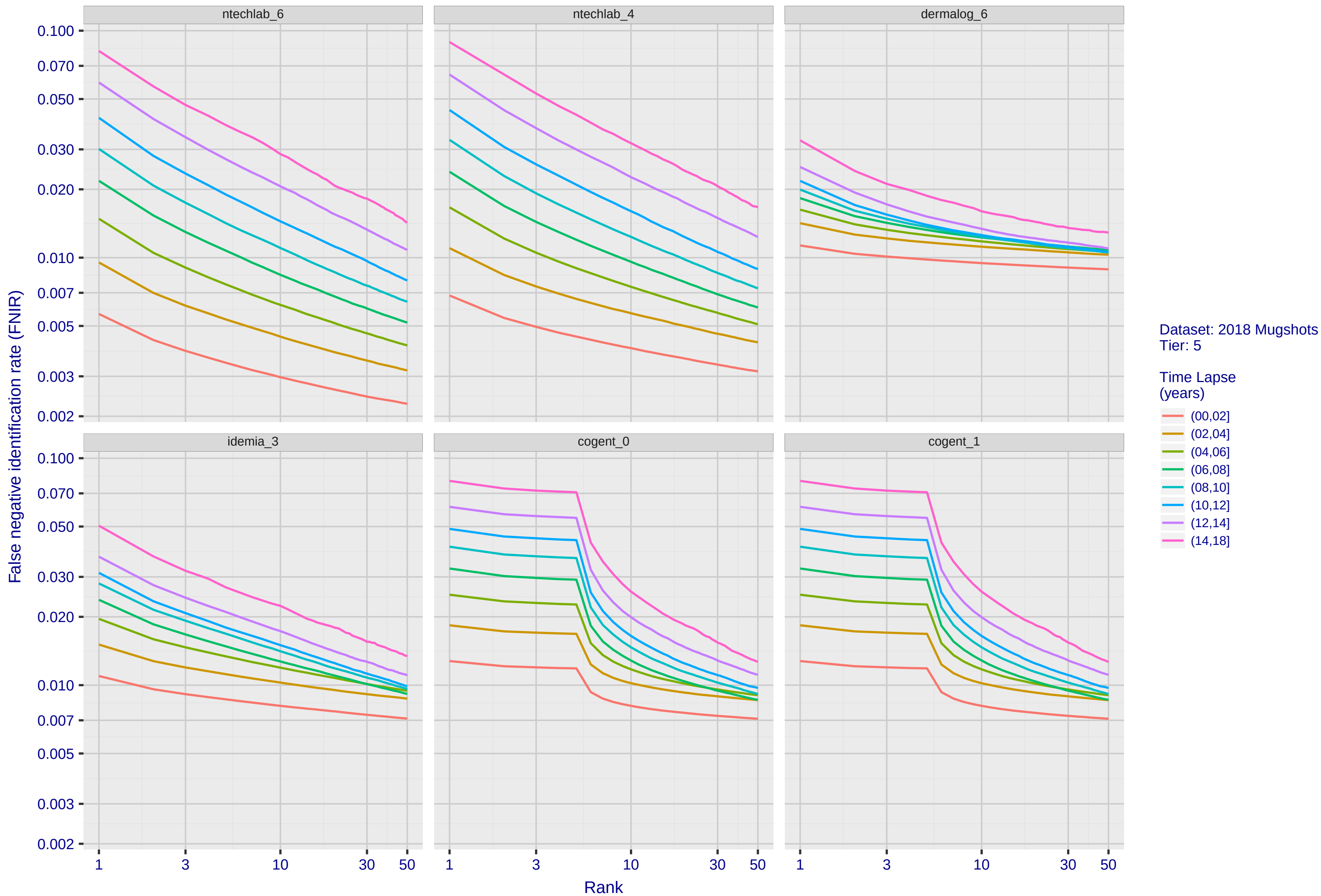

Figure 66: **[FRVT-2018 Mugshot Ageing Dataset] Identification miss rates vs. rank by time-elapsed**. *The oldest image of each individual is enrolled. Thereafter, all more recent images are searched. Miss rates are computed over all searches noted in row 17 of Table 5 and binned by number of years between search and initial enrollment.*

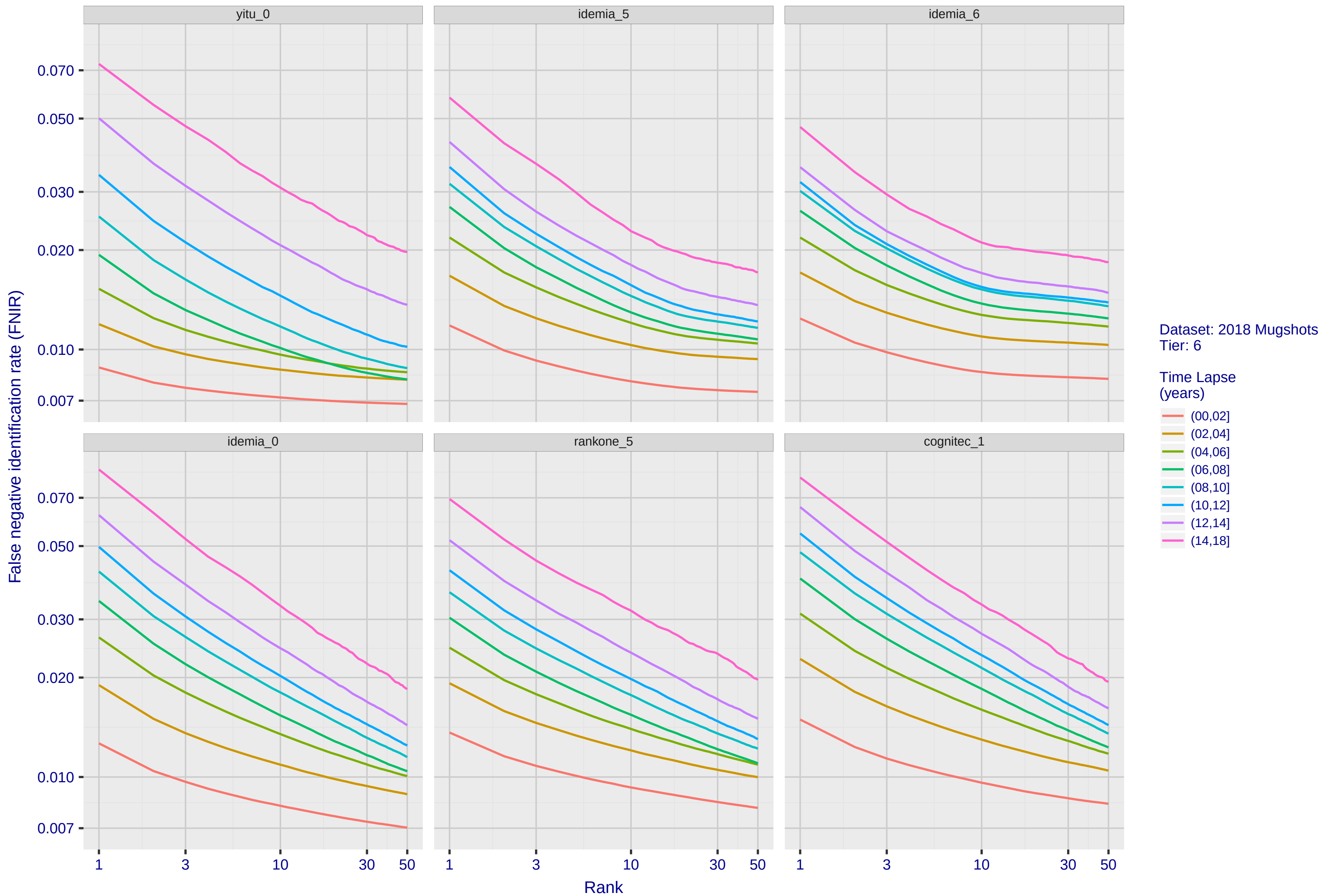

Figure 67: **[FRVT-2018 Mugshot Ageing Dataset] Identification miss rates vs. rank by time-elapsed**. *The oldest image of each individual is enrolled. Thereafter, all more recent images are searched. Miss rates are computed over all searches noted in row 17 of Table 5 and binned by number of years between search and initial enrollment.*

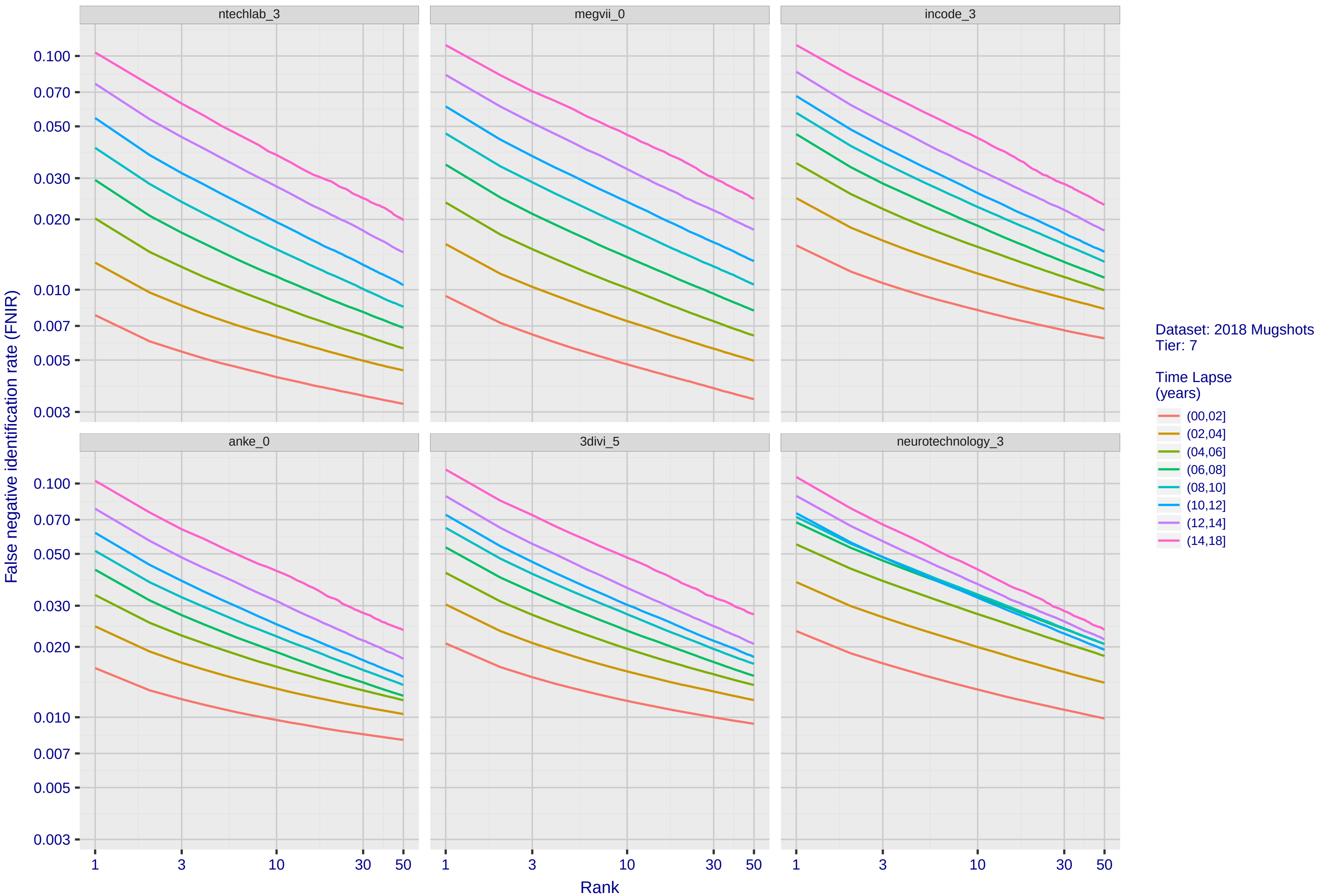

Figure 68: **[FRVT-2018 Mugshot Ageing Dataset] Identification miss rates vs. rank by time-elapsed**. *The oldest image of each individual is enrolled. Thereafter, all more recent images are searched. Miss rates are computed over all searches noted in row 17 of Table 5 and binned by number of years between search and initial enrollment.*

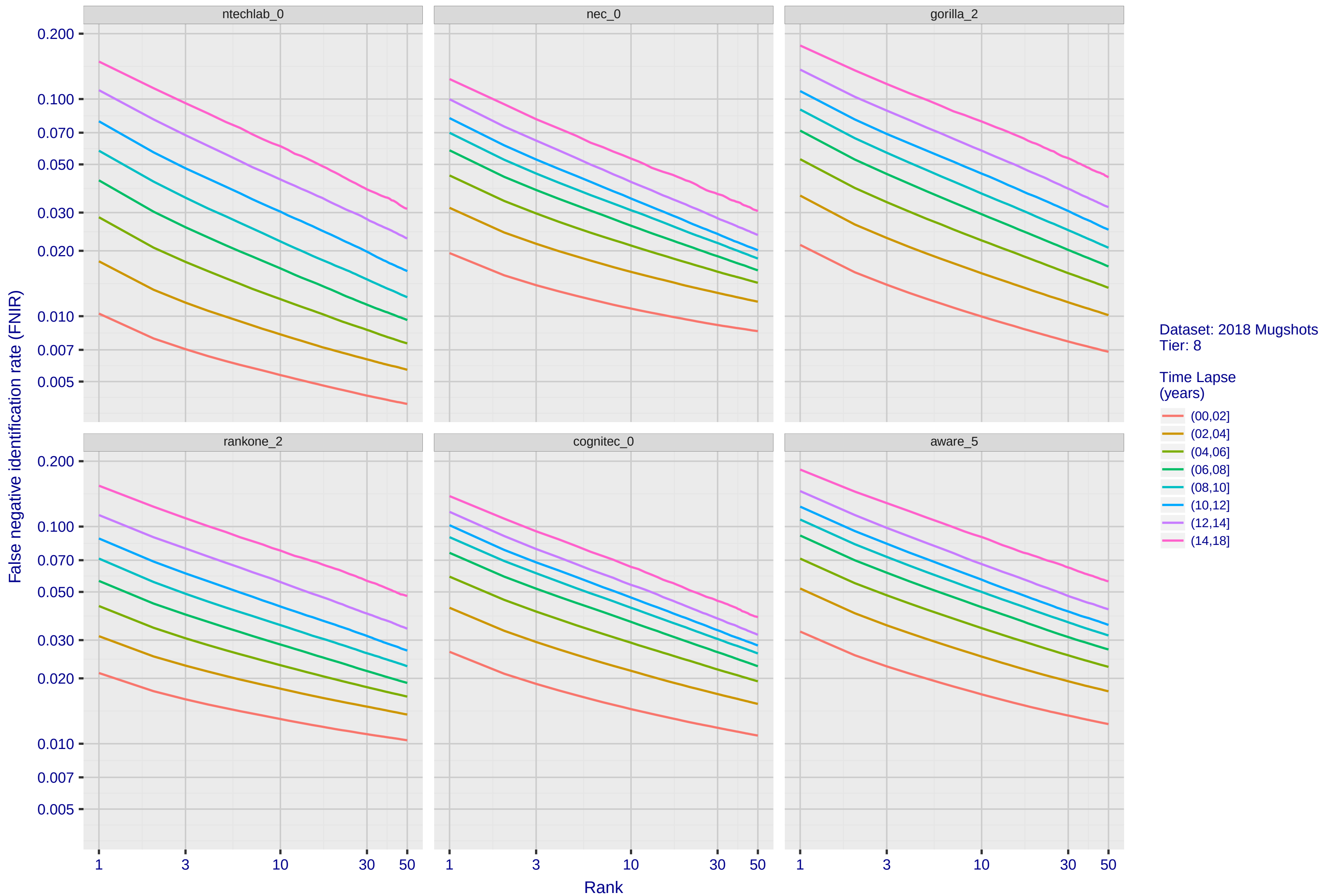

Figure 69: **[FRVT-2018 Mugshot Ageing Dataset] Identification miss rates vs. rank by time-elapsed**. *The oldest image of each individual is enrolled. Thereafter, all more recent images are searched. Miss rates are computed over all searches noted in row 17 of Table 5 and binned by number of years between search and initial enrollment.*

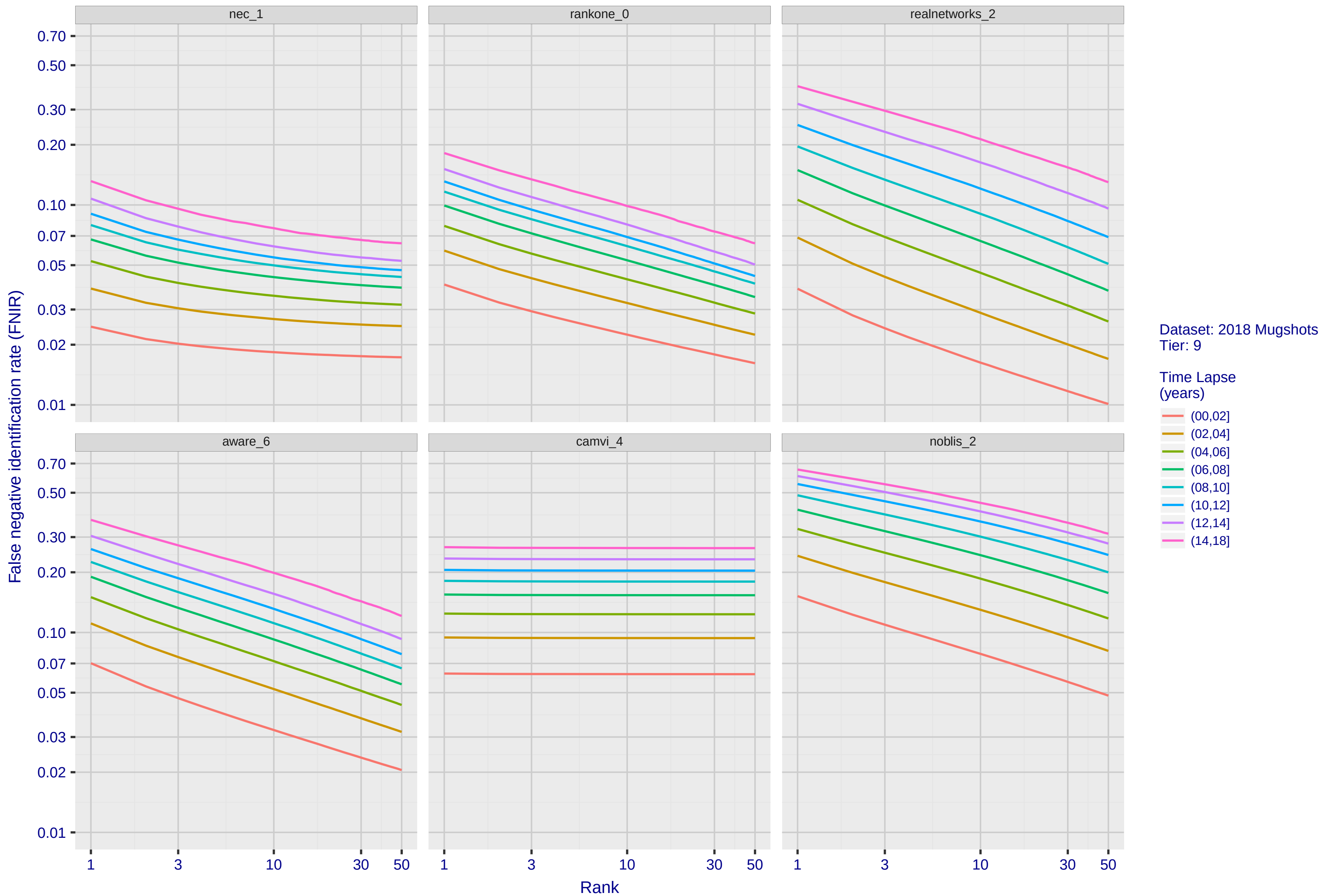

Figure 70: **[FRVT-2018 Mugshot Ageing Dataset] Identification miss rates vs. rank by time-elapsed**. *The oldest image of each individual is enrolled. Thereafter, all more recent images are searched. Miss rates are computed over all searches noted in row 17 of Table 5 and binned by number of years between search and initial enrollment.*

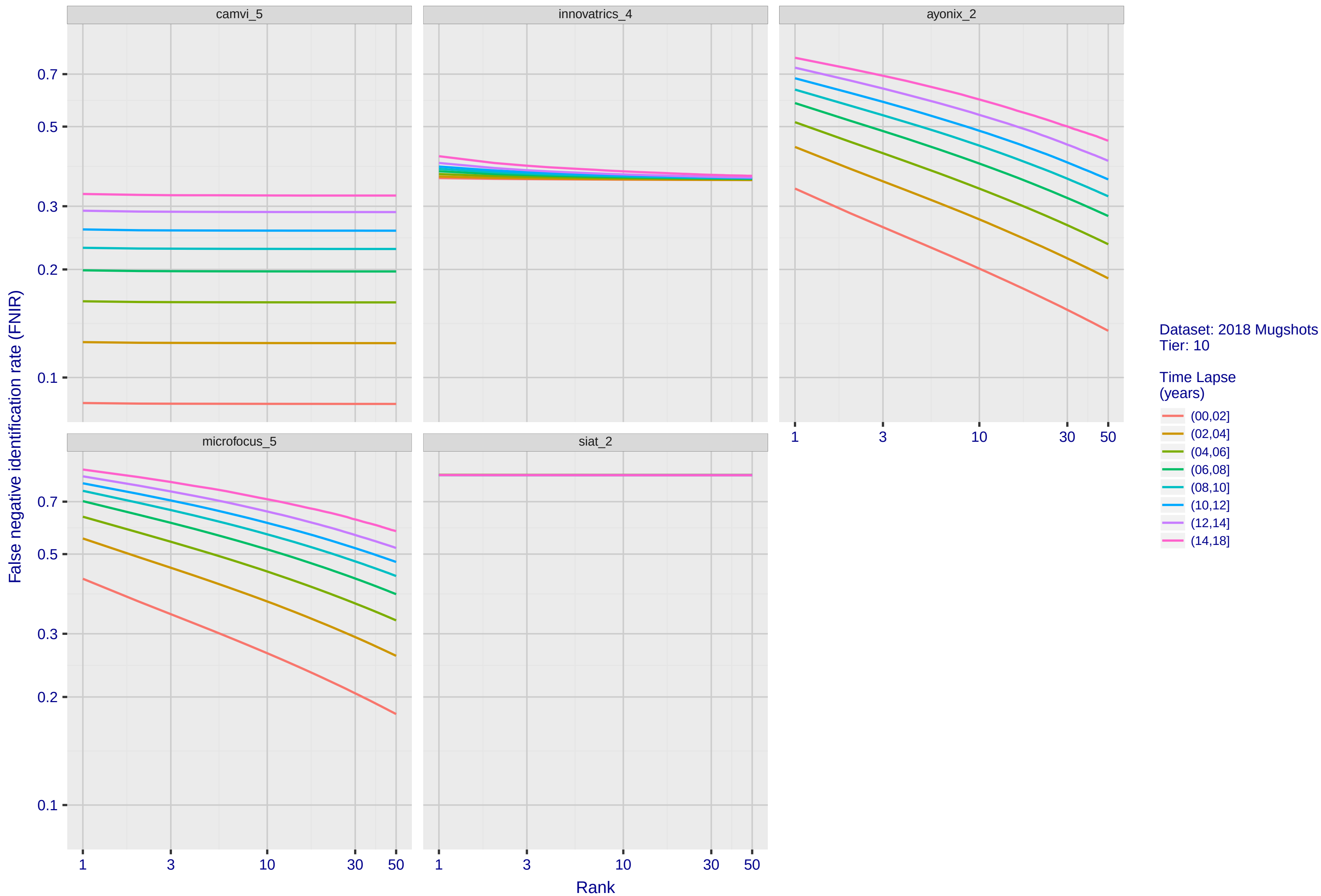

Figure 71: **[FRVT-2018 Mugshot Ageing Dataset] Identification miss rates vs. rank by time-elapsed**. *The oldest image of each individual is enrolled. Thereafter, all more recent images are searched. Miss rates are computed over all searches noted in row 17 of Table 5 and binned by number of years between search and initial enrollment.*

2019/09/11	FNIR(N, R, T) =	False neg. identification rate	N = Num. enrolled subjects	T = Threshold	$T = 0 \rightarrow$ Investigation
16:09:13	FPIR(N, T) =	False pos. identification rate	R = Num. candidates examined		$T > 0 \rightarrow$ Identification

FNIR(N, R, T) = False neg. identification rate
FPIR(N, T) = False pos. identification rate
N = Num. enrolled subjects
R = Num. candidates examined
T = Threshold
T = 0 → Investigation
T > 0 → Identification

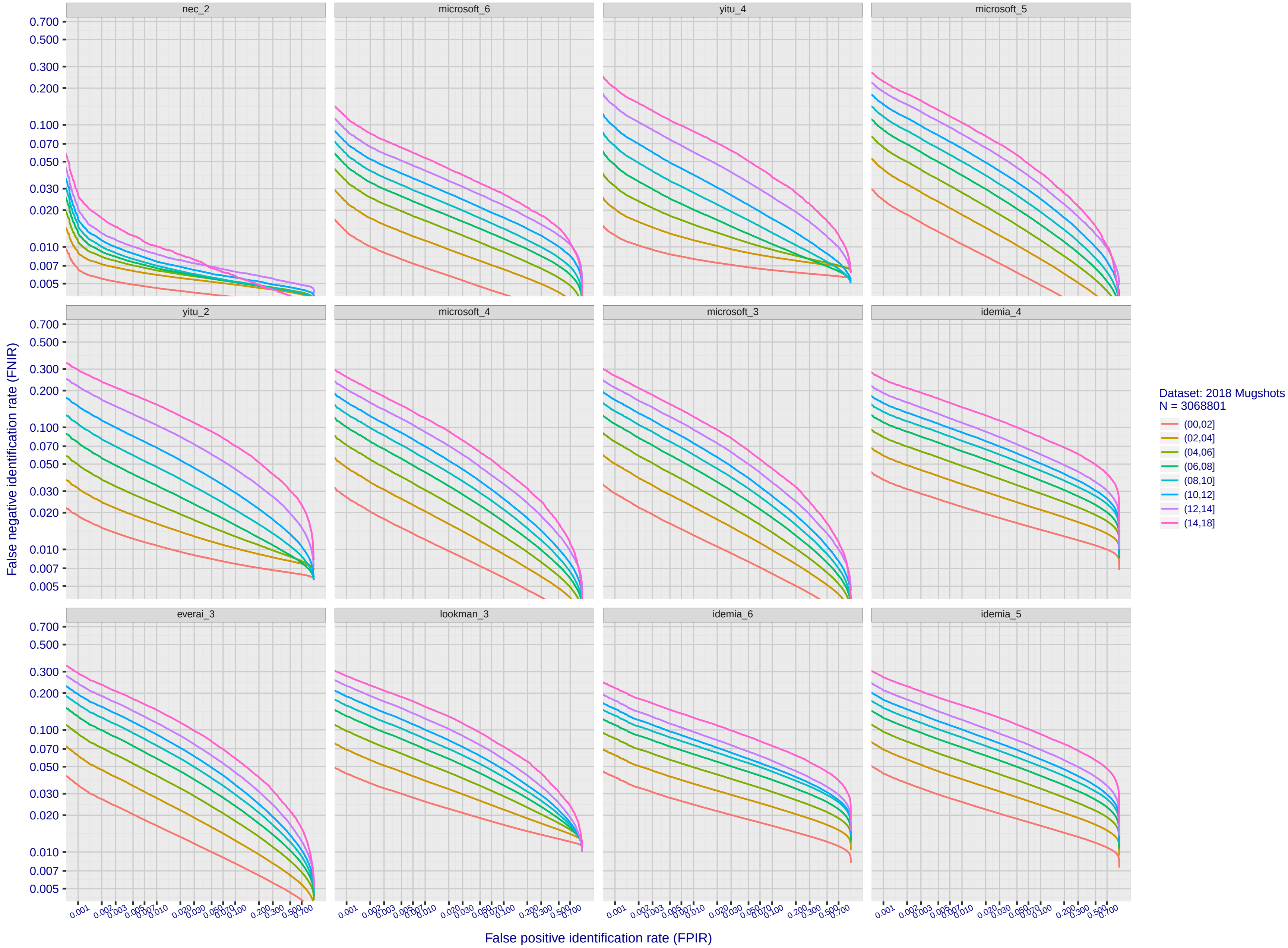

Figure 72: **[FRVT-2018 Mugshot Ageing Dataset] Identification miss rates vs. FPIR by time-elapsed**. *The oldest image of each individual is enrolled. Thereafter, all more recent images are searched. Miss rates are computed over all searches noted in row 17 of Table 5 and binned by number of years between search and initial enrollment. FPIR is computed from the same FRVT 2018 non-mates noted in row 3 of Table 5 with N = 3 000 000.*

FNIR(N, R, T) = False neg. identification rate
FPIR(N, T) = False pos. identification rate
N = Num. enrolled subjects
R = Num. candidates examined
T = Threshold
T = 0 → Investigation
T > 0 → Identification

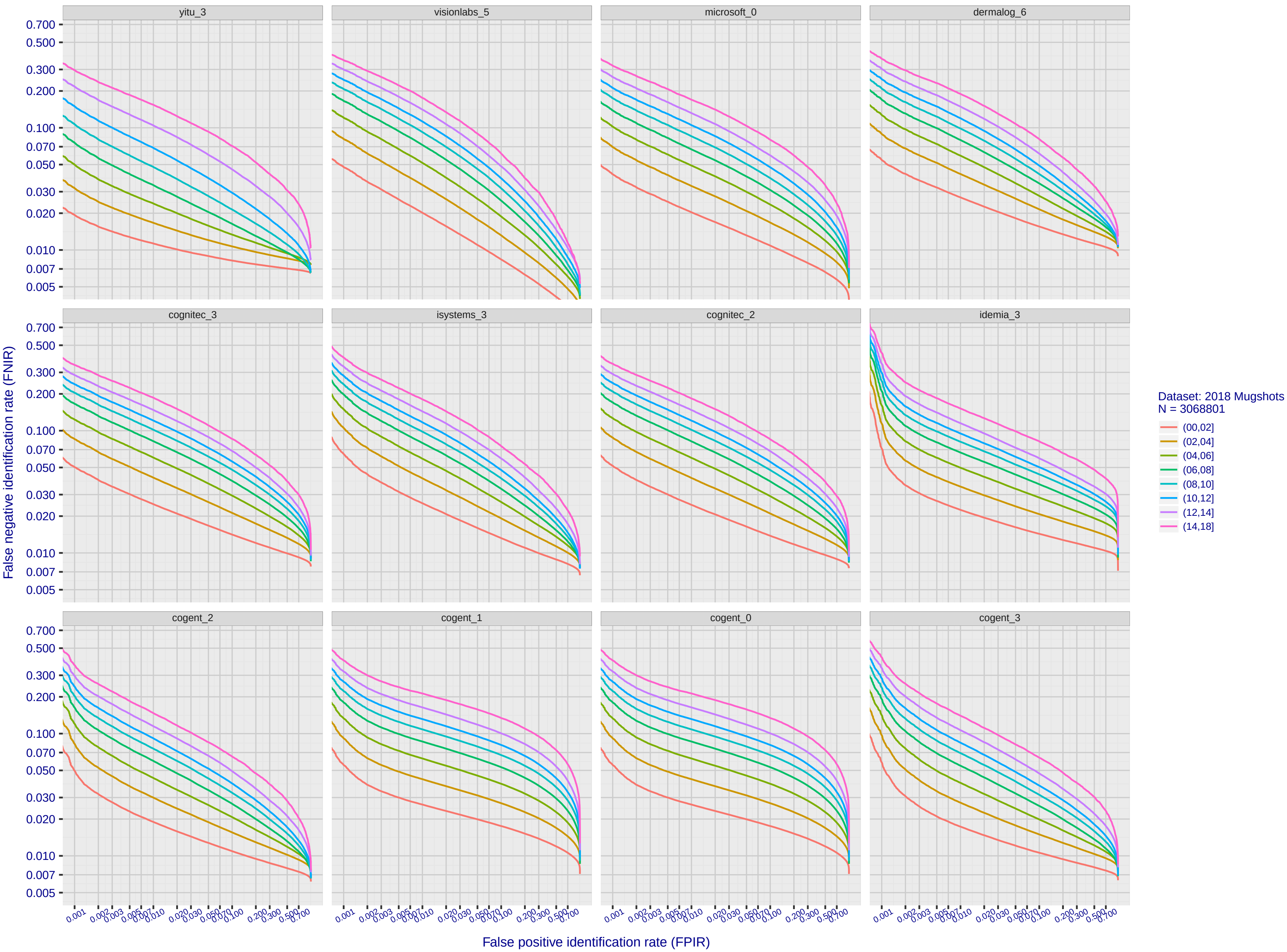

Figure 73: **[FRVT-2018 Mugshot Ageing Dataset] Identification miss rates vs. FPIR by time-elapsed**. *The oldest image of each individual is enrolled. Thereafter, all more recent images are searched. Miss rates are computed over all searches noted in row 17 of Table 5 and binned by number of years between search and initial enrollment. FPIR is computed from the same FRVT 2018 non-mates noted in row 3 of Table 5 with N = 3 000 000.*

FNIR(N, R, T) = False neg. identification rate
FPIR(N, T) = False pos. identification rate
N = Num. enrolled subjects
R = Num. candidates examined
T = Threshold
T = 0 → Investigation
T > 0 → Identification

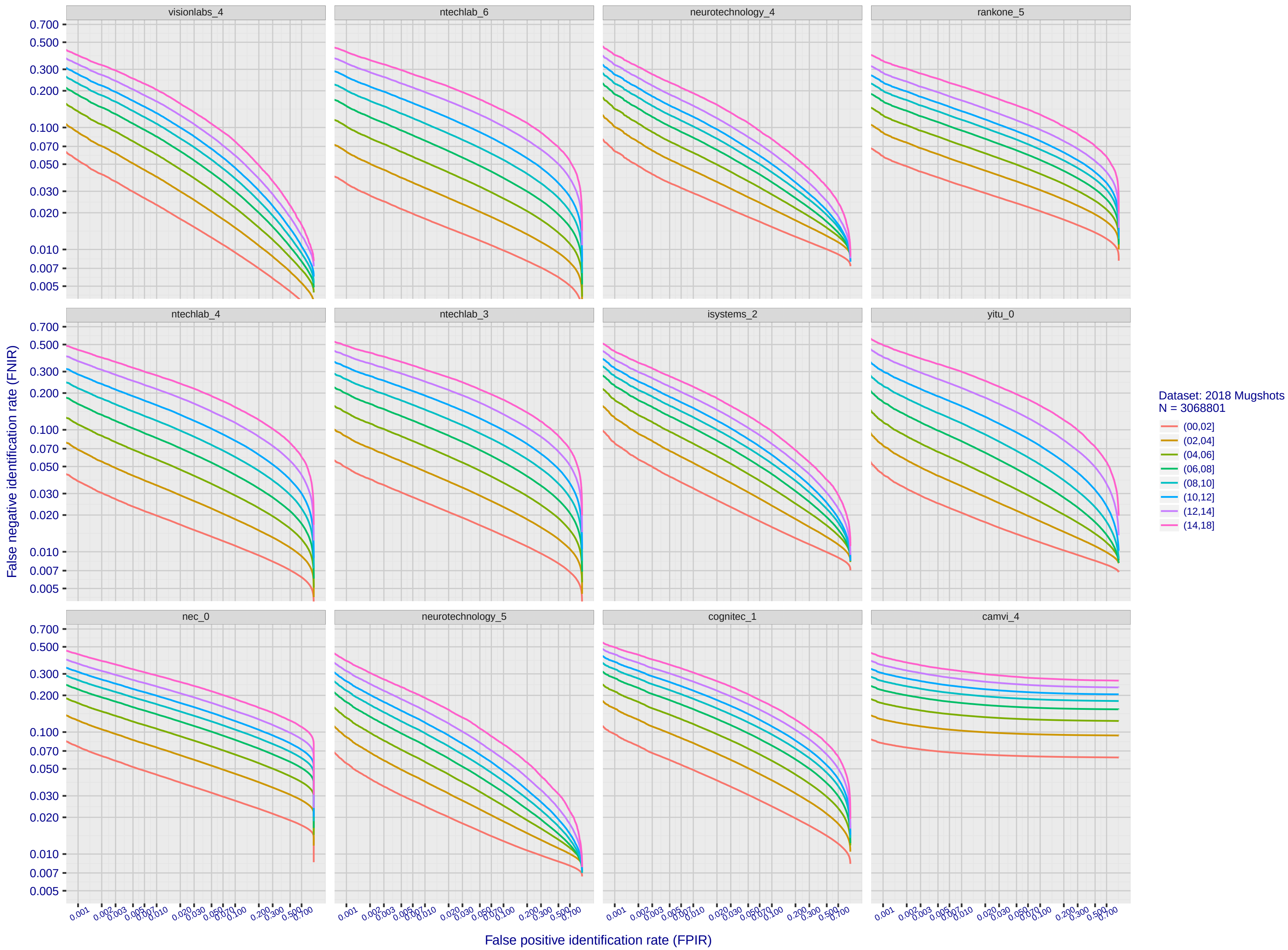

Figure 74: **[FRVT-2018 Mugshot Ageing Dataset] Identification miss rates vs. FPIR by time-elapsed**. *The oldest image of each individual is enrolled. Thereafter, all more recent images are searched. Miss rates are computed over all searches noted in row 17 of Table 5 and binned by number of years between search and initial enrollment. FPIR is computed from the same FRVT 2018 non-mates noted in row 3 of Table 5 with N = 3 000 000.*

2019/09/11
16:09:13

FNIR(N, R, T) = False neg. identification rate
FPIR(N, T) = False pos. identification rate
N = Num. enrolled subjects
R = Num. candidates examined
T = Threshold
T = 0 → Investigation
T > 0 → Identification

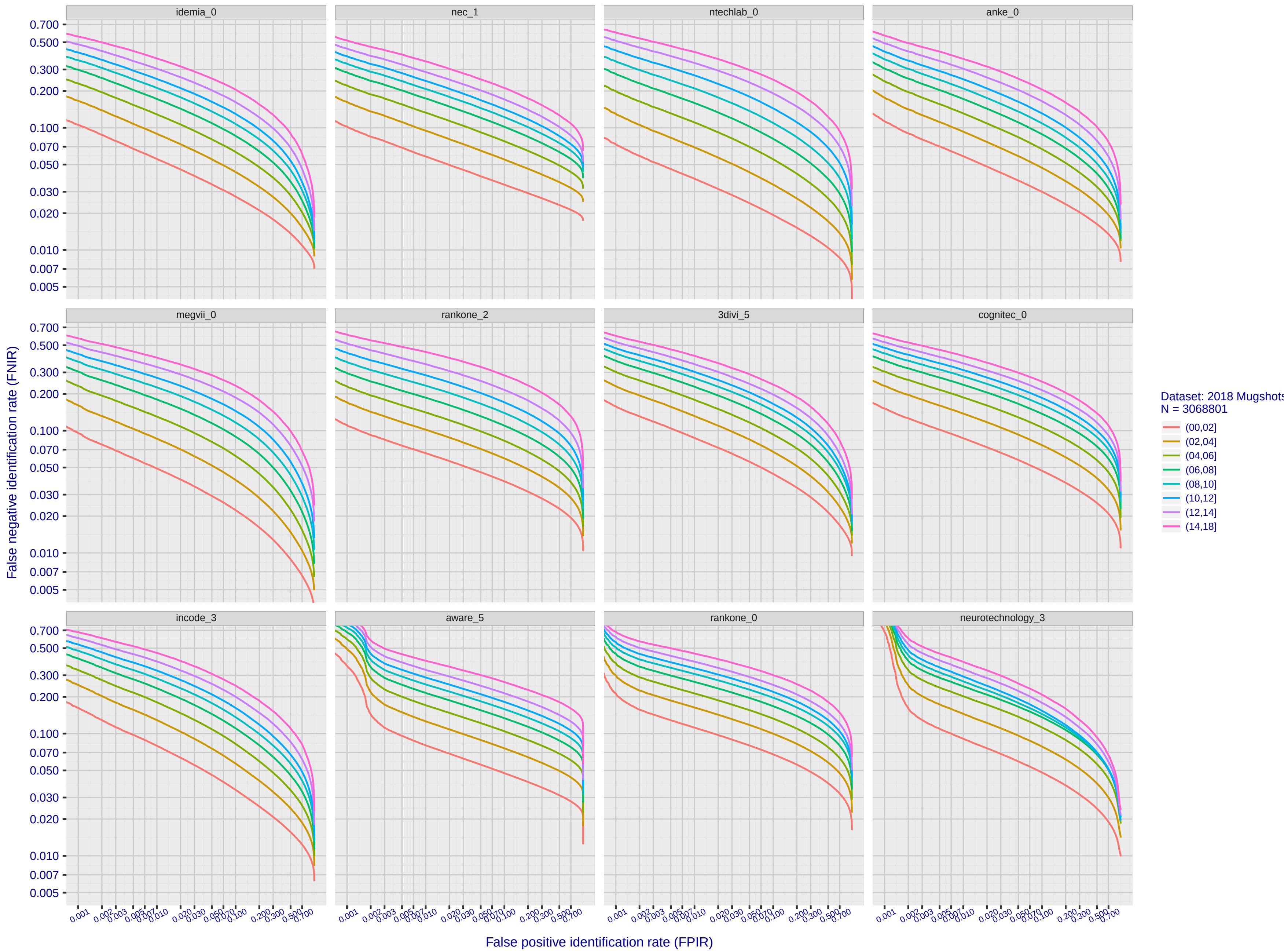

Figure 75: **[FRVT-2018 Mugshot Ageing Dataset] Identification miss rates vs. FPIR by time-elapsed**. *The oldest image of each individual is enrolled. Thereafter, all more recent images are searched. Miss rates are computed over all searches noted in row 17 of Table 5 and binned by number of years between search and initial enrollment. FPIR is computed from the same FRVT 2018 non-mates noted in row 3 of Table 5 with N = 3 000 000.*

FNIR(N, R, T) = False neg. identification rate
FPIR(N, T) = False pos. identification rate
N = Num. enrolled subjects
R = Num. candidates examined
T = Threshold
T = 0 → Investigation
T > 0 → Identification

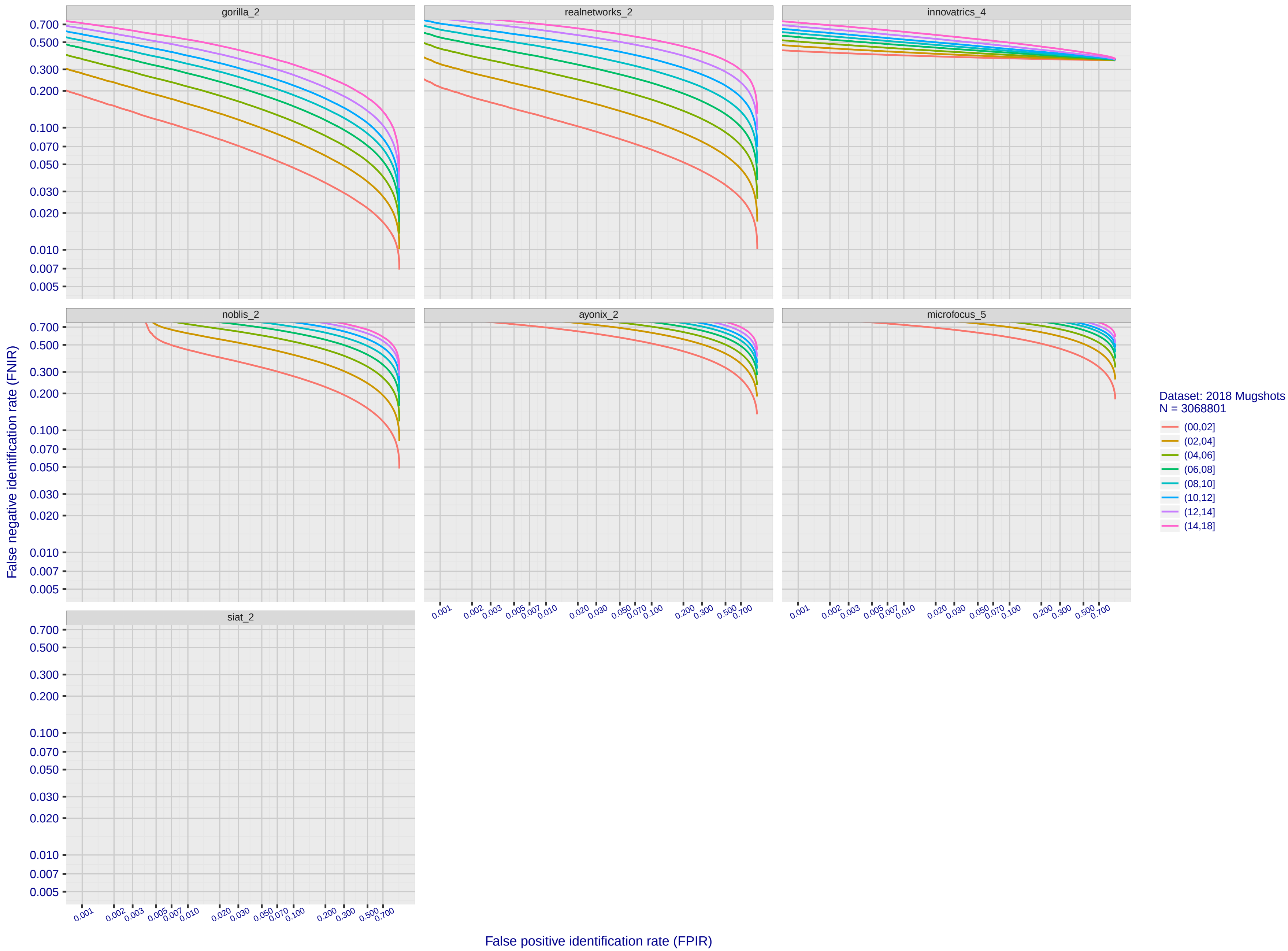

Figure 76: **[FRVT-2018 Mugshot Ageing Dataset] Identification miss rates vs. FPIR by time-elapsed**. *The oldest image of each individual is enrolled. Thereafter, all more recent images are searched. Miss rates are computed over all searches noted in row 17 of Table 5 and binned by number of years between search and initial enrollment. FPIR is computed from the same FRVT 2018 non-mates noted in row 3 of Table 5 with N = 3 000 000.*

2019/09/11	FNIR(N, R, T) =	False neg. identification rate	N = Num. enrolled subjects	T = Threshold	T = 0 → Investigation
16:09:13	FPIR(N, T) =	False pos. identification rate	R = Num. candidates examined		T > 0 → Identification

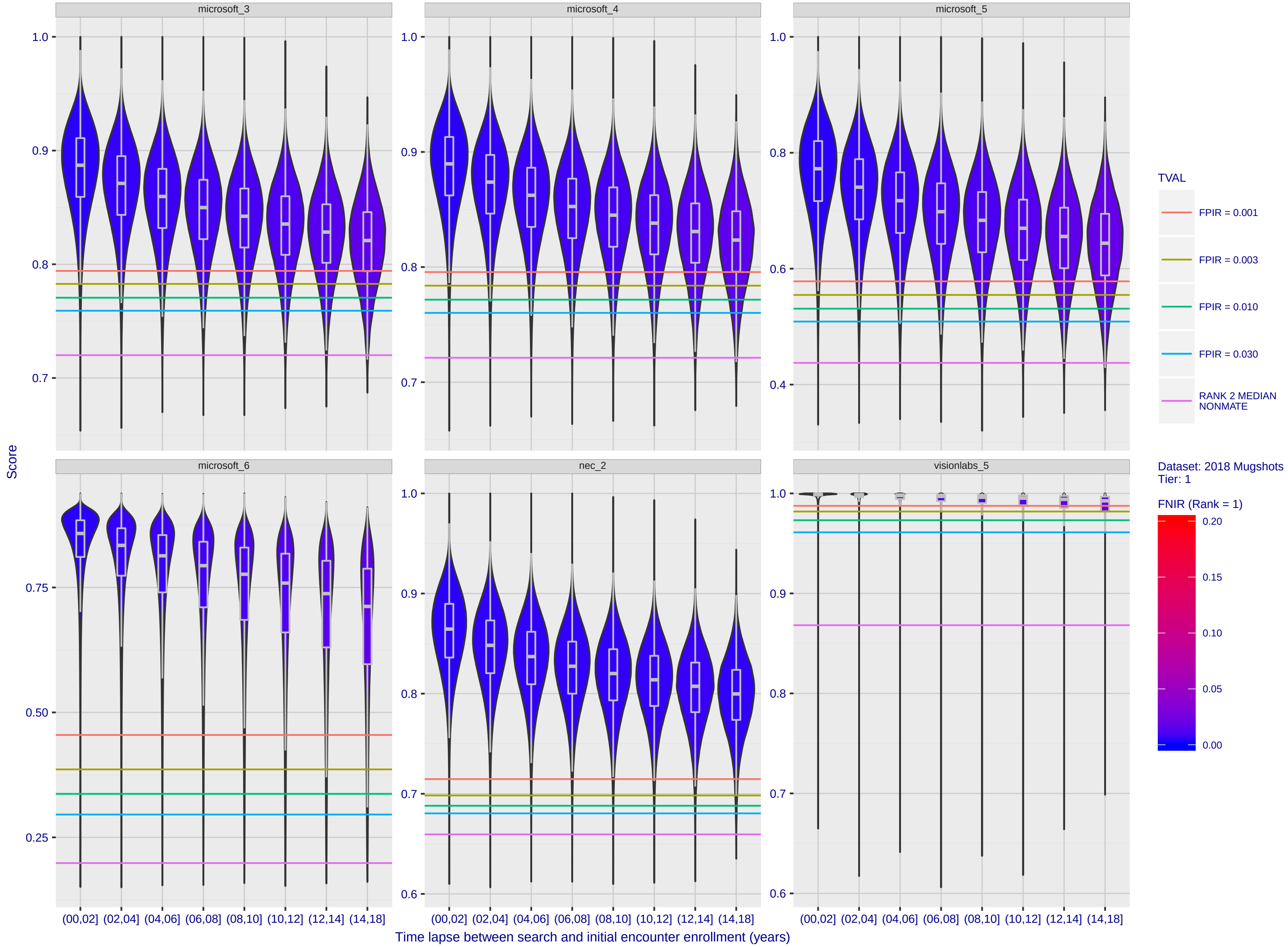

Figure 77: **[FRVT-2018 Mugshot Ageing Dataset] Native mate scores vs. time-elapsed**. *The oldest image of each individual is enrolled. Thereafter, all more recent images are searched. Mated score distributions are computed over all searches noted in row 17 of Table 5 binned by number of years between search and initial enrollment.*

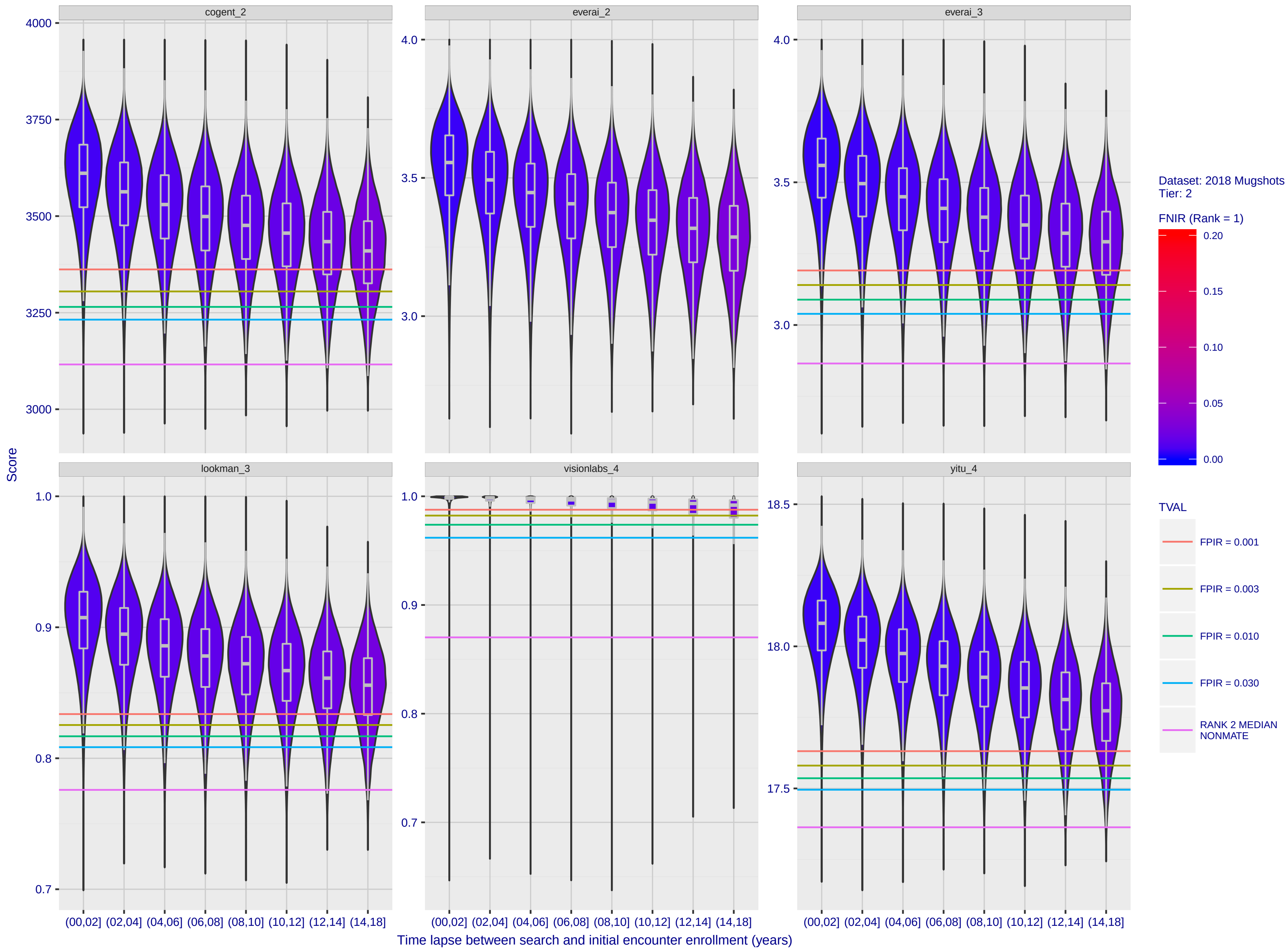

Figure 78: **[FRVT-2018 Mugshot Ageing Dataset] Native mate scores vs. time-elapsed**. *The oldest image of each individual is enrolled. Thereafter, all more recent images are searched. Mated score distributions are computed over all searches noted in row 17 of Table 5 binned by number of years between search and initial enrollment.*

FNIR(N, R, T) = False neg. identification rate
FPIR(N, T) = False pos. identification rate
N = Num. enrolled subjects
R = Num. candidates examined
T = Threshold
T = 0 → Investigation
T > 0 → Identification

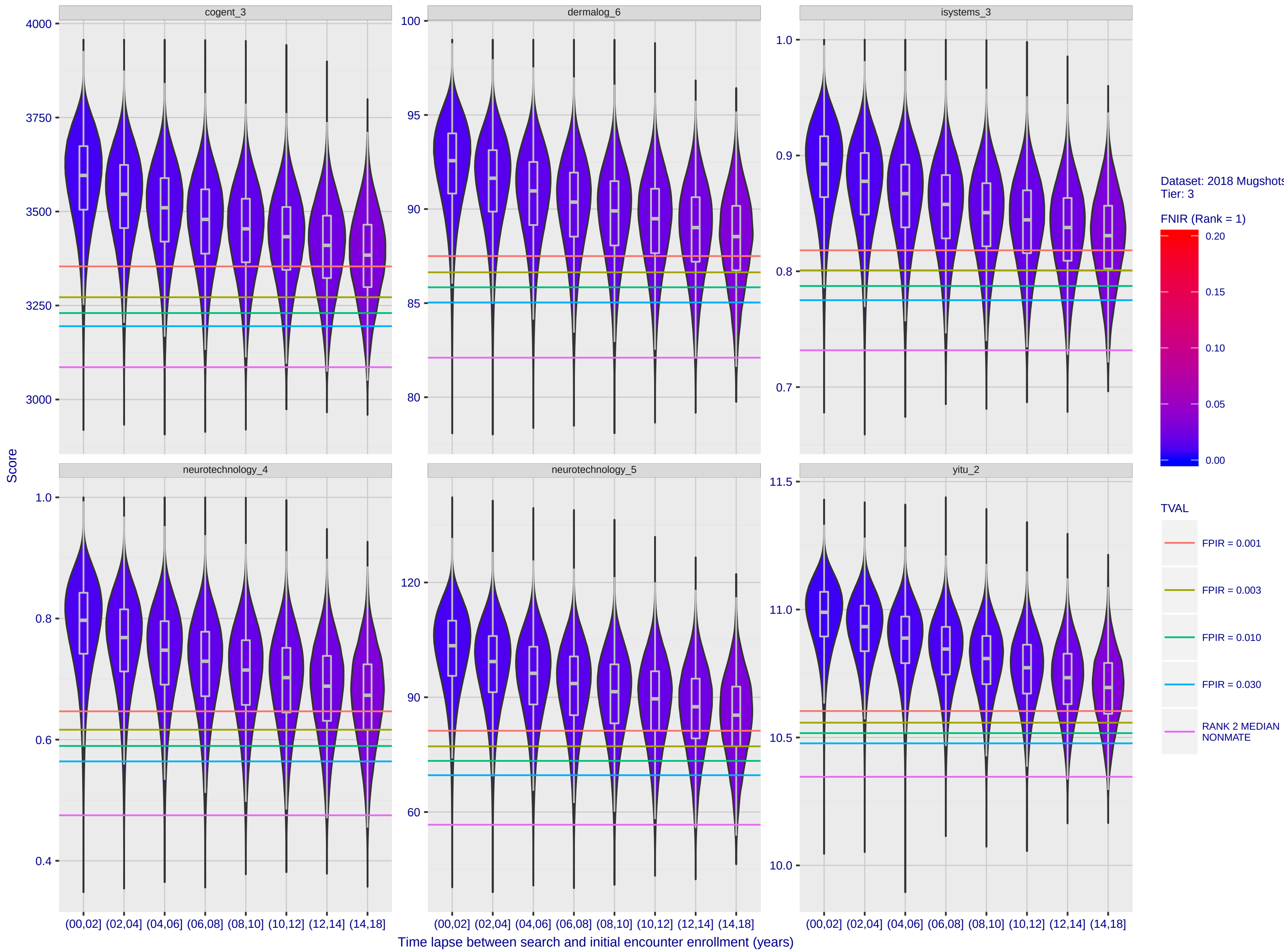

Figure 79: **[FRVT-2018 Mugshot Ageing Dataset] Native mate scores vs. time-elapsed**. *The oldest image of each individual is enrolled. Thereafter, all more recent images are searched. Mated score distributions are computed over all searches noted in row 17 of Table 5 binned by number of years between search and initial enrollment.*

FNIR(N, R, T) = False neg. identification rate
FPIR(N, T) = False pos. identification rate
N = Num. enrolled subjects
R = Num. candidates examined
T = Threshold
T = 0 → Investigation
T > 0 → Identification

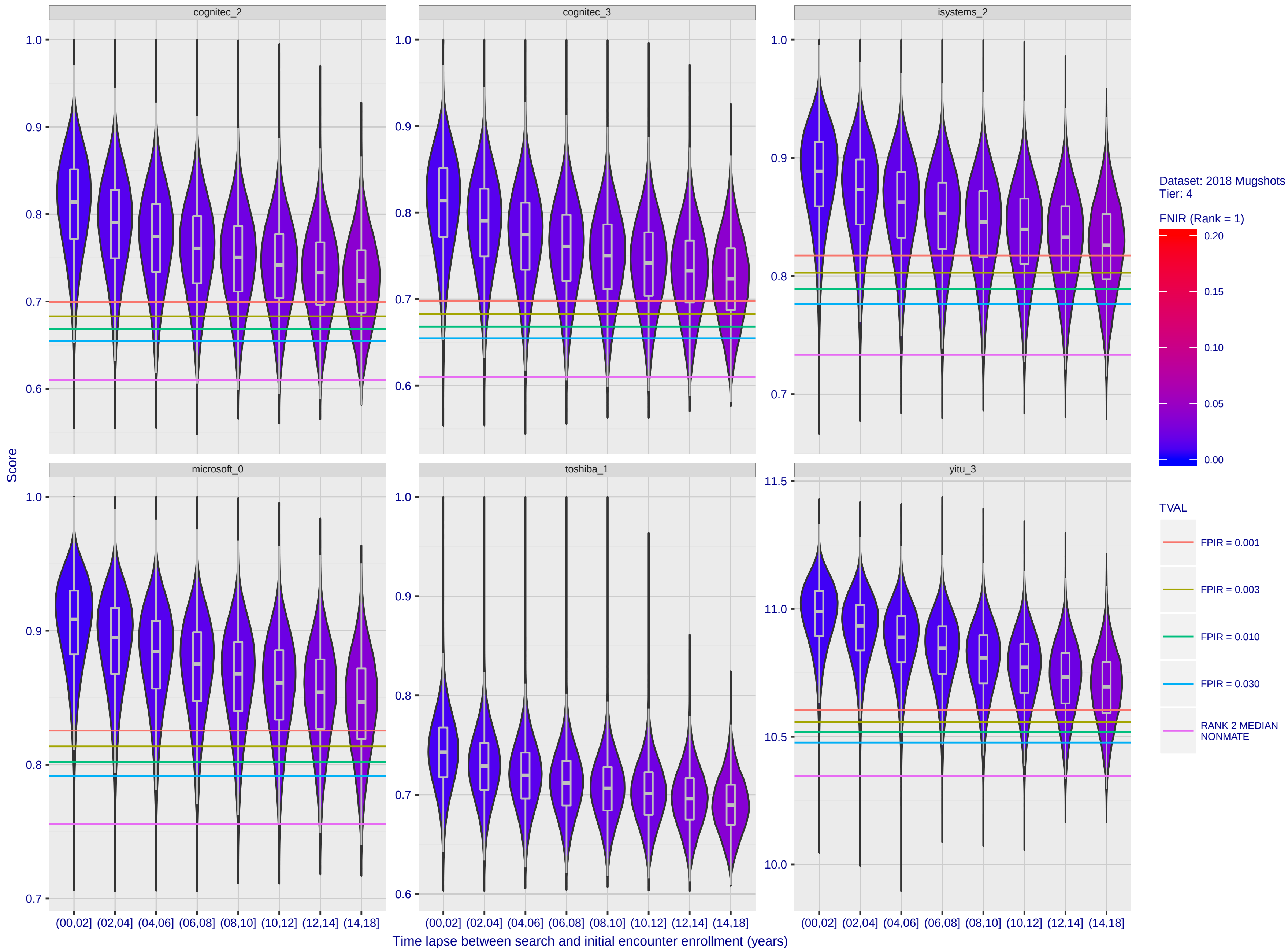

Figure 80: **[FRVT-2018 Mugshot Ageing Dataset] Native mate scores vs. time-elapsed**. *The oldest image of each individual is enrolled. Thereafter, all more recent images are searched. Mated score distributions are computed over all searches noted in row 17 of Table 5 binned by number of years between search and initial enrollment.*

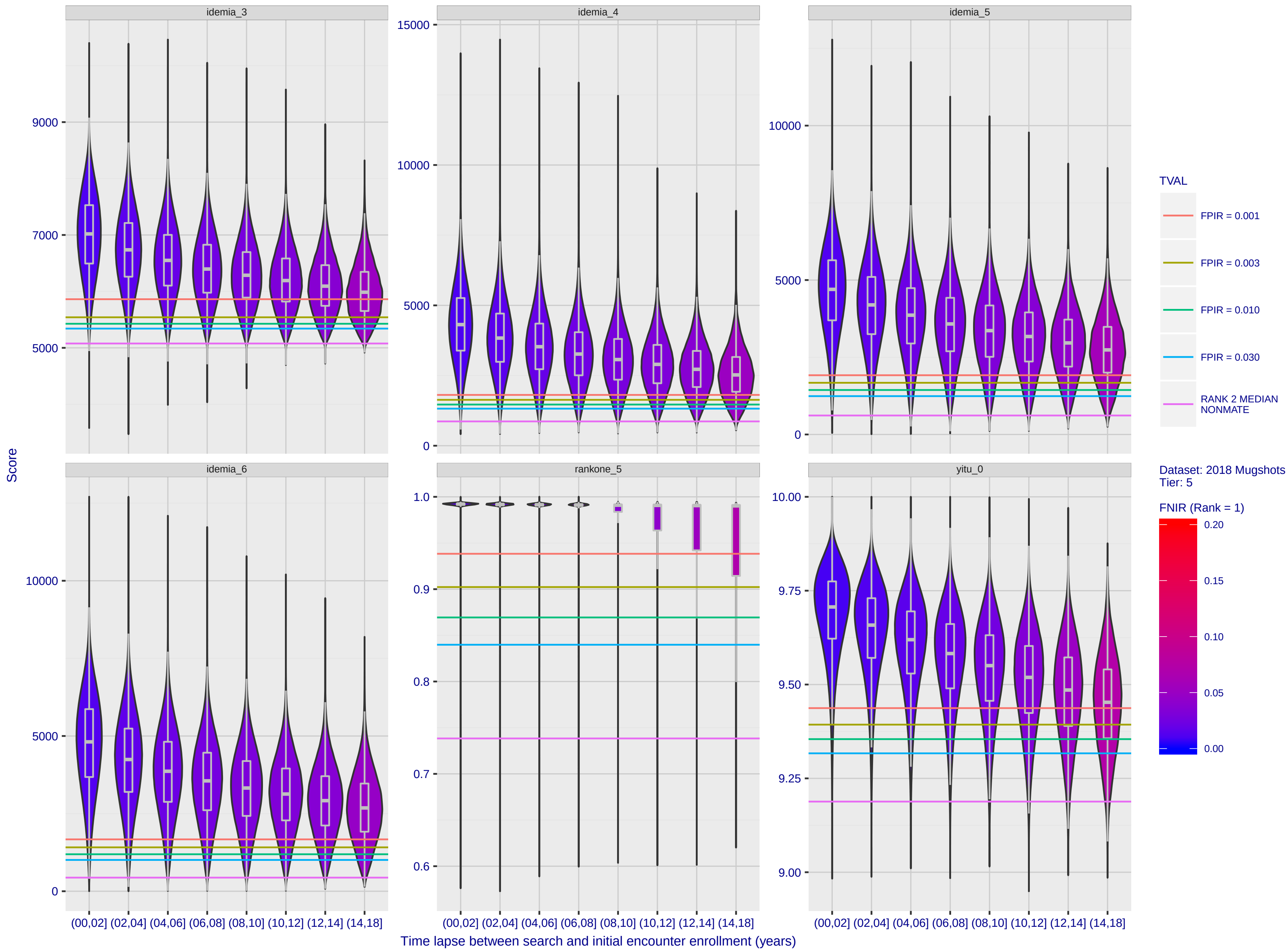

Figure 81: **[FRVT-2018 Mugshot Ageing Dataset] Native mate scores vs. time-elapsed**. *The oldest image of each individual is enrolled. Thereafter, all more recent images are searched. Mated score distributions are computed over all searches noted in row 17 of Table 5 binned by number of years between search and initial enrollment.*

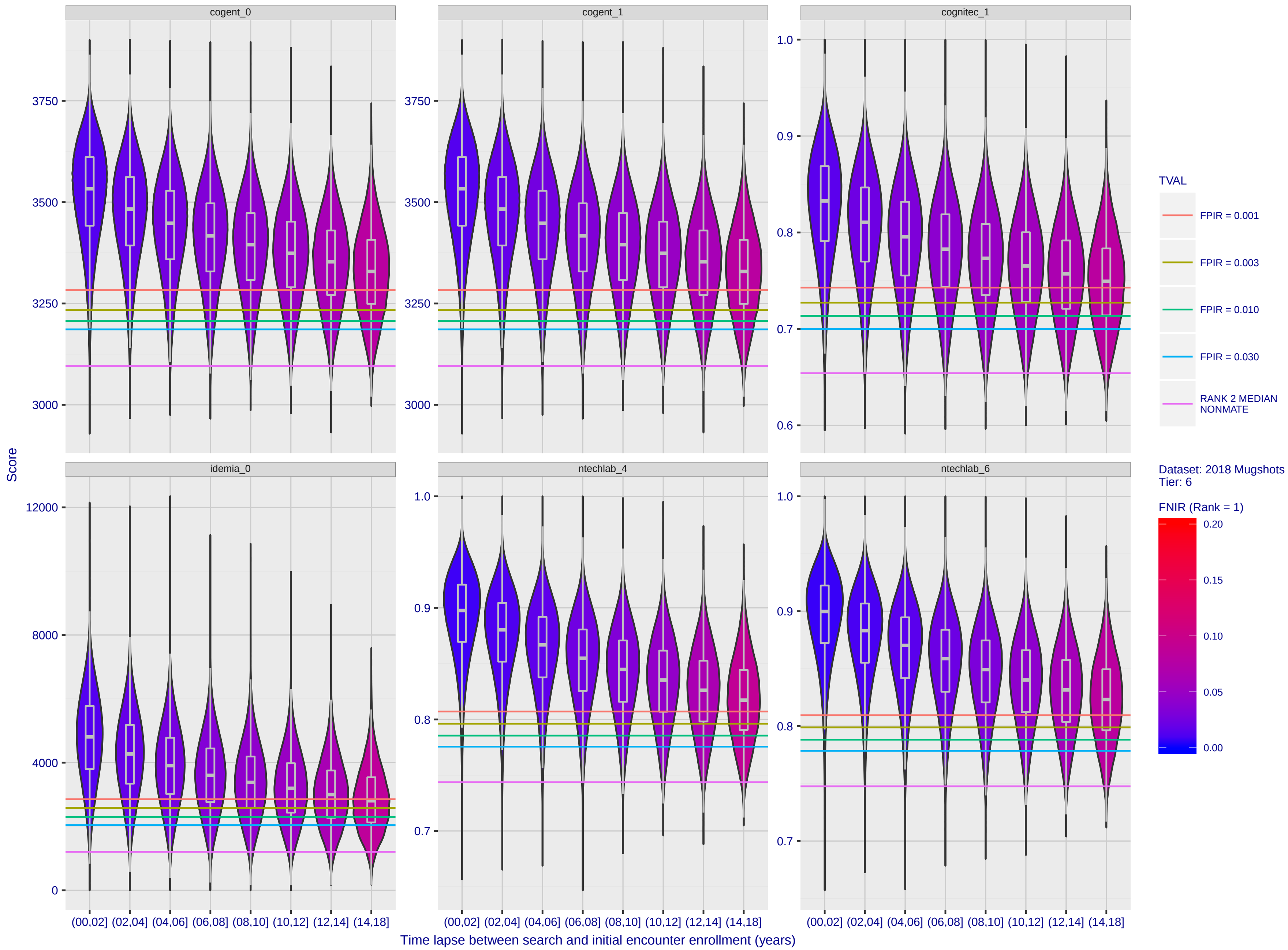

Figure 82: **[FRVT-2018 Mugshot Ageing Dataset] Native mate scores vs. time-elapsed**. *The oldest image of each individual is enrolled. Thereafter, all more recent images are searched. Mated score distributions are computed over all searches noted in row 17 of Table 5 binned by number of years between search and initial enrollment.*

FNIR(N, R, T) = False neg. identification rate
FPIR(N, T) = False pos. identification rate
N = Num. enrolled subjects
R = Num. candidates examined
T = Threshold
T = 0 → Investigation
T > 0 → Identification

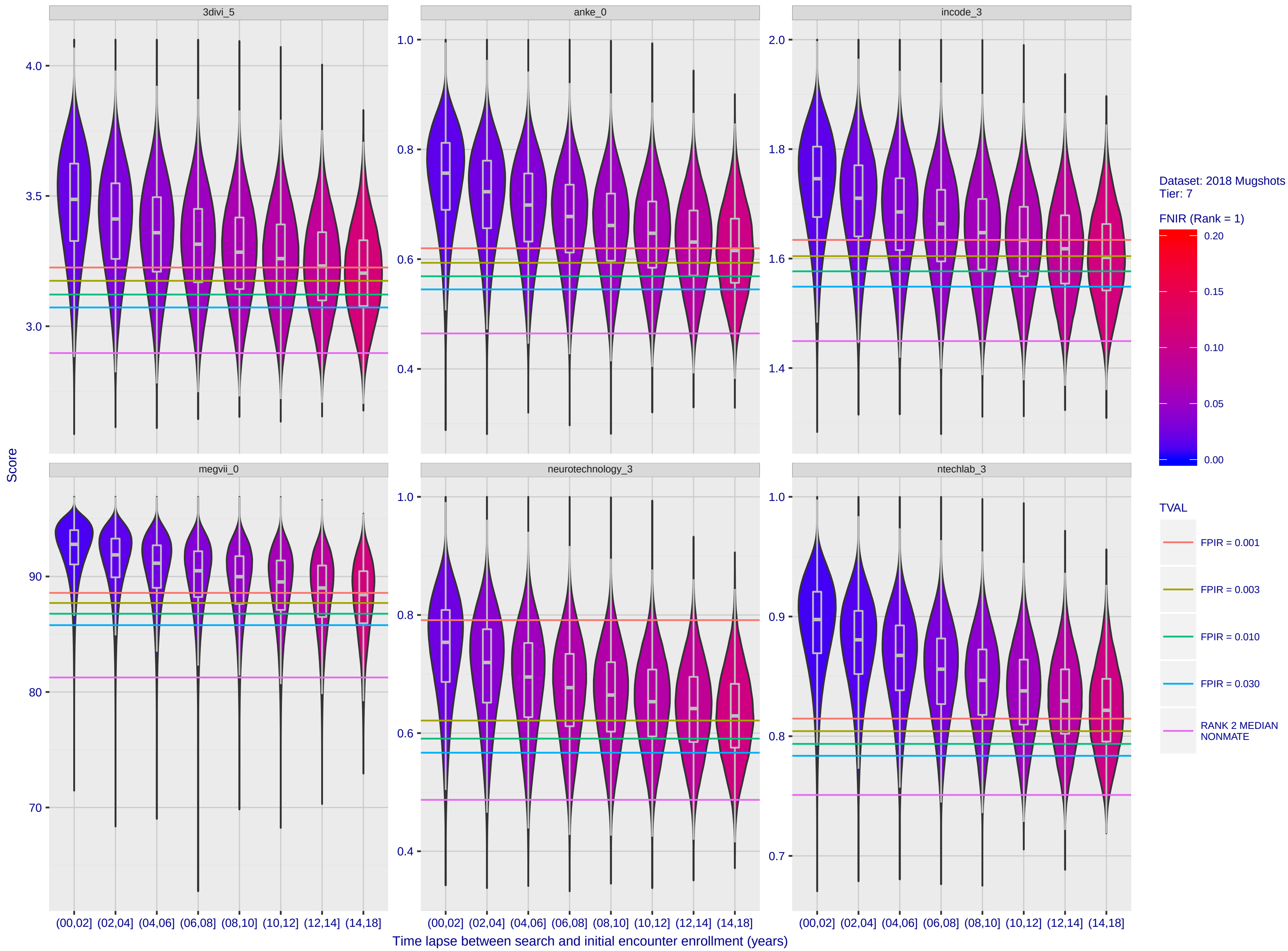

Figure 83: **[FRVT-2018 Mugshot Ageing Dataset] Native mate scores vs. time-elapsed**. *The oldest image of each individual is enrolled. Thereafter, all more recent images are searched. Mated score distributions are computed over all searches noted in row 17 of Table 5 binned by number of years between search and initial enrollment.*

This publication is available free of charge from: https://doi.org/10.6028/NIST.IR.8271

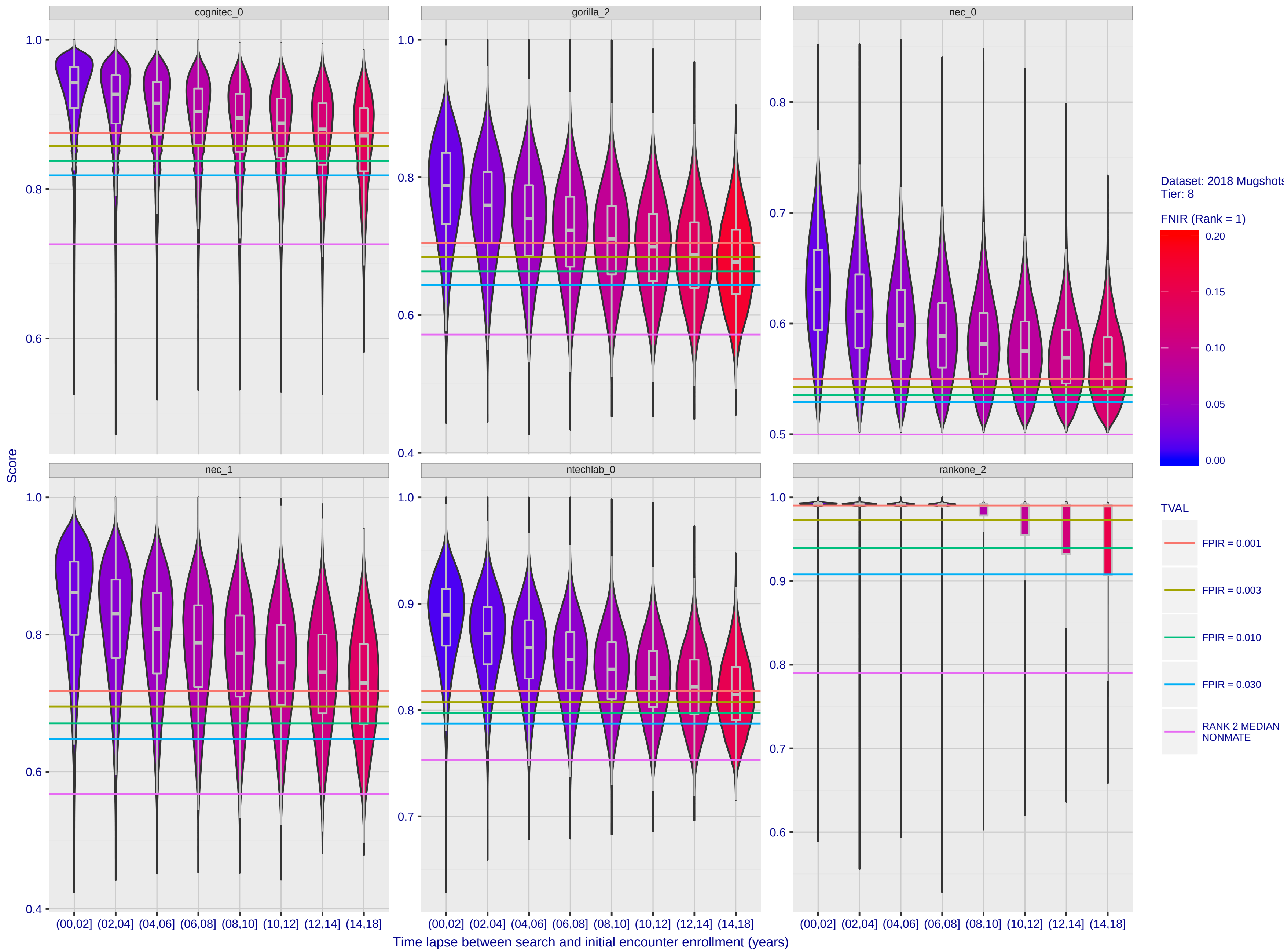

Figure 84: **[FRVT-2018 Mugshot Ageing Dataset] Native mate scores vs. time-elapsed**. *The oldest image of each individual is enrolled. Thereafter, all more recent images are searched. Mated score distributions are computed over all searches noted in row 17 of Table 5 binned by number of years between search and initial enrollment.*

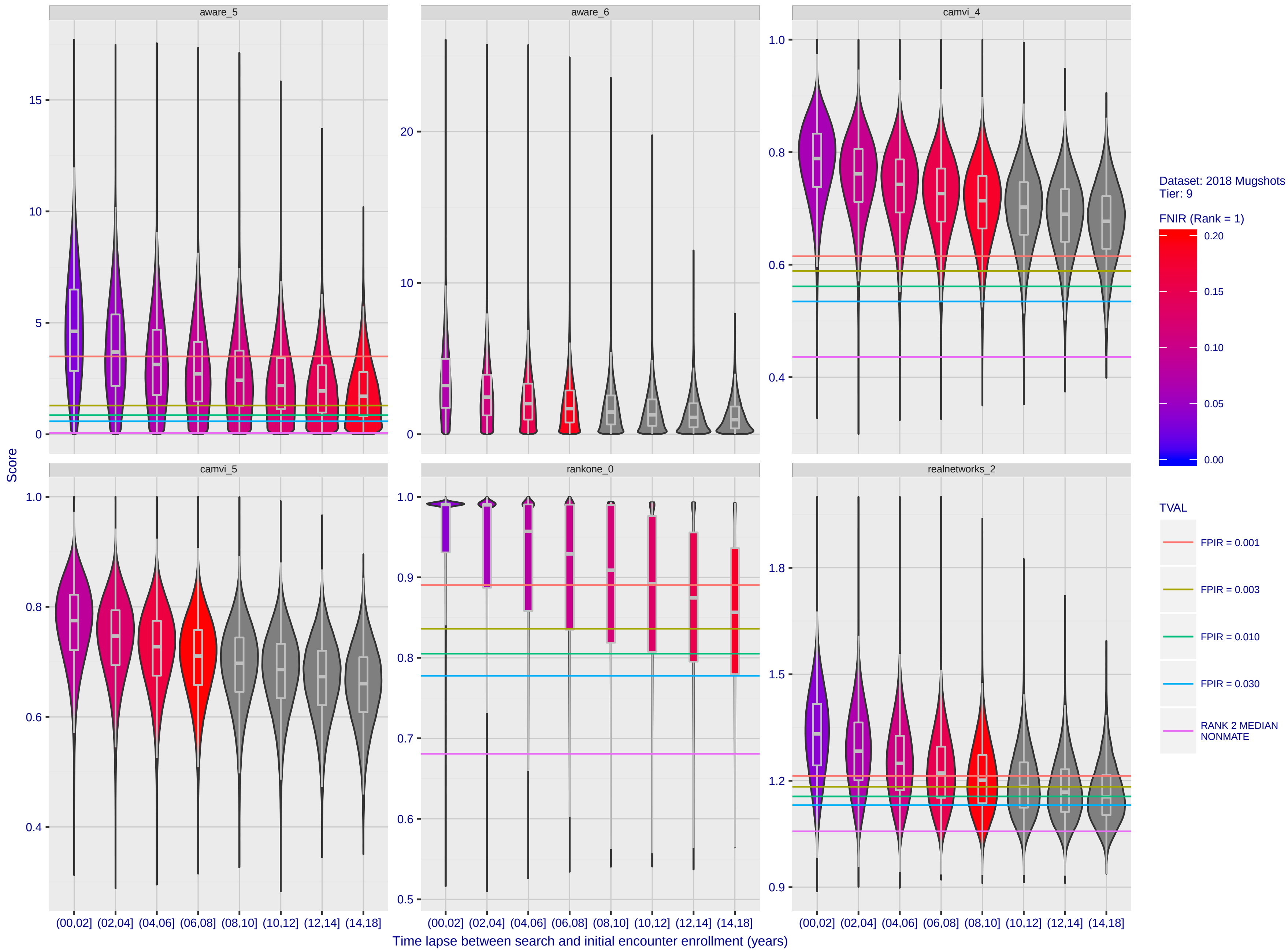

Figure 85: **[FRVT-2018 Mugshot Ageing Dataset] Native mate scores vs. time-elapsed**. *The oldest image of each individual is enrolled. Thereafter, all more recent images are searched. Mated score distributions are computed over all searches noted in row 17 of Table 5 binned by number of years between search and initial enrollment.*

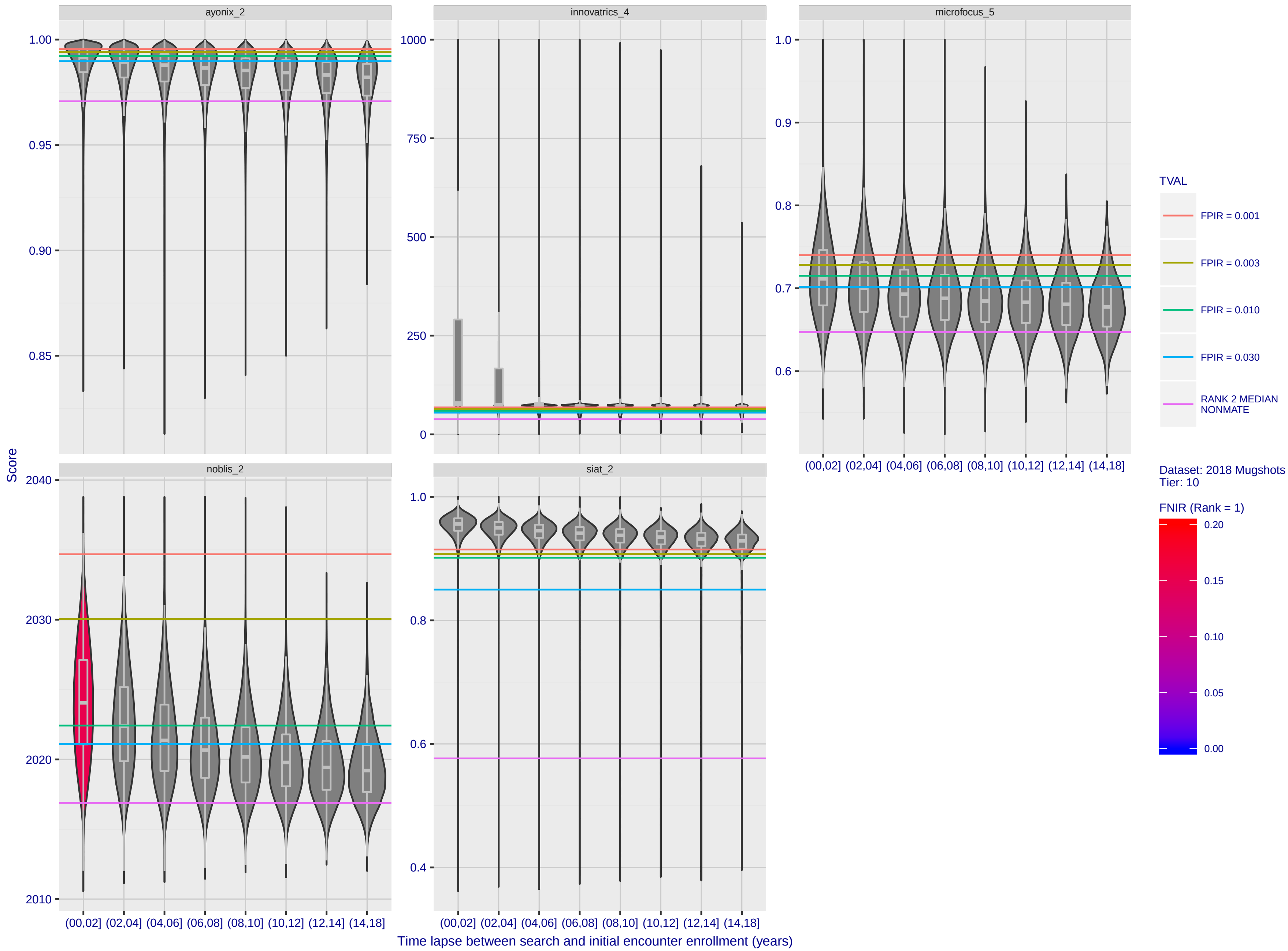

Figure 86: **[FRVT-2018 Mugshot Ageing Dataset] Native mate scores vs. time-elapsed**. *The oldest image of each individual is enrolled. Thereafter, all more recent images are searched. Mated score distributions are computed over all searches noted in row 17 of Table 5 binned by number of years between search and initial enrollment.*

Appendix C Effect of enrolling multiple images

FNIR(N, R, T) = False neg. identification rate
FPIR(N, T) = False pos. identification rate
N = Num. enrolled subjects
R = Num. candidates examined
T = Threshold
T = 0 → Investigation
T > 0 → Identification

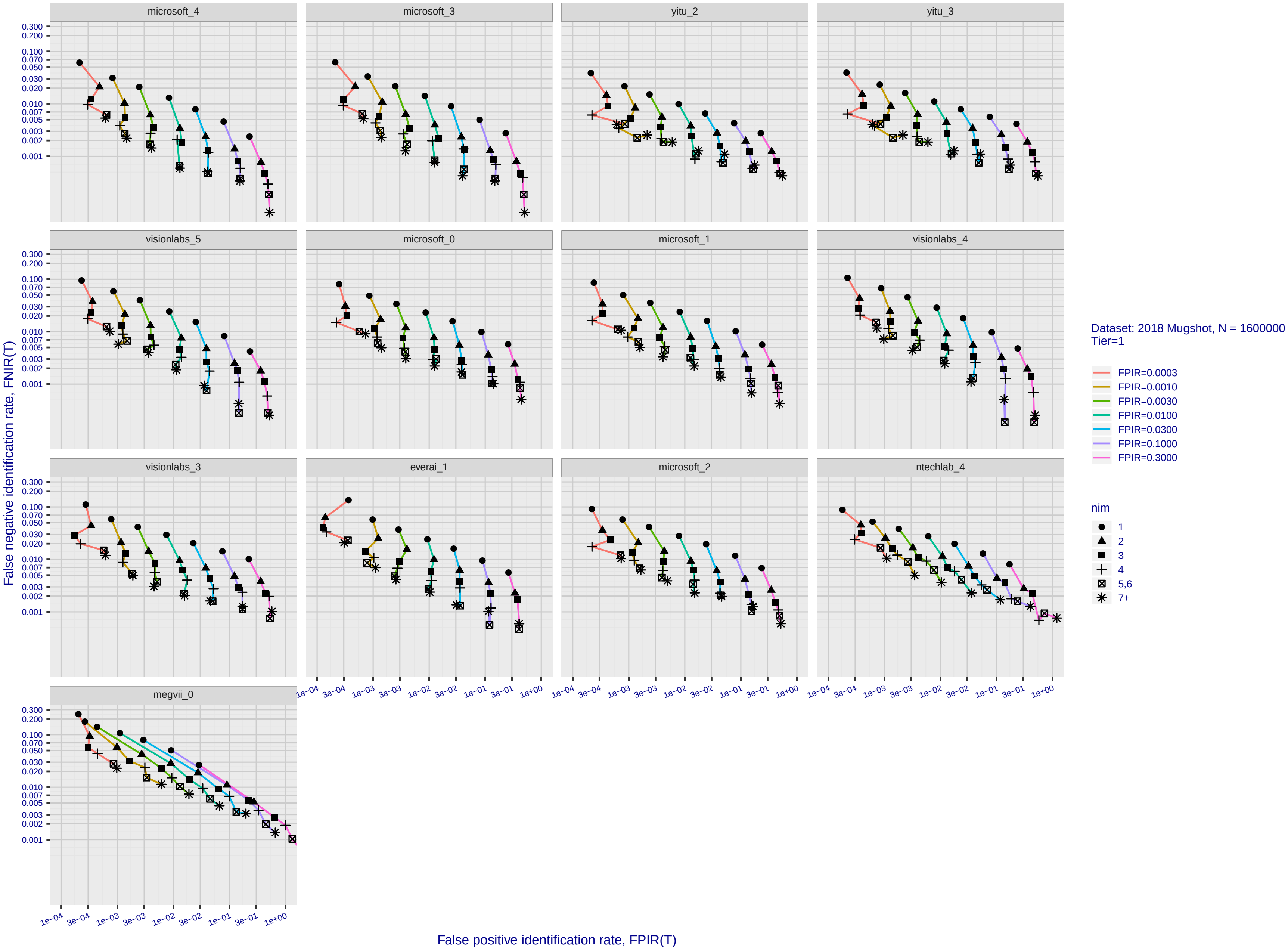

Figure 87: **[FRVT-2018 Mugshot Dataset] Effect of enrolling multiple images for each identity**. *The plot shows an identification miss rates vs. false positive rates, at seven operating thresholds. The enrolled population size is fixed. The images are enrolled with lifetime-consolidation - see section 2.3.*

2019/09/11
16:09:13

FNIR(N, R, T) = False neg. identification rate
FPIR(N, T) = False pos. identification rate

N = Num. enrolled subjects
R = Num. candidates examined

T = Threshold

T = 0 → Investigation
T > 0 → Identification

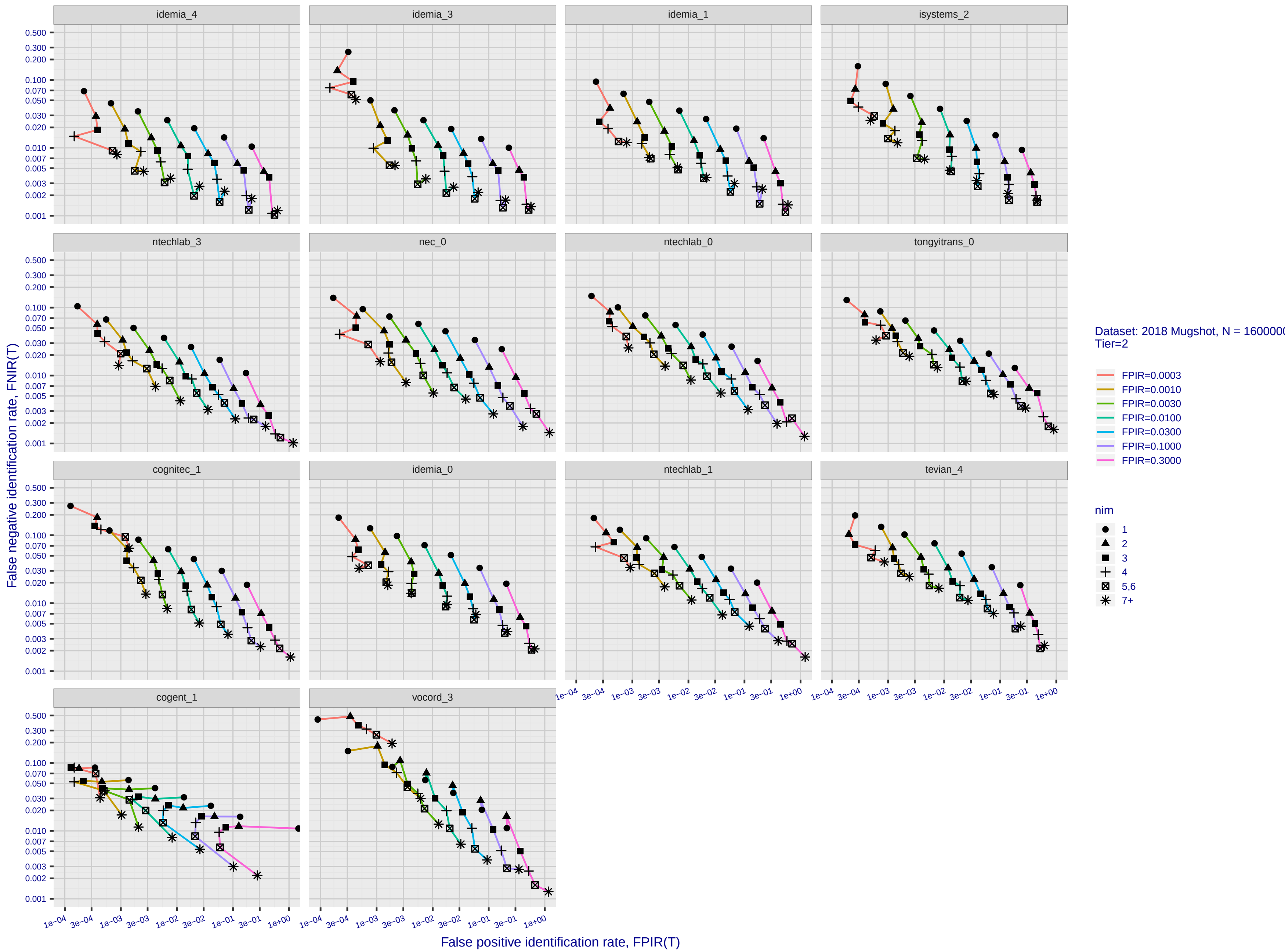

Figure 88: **[FRVT-2018 Mugshot Dataset] Effect of enrolling multiple images for each identity**. *The plot shows an identification miss rates vs. false positive rates, at seven operating thresholds. The enrolled population size is fixed. The images are enrolled with lifetime-consolidation - see section 2.3.*

FNIR(N, R, T) = False neg. identification rate
FPIR(N, T) = False pos. identification rate
N = Num. enrolled subjects
R = Num. candidates examined
T = Threshold
T = 0 → Investigation
T > 0 → Identification

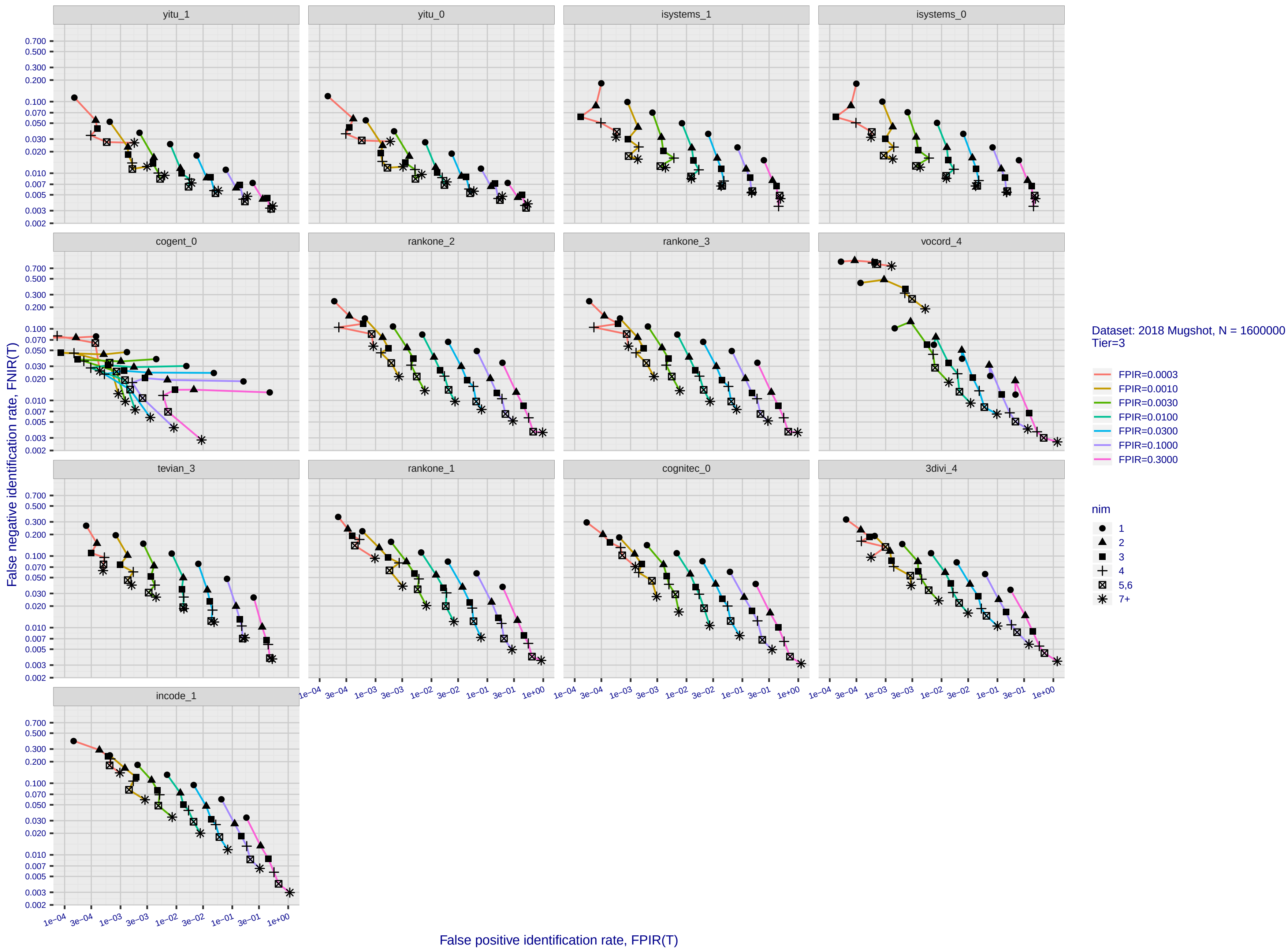

Figure 89: **[FRVT-2018 Mugshot Dataset] Effect of enrolling multiple images for each identity**. *The plot shows an identification miss rates vs. false positive rates, at seven operating thresholds. The enrolled population size is fixed. The images are enrolled with lifetime-consolidation - see section 2.3.*

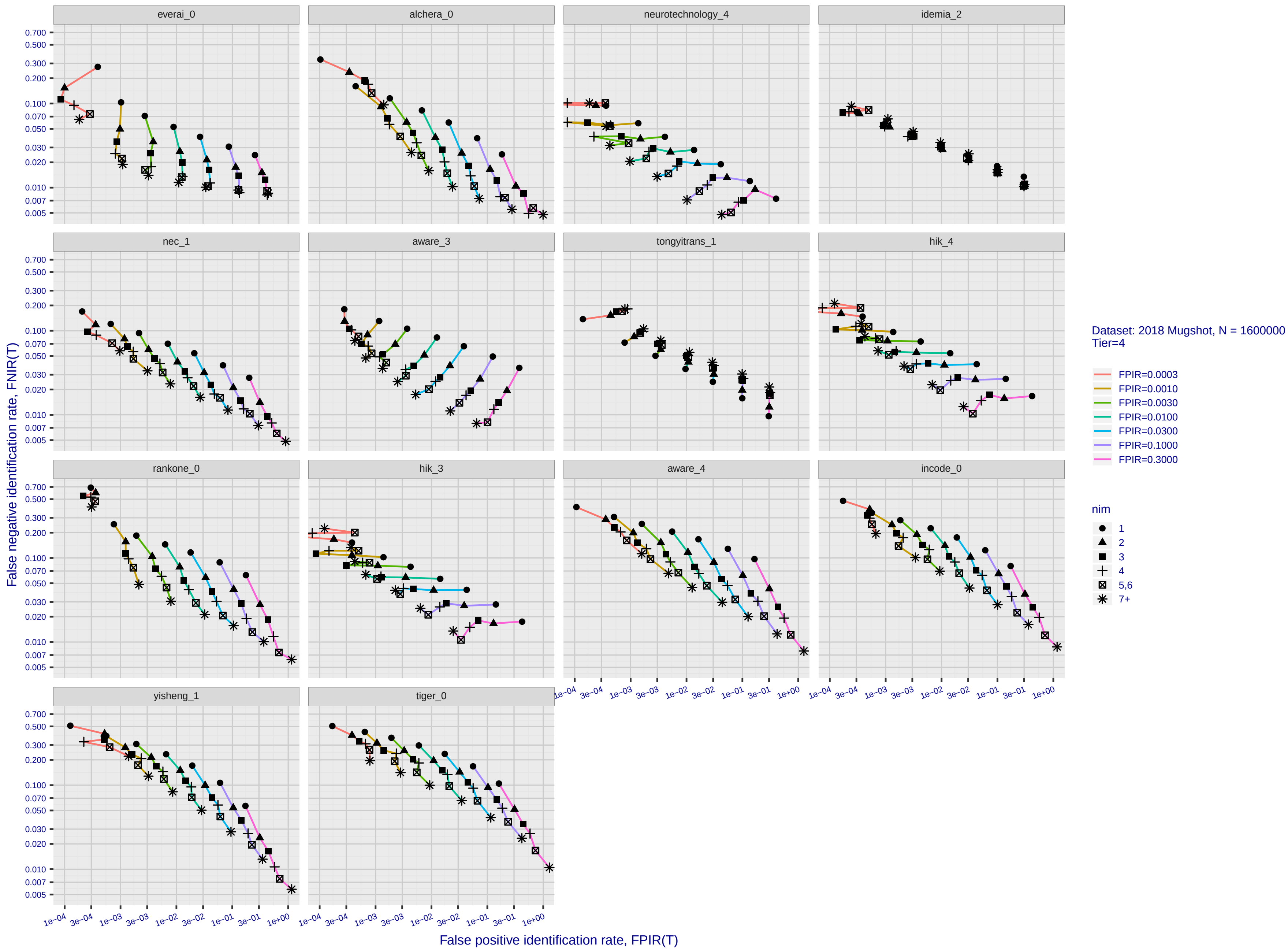

Figure 90: **[FRVT-2018 Mugshot Dataset] Effect of enrolling multiple images for each identity**. *The plot shows an identification miss rates vs. false positive rates, at seven operating thresholds. The enrolled population size is fixed. The images are enrolled with lifetime-consolidation - see section 2.3.*

FNIR(N, R, T) = False neg. identification rate
FPIR(N, T) = False pos. identification rate
N = Num. enrolled subjects
R = Num. candidates examined
T = Threshold
T = 0 → Investigation
T > 0 → Identification

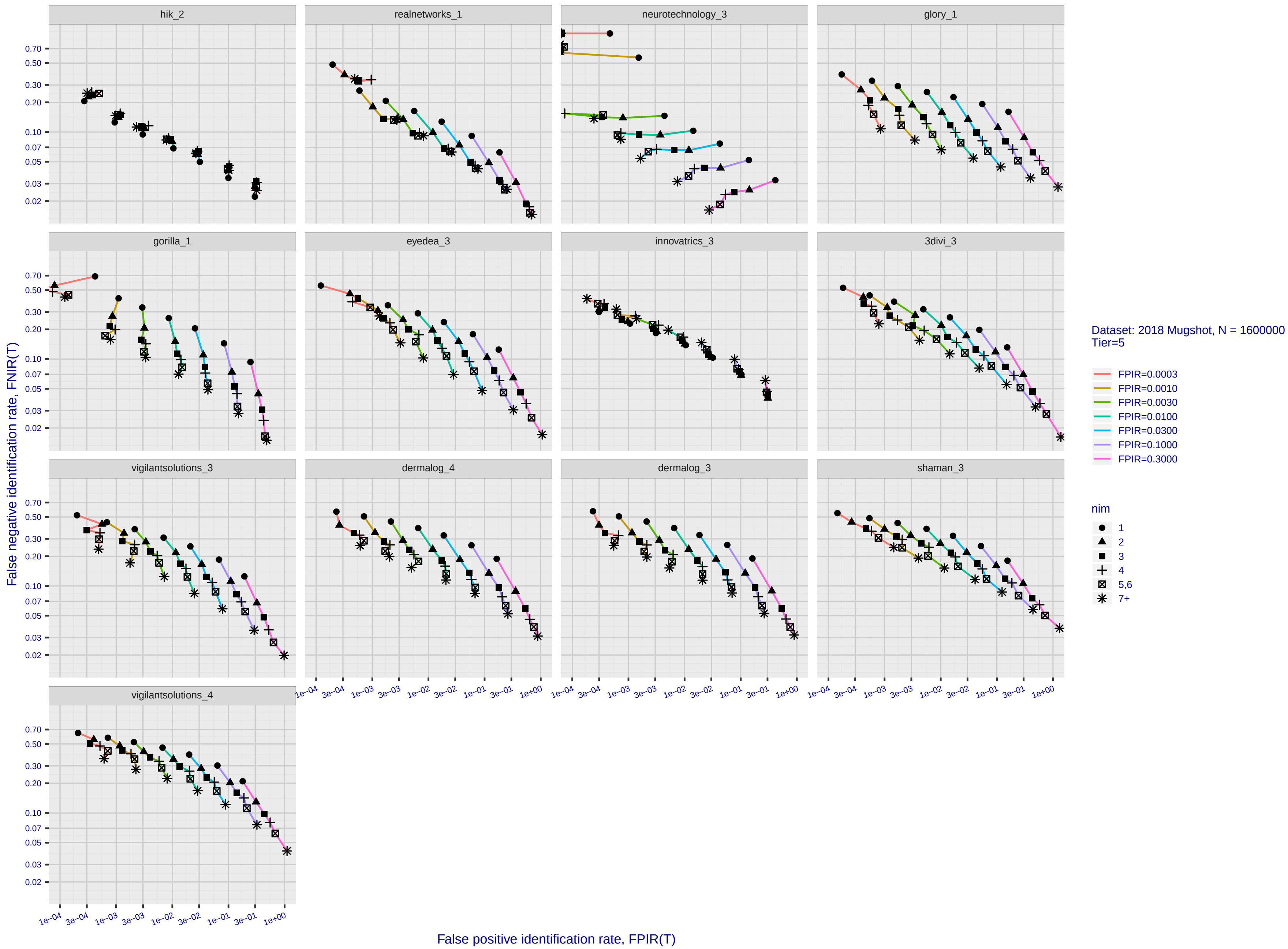

Figure 91: **[FRVT-2018 Mugshot Dataset] Effect of enrolling multiple images for each identity**. *The plot shows an identification miss rates vs. false positive rates, at seven operating thresholds. The enrolled population size is fixed. The images are enrolled with lifetime-consolidation - see section 2.3.*

2019/09/11 16:09:13

FNIR(N, R, T) = False neg. identification rate
FPIR(N, T) = False pos. identification rate
N = Num. enrolled subjects
R = Num. candidates examined
T = Threshold
T = 0 → Investigation
T > 0 → Identification

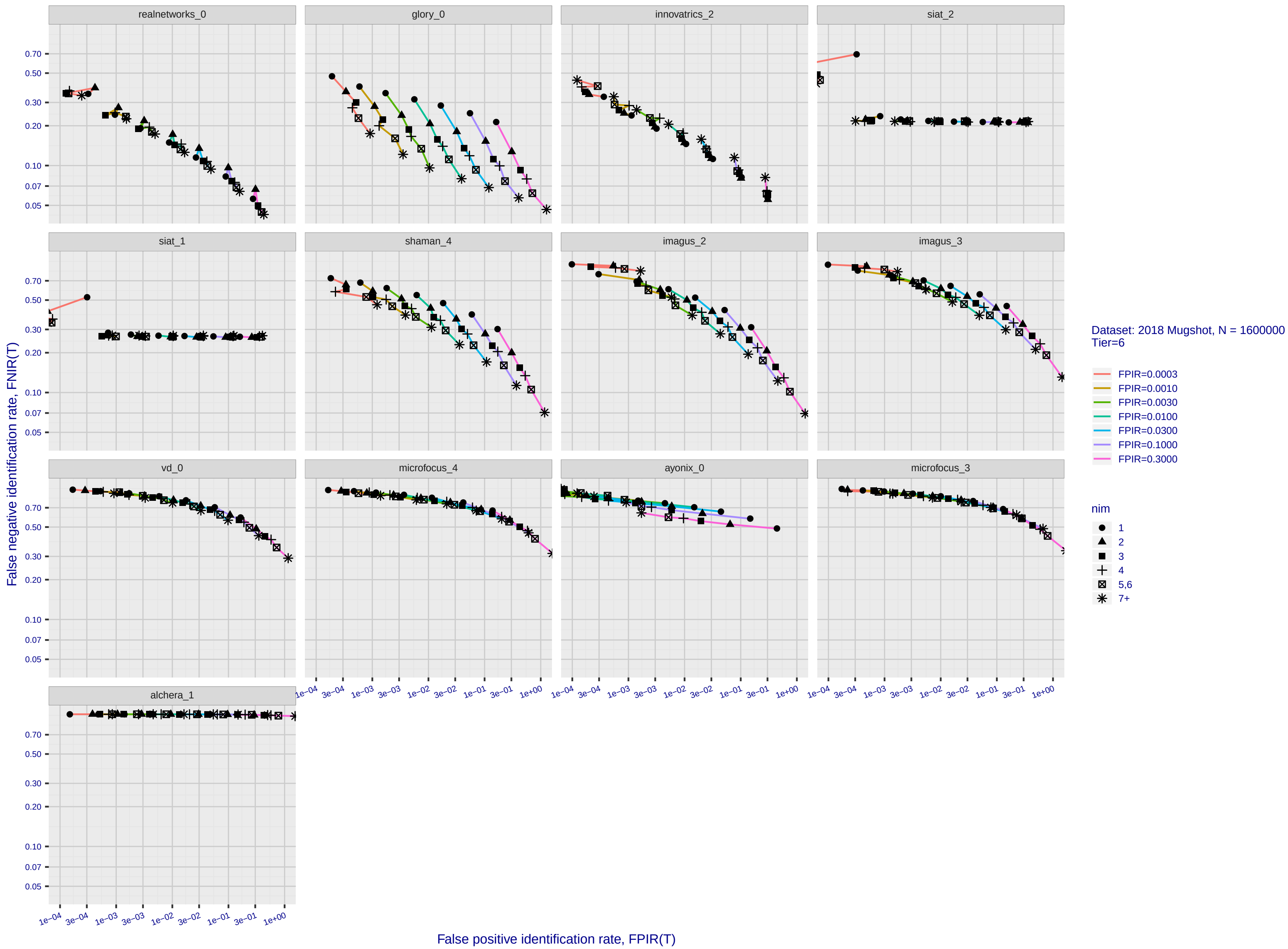

Figure 92: **[FRVT-2018 Mugshot Dataset] Effect of enrolling multiple images for each identity**. *The plot shows an identification miss rates vs. false positive rates, at seven operating thresholds. The enrolled population size is fixed. The images are enrolled with lifetime-consolidation - see section 2.3.*

Appendix D Accuracy with poor quality webcam images

2019/09/11	FNIR(N, R, T) =	False neg. identification rate	N = Num. enrolled subjects	T = Threshold	$T = 0 \rightarrow$ Investigation
16:09:13	FPIR(N, T) =	False pos. identification rate	R = Num. candidates examined		$T > 0 \rightarrow$ Identification

FNIR(N, R, T) = False neg. identification rate
FPIR(N, T) = False pos. identification rate
N = Num. enrolled subjects
R = Num. candidates examined
T = Threshold
T = 0 → Investigation
T > 0 → Identification

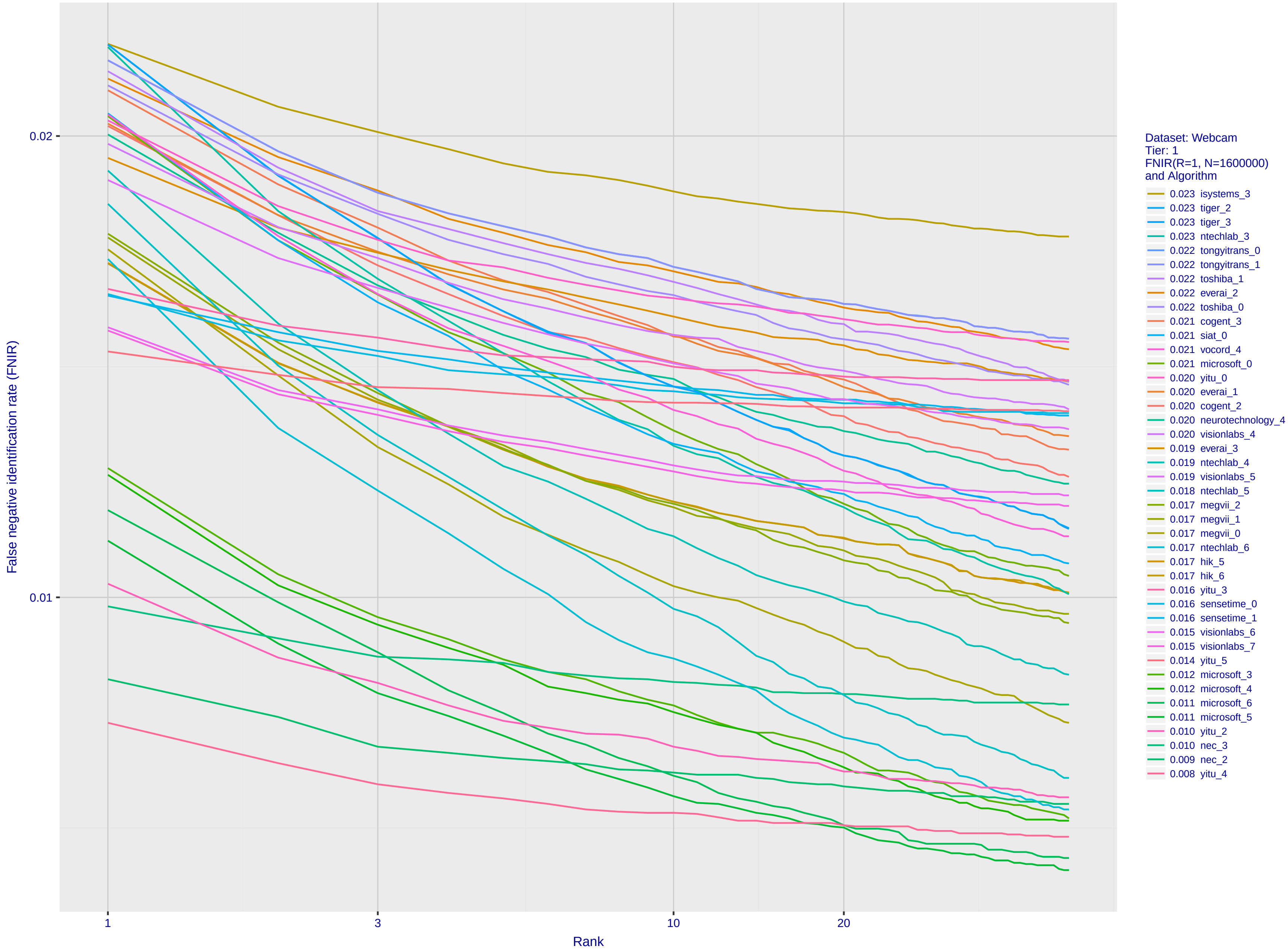

Figure 93: **[Webcam Dataset] Identification miss rates vs. rank**. *The results apply to cross-domain recognition in which webcams are searched against enrolled mugshots. The FNIR values are higher than those for mugshot-mugshot identification due to low image resolution, lighting and less constrained subject pose in webcam images - see Figure 4.*

This publication is available free of charge from: https://doi.org/10.6028/NIST.IR.8271

FNIR(N, R, T) = False neg. identification rate
FPIR(N, T) = False pos. identification rate
N = Num. enrolled subjects
R = Num. candidates examined
T = Threshold
T = 0 → Investigation
T > 0 → Identification

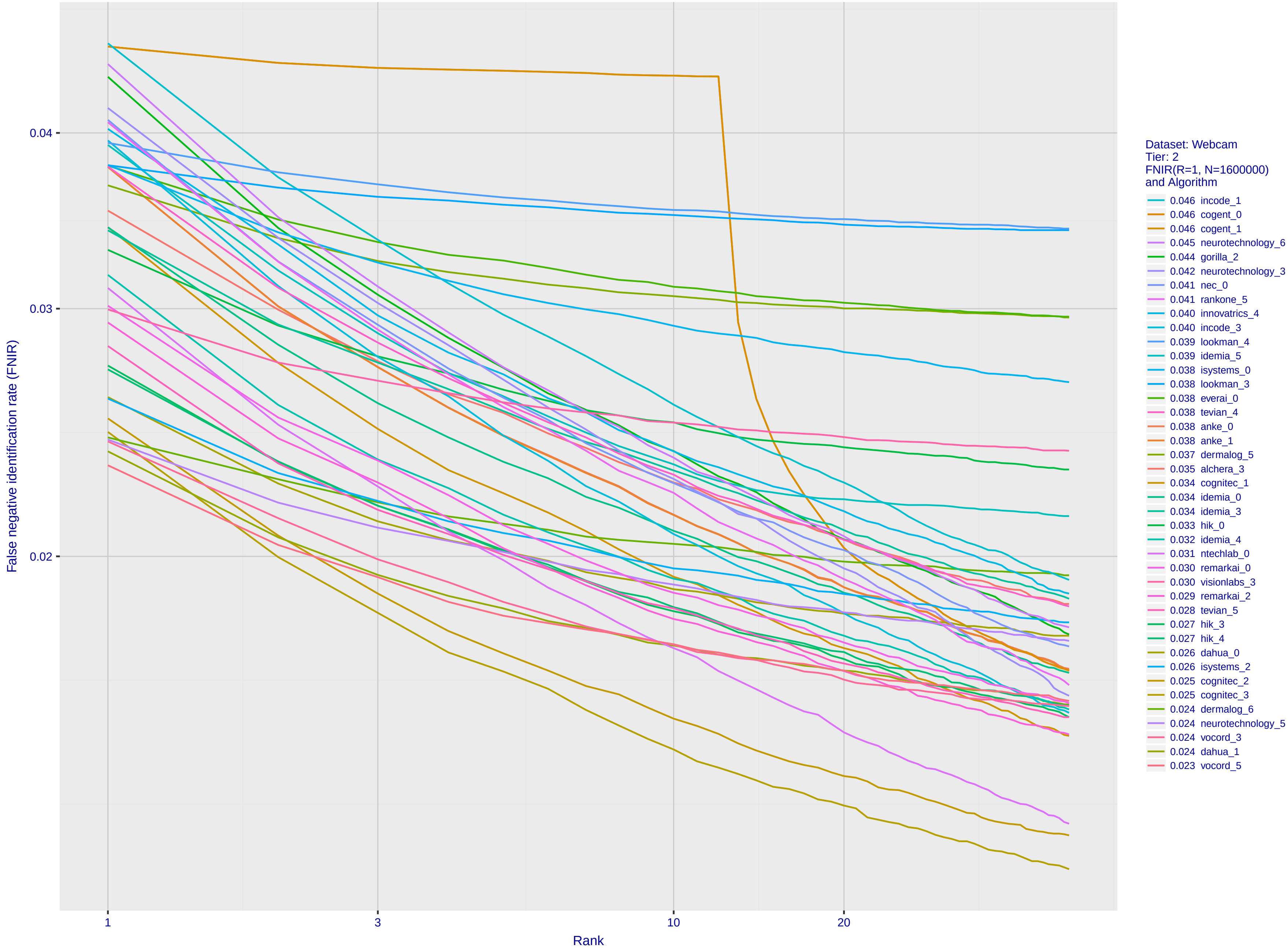

Figure 94: **[Webcam Dataset] Identification miss rates vs. rank**. *The results apply to cross-domain recognition in which webcams are searched against enrolled mugshots. The FNIR values are higher than those for mugshot-mugshot identification due to low image resolution, lighting and less constrained subject pose in webcam images - see Figure 4.*

FNIR(N, R, T) = False neg. identification rate
FPIR(N, T) = False pos. identification rate
N = Num. enrolled subjects
R = Num. candidates examined
T = Threshold
T = 0 → Investigation
T > 0 → Identification

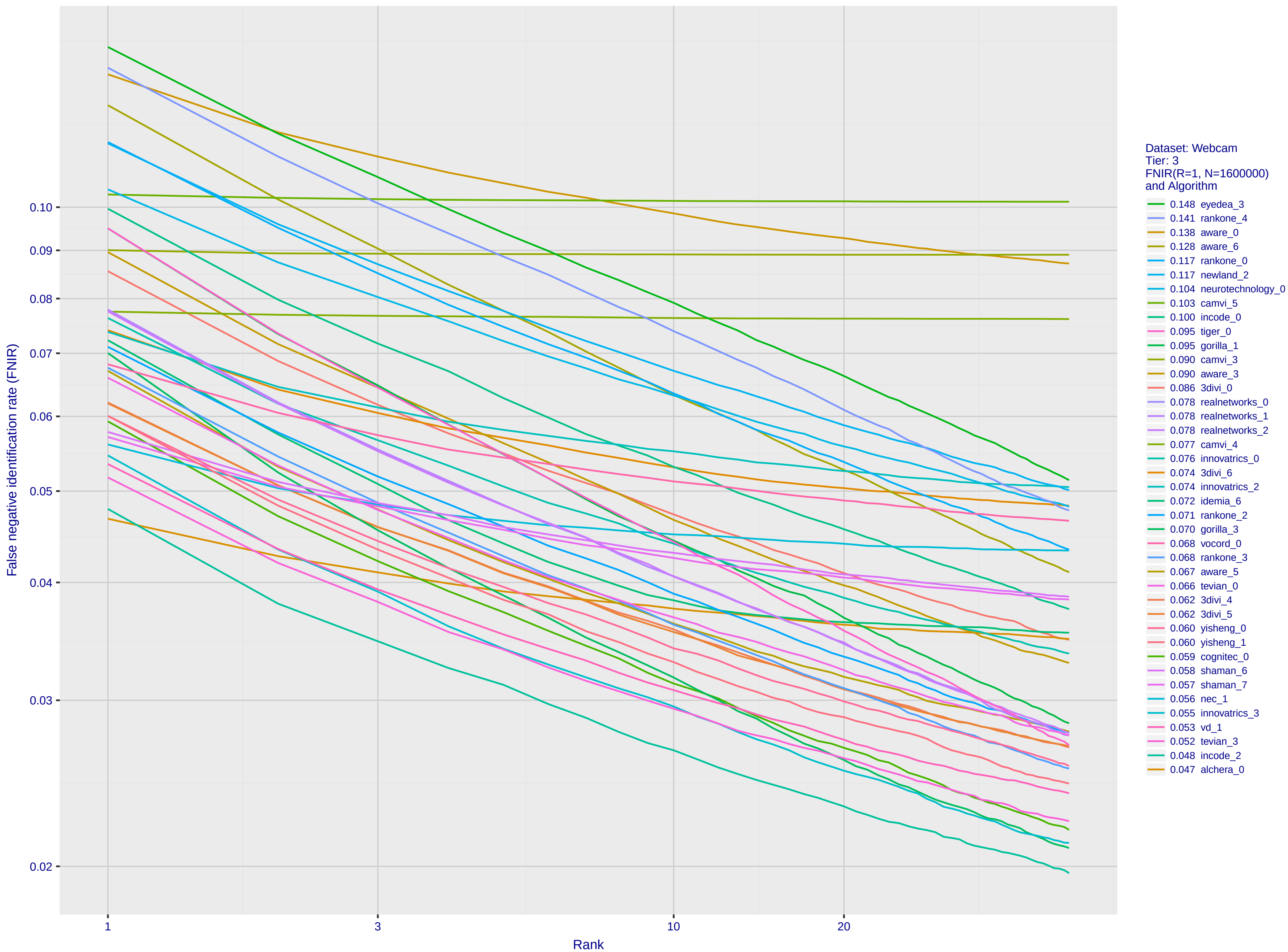

Figure 95: **[Webcam Dataset] Identification miss rates vs. rank**. *The results apply to cross-domain recognition in which webcams are searched against enrolled mugshots. The FNIR values are higher than those for mugshot-mugshot identification due to low image resolution, lighting and less constrained subject pose in webcam images - see Figure 4.*

This publication is available free of charge from: https://doi.org/10.6028/NIST.IR.8271

FNIR(N, R, T) = False neg. identification rate
FPIR(N, T) = False pos. identification rate
N = Num. enrolled subjects
R = Num. candidates examined
T = Threshold
T = 0 → Investigation
T > 0 → Identification

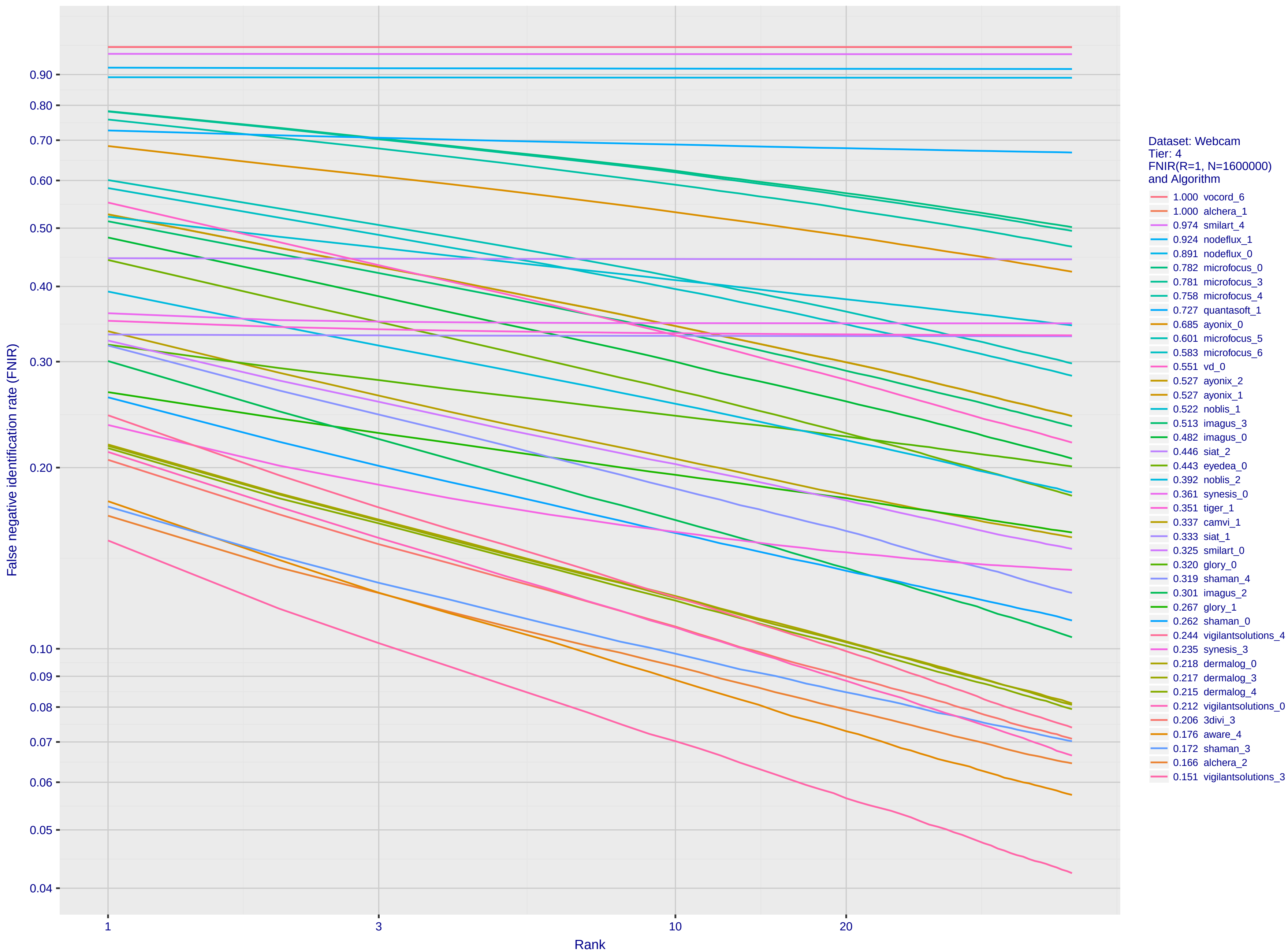

Figure 96: **[Webcam Dataset] Identification miss rates vs. rank**. *The results apply to cross-domain recognition in which webcams are searched against enrolled mugshots. The FNIR values are higher than those for mugshot-mugshot identification due to low image resolution, lighting and less constrained subject pose in webcam images - see Figure 4.*

FNIR(N, R, T) = False neg. identification rate
FPIR(N, T) = False pos. identification rate
N = Num. enrolled subjects
R = Num. candidates examined
T = Threshold
T = 0 → Investigation
T > 0 → Identification

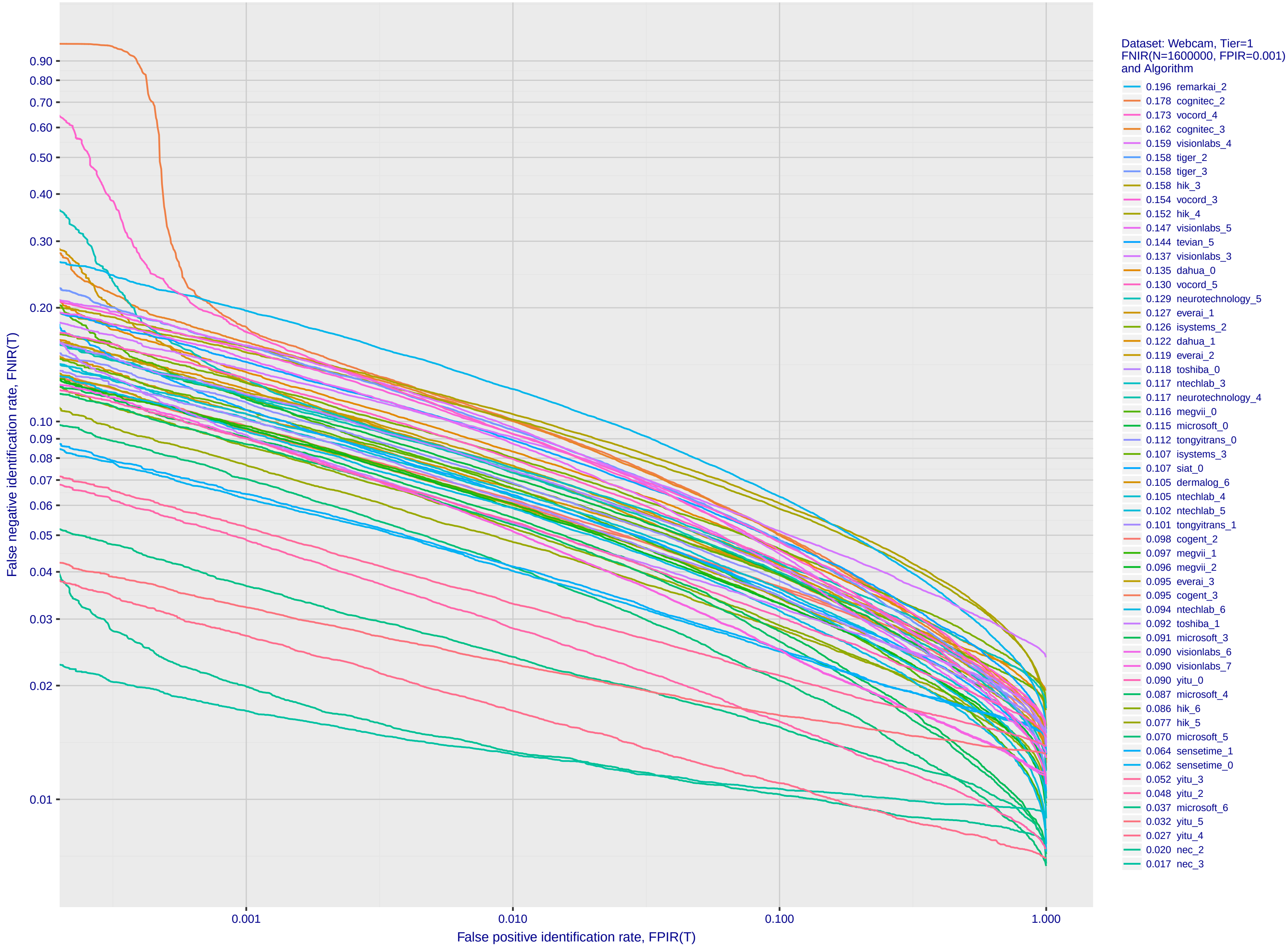

Figure 97: **[Webcam Dataset] Identification miss rates vs. false positive rates**. *The results apply to cross-domain recognition in which webcams are searched against enrolled mugshots. The FNIR values are higher than those for mugshot-mugshot identification due to low image resolution, lighting and less constrained subject pose in webcam images - see Figure 4.*

FNIR(N, R, T) = False neg. identification rate
FPIR(N, T) = False pos. identification rate
N = Num. enrolled subjects
R = Num. candidates examined
T = Threshold
T = 0 → Investigation
T > 0 → Identification

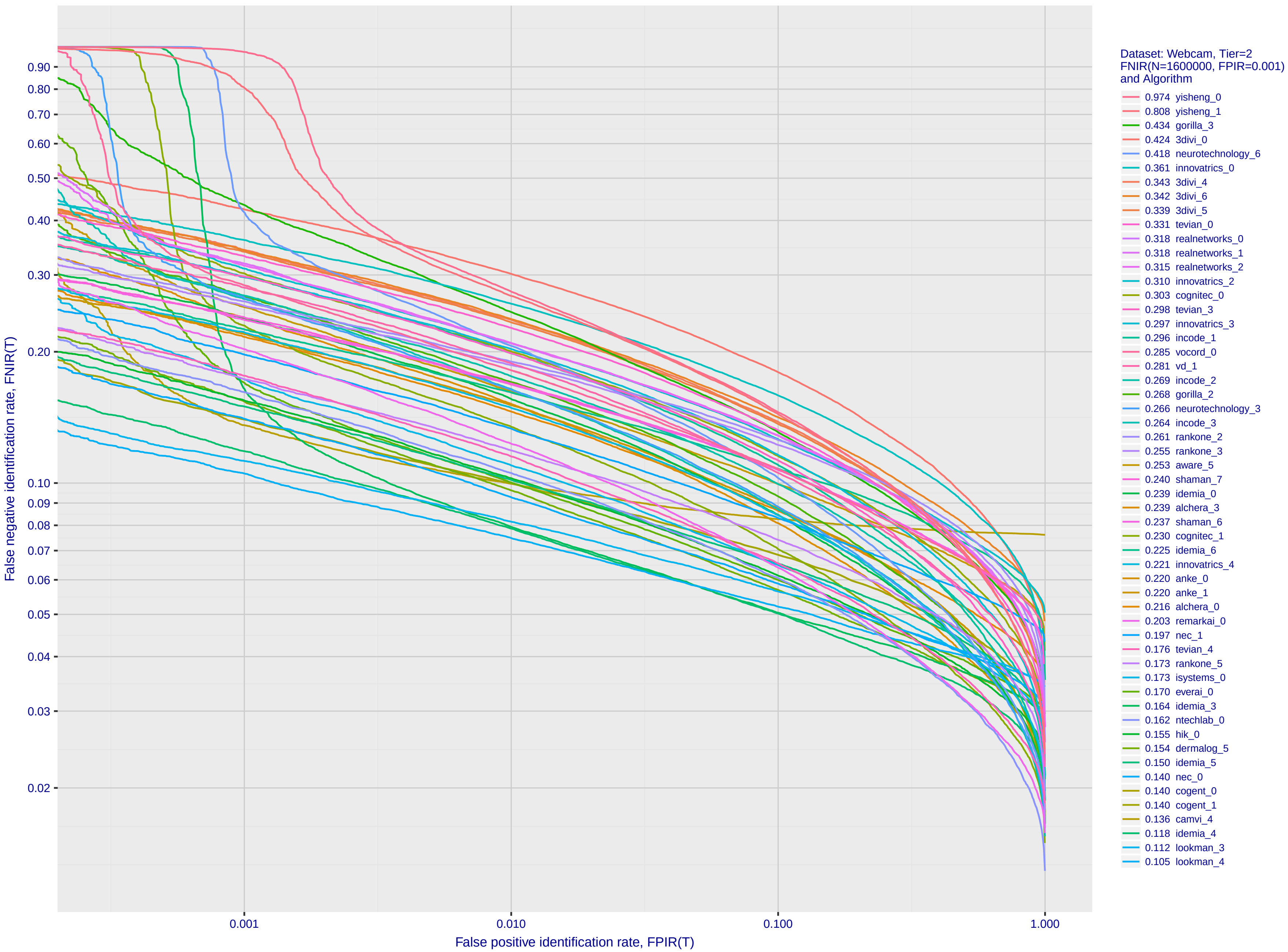

Figure 98: **[Webcam Dataset] Identification miss rates vs. false positive rates**. *The results apply to cross-domain recognition in which webcams are searched against enrolled mugshots. The FNIR values are higher than those for mugshot-mugshot identification due to low image resolution, lighting and less constrained subject pose in webcam images - see Figure 4.*

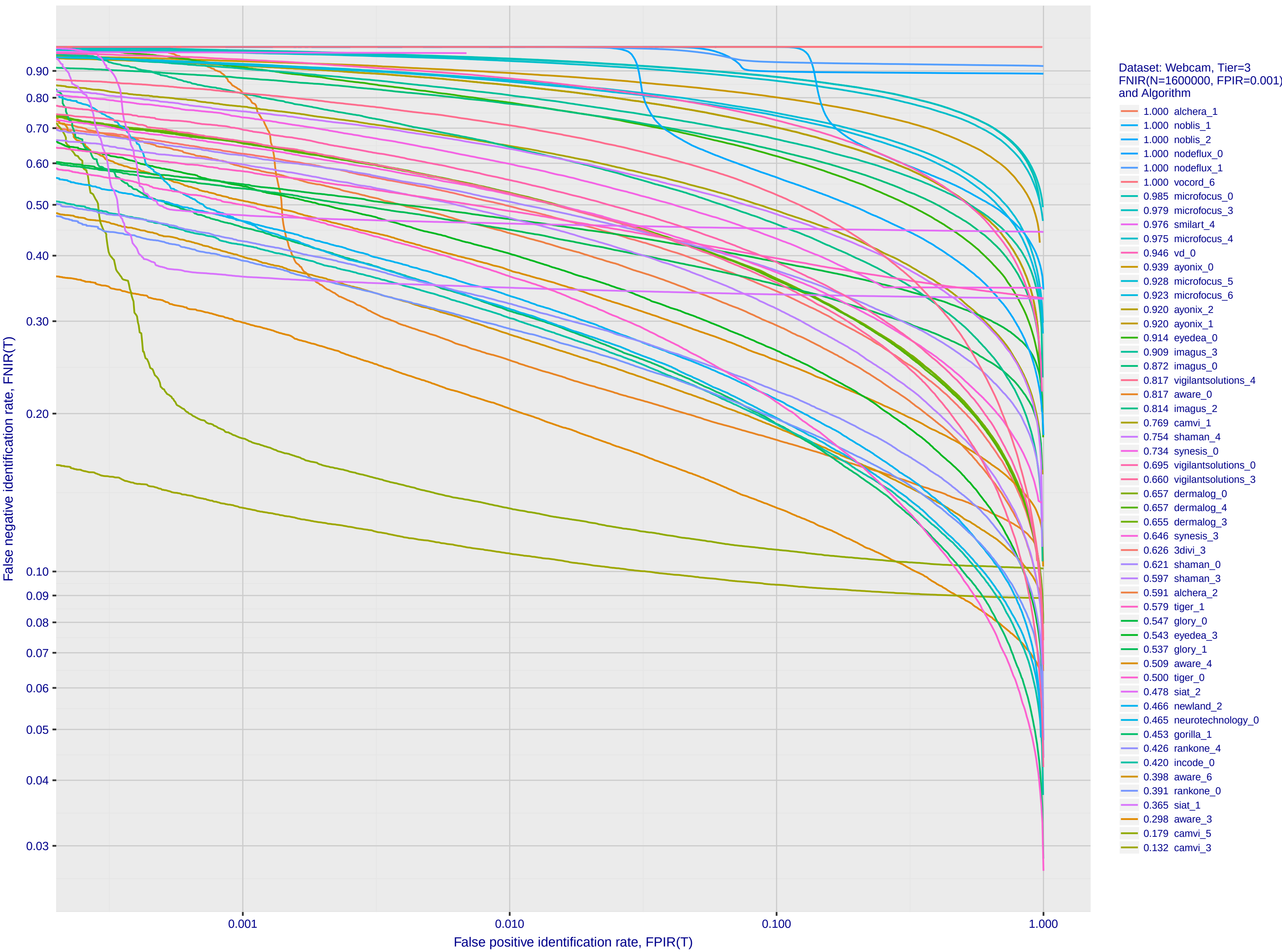

Figure 99: **[Webcam Dataset] Identification miss rates vs. false positive rates**. *The results apply to cross-domain recognition in which webcams are searched against enrolled mugshots. The FNIR values are higher than those for mugshot-mugshot identification due to low image resolution, lighting and less constrained subject pose in webcam images - see Figure 4.*

Appendix E Accuracy for profile-view to frontal recognition

Figures 100 - 102 gives accuracy results for searching 100 000 mated and 100 000 non-mated profile-view images against the same FRVT 2018 frontal enrollment dataset, N = 1 600 000, used in the main mugshot trials. This experiment corresponds to row-13 of Table 5. An example of profile-view image is given in Figure 5.

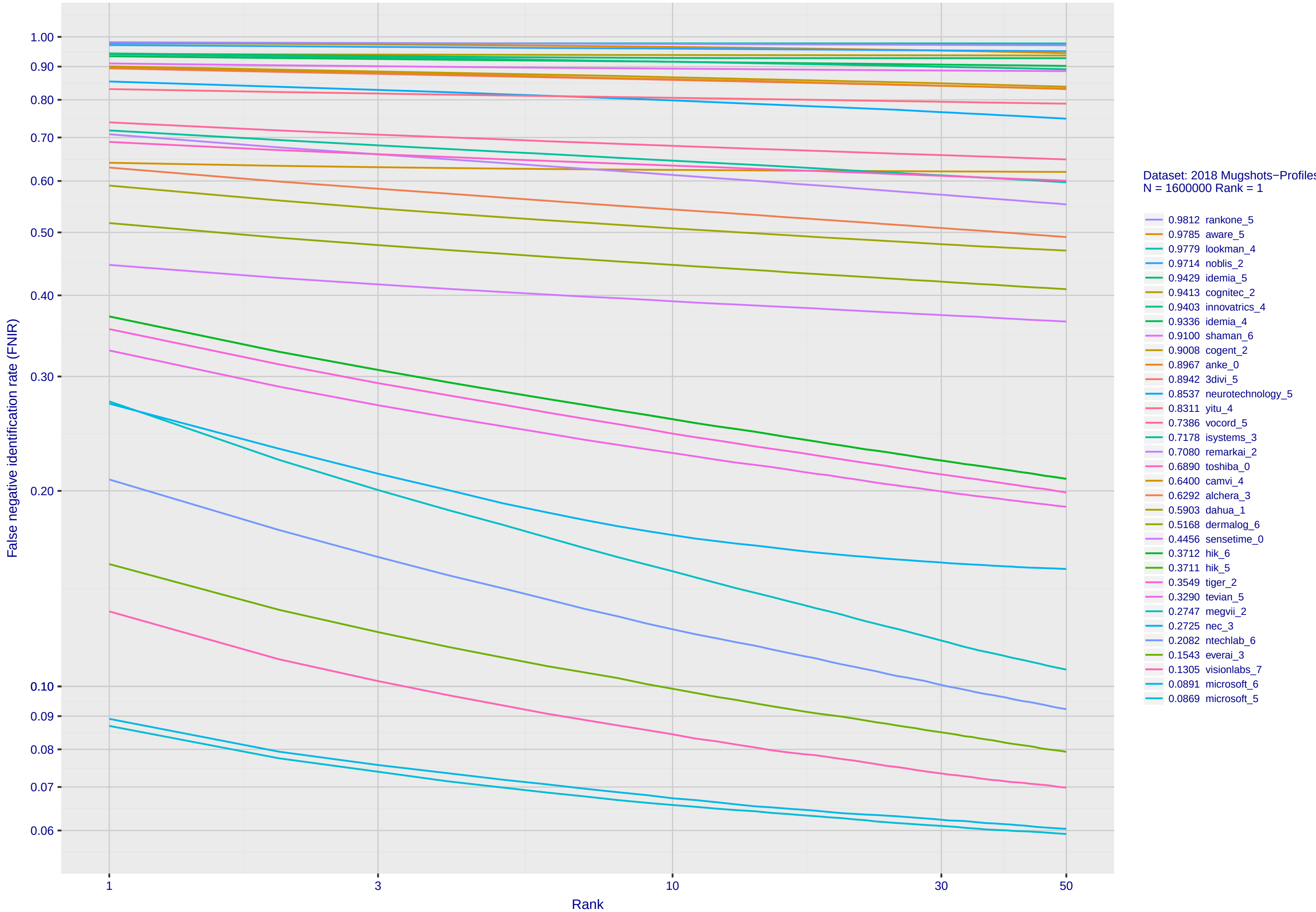

Figure 100: **[Mugshot and profile-view dataset] Rank-based accuracy**. *For some of the more accurate Phase 3 algorithms the figure plots error tradeoff characteristics for frontal and profile-view searches into an enrolled set of N = 1 600 000 frontal images. Note that some algorithms fail on profile-view images with FNIR → 1 - this evaluation did not ask developers to provide profile-view capability. Some algorithms, on the other hand, give FNIR approaching that for frontal-view searches using c. 2010 algorithms. The best result is that 91% of profile-view searches yield the correct mate at rank 1, and better than 94% in the top-50 candidates.*

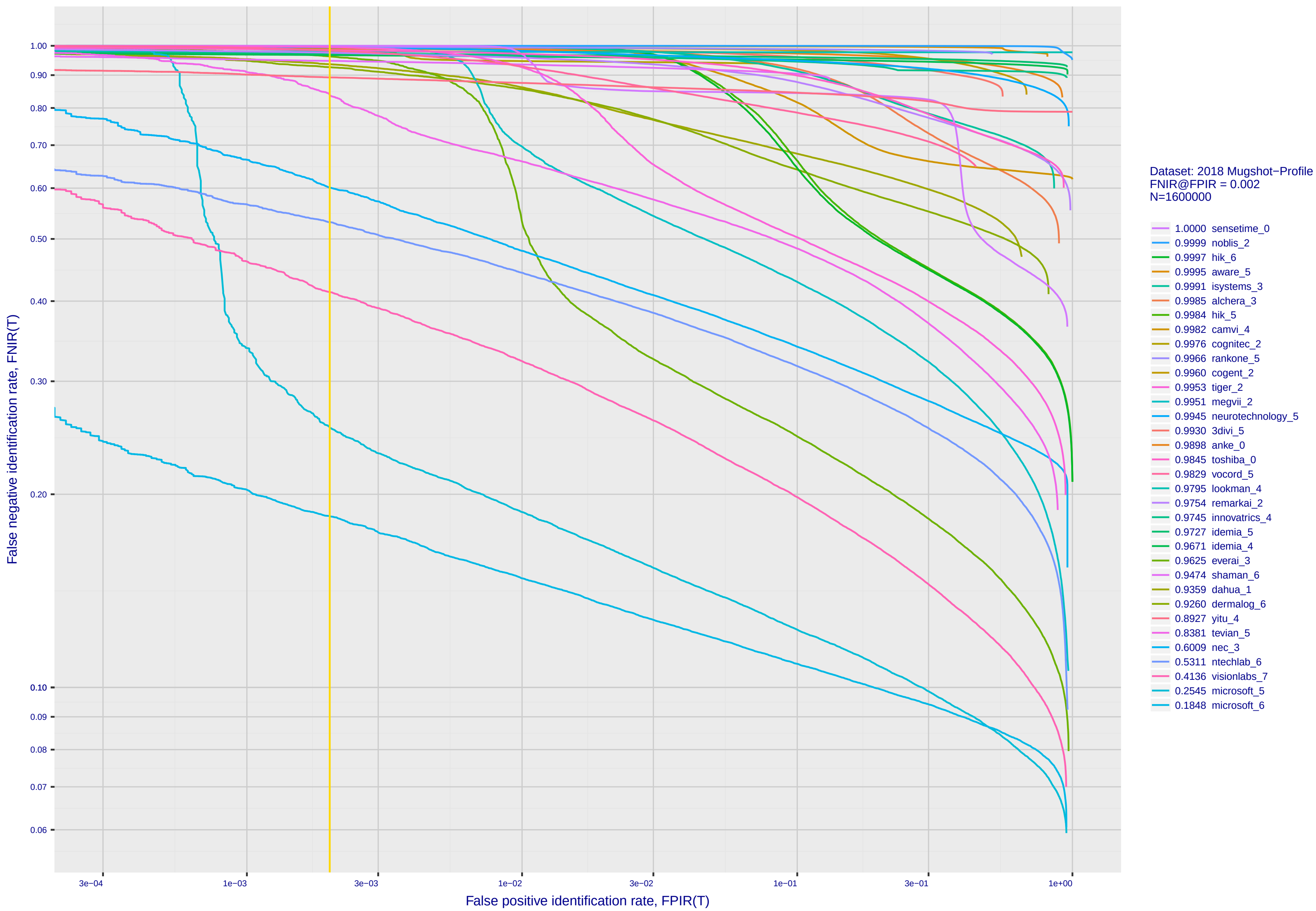

Figure 101: **[Mugshot and profile-view dataset] Threshold-based accuracy**. *For some of the more accurate Phase 3 algorithms the figure plots error tradeoff characteristics for frontal and profile-view searches into an enrolled set of N = 1 600 000 frontal images. Note that some algorithms fail on profile-view images with FNIR → 1 - this evaluation did not ask developers to provide profile-view capability. Some algorithms, on the other hand, give FNIR approaching that for frontal-view searches using c. 2010 algorithms.*

FNIR(N, R, T) = False neg. identification rate
FPIR(N, T) = False pos. identification rate
N = Num. enrolled subjects
R = Num. candidates examined
T = Threshold
T = 0 → Investigation
T > 0 → Identification

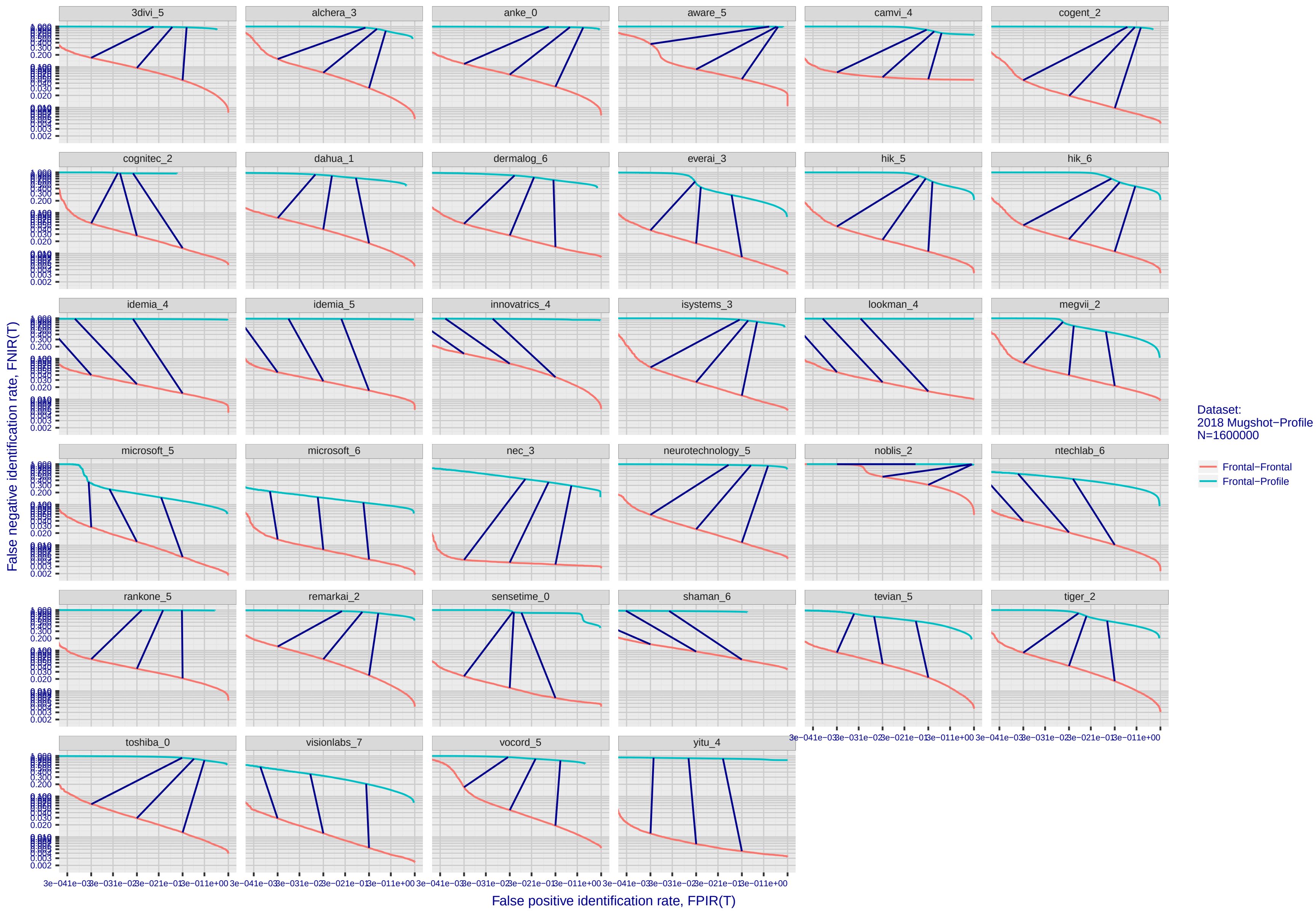

Figure 102: **[Mugshot and profile-view dataset] Speed-accuracy tradeoff**. *For some of the more accurate Phase 3 algorithms the figure plots error tradeoff characteristics for frontal and profile-view searches into an enrolled set of $N = 1\,600\,000$ frontal images. Some algorithms fail on profile-view images with FNIR $\rightarrow 1$ - this evaluation did not ask developers to provide profile-view capability. Some algorithms, on the other hand, give FNIR approaching that for frontal-view searches using c. 2010 algorithms. Blue lines connect points of equal threshold from which it is evident that some algorithms would give markedly higher false positive outcomes if profile-view images were searched in a system configured for frontal searches. This would be a vulnerability in an access control system.*

Appendix F Accuracy when identifying wild images

2019/09/11	FNIR(N, R, T) =	False neg. identification rate	N = Num. enrolled subjects	T = Threshold	$T = 0 \rightarrow$ Investigation
16:09:13	FPIR(N, T) =	False pos. identification rate	R = Num. candidates examined		$T > 0 \rightarrow$ Identification

FNIR(N, R, T) = False neg. identification rate
FPIR(N, T) = False pos. identification rate
N = Num. enrolled subjects
R = Num. candidates examined
T = Threshold
T = 0 → Investigation
T > 0 → Identification

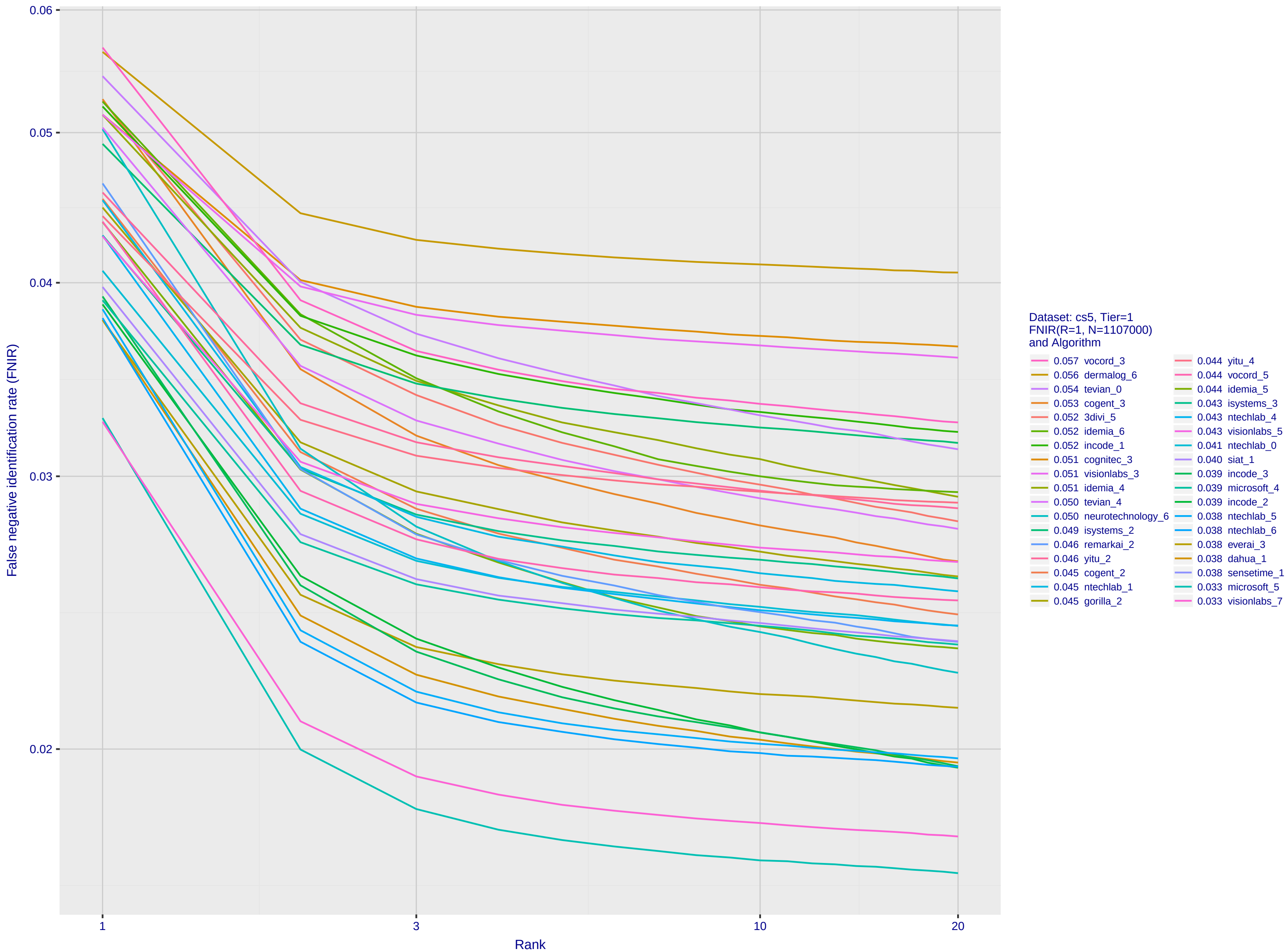

Figure 103: **[Wild Dataset] Identification miss rates vs. rank**. *For the wild dataset, the figure shows false negative identification rates (FNIR) vs. rank when the threshold is set to zero. This metric is relevant to human reviewers who will traverse candidate lists checking whether any of the returned identities match to the search imagery. Specifically, wild images were searched against 1.1 million individuals enrolled with wild images as well.*

FNIR(N, R, T) = False neg. identification rate
FPIR(N, T) = False pos. identification rate
N = Num. enrolled subjects
R = Num. candidates examined
T = Threshold
T = 0 → Investigation
T > 0 → Identification

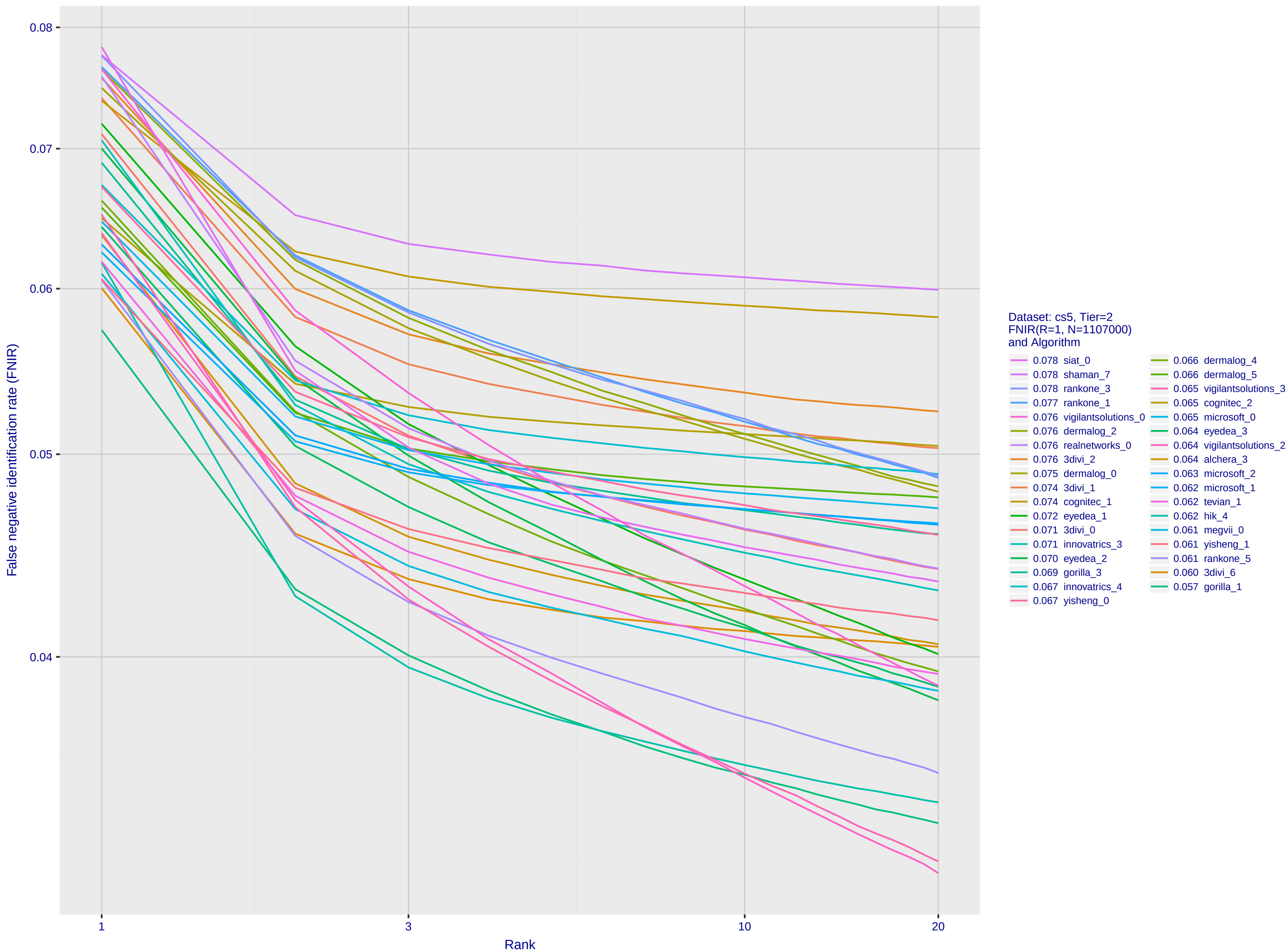

Figure 104: **[Wild Dataset] Identification miss rates vs. rank**. *For the wild dataset, the figure shows false negative identification rates (FNIR) vs. rank when the threshold is set to zero. This metric is relevant to human reviewers who will traverse candidate lists checking whether any of the returned identities match to the search imagery. Specifically, wild images were searched against 1.1 million individuals enrolled with wild images as well.*

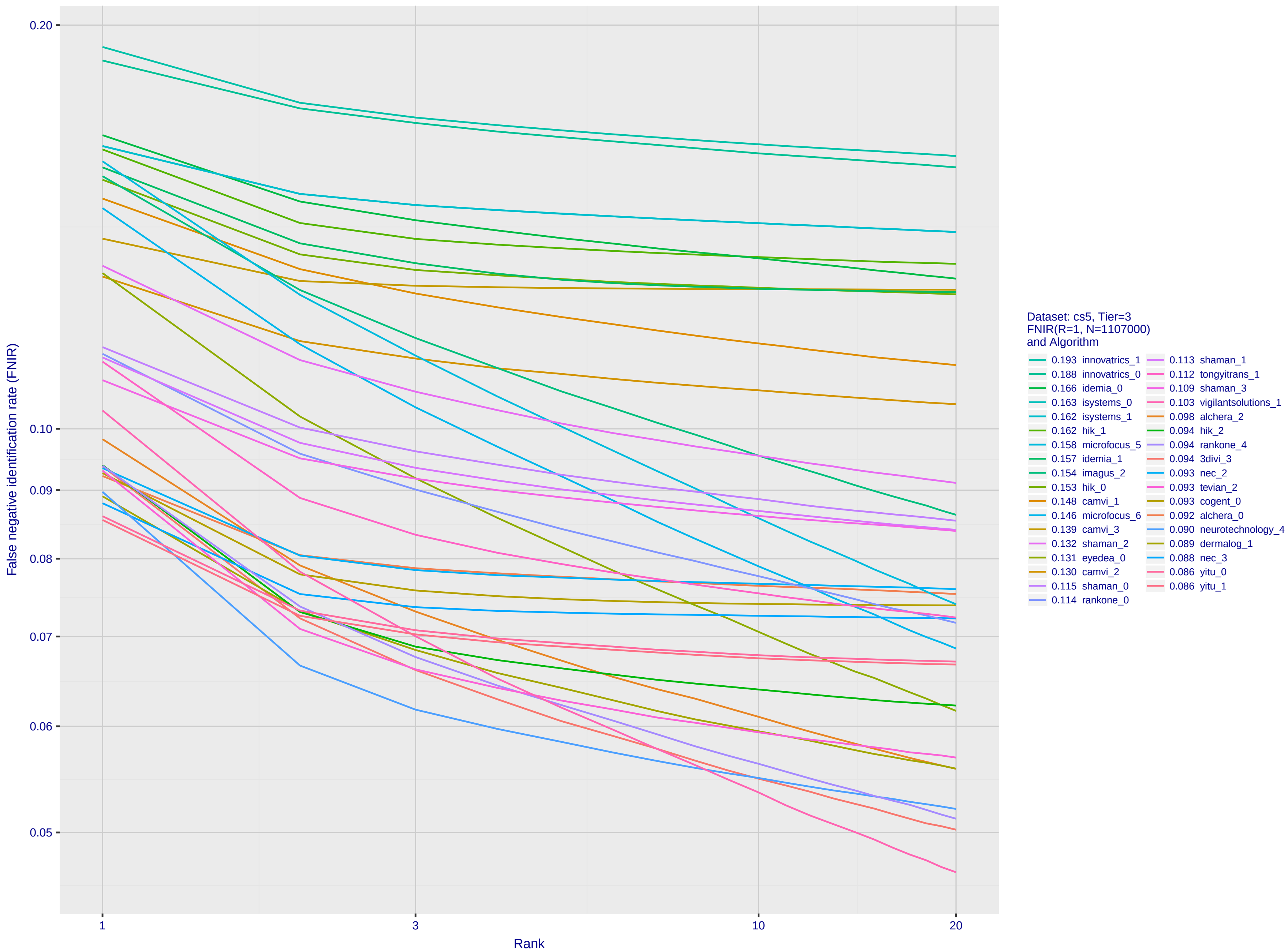

Figure 105: **[Wild Dataset] Identification miss rates vs. rank**. *For the wild dataset, the figure shows false negative identification rates (FNIR) vs. rank when the threshold is set to zero. This metric is relevant to human reviewers who will traverse candidate lists checking whether any of the returned identities match to the search imagery. Specifically, wild images were searched against 1.1 million individuals enrolled with wild images as well.*

FNIR(N, R, T) = False neg. identification rate
FPIR(N, T) = False pos. identification rate
N = Num. enrolled subjects
R = Num. candidates examined
T = Threshold
T = 0 → Investigation
T > 0 → Identification

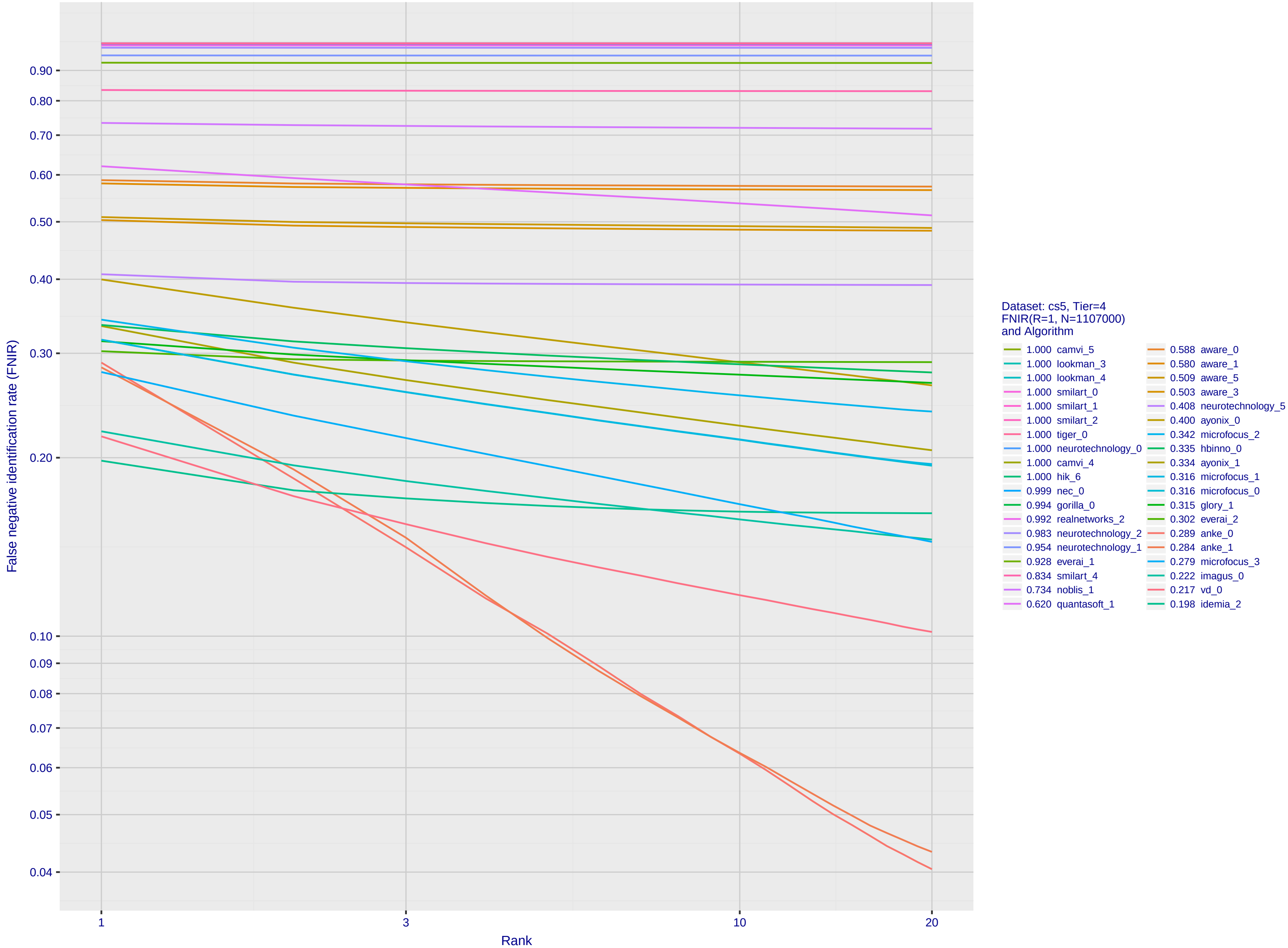

Figure 106: **[Wild Dataset] Identification miss rates vs. rank**. *For the wild dataset, the figure shows false negative identification rates (FNIR) vs. rank when the threshold is set to zero. This metric is relevant to human reviewers who will traverse candidate lists checking whether any of the returned identities match to the search imagery. Specifically, wild images were searched against 1.1 million individuals enrolled with wild images as well.*

2019/09/11	FNIR(N, R, T) =	False neg. identification rate	N = Num. enrolled subjects	T = Threshold	$T = 0 \rightarrow$ Investigation
16:09:13	FPIR(N, T) =	False pos. identification rate	R = Num. candidates examined		$T > 0 \rightarrow$ Identification

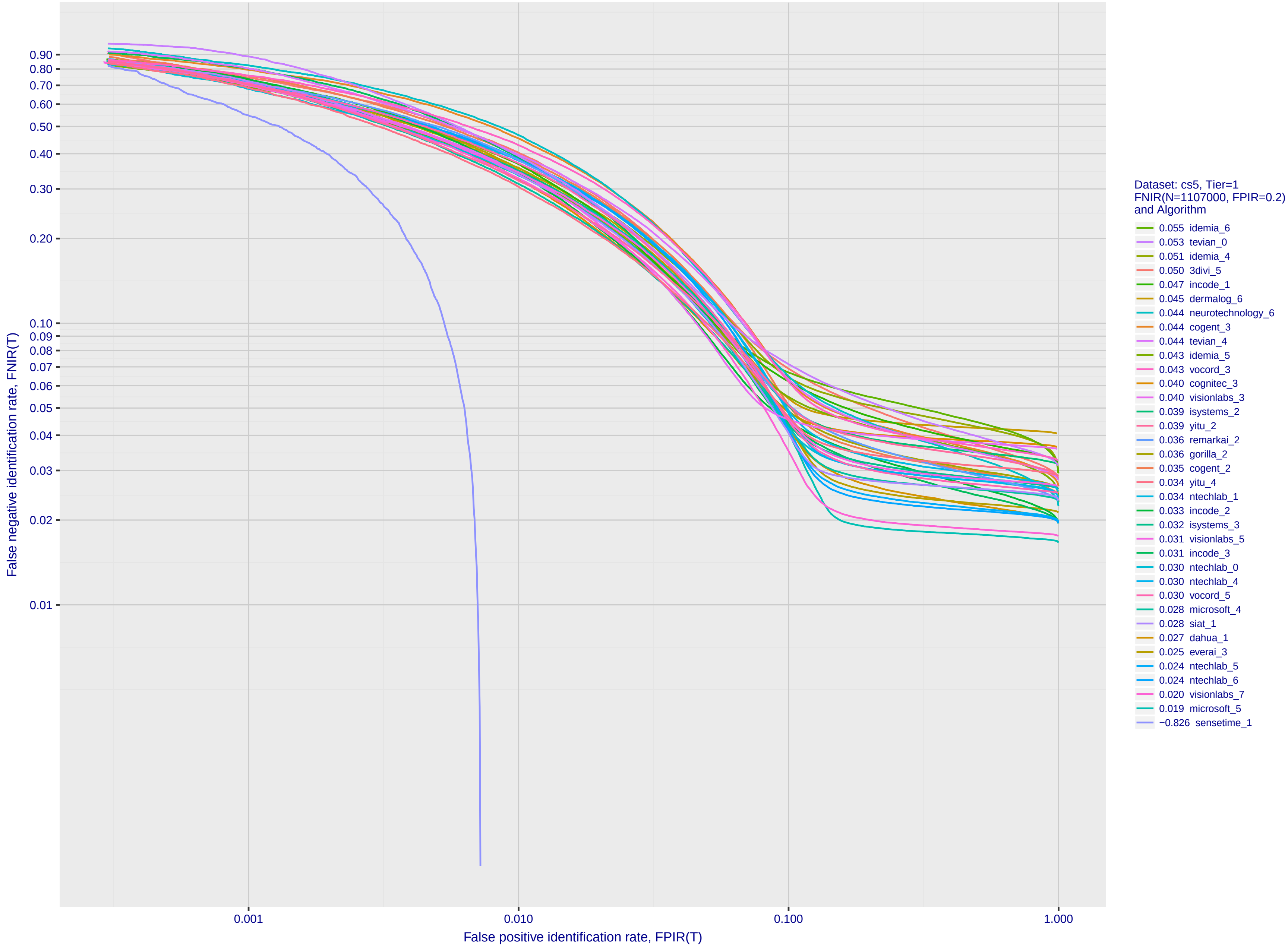

Figure 107: **[Wild Dataset] Identification miss rates vs. false positive rates**. *The figure shows accuracy of algorithms on wild images searched against wild images of 1.1 million individuals enrolled into a gallery. On the vertical axis is miss rate FNIR(N, T, L) with N = 1 107 000, as a function of false positive identification FPIR(N, T). The rapid increase in FNIR below FPIR = 0.1 suggests that some background identities in the gallery are actually present in the non-mated search sets. This issue will be addressed in the 2019 revision of this report.*

This publication is available free of charge from: https://doi.org/10.6028/NIST.IR.8271

FNIR(N, R, T) = False neg. identification rate N = Num. enrolled subjects T = Threshold T = 0 → Investigation
FPIR(N, T) = False pos. identification rate R = Num. candidates examined T > 0 → Identification

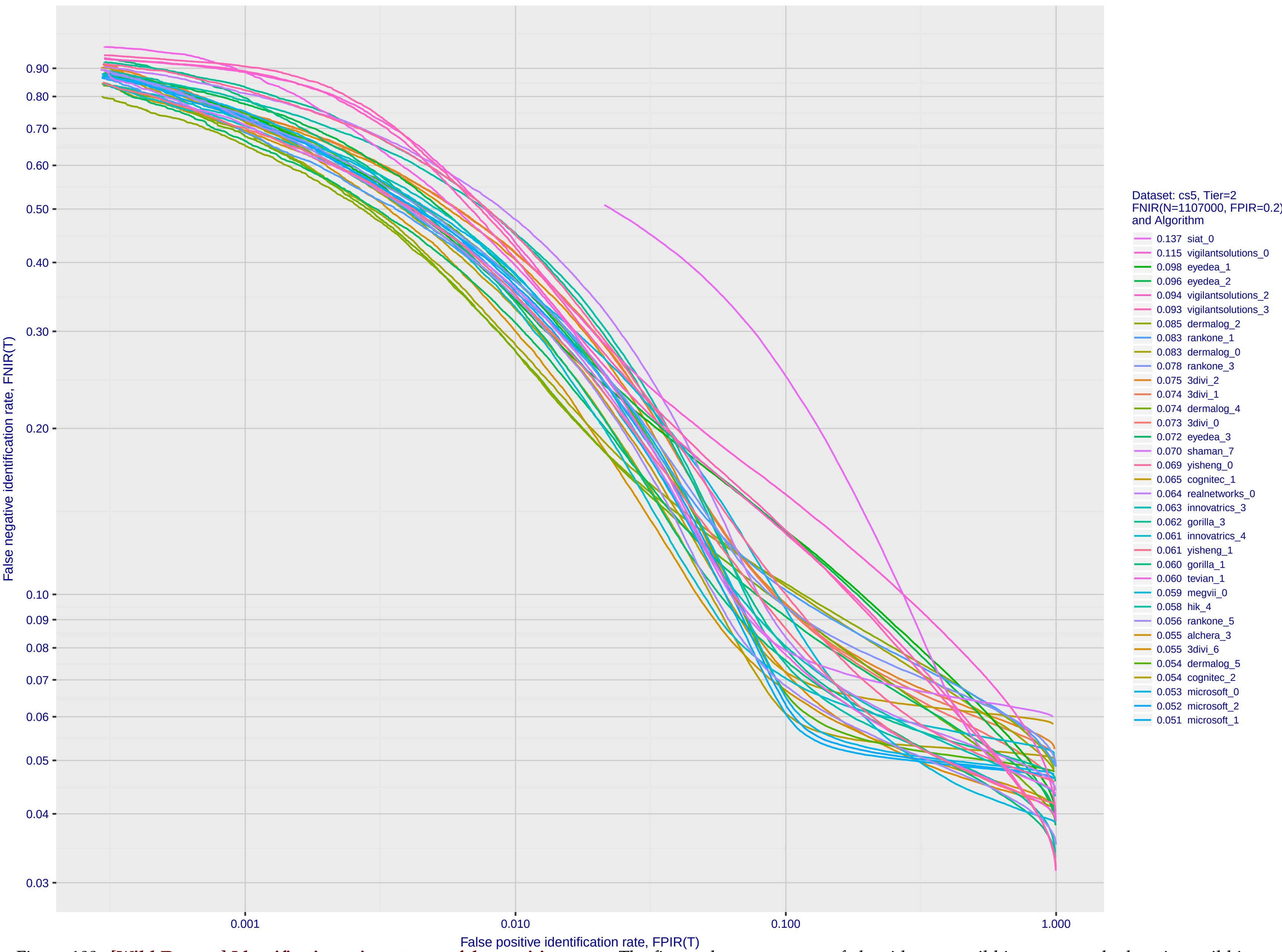

Figure 108: **[Wild Dataset] Identification miss rates vs. false positive rates**. *The figure shows accuracy of algorithms on wild images searched against wild images of 1.1 million individuals enrolled into a gallery. On the vertical axis is miss rate FNIR(N, T, L) with N = 1 107 000, as a function of false positive identification FPIR(N, T). The rapid increase in FNIR below FPIR = 0.1 suggests that some background identities in the gallery are actually present in the non-mated search sets. This issue will be addressed in the 2019 revision of this report.*

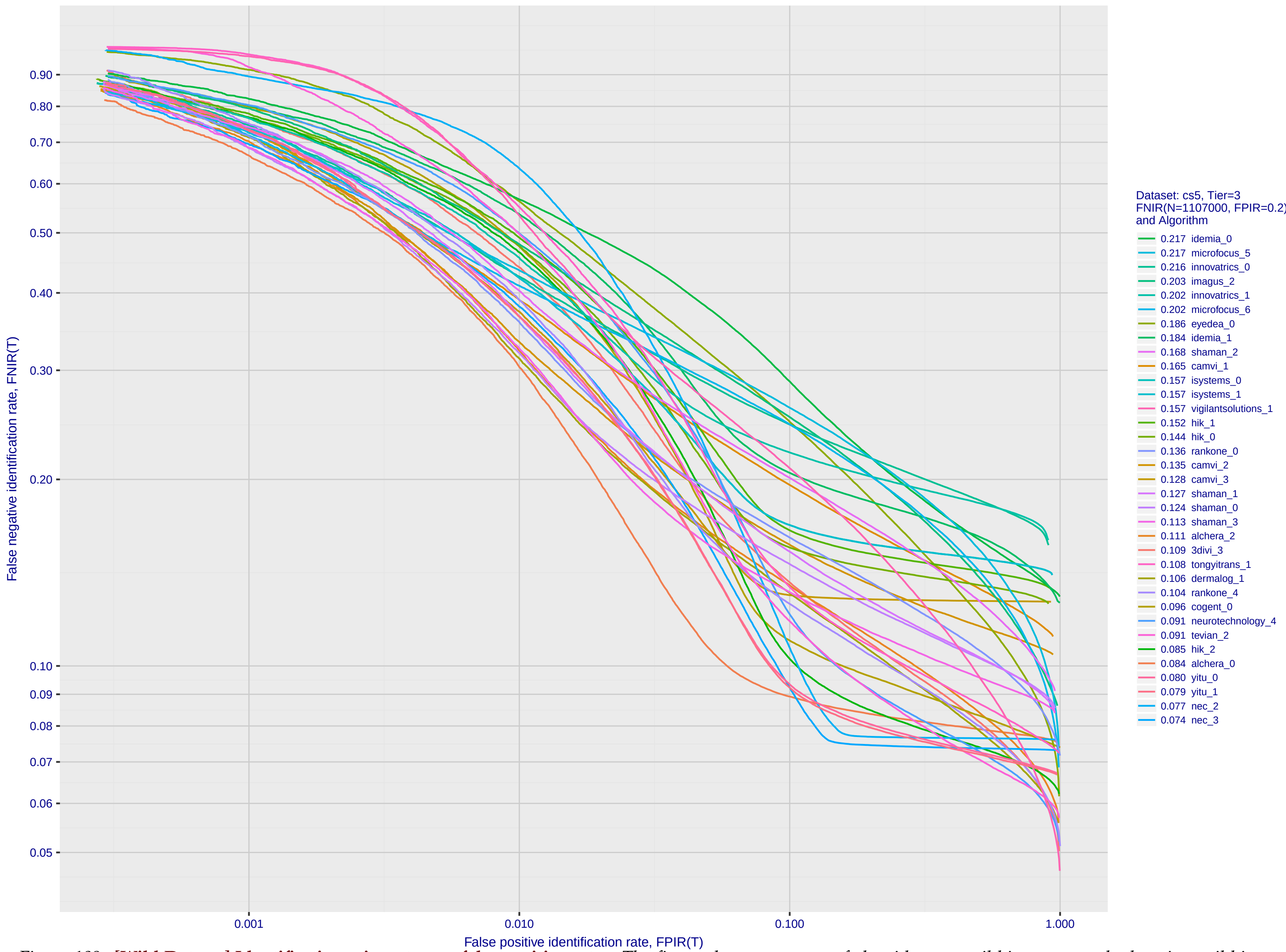

Figure 109: **[Wild Dataset] Identification miss rates vs. false positive rates**. *The figure shows accuracy of algorithms on wild images searched against wild images of 1.1 million individuals enrolled into a gallery. On the vertical axis is miss rate FNIR(N, T, L) with N = 1 107 000, as a function of false positive identification FPIR(N, T). The rapid increase in FNIR below FPIR = 0.1 suggests that some background identities in the gallery are actually present in the non-mated search sets. This issue will be addressed in the 2019 revision of this report.*

FNIR(N, R, T) = False neg. identification rate
FPIR(N, T) = False pos. identification rate
N = Num. enrolled subjects
R = Num. candidates examined
T = Threshold
T = 0 → Investigation
T > 0 → Identification

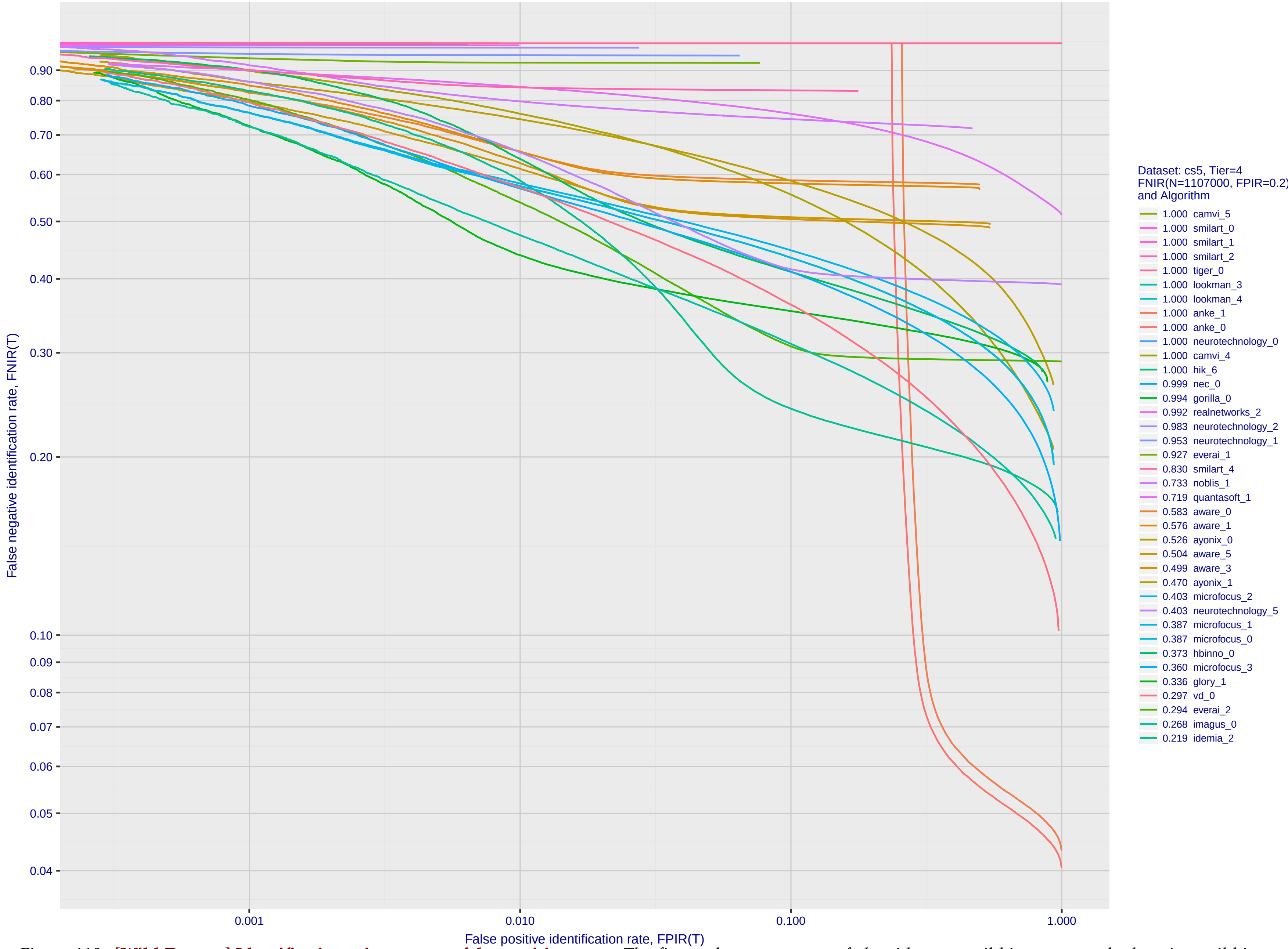

Figure 110: **[Wild Dataset] Identification miss rates vs. false positive rates**. *The figure shows accuracy of algorithms on wild images searched against wild images of 1.1 million individuals enrolled into a gallery. On the vertical axis is miss rate FNIR(N, T, L) with N = 1 107 000, as a function of false positive identification FPIR(N, T). The rapid increase in FNIR below FPIR = 0.1 suggests that some background identities in the gallery are actually present in the non-mated search sets. This issue will be addressed in the 2019 revision of this report.*

Appendix G Search duration

As in and prior tests, this section documents search speeds spanning three orders of magnitude. In applications where search volumes are high enough, this will have implications for hardware requirements especially for large N or when search duration is appreciably larger than the time it takes to prepare a template from the search image(s). Further, given very large (and growing) operational databases, the scalability of algorithms is important. It has been reported previously [8] that search duration can scale sublinearly with enrolled population size N. Further there has been considerable recent research on indexing, exact [13] and approximate nearest neighbor search [1,13] and fast-search [14,16].

Figure 111 charts the search duration measurements presented earlier in Tables 6 - 9.

- ▷ Most algorithms scale linearly. For those in that category, there is a wide range in speed with search durations ranging from 82 milliseconds for a 12 million gallery (for NEC-3) to more than 40 seconds (for Yitu-3, Toshiba-2) and even higher for less accurate algorithms.
- ▷ Some developers (Camvi, Dermalog, EverAI, Innovatrics, and Visionlabs) provide algorithms whose template search durations grow logarithmically i.e. approximately $T(N) = a \log N$ with the constant a varying between implementations. In the figure this model is fit using the point $T(1) = 0$, and $T(640\,000)$. This very sublinear behaviour affords extremely fast search times in very large galleries. One caveat for the sublinear algorithms is that the fast-search data structures require considerable computation time - on the order of hours - for N in the millions, and this scales mildy super-linearly, i.e. $O(N^b), b > 1$. There are exceptions: the Camvi algorithms take minutes; and Innvovatrics' scale sublinearly.

This publication is available free of charge from: https://doi.org/10.6028/NIST.IR.8271

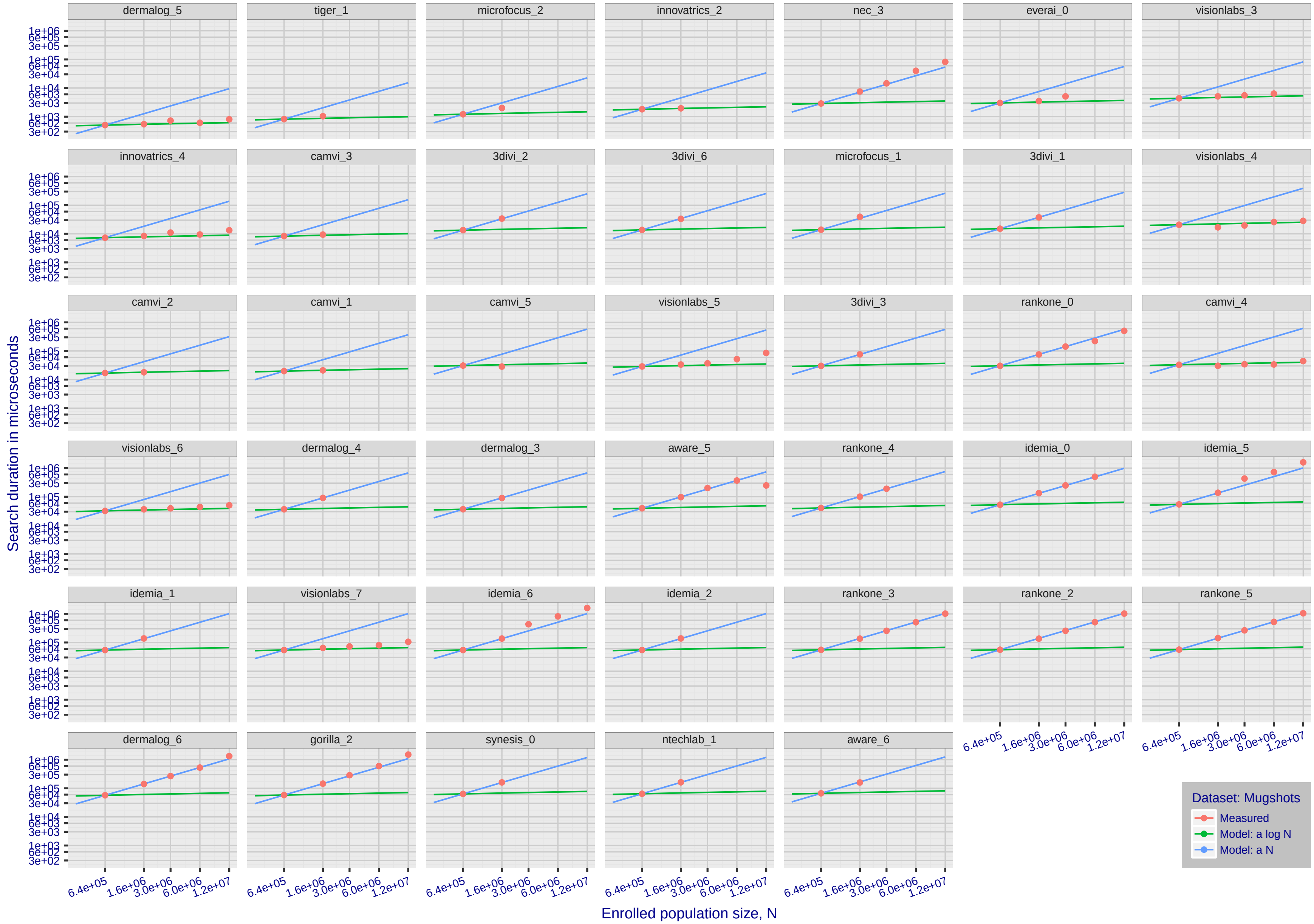

Figure 111: **[Mugshot Dataset] Search duration vs. enrolled population size**. *In red are the actual point durations measured on a single c. 2016 core. The blue shows linear growth from $N = 640\,000$. The green line shows logathmic growth from that point to $N = 1\,600\,000$. Note the sublinear growth from algorithms from Camvi, Dermalog, EverAI, Innovatrics, and Visionlabs. The tiger_1 algorithm is also sublinear, but inaccurate and inoperable at $N \geq 3000000$. This capability sometimes comes at the additional expense of converting a linear gallery data structure into whatever fast-search data structure is used. Note that search times are sometimes dominated by the template generation times shown in Table 16.*

This publication is available free of charge from: https://doi.org/10.6028/NIST.IR.8271

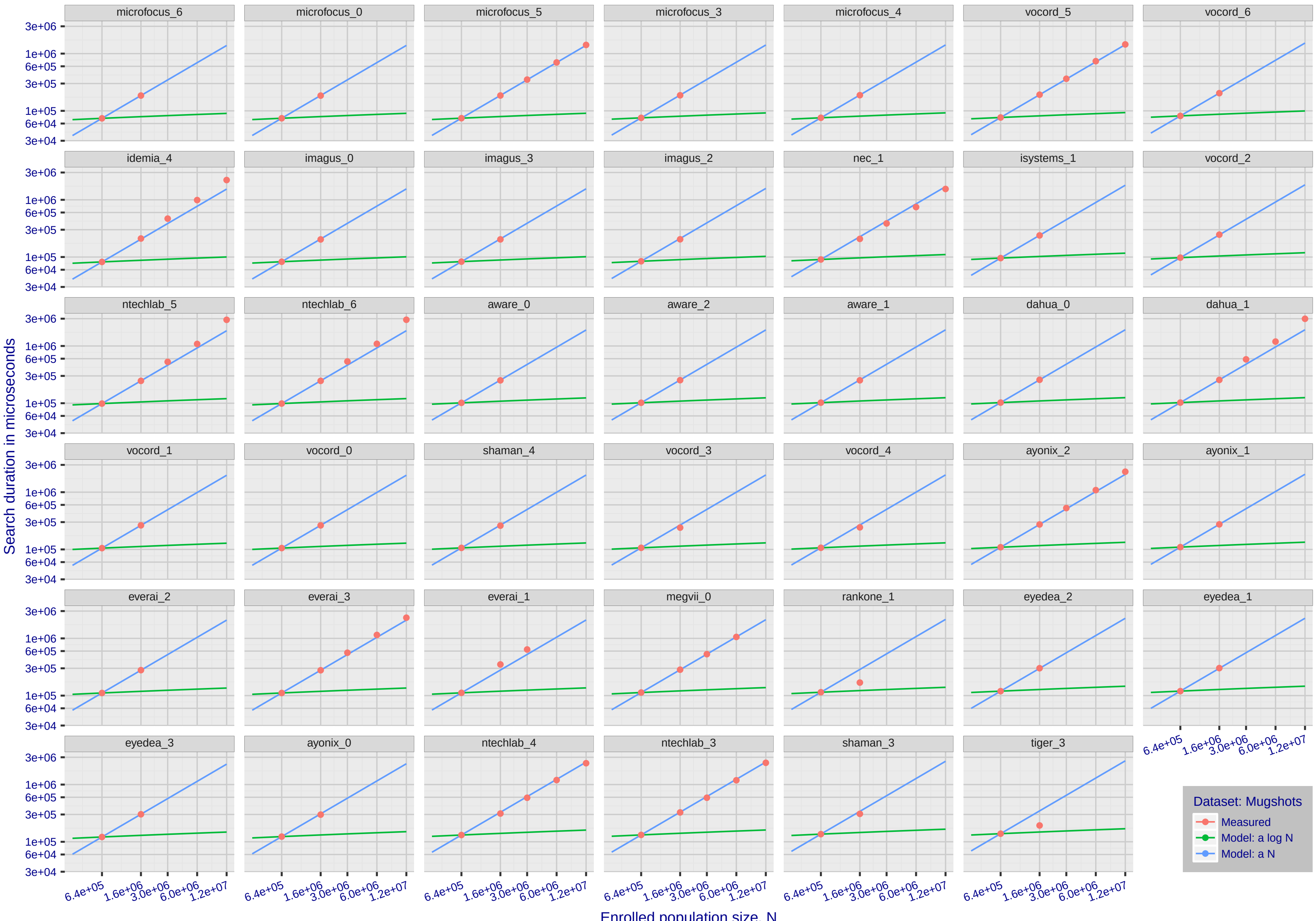

Figure 112: **[Mugshot Dataset] Search duration vs. enrolled population size**. *In red are the actual point durations measured on a single c. 2016 core. The blue shows linear growth from $N = 640\,000$. The green line shows logathmic growth from that point to $N = 1\,600\,000$. Note the sublinear growth from algorithms from Camvi, Dermalog, EverAI, Innovatrics, and Visionlabs. The tiger_1 algorithm is also sublinear, but inaccurate and inoperable at $N \geq 3000000$. This capability sometimes comes at the additional expense of converting a linear gallery data structure into whatever fast-search data structure is used. Note that search times are sometimes dominated by the template generation times shown in Table 16.*

FNIR(N, R, T) = False neg. identification rate
FPIR(N, T) = False pos. identification rate
N = Num. enrolled subjects
R = Num. candidates examined
T = Threshold
T = 0 → Investigation
T > 0 → Identification

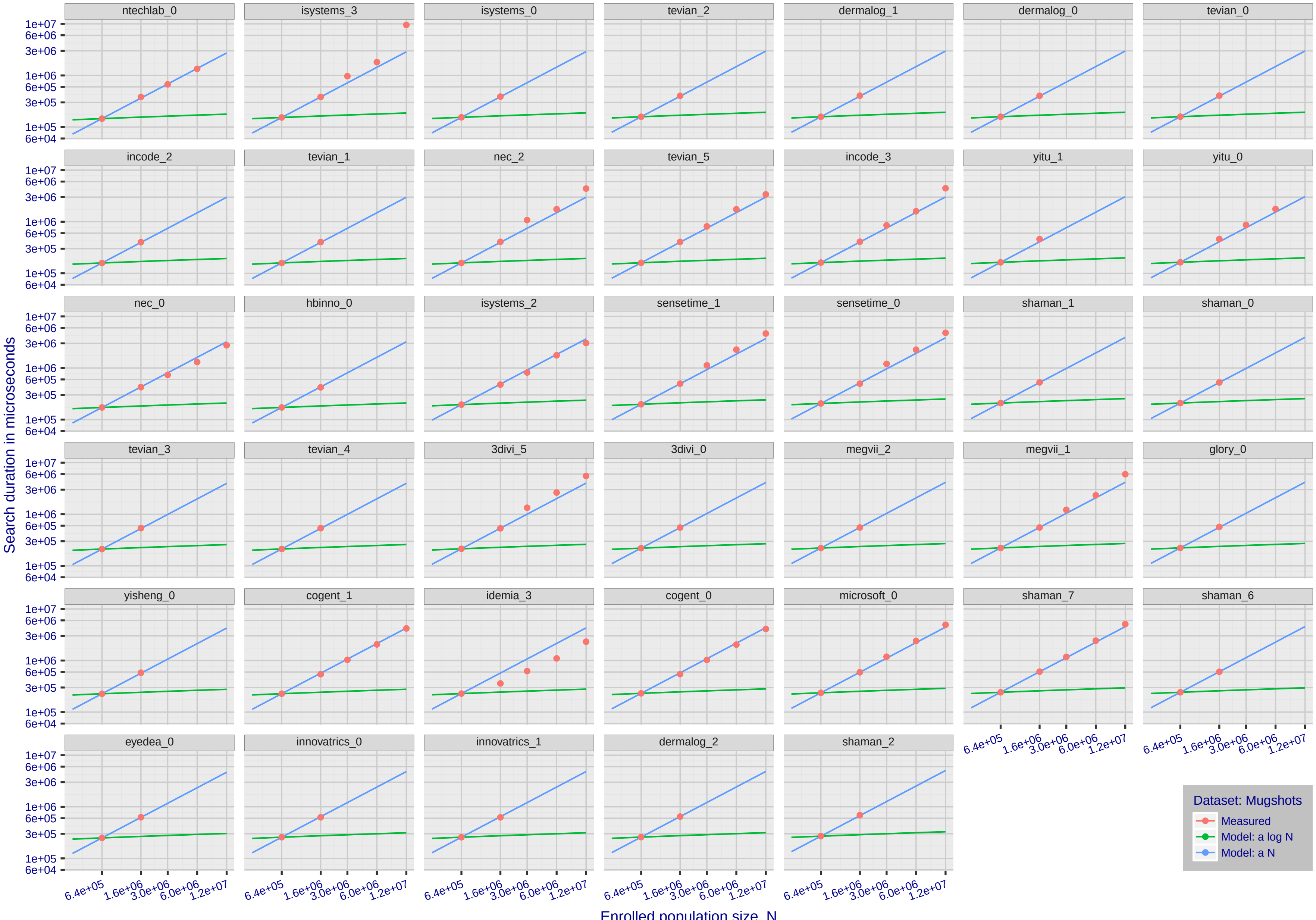

Figure 113: **[Mugshot Dataset] Search duration vs. enrolled population size**. *In red are the actual point durations measured on a single c. 2016 core. The blue shows linear growth from $N = 640\,000$. The green line shows logathmic growth from that point to $N = 1\,600\,000$. Note the sublinear growth from algorithms from Camvi, Dermalog, EverAI, Innovatrics, and Visionlabs. The tiger_1 algorithm is also sublinear, but inaccurate and inoperable at $N \geq 3000000$. This capability sometimes comes at the additional expense of converting a linear gallery data structure into whatever fast-search data structure is used. Note that search times are sometimes dominated by the template generation times shown in Table 16.*

FNIR(N, R, T) = False neg. identification rate
FPIR(N, T) = False pos. identification rate
N = Num. enrolled subjects
R = Num. candidates examined
T = Threshold
T = 0 → Investigation
T > 0 → Identification

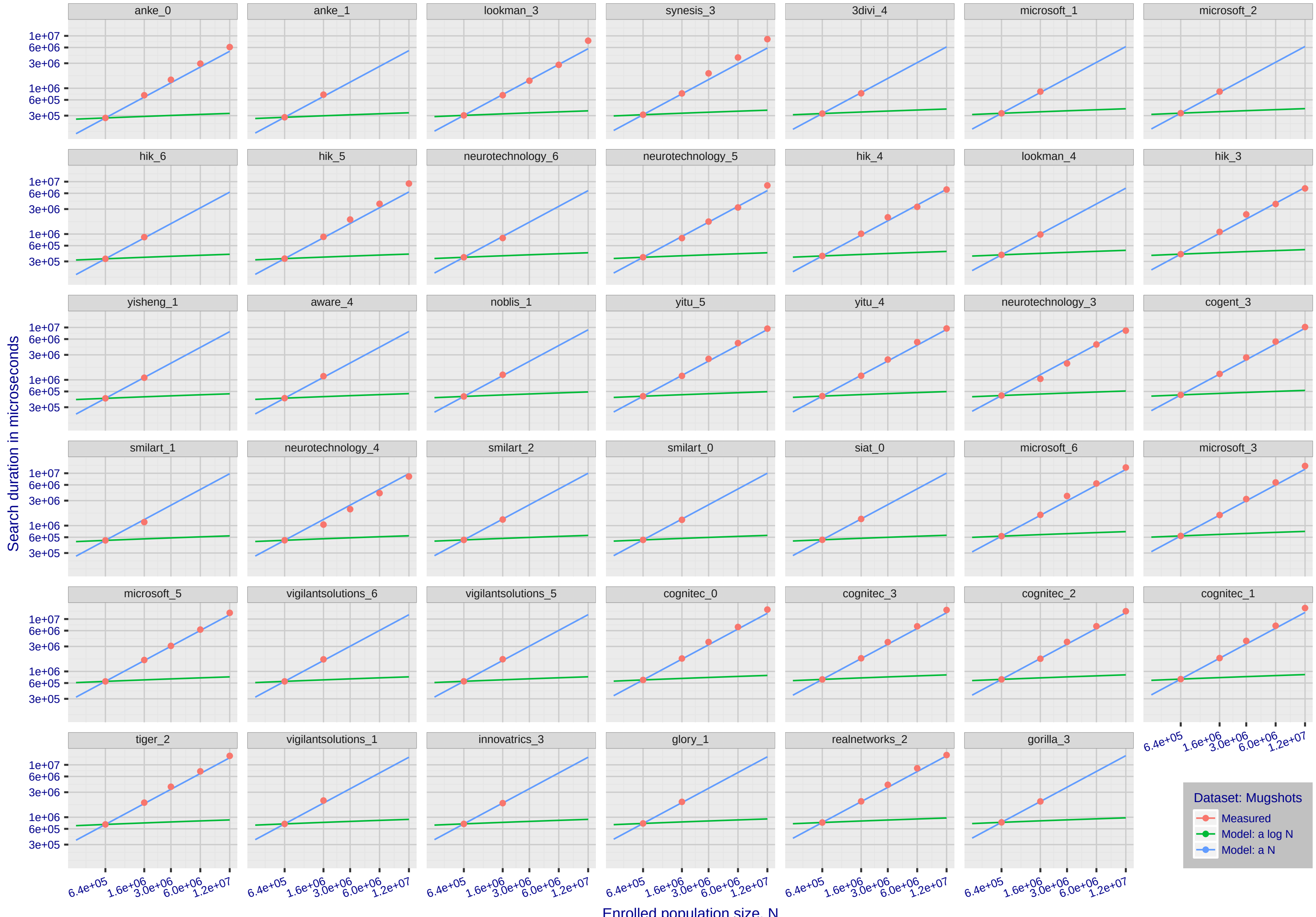

Figure 114: **[Mugshot Dataset] Search duration vs. enrolled population size**. *In red are the actual point durations measured on a single c. 2016 core. The blue shows linear growth from $N = 640\,000$. The green line shows logathmic growth from that point to $N = 1\,600\,000$. Note the sublinear growth from algorithms from Camvi, Dermalog, EverAI, Innovatrics, and Visionlabs. The tiger_1 algorithm is also sublinear, but inaccurate and inoperable at $N \geq 3000000$. This capability sometimes comes at the additional expense of converting a linear gallery data structure into whatever fast-search data structure is used. Note that search times are sometimes dominated by the template generation times shown in Table 16.*

FNIR(N, R, T) = False neg. identification rate
FPIR(N, T) = False pos. identification rate
N = Num. enrolled subjects
R = Num. candidates examined
T = Threshold
T = 0 → Investigation
T > 0 → Identification

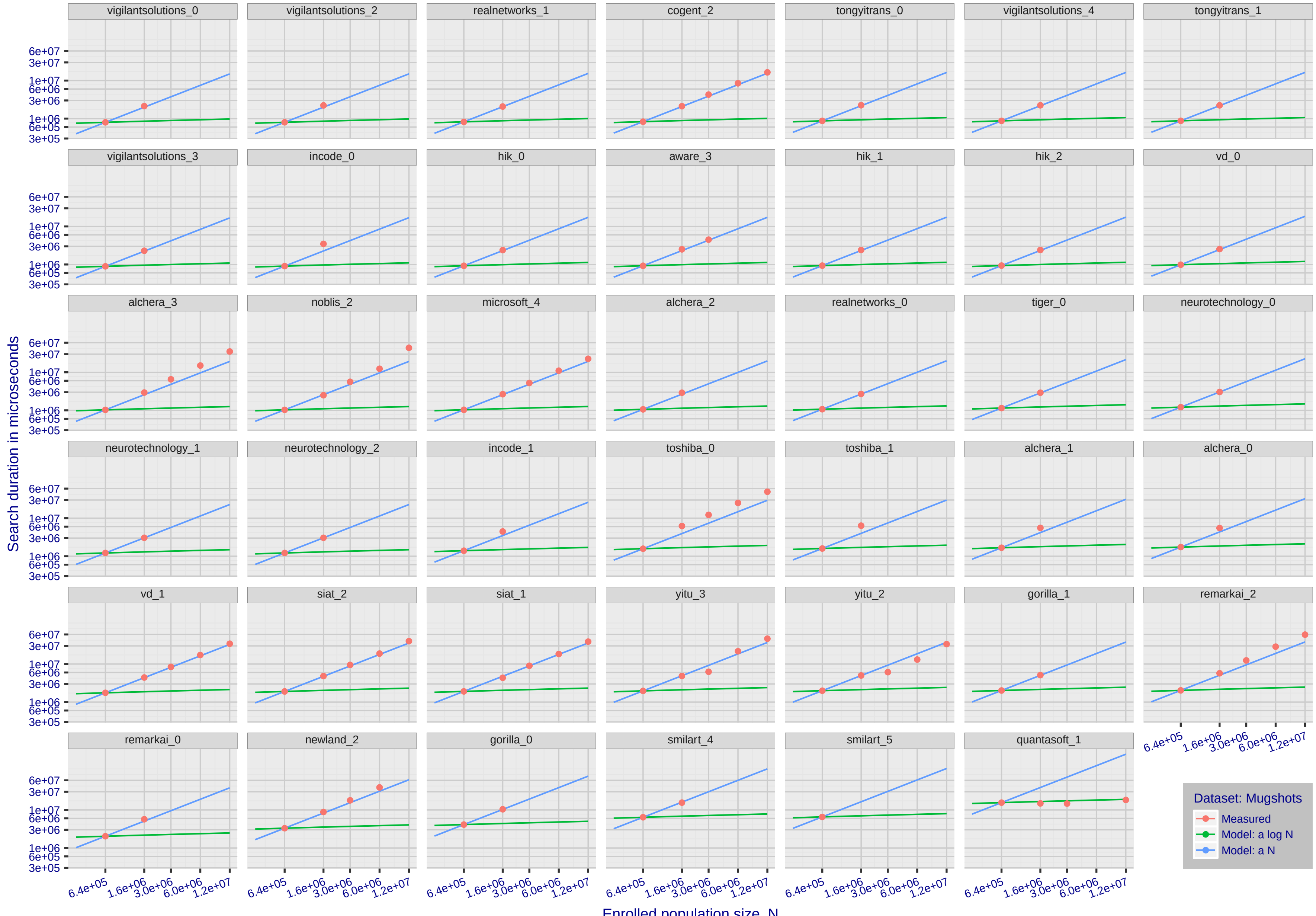

Figure 115: **[Mugshot Dataset] Search duration vs. enrolled population size**. *In red are the actual point durations measured on a single c. 2016 core. The blue shows linear growth from $N = 640\,000$. The green line shows logathmic growth from that point to $N = 1\,600\,000$. Note the sublinear growth from algorithms from Camvi, Dermalog, EverAI, Innovatrics, and Visionlabs. The tiger_1 algorithm is also sublinear, but inaccurate and inoperable at $N \geq 3000000$. This capability sometimes comes at the additional expense of converting a linear gallery data structure into whatever fast-search data structure is used. Note that search times are sometimes dominated by the template generation times shown in Table 16.*

Appendix H Gallery Insertion Timing

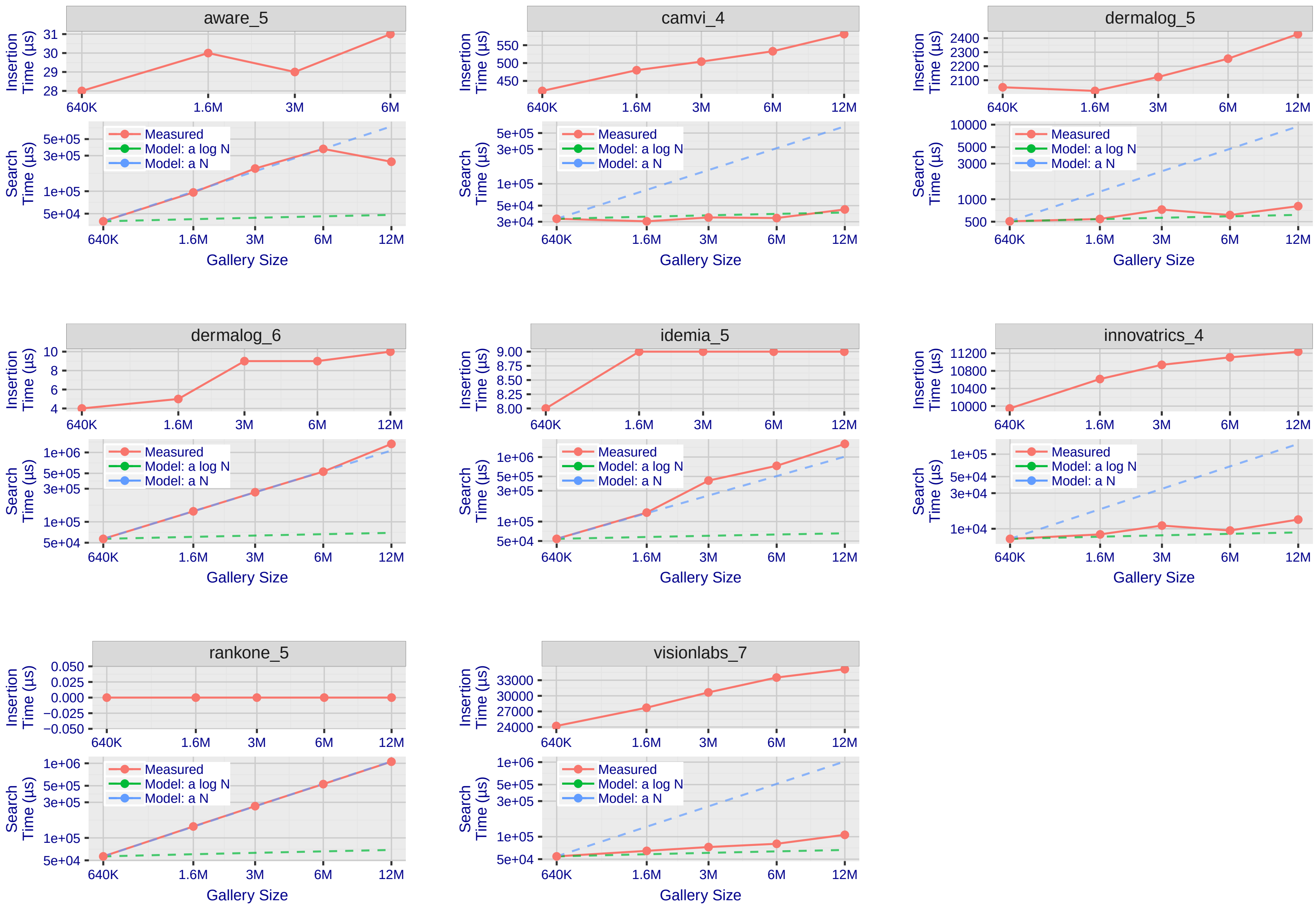

Figure 116: **[Mugshot Dataset] Gallery insertion duration vs. enrolled population size**. *This chart plots the time it takes to insert a single template into a finalized gallery, illustrated over increasing gallery sizes. For reference, search times on finalized galleries of corresponding sizes are plotted right underneath. Gallery insertion time plots were generated on algorithms that 1) successfully implemented gallery insertion with no errors and 2) that were run on galleries with N up to 12 000 000. Generally, only the more accurate algorithms were run on galleries with N up to 12 000 000.*

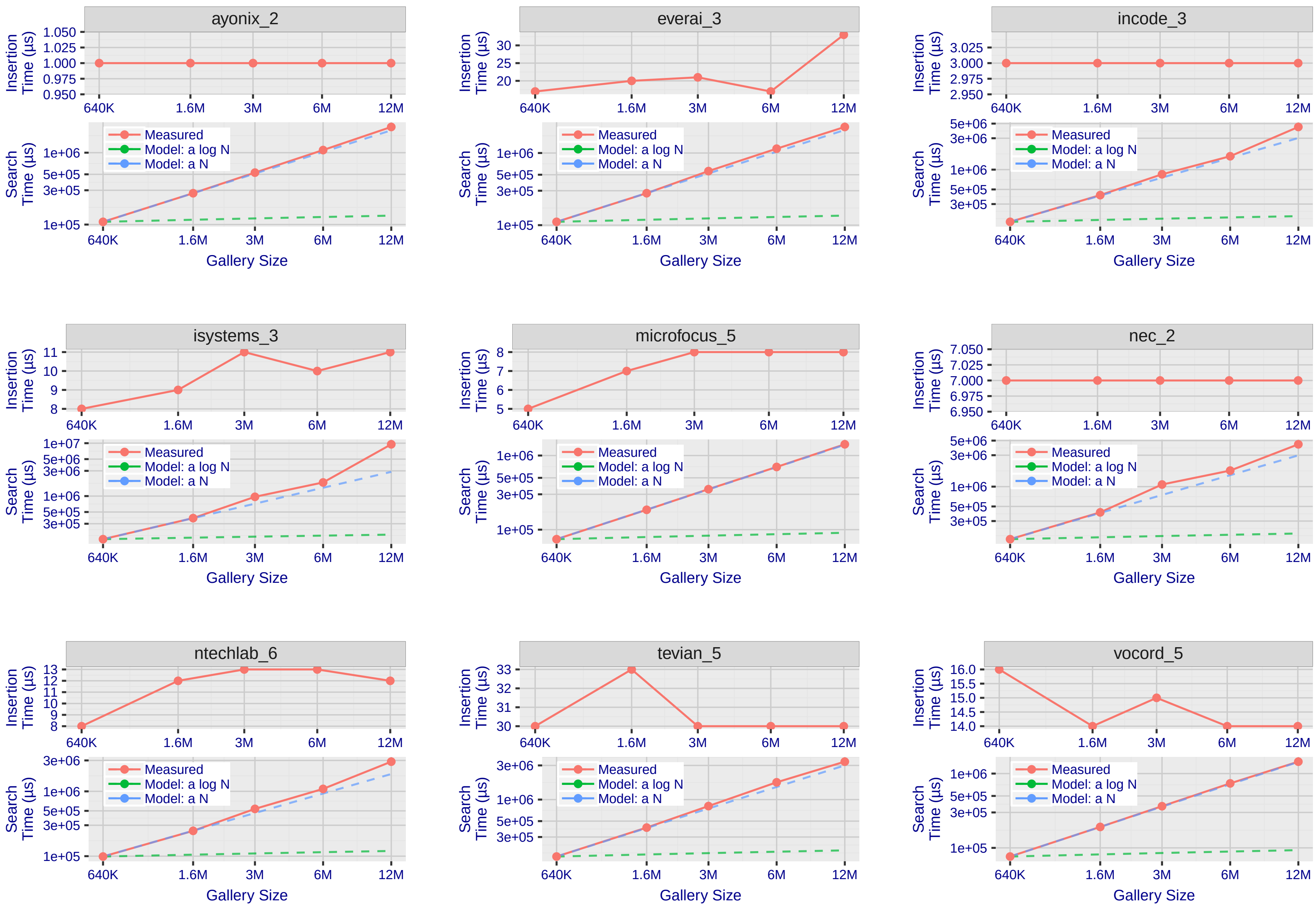

Figure 117: **[Mugshot Dataset] Gallery insertion duration vs. enrolled population size**. *This chart plots the time it takes to insert a single template into a finalized gallery, illustrated over increasing gallery sizes. For reference, search times on finalized galleries of corresponding sizes are plotted right underneath. Gallery insertion time plots were generated on algorithms that 1) successfully implemented gallery insertion with no errors and 2) that were run on galleries with N up to 12 000 000. Generally, only the more accurate algorithms were run on galleries with N up to 12 000 000.*

2019/09/11
16:09:13

FNIR(N, R, T) = False neg. identification rate
FPIR(N, T) = False pos. identification rate
N = Num. enrolled subjects
R = Num. candidates examined
T = Threshold
T = 0 → Investigation
T > 0 → Identification

This publication is available free of charge from: https://doi.org/10.6028/NIST.IR.8271

FNIR(N, R, T) = False neg. identification rate
FPIR(N, T) = False pos. identification rate
N = Num. enrolled subjects
R = Num. candidates examined
T = Threshold
T = 0 → Investigation
T > 0 → Identification

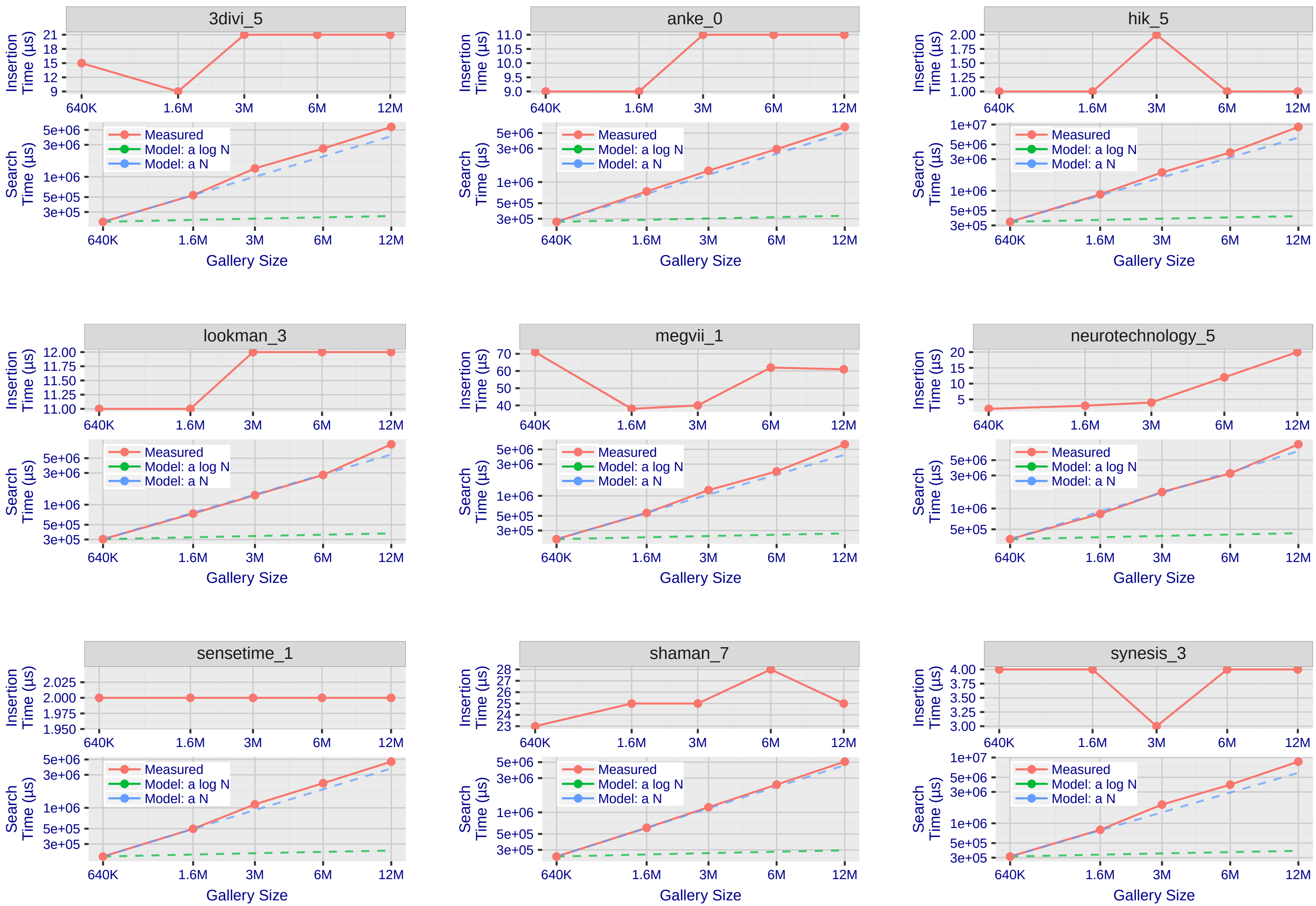

Figure 118: **[Mugshot Dataset] Gallery insertion duration vs. enrolled population size**. *This chart plots the time it takes to insert a single template into a finalized gallery, illustrated over increasing gallery sizes. For reference, search times on finalized galleries of corresponding sizes are plotted right underneath. Gallery insertion time plots were generated on algorithms that 1) successfully implemented gallery insertion with no errors and 2) that were run on galleries with N up to 12 000 000. Generally, only the more accurate algorithms were run on galleries with N up to 12 000 000.*

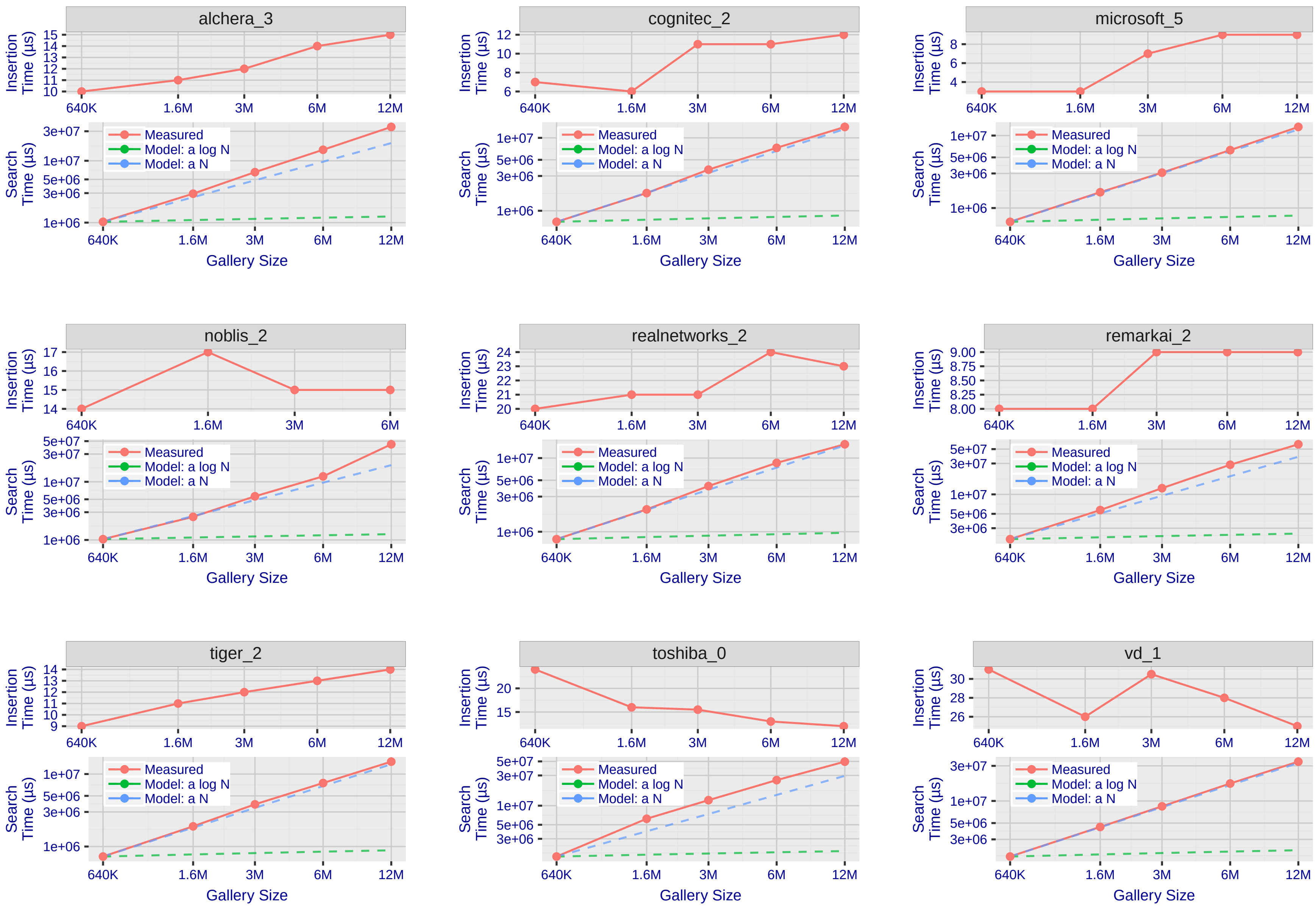

Figure 119: **[Mugshot Dataset] Gallery insertion duration vs. enrolled population size**. *This chart plots the time it takes to insert a single template into a finalized gallery, illustrated over increasing gallery sizes. For reference, search times on finalized galleries of corresponding sizes are plotted right underneath. Gallery insertion time plots were generated on algorithms that 1) successfully implemented gallery insertion with no errors and 2) that were run on galleries with N up to 12 000 000. Generally, only the more accurate algorithms were run on galleries with N up to 12 000 000.*

References

[1] Artem Babenko and Victor Lempitsky. Efficient indexing of billion-scale datasets of deep descriptors. In *The IEEE Conference on Computer Vision and Pattern Recognition (CVPR)*, June 2016.

[2] L. Best-Rowden and A. K. Jain. Longitudinal study of automatic face recognition. *IEEE Transactions on Pattern Analysis and Machine Intelligence*, 40(1):148–162, Jan 2018.

[3] Blumstein, Cohen, Roth, and Visher, editors. *Random parameter stochastic models of criminal careers*. National Academy of Sciences Press, 1986.

[4] Thomas P. Bonczar and Lauren E. Glaze. Probation and parole in the united statesm 2007, statistical tables. Technical report, Bureau of Justice Statistics, December 2008.

[5] White D., Kemp R. I., Jenkins R., Matheson M, and Burton A. M. Passport officers errors in face matching. *PLoS ONE*, 9(8), 2014. e103510. doi:10.1371/journal. pone.0103510.

[6] P. Grother, G. W. Quinn, and P. J. Phillips. Evaluation of 2d still-image face recognition algorithms. NIST Interagency Report 7709, National Institute of Standards and Technology, 8 2010. http://face.nist.gov/mbe as MBE2010 FRVT2010.

[7] P. J. Grother, R. J. Micheals, and P. J. Phillips. Performance metrics for the frvt 2002 evaluation. In *Proceedings of Audio and Video Based Person Authentication Conference (AVBPA)*, June 2003.

[8] Patrick Grother and Mei Ngan. Interagency report 8009, performance of face identification algorithms. *Face Recognition Vendor Test (FRVT)*, May 2014.

[9] Patrick Grother, George Quinn, and Mei Ngan. Face in video evaluation (five) face recognition of non-cooperative subjects. Interagency Report 8173, National Institute of Standards and Technology, March 2017. https://doi.org/10.6028/NIST.IR.8173.

[10] Patrick Grother, George W. Quinn, and Mei Ngan. Face recognition vendor test - still face image and video concept, evaluation plan and api. Technical report, National Institute of Standards and Technology, 7 2013. http://biometrics.nist.gov/cs_links/face/frvt/frvt2012/NIST_FRVT2012_api_Aug15.pdf.

[11] K. He, X. Zhang, S. Ren, and J. Sun. Deep residual learning for image recognition. In *2016 IEEE Conference on Computer Vision and Pattern Recognition (CVPR)*, pages 770–778, June 2016.

[12] Gary B. Huang, Manu Ramesh, Tamara Berg, and Erik Learned-Miller. Labeled faces in the wild: A database for studying face recognition in unconstrained environments. Technical Report 07-49, University of Massachusetts, Amherst, October 2007.

[13] Masato Ishii, Hitoshi Imaoka, and Atsushi Sato. Fast k-nearest neighbor search for face identification using bounds of residual score. In *2017 12th IEEE International Conference on Automatic Face & Gesture Recognition (FG 2017)*, pages 194–199, Los Alamitos, CA, USA, May 2017. IEEE Computer Society.

[14] Jeff Johnson, Matthijs Douze, and Hervé Jégou. Billion-scale similarity search with gpus. *CoRR*, abs/1702.08734, 2017.

[15] Ira Kemelmacher-Shlizerman, Steven M. Seitz, Daniel Miller, and Evan Brossard. The megaface benchmark: 1 million faces for recognition at scale. *CoRR*, abs/1512.00596, 2015.

[16] Yury A. Malkov and D. A. Yashunin. Efficient and robust approximate nearest neighbor search using hierarchical navigable small world graphs. *CoRR*, abs/1603.09320, 2016.

[17] Joyce A. Martin, Brady E. Hamilton, Michelle J.K. Osterman, Anne K. Driscoll, , and Patrick Drake. National vital statistics reports. Technical Report 8, Centers for Disease Control and Prevention, National Center for Health Statistics, National Vital Statistics System, Division of Vital Statistics, November 2018.

[18] O. M. Parkhi, A. Vedaldi, and A. Zisserman. Deep face recognition. In *British Machine Vision Conference*, 2015.

[19] P. Jonathon Phillips, Amy N. Yates, Ying Hu, Carina A. Hahn, Eilidh Noyes, Kelsey Jackson, Jacqueline G. Cavazos, Géraldine Jeckeln, Rajeev Ranjan, Swami Sankaranarayanan, Jun-Cheng Chen, Carlos D. Castillo, Rama Chellappa, David White, and Alice J. O'Toole. Face recognition accuracy of forensic examiners, superrecognizers, and face recognition algorithms. *Proceedings of the National Academy of Sciences*, 115(24):6171–6176, 2018.

[20] Florian Schroff, Dmitry Kalenichenko, and James Philbin. Facenet: A unified embedding for face recognition and clustering. *CoRR*, abs/1503.03832, 2015.

[21] K. Simonyan and A. Zisserman. Very deep convolutional networks for large-scale image recognition. *CoRR*, abs/1409.1556, 2014.

[22] Jeroen Smits and Christiaan Monden. Twinning across the developing world. *PLOS ONE*, 6(9):1–5, 09 2011.

[23] Christian Szegedy, Wei Liu, Yangqing Jia, Pierre Sermanet, Scott E. Reed, Dragomir Anguelov, Dumitru Erhan, Vincent Vanhoucke, and Andrew Rabinovich. Going deeper with convolutions. *CoRR*, abs/1409.4842, 2014.

[24] Yaniv Taigman, Ming Yang, Marc'Aurelio Ranzato, and Lior Wolf. Deepface: Closing the gap to human-level performance in face verification. In *Proceedings of the 2014 IEEE Conference on Computer Vision and Pattern Recognition*, CVPR '14, pages 1701–1708, Washington, DC, USA, 2014. IEEE Computer Society.

[25] A. Towler, R. I. Kemp, and D White. *Unfamiliar face matching systems in applied settings*. Nova Science, 2017.

[26] Working Group 3. Ed. M. Werner. *ISO/IEC 19794-5 Information Technology - Biometric Data Interchange Formats - Part 5: Face image data*. JTC1 :: SC37, 2 edition, 2011. http://webstore.ansi.org.

[27] David White, James D. Dunn, Alexandra C. Schmid, and Richard I. Kemp. Error rates in users of automatic face recognition software. *PLoS ONE*, 10:1–14, October 2015.

[28] Bradford Wing and R. Michael McCabe. Special publication 500-271: American national standard for information systems data format for the interchange of fingerprint, facial, and other biometric information part 1. Technical report, NIST, September 2015. ANSI/NIST ITL 1-2015.

[29] Andreas Wolf. Portrait quality - (reference facial images for mrtd). Technical report, ICAO, April 2018.

[30] D. Yadav, N. Kohli, P. Pandey, R. Singh, M. Vatsa, and A. Noore. Effect of illicit drug abuse on face recognition. In *2016 IEEE Winter Conference on Applications of Computer Vision (WACV)*, pages 1–7, Los Alamitos, CA, USA, mar 2016. IEEE Computer Society.